

OPTICAL AND INFRARED TRANSFER FUNCTION  
OF THE LAGEOS RETROREFLECTOR ARRAY

Grant NGR 09-015-002

Author: David A. Arnold

May 1978

Prepared for  
National Aeronautics and Space Administration  
Washington, D. C. 20546

Smithsonian Institution  
Astrophysical Observatory  
Cambridge, Massachusetts 02138

The Smithsonian Astrophysical Observatory  
and the Harvard College Observatory  
are members of the  
Center for Astrophysics

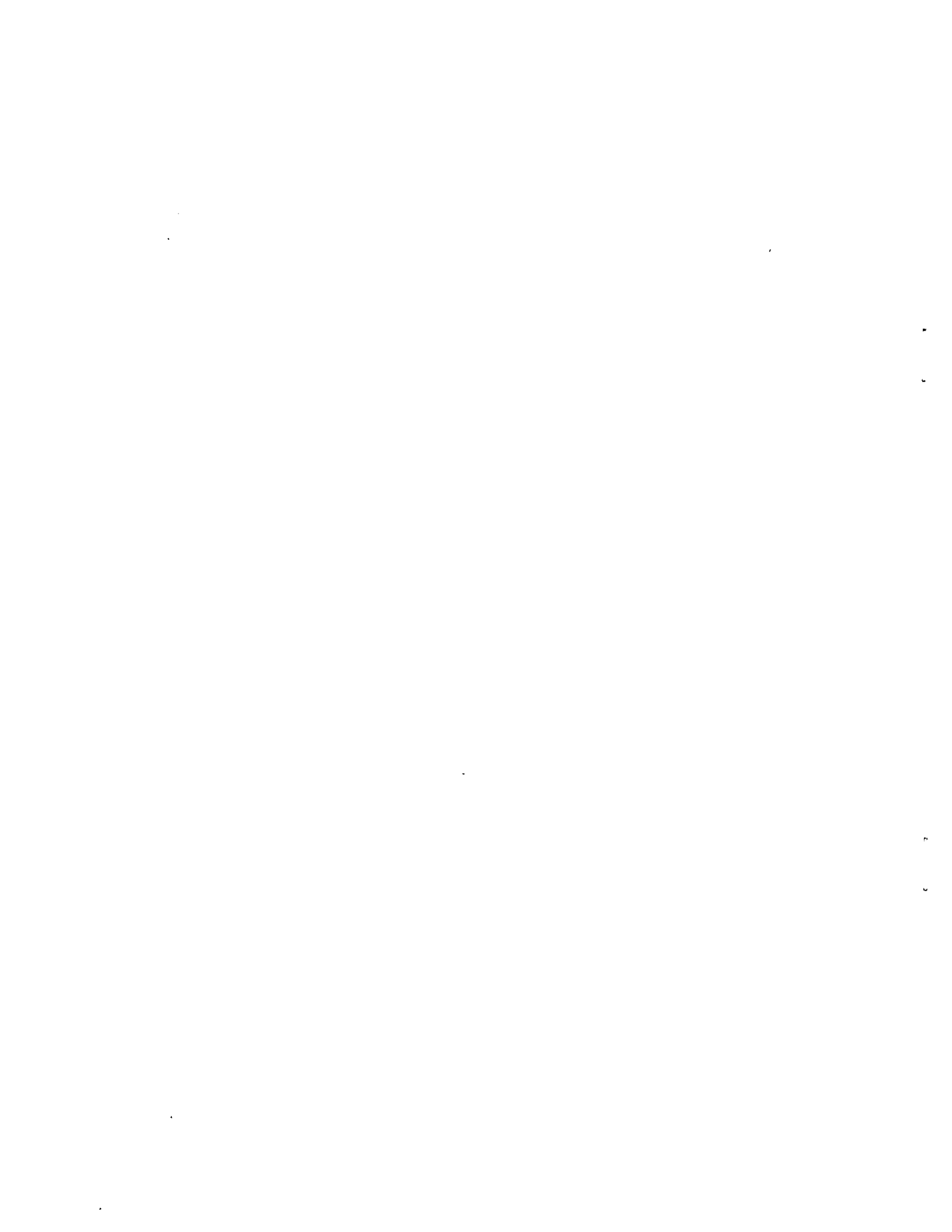


## TABLE OF CONTENTS

	<u>Page</u>
ABSTRACT .....	vi
1 INTRODUCTION .....	1
2 CUBE-CORNER SPECIFICATIONS.....	3
3 GEOMETRY OF THE ARRAY .....	5
4 METHOD OF COMPUTING THE TRANSFER FUNCTION .....	19
5 SIGNAL-STRENGTH COMPUTATION .....	21
6 OPTICAL CUBE-CORNER REFLECTIVITY.....	23
7 VARIATION OF TRANSFER FUNCTION WITH SATELLITE ORIENTA- TION.....	43
8 REFLECTIVITY HISTOGRAM .....	45
9 ARRAY REFLECTIVITY.....	53
10 RANGE CORRECTION .....	105
11 EFFECT OF OPTICAL COHERENCE .....	159
12 ACCURACY OF RESULTS.....	177
13 INFRARED TRANSFER FUNCTION .....	179
14 ACKNOWLEDGMENTS.....	189
15 REFERENCES .....	191

## LIST OF FIGURES

<u>Figure</u>		<u>Page</u>
1	The Lageos satellite. . . . .	6
2	Cube-corner mount assembly. . . . .	7
3	Coordinate system for cube-corner orientation. . . . .	8
4	Coordinate system for incidence angles on cube-corner entrance face.	23
5	Asymmetry of the input polarization vector with respect to $\theta = 30^\circ$ . . .	26
6	Total reflectivity and average reflectivity in the 32- to 41- $\mu$ rad annulus for a Lageos optical cube corner. . . . .	28
7	Reflectivity histogram of Lageos . . . . .	47
8	Diffraction-pattern coordinate system . . . . .	54
9	Contour plots of the gain-function matrices . . . . .	87
10	Contour plots of the centroid range correction matrices. . . . .	142
11	Sample incoherent and coherent reflected pulse shapes. . . . .	162
12	Reflectivity of a Lageos infrared cube corner. . . . .	182

## LIST OF TABLES

<u>Table</u>	<u>Page</u>
1 Specifications for the rings of cube corners . . . . .	5
2 Cube-corner positions and orientations . . . . .	9
3 Cutoff angles for total internal reflection . . . . .	25
4 Average reflectivity of a Lageos optical cube corner in the 32- to 41- $\mu$ rad annulus. . . . .	27
5 Apparent reflection points for various cube-corner incidence angles. .	46
6 Percentage of total return in each 1-cm interval. . . . .	50
7 Gain function matrices . . . . .	55
8 Gain function vs. velocity aberration. . . . .	71
9 Average gain in the 32-41 $\mu$ rad annulus . . . . .	104
10 Variation of range correction with pulse length. . . . .	105
11 Codes for range contour plots in Figure 10. . . . .	106
12 Average range correction in the 32-41 $\mu$ rad annulus for various cases. . . . .	106
13 Range correction for four pulse detection techniques at selected points in the far field . . . . .	108
14 Centroid range correction matrices . . . . .	110
15 Centroid range correction vs. velocity aberration. . . . .	126
16 Difference between the average range correction for a set of coherent returns and the range correction for the incoherent return . . . . .	160
17 Central angles between pairs of infrared cube corners . . . . .	179
18 Reflectivity of a Lageos infrared cube corner . . . . .	181
19 Polarization of the reflection from a Lageos infrared cube corner . . .	183
20 Absorptance/cm and transmission factor for the Lageos infrared reflectors. . . . .	183
21 Probability of getting reflections from more than one infrared reflector . . . . .	184
22 Infrared range correction vs. incidence angle. . . . .	186

## ABSTRACT

This report covers work done under NASA Grant NGR 09-015-002. The transfer function of the retroreflector array carried by the LAGEOS satellite (1976 39A) has been computed at three wavelengths: 5230, 6943, and 106000 Å. The range correction is given for extrapolating laser range measurements to the center of gravity of the satellite. The reflectivity of the array has been computed for estimating laser-echo signal strengths.

# OPTICAL AND INFRARED TRANSFER FUNCTION OF THE LAGEOS RETROREFLECTOR ARRAY

David A. Arnold

## 1. INTRODUCTION

This is the fifth in a series of reports giving transfer functions for satellites with retroreflector arrays (Arnold, 1972, 1974, 1975a, b). A special analysis has been done for the infrared cube corners designed for use with lasers operating at  $\lambda = 106000 \text{ \AA}$ . The optical transfer function of the array was measured experimentally at Goddard Space Flight Center before the satellite was launched (Fitzmaurice, Minott, Abshire, and Rowe, 1977). Some preliminary transfer function analyses done on an earlier design of the satellite are given (Weiffenbach, 1973).

Data on the Lageos retroreflector array were obtained from Marshall Space Flight Center.





## 2. CUBE-CORNER SPECIFICATIONS

The cube corners on Lageos have a circular entrance face  $1.15$  (3.81 cm) in diameter, which gives an aperture of  $11.4009 \text{ cm}^2$ . The length from vertex to face is 1.096 in. (2.78384 cm). The optical cube corners are made of fused silica and rely on total internal reflection rather than reflective coatings on the back faces. The dihedral angles between the back faces are  $90^\circ + 1.25 \pm 0.5$  in order to compensate for velocity aberration. The infrared cube corners are made of single-crystal germanium and are also uncoated. The dihedral angles between the back faces are  $90^\circ \pm 0.5$  with no offset.

The index of refraction of the fused silica is 1.455 at  $6943 \text{ \AA}$  and 1.461 at  $5320 \text{ \AA}$ . The refractive index of the germanium cube corners at  $106000 \text{ \AA}$  is 4.003. The surface flatness tolerance is  $\lambda/10$  peak to peak for the optical cubes and  $\lambda/4$  for the infrared cubes, where  $\lambda$  is the helium-neon wavelength used in measuring the flatness.



### 3. GEOMETRY OF THE ARRAY

The Lageos satellite is a sphere 60 cm in diameter with 426 retroreflectors distributed over the surface (Figure 1). Four of the cube corners are made of germanium for infrared wavelengths and the other 422 are made of fused silica for use at visible wavelengths. The sphere consists of two hemispheres bolted together. The cube corners are arranged in rings about the pole of each hemisphere. Table 1 lists for each ring, the number of cubes, the latitude, and the angle between the cubes as measured from the axis of the hemisphere.

Table 1. Specifications for the rings of cube corners on each hemisphere.

Ring number	Number of cubes	Latitude (deg.)	Angle between cubes (deg.)
1	32	4.865	11.250
2	32	13.252	11.250
3	31	22.982	11.613
4	31	31.231	11.613
5	27	40.961	13.333
6	23	50.691	15.652
7	18	60.421	20.000
8	12	70.151	30.000
9	6	79.881	60.000
10	1	90.000	360.000

Adjacent rings having the same number of cubes are meshed in order to get as many cubes on the sphere as possible. The cubes in ring two are positioned above the space between the cubes in row one. The cubes in rings three and four are meshed in a similar manner.

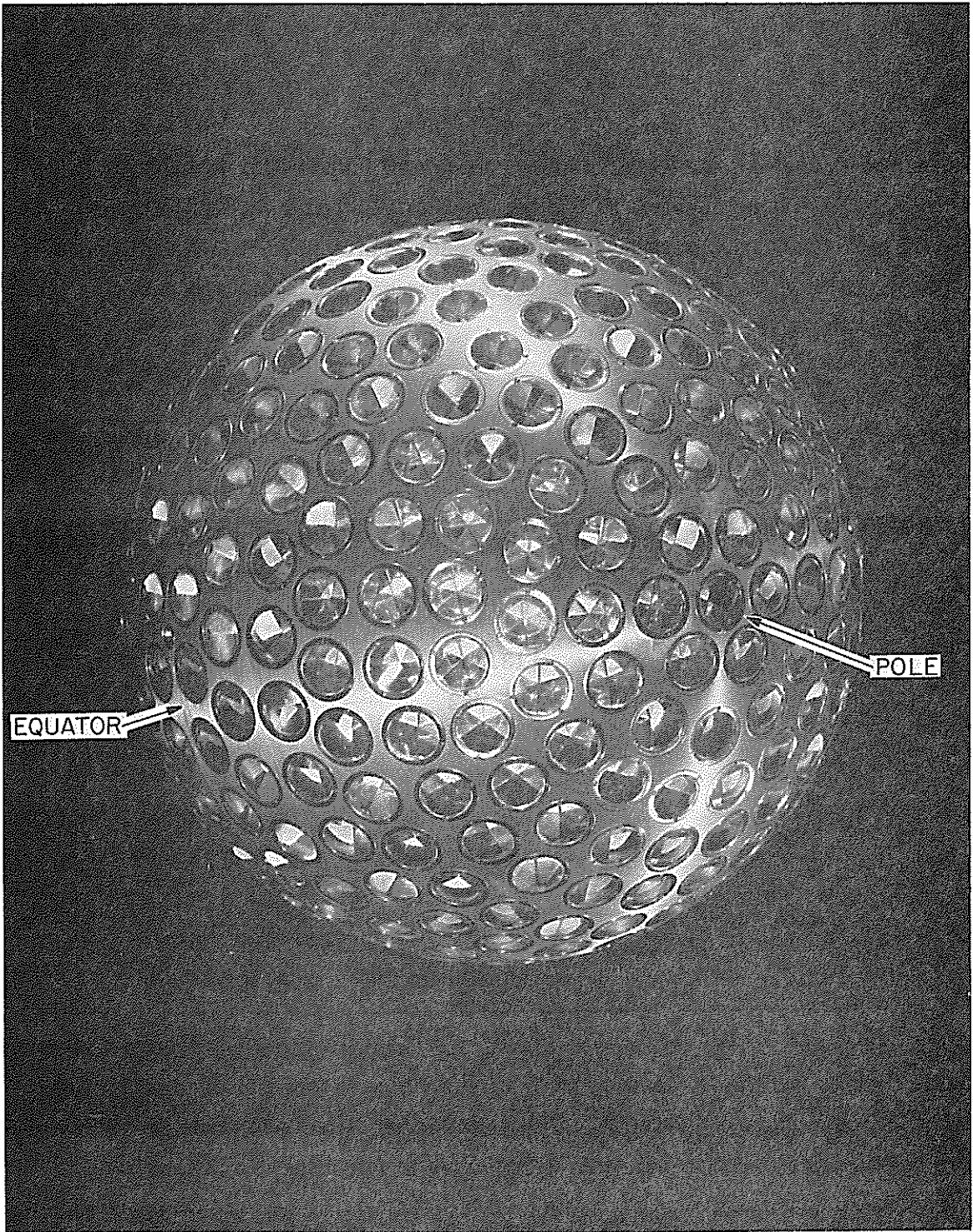


Figure 1. The Lageos satellite.

The retroreflectors are recessed slightly below the surface of the sphere in order to prevent them from being damaged during handling. This recession, together with the fact that the front face of a cube corner is flat, places the center of the front face closer to the center of the satellite than the surface of the sphere. The cube corner is held in place by upper and lower mounting rings, which fit over tabs projecting from the cube corner. In order to minimize thermal conductance across the mounting tabs, there is a slight clearance between the tabs and the rings. The outermost hole into which the cube corner assembly is placed is 2.3813 cm in radius and 1.0236 cm deep (Figure 2). The bottom of the mounting rings are therefore

$$\sqrt{30^2 - 2.3813^2} - 1.0236 = 28.8818 \text{ cm}$$

from the center of the sphere. Adding to this the distance from the bottom of the rings to the center of the tab (0.5436 cm) and the distance from the center of the tab to the front face of the cube corner (0.3810 cm) places the front face at 29.807 cm from the center of the sphere.

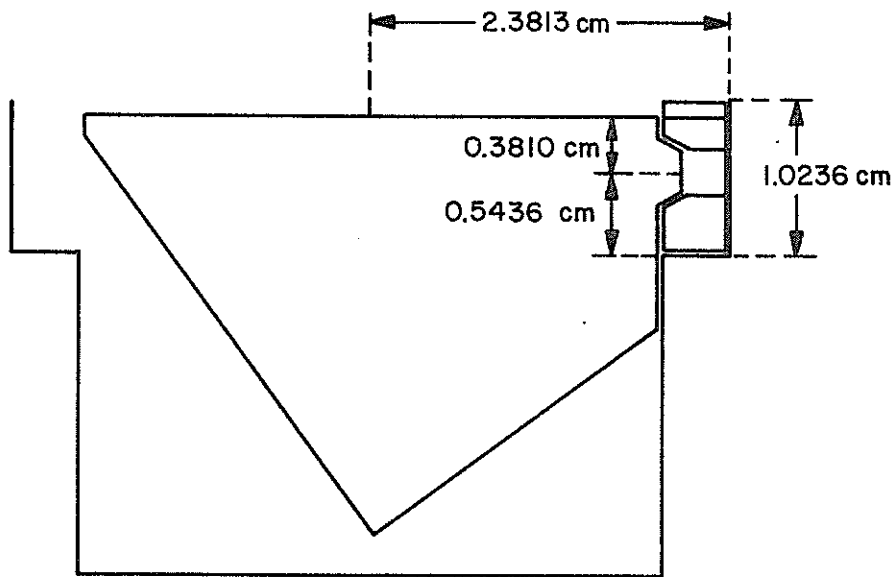


Figure 2. Cube-corner mount assembly.

Since the cube corners have no reflective coating on the back faces, retroreflection is by total internal reflection, which occurs only for certain directions of the incident beam. Any beam making an angle of less than about  $17^\circ$  with the normal to the front face will undergo total reflection. Beyond  $17^\circ$ , only certain azimuths give total reflection. In order to make the transfer function of the sphere more independent of satellite orientation, the cube corners have been installed so as to give a uniform distribution of orientations. In this way there is no satellite orientation where all the cube corners at greater than  $17^\circ$  incidence angle are either all totally reflecting or not totally reflecting, which would give an anomalous transfer function.

The coordinate system used to describe the geometry of the array is as follows. The position and orientation of each cube corner in the array are given by the six numbers,  $x, y, z, \theta, \phi, \alpha$ . The origin of the  $x$ - $y$ - $z$  coordinate system is the center of the satellite. The angles  $\theta$  and  $\phi$  are given in an  $x'$ - $y'$ - $z'$  coordinate, which is parallel to the  $x$ - $y$ - $z$  system (Figure 3a). The angle  $\alpha$  is shown in Figure 3b. The  $\beta$  and  $\gamma$  axes point east and north, respectively; in other words,  $\gamma$  is in the direction of decreasing  $\phi$ , and  $\beta$  is in the direction of increasing  $\theta$ .

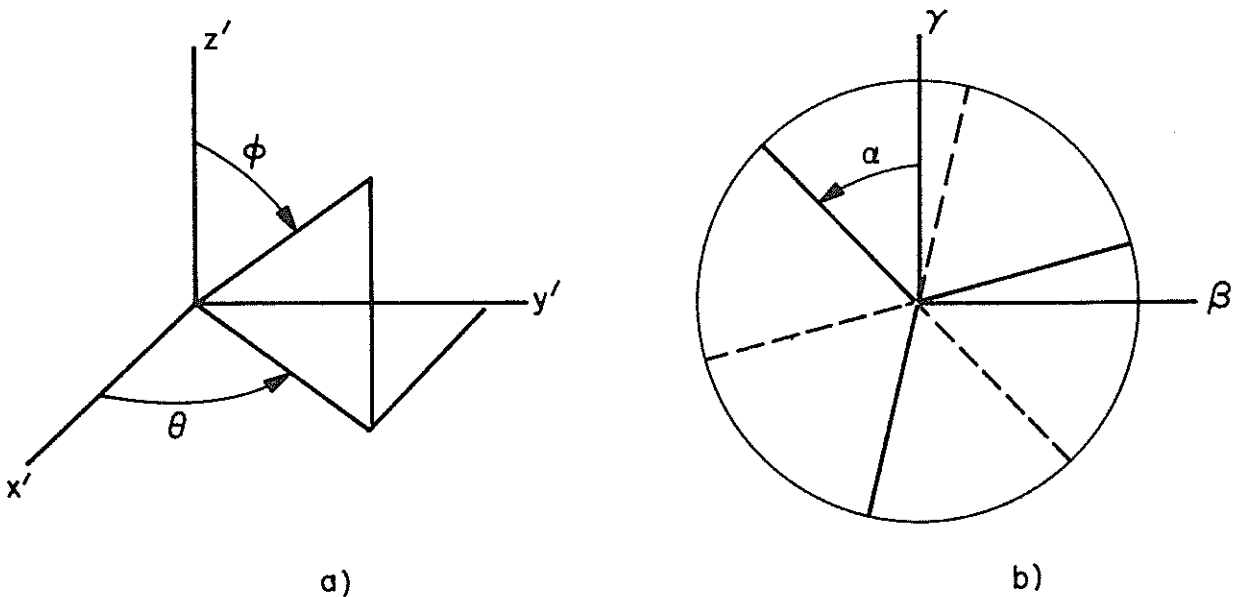


Figure 3. Coordinate system for cube-corner orientation.

Table 2 lists the position and orientation of the cube corners in the array.

Table 2. Cube corner positions (m) and orientations (degrees).

a) Infrared cube corners

HEMISPHERE	RING	RETRO	X	Y	Z	THETA	PHI	ALPHA
1	10	1	0.00000	0.00000	.29807	0.000	0.000	115.000
2	3	1	.27300	.02776	-.11638	5.806	112.982	170.000
2	3	11	-.14515	.23287	-.11638	121.936	112.982	150.000
2	3	21	-.14515	-.23287	-.11638	238.065	112.982	130.000

Table 2. (Cont.)

b) Optical cube corners.

HEMISPHERE	RING	RETRO	X	Y	Z	THETA	PHI	ALPHA
1	1	1	.29556	.02911	.02528	5.625	85.135	107.000
2	1	1	.29556	.02911	-.02528	5.625	94.865	154.000
1	1	2	.28421	.08621	.02528	16.875	85.135	81.000
2	1	2	.28421	.08621	-.02528	16.875	94.865	128.000
1	1	3	.26192	.14000	.02528	28.125	85.135	175.000
2	1	3	.26192	.14000	-.02528	28.125	94.865	102.000
1	1	4	.22958	.18841	.02528	39.375	85.135	149.000
2	1	4	.22958	.18841	-.02528	39.375	94.865	76.000
1	1	5	.18841	.22958	.02528	50.625	85.135	123.000
2	1	5	.18841	.22958	-.02528	50.625	94.865	170.000
1	1	6	.14000	.26192	.02528	61.875	85.135	97.000
2	1	6	.14000	.26192	-.02528	61.875	94.865	144.000
1	1	7	.08621	.28421	.02528	73.125	85.135	71.000
2	1	7	.08621	.28421	-.02528	73.125	94.865	118.000
1	1	8	.02911	.29556	.02528	84.375	85.135	165.000
2	1	8	.02911	.29556	-.02528	84.375	94.865	92.000
1	1	9	-.02911	.29556	.02528	95.625	85.135	139.000
2	1	9	-.02911	.29556	-.02528	95.625	94.865	66.000
1	1	10	-.08621	.28421	.02528	106.875	85.135	113.000
2	1	10	-.08621	.28421	-.02528	106.875	94.865	160.000
1	1	11	-.14000	.26192	.02528	118.125	85.135	87.000
2	1	11	-.14000	.26192	-.02528	118.125	94.865	134.000
1	1	12	-.18841	.22958	.02528	129.375	85.135	61.000
2	1	12	-.18841	.22958	-.02528	129.375	94.865	108.000
1	1	13	-.22958	.18841	.02528	140.625	85.135	155.000
2	1	13	-.22958	.18841	-.02528	140.625	94.865	82.000
1	1	14	-.26192	.14000	.02528	151.875	85.135	129.000
2	1	14	-.26192	.14000	-.02528	151.875	94.865	176.000
1	1	15	-.28421	.08621	.02528	163.125	85.135	103.000
2	1	15	-.28421	.08621	-.02528	163.125	94.865	150.000
1	1	16	-.29556	.02911	.02528	174.375	85.135	77.000
2	1	16	-.29556	.02911	-.02528	174.375	94.865	124.000
1	1	17	-.29556	-.02911	.02528	185.625	85.135	171.000
2	1	17	-.29556	-.02911	-.02528	185.625	94.865	98.000
1	1	18	-.28421	-.08621	.02528	196.875	85.135	145.000
2	1	18	-.28421	-.08621	-.02528	196.875	94.865	72.000
1	1	19	-.26192	-.14000	.02528	208.125	85.135	119.000
2	1	19	-.26192	-.14000	-.02528	208.125	94.865	166.000
1	1	20	-.22958	-.18841	.02528	219.375	85.135	93.000
2	1	20	-.22958	-.18841	-.02528	219.375	94.865	140.000
1	1	21	-.18841	-.22958	.02528	230.625	85.135	67.000
2	1	21	-.18841	-.22958	-.02528	230.625	94.865	114.000
1	1	22	-.14000	-.26192	.02528	241.875	85.135	161.000
2	1	22	-.14000	-.26192	-.02528	241.875	94.865	88.000
1	1	23	-.08621	-.28421	.02528	253.125	85.135	135.000
2	1	23	-.08621	-.28421	-.02528	253.125	94.865	62.000
1	1	24	-.02911	-.29556	.02528	264.375	85.135	109.000
2	1	24	-.02911	-.29556	-.02528	264.375	94.865	156.000
1	1	25	.02911	-.29556	.02528	275.625	85.135	83.000
2	1	25	.02911	-.29556	-.02528	275.625	94.865	130.000



Table 2. (Cont.)

HEMISPHERE	RING	RETRO	X	Y	Z	THETA	PHI	ALPHA
1	1	26	.08621	-.28421	.02528	286.875	85.135	177.000
2	1	26	.08621	-.28421	-.02528	286.875	94.865	104.000
1	1	27	.14000	-.26192	.02528	298.125	85.135	151.000
2	1	27	.14000	-.26192	-.02528	298.125	94.865	78.000
1	1	28	.18841	-.22958	.02528	309.375	85.135	125.000
2	1	28	.18841	-.22958	-.02528	309.375	94.865	172.000
1	1	29	.22958	-.18841	.02528	320.625	85.135	99.000
2	1	29	.22958	-.18841	-.02528	320.625	94.865	146.000
1	1	30	.26192	-.14000	.02528	331.875	85.135	73.000
2	1	30	.26192	-.14000	-.02528	331.875	94.865	120.000
1	1	31	.28421	-.08621	.02528	343.125	85.135	167.000
2	1	31	.28421	-.08621	-.02528	343.125	94.865	94.000
1	1	32	.29556	-.02911	.02528	354.375	85.135	141.000
2	1	32	.29556	-.02911	-.02528	354.375	94.865	68.000
1	2	1	.29013	0.00000	.06833	0.000	76.748	115.000
2	2	1	.29013	0.00000	-.06833	0.000	103.252	162.000
1	2	2	.28456	.05660	.06833	11.250	76.748	89.000
2	2	2	.28456	.05660	-.06833	11.250	103.252	136.000
1	2	3	.26804	.11103	.06833	22.500	76.748	63.000
2	2	3	.26804	.11103	-.06833	22.500	103.252	110.000
1	2	4	.24124	.16119	.06833	33.750	76.748	157.000
2	2	4	.24124	.16119	-.06833	33.750	103.252	84.000
1	2	5	.20515	.20515	.06833	45.000	76.748	131.000
2	2	5	.20515	.20515	-.06833	45.000	103.252	178.000
1	2	6	.16119	.24124	.06833	56.250	76.748	105.000
2	2	6	.16119	.24124	-.06833	56.250	103.252	152.000
1	2	7	.11103	.26804	.06833	67.500	76.748	79.000
2	2	7	.11103	.26804	-.06833	67.500	103.252	126.000
1	2	8	.05660	.28456	.06833	78.750	76.748	173.000
2	2	8	.05660	.28456	-.06833	78.750	103.252	100.000
1	2	9	0.00000	.29013	.06833	90.000	76.748	147.000
2	2	9	0.00000	.29013	-.06833	90.000	103.252	74.000
1	2	10	-.05660	.28456	.06833	101.250	76.748	121.000
2	2	10	-.05660	.28456	-.06833	101.250	103.252	168.000
1	2	11	-.11103	.26804	.06833	112.500	76.748	95.000
2	2	11	-.11103	.26804	-.06833	112.500	103.252	142.000
1	2	12	-.16119	.24124	.06833	123.750	76.748	69.000
2	2	12	-.16119	.24124	-.06833	123.750	103.252	116.000
1	2	13	-.20515	.20515	.06833	135.000	76.748	163.000
2	2	13	-.20515	.20515	-.06833	135.000	103.252	90.000
1	2	14	-.24124	.16119	.06833	146.250	76.748	137.000
2	2	14	-.24124	.16119	-.06833	146.250	103.252	64.000
1	2	15	-.26804	.11103	.06833	157.500	76.748	111.000
2	2	15	-.26804	.11103	-.06833	157.500	103.252	158.000
1	2	16	-.28456	.05660	.06833	168.750	76.748	85.000
2	2	16	-.28456	.05660	-.06833	168.750	103.252	132.000
1	2	17	-.29013	0.00000	.06833	180.000	76.748	179.000
2	2	17	-.29013	0.00000	-.06833	180.000	103.252	106.000
1	2	18	-.28456	-.05660	.06833	191.250	76.748	153.000
2	2	18	-.28456	-.05660	-.06833	191.250	103.252	80.000

Table 2. (Cont.)

HEMISPHERE	RING	RETRO	X	Y	Z	THETA	PHI	ALPHA
1	2	19	-.26804	-.11103	.06833	202.500	76.748	127.000
2	2	19	-.26804	-.11103	-.06833	202.500	103.252	174.000
1	2	20	-.24124	-.16119	.06833	213.750	76.748	101.000
2	2	20	-.24124	-.16119	-.06833	213.750	103.252	148.000
1	2	21	-.20515	-.20515	.06833	225.000	76.748	75.000
2	2	21	-.20515	-.20515	-.06833	225.000	103.252	122.000
1	2	22	-.16119	-.24124	.06833	236.250	76.748	169.000
2	2	22	-.16119	-.24124	-.06833	236.250	103.252	96.000
1	2	23	-.11103	-.26804	.06833	247.500	76.748	143.000
2	2	23	-.11103	-.26804	-.06833	247.500	103.252	70.000
1	2	24	-.05660	-.28456	.06833	258.750	76.748	117.000
2	2	24	-.05660	-.28456	-.06833	258.750	103.252	164.000
1	2	25	0.00000	-.29013	.06833	270.000	76.748	91.000
2	2	25	0.00000	-.29013	-.06833	270.000	103.252	138.000
1	2	26	.05660	-.28456	.06833	281.250	76.748	65.000
2	2	26	.05660	-.28456	-.06833	281.250	103.252	112.000
1	2	27	.11103	-.26804	.06833	292.500	76.748	159.000
2	2	27	.11103	-.26804	-.06833	292.500	103.252	86.000
1	2	28	.16119	-.24124	.06833	303.750	76.748	133.000
2	2	28	.16119	-.24124	-.06833	303.750	103.252	180.000
1	2	29	.20515	-.20515	.06833	315.000	76.748	107.000
2	2	29	.20515	-.20515	-.06833	315.000	103.252	154.000
1	2	30	.24124	-.16119	.06833	326.250	76.748	81.000
2	2	30	.24124	-.16119	-.06833	326.250	103.252	128.000
1	2	31	.26804	-.11103	.06833	337.500	76.748	175.000
2	2	31	.26804	-.11103	-.06833	337.500	103.252	102.000
1	2	32	.28456	-.05660	.06833	348.750	76.748	149.000
2	2	32	.28456	-.05660	-.06833	348.750	103.252	76.000
1	3	1	.27300	.02776	.11638	5.806	67.018	123.000
1	3	2	.26182	.08215	.11638	17.420	67.018	97.000
2	3	2	.26182	.08215	-.11638	17.420	112.982	144.000
1	3	3	.23992	.13317	.11638	29.032	67.018	71.000
2	3	3	.23992	.13317	-.11638	29.032	112.982	118.000
1	3	4	.20821	.17874	.11638	40.645	67.018	165.000
2	3	4	.20821	.17874	-.11638	40.645	112.982	92.000
1	3	5	.16797	.21699	.11638	52.258	67.018	139.000
2	3	5	.16797	.21699	-.11638	52.258	112.982	66.000
1	3	6	.12085	.24636	.11638	63.871	67.018	113.000
2	3	6	.12085	.24636	-.11638	63.871	112.982	160.000
1	3	7	.06878	.26565	.11638	75.484	67.018	87.000
2	3	7	.06878	.26565	-.11638	75.484	112.982	134.000
1	3	8	.01390	.27405	.11638	87.097	67.018	61.000
2	3	8	.01390	.27405	-.11638	87.097	112.982	108.000
1	3	9	-.04155	.27124	.11638	98.710	67.018	155.000
2	3	9	-.04155	.27124	-.11638	98.710	112.982	82.000
1	3	10	-.09530	.25732	.11638	110.322	67.018	129.000
2	3	10	-.09530	.25732	-.11638	110.322	112.982	176.000
1	3	11	-.14515	.23287	.11638	121.936	67.018	103.000
1	3	12	-.18905	.19889	.11638	133.548	67.018	77.000
2	3	12	-.18905	.19889	-.11638	133.548	112.982	124.000

Table 2. (Cont.)

HEMISPHERE	RING	RETRO	X	Y	Z	THETA	PHI	ALPHA
1	3	13	-.22522	.15676	.11638	145.161	67.018	171.000
2	3	13	-.22522	.15676	-.11638	145.161	112.982	98.000
1	3	14	-.25217	.10822	.11638	156.774	67.018	145.000
2	3	14	-.25217	.10822	-.11638	156.774	112.982	72.000
1	3	15	-.26879	.05524	.11638	168.387	67.018	119.000
2	3	15	-.26879	.05524	-.11638	168.387	112.982	166.000
1	3	16	-.27441	0.00000	.11638	180.000	67.018	93.000
2	3	16	-.27441	0.00000	-.11638	180.000	112.982	140.000
1	3	17	-.26879	-.05524	.11638	191.613	67.018	67.000
2	3	17	-.26879	-.05524	-.11638	191.613	112.982	114.000
1	3	18	-.25217	-.10822	.11638	203.226	67.018	161.000
2	3	18	-.25217	-.10822	-.11638	203.226	112.982	88.000
1	3	19	-.22522	-.15676	.11638	214.839	67.018	135.000
2	3	19	-.22522	-.15676	-.11638	214.839	112.982	62.000
1	3	20	-.18905	-.19889	.11638	226.452	67.018	109.000
2	3	20	-.18905	-.19889	-.11638	226.452	112.982	156.000
1	3	21	-.14515	-.23287	.11638	238.065	67.018	83.000
1	3	22	-.09530	-.25732	.11638	249.677	67.018	177.000
2	3	22	-.09530	-.25732	-.11638	249.677	112.982	104.000
1	3	23	-.04155	-.27124	.11638	261.291	67.018	151.000
2	3	23	-.04155	-.27124	-.11638	261.291	112.982	78.000
1	3	24	.01390	-.27405	.11638	272.903	67.018	125.000
2	3	24	.01390	-.27405	-.11638	272.903	112.982	172.000
1	3	25	.06878	-.26565	.11638	284.516	67.018	99.000
2	3	25	.06878	-.26565	-.11638	284.516	112.982	146.000
1	3	26	.12085	-.24636	.11638	296.129	67.018	73.000
2	3	26	.12085	-.24636	-.11638	296.129	112.982	120.000
1	3	27	.16797	-.21609	.11638	307.742	67.018	167.000
2	3	27	.16797	-.21609	-.11638	307.742	112.982	94.000
1	3	28	.20821	-.17874	.11638	319.355	67.018	141.000
2	3	28	.20821	-.17874	-.11638	319.355	112.982	68.000
1	3	29	.23992	-.13317	.11638	330.968	67.018	115.000
2	3	29	.23992	-.13317	-.11638	330.968	112.982	162.000
1	3	30	.26182	-.08215	.11638	342.581	67.018	89.000
2	3	30	.26182	-.08215	-.11638	342.581	112.982	136.000
1	3	31	.27300	-.02776	.11638	354.193	67.018	63.000
2	3	31	.27300	-.02776	-.11638	354.193	112.982	110.000
1	4	1	.25487	0.00000	.15455	0.000	58.769	157.000
2	4	1	.25487	0.00000	-.15455	0.000	121.231	84.000
1	4	2	.24965	.05131	.15455	11.613	58.769	131.000
2	4	2	.24965	.05131	-.15455	11.613	121.231	178.000
1	4	3	.23422	.10051	.15455	23.226	58.769	105.000
2	4	3	.23422	.10051	-.15455	23.226	121.231	152.000
1	4	4	.20919	.14560	.15455	34.839	58.769	79.000
2	4	4	.20919	.14560	-.15455	34.839	121.231	126.000
1	4	5	.17560	.18473	.15455	46.451	58.769	173.000
2	4	5	.17560	.18473	-.15455	46.451	121.231	100.000
1	4	6	.13482	.21630	.15455	58.065	58.769	147.000
2	4	6	.13482	.21630	-.15455	58.065	121.231	74.000
1	4	7	.08852	.23901	.15455	69.677	58.769	121.000

Table 2. (Cont.)

HEMISPHERE	RING	RETRO	X	Y	Z	THETA	PHI	ALPHA
2	4	7	.08852	.23901	-.15455	69.677	121.231	168.000
1	4	8	.03860	.25194	.15455	81.290	58.769	95.000
2	4	8	.03860	.25194	-.15455	81.290	121.231	142.000
1	4	9	-.01291	.25455	.15455	92.903	58.769	69.000
2	4	9	-.01291	.25455	-.15455	92.903	121.231	116.000
1	4	10	-.06389	.24674	.15455	104.516	58.769	163.000
2	4	10	-.06389	.24674	-.15455	104.516	121.231	90.000
1	4	11	-.11224	.22883	.15455	116.129	58.769	137.000
2	4	11	-.11224	.22883	-.15455	116.129	121.231	64.000
1	4	12	-.15601	.20154	.15455	127.742	58.769	111.000
2	4	12	-.15601	.20154	-.15455	127.742	121.231	158.000
1	4	13	-.19339	.16601	.15455	139.355	58.769	85.000
2	4	13	-.19339	.16601	-.15455	139.355	121.231	132.000
1	4	14	-.22285	.12369	.15455	150.968	58.769	179.000
2	4	14	-.22285	.12369	-.15455	150.968	121.231	106.000
1	4	15	-.24318	.07630	.15455	162.581	58.769	153.000
2	4	15	-.24318	.07630	-.15455	162.581	121.231	80.000
1	4	16	-.25357	.02578	.15455	174.193	58.769	127.000
2	4	16	-.25357	.02578	-.15455	174.193	121.231	174.000
1	4	17	-.25357	-.02578	.15455	185.806	58.769	101.000
2	4	17	-.25357	-.02578	-.15455	185.806	121.231	148.000
1	4	18	-.24318	-.07630	.15455	197.419	58.769	75.000
2	4	18	-.24318	-.07630	-.15455	197.419	121.231	122.000
1	4	19	-.22285	-.12369	.15455	209.032	58.769	169.000
2	4	19	-.22285	-.12369	-.15455	209.032	121.231	96.000
1	4	20	-.19339	-.16601	.15455	220.645	58.769	143.000
2	4	20	-.19339	-.16601	-.15455	220.645	121.231	70.000
1	4	21	-.15601	-.20154	.15455	232.258	58.769	117.000
2	4	21	-.15601	-.20154	-.15455	232.258	121.231	164.000
1	4	22	-.11224	-.22883	.15455	243.871	58.769	91.000
2	4	22	-.11224	-.22883	-.15455	243.871	121.231	138.000
1	4	23	-.06389	-.24674	.15455	255.484	58.769	65.000
2	4	23	-.06389	-.24674	-.15455	255.484	121.231	112.000
1	4	24	-.01291	-.25455	.15455	267.097	58.769	159.000
2	4	24	-.01291	-.25455	-.15455	267.097	121.231	86.000
1	4	25	.03859	-.25194	.15455	278.710	58.769	133.000
2	4	25	.03859	-.25194	-.15455	278.710	121.231	180.000
1	4	26	.08852	-.23901	.15455	290.322	58.769	107.000
2	4	26	.08852	-.23901	-.15455	290.322	121.231	154.000
1	4	27	.13482	-.21630	.15455	301.936	58.769	81.000
2	4	27	.13482	-.21630	-.15455	301.936	121.231	128.000
1	4	28	.17560	-.18473	.15455	313.548	58.769	175.000
2	4	28	.17560	-.18473	-.15455	313.548	121.231	102.000
1	4	29	.20919	-.14560	.15455	325.161	58.769	149.000
2	4	29	.20919	-.14560	-.15455	325.161	121.231	76.000
1	4	30	.23422	-.10051	.15455	336.774	58.769	123.000
2	4	30	.23422	-.10051	-.15455	336.774	121.231	170.000
1	4	31	.24965	-.05131	.15455	348.387	58.769	97.000
2	4	31	.24965	-.05131	-.15455	348.387	121.231	144.000
1	5	1	.22509	0.00000	.19539	0.000	49.039	71.000

Table 2. (Cont.)

HEMISPHERE	RING	RETRO	X	Y	Z	THETA	PHI	ALPHA
2	5	1	.22509	0.00000	-.19539	0.000	130.961	118.000
1	5	2	.21902	.05190	.19539	13.333	49.039	165.000
2	5	2	.21902	.05190	-.19539	13.333	130.961	92.000
1	5	3	.20115	.10102	.19539	26.667	49.039	139.000
2	5	3	.20115	.10102	-.19539	26.667	130.961	66.000
1	5	4	.17242	.14468	.19539	40.000	49.039	113.000
2	5	4	.17242	.14468	-.19539	40.000	130.961	160.000
1	5	5	.13441	.18055	.19539	53.333	49.039	87.000
2	5	5	.13441	.18055	-.19539	53.333	130.961	134.000
1	5	6	.08915	.20668	.19539	66.667	49.039	61.000
2	5	6	.08915	.20668	-.19539	66.667	130.961	108.000
1	5	7	.03909	.22166	.19539	80.000	49.039	155.000
2	5	7	.03909	.22166	-.19539	80.000	130.961	82.000
1	5	8	-.01309	.22470	.19539	93.333	49.039	129.000
2	5	8	-.01309	.22470	-.19539	93.333	130.961	176.000
1	5	9	-.06455	.21563	.19539	106.666	49.039	103.000
2	5	9	-.06455	.21563	-.19539	106.666	130.961	150.000
1	5	10	-.11254	.19493	.19539	120.000	49.039	77.000
2	5	10	-.11254	.19493	-.19539	120.000	130.961	124.000
1	5	11	-.15446	.16372	.19539	133.333	49.039	171.000
2	5	11	-.15446	.16372	-.19539	133.333	130.961	98.000
1	5	12	-.18805	.12369	.19539	146.666	49.039	145.000
2	5	12	-.18805	.12369	-.19539	146.666	130.961	72.000
1	5	13	-.21151	.07698	.19539	160.000	49.039	119.000
2	5	13	-.21151	.07698	-.19539	160.000	130.961	166.000
1	5	14	-.22356	.02613	.19539	173.333	49.039	93.000
2	5	14	-.22356	.02613	-.19539	173.333	130.961	140.000
1	5	15	-.22356	-.02613	.19539	186.666	49.039	67.000
2	5	15	-.22356	-.02613	-.19539	186.666	130.961	114.000
1	5	16	-.21151	-.07698	.19539	200.000	49.039	161.000
2	5	16	-.21151	-.07698	-.19539	200.000	130.961	88.000
1	5	17	-.18806	-.12369	.19539	213.333	49.039	135.000
2	5	17	-.18806	-.12369	-.19539	213.333	130.961	62.000
1	5	18	-.15447	-.16372	.19539	226.666	49.039	109.000
2	5	18	-.15447	-.16372	-.19539	226.666	130.961	156.000
1	5	19	-.11254	-.19493	.19539	239.999	49.039	83.000
2	5	19	-.11254	-.19493	-.19539	239.999	130.961	130.000
1	5	20	-.06456	-.21563	.19539	253.333	49.039	177.000
2	5	20	-.06456	-.21563	-.19539	253.333	130.961	104.000
1	5	21	-.01310	-.22470	.19539	266.666	49.039	151.000
2	5	21	-.01310	-.22470	-.19539	266.666	130.961	78.000
1	5	22	.03909	-.22166	.19539	279.999	49.039	125.000
2	5	22	.03909	-.22166	-.19539	279.999	130.961	172.000
1	5	23	.08915	-.20668	.19539	293.333	49.039	99.000
2	5	23	.08915	-.20668	-.19539	293.333	130.961	146.000
1	5	24	.13441	-.18055	.19539	306.666	49.039	73.000
2	5	24	.13441	-.18055	-.19539	306.666	130.961	120.000
1	5	25	.17242	-.14468	.19539	319.999	49.039	167.000
2	5	25	.17242	-.14468	-.19539	319.999	130.961	94.000
1	5	26	.20115	-.10103	.19539	333.333	49.039	141.000

Table 2. (Cont.)

HEMISPHERE	RING	RETRO	X	Y	Z	THETA	PHI	ALPHA
2	5	26	.20115	-.10103	-.19539	333.333	130.961	68.000
1	5	27	.21902	-.05191	.19539	346.666	49.039	115.000
2	5	27	.21902	-.05191	-.19539	346.666	130.961	162.000
1	6	1	.18883	0.00000	.23063	0.000	39.309	89.000
2	6	1	.18883	0.00000	-.23063	0.000	140.691	136.000
1	6	2	.18182	.05095	.23063	15.652	39.309	63.000
2	6	2	.18182	.05095	-.23063	15.652	140.691	110.000
1	6	3	.16133	.09811	.23063	31.304	39.309	157.000
2	6	3	.16133	.09811	-.23063	31.304	140.691	84.000
1	6	4	.12888	.13801	.23063	46.957	39.309	131.000
2	6	4	.12888	.13801	-.23063	46.957	140.691	178.000
1	6	5	.08688	.16765	.23063	62.609	39.309	105.000
2	6	5	.08688	.16765	-.23063	62.609	140.691	152.000
1	6	6	.03842	.18488	.23063	78.261	39.309	79.000
2	6	6	.03842	.18488	-.23063	78.261	140.691	126.000
1	6	7	-.01289	.18839	.23063	93.913	39.309	173.000
2	6	7	-.01289	.18839	-.23063	93.913	140.691	100.000
1	6	8	-.06323	.17793	.23063	109.566	39.309	147.000
2	6	8	-.06323	.17793	-.23063	109.566	140.691	74.000
1	6	9	-.10889	.15427	.23063	125.218	39.309	121.000
2	6	9	-.10889	.15427	-.23063	125.218	140.691	168.000
1	6	10	-.14647	.11917	.23063	140.870	39.309	95.000
2	6	10	-.14647	.11917	-.23063	140.870	140.691	142.000
1	6	11	-.17320	.07523	.23063	156.522	39.309	69.000
2	6	11	-.17320	.07523	-.23063	156.522	140.691	116.000
1	6	12	-.18707	.02571	.23063	172.174	39.309	163.000
2	6	12	-.18707	.02571	-.23063	172.174	140.691	90.000
1	6	13	-.18707	-.02571	.23063	187.826	39.309	137.000
2	6	13	-.18707	-.02571	-.23063	187.826	140.691	64.000
1	6	14	-.17320	-.07523	.23063	203.479	39.309	111.000
2	6	14	-.17320	-.07523	-.23063	203.479	140.691	158.000
1	6	15	-.14647	-.11917	.23063	219.131	39.309	85.000
2	6	15	-.14647	-.11917	-.23063	219.131	140.691	132.000
1	6	16	-.10889	-.15427	.23063	234.783	39.309	179.000
2	6	16	-.10889	-.15427	-.23063	234.783	140.691	106.000
1	6	17	-.06323	-.17793	.23063	250.435	39.309	153.000
2	6	17	-.06323	-.17793	-.23063	250.435	140.691	80.000
1	6	18	-.01289	-.18839	.23063	266.087	39.309	127.000
2	6	18	-.01289	-.18839	-.23063	266.087	140.691	174.000
1	6	19	.03842	-.18488	.23063	281.739	39.309	101.000
2	6	19	.03842	-.18488	-.23063	281.739	140.691	148.000
1	6	20	.08688	-.16765	.23063	297.392	39.309	75.000
2	6	20	.08688	-.16765	-.23063	297.392	140.691	122.000
1	6	21	.12888	-.13800	.23063	313.044	39.309	169.000
2	6	21	.12888	-.13800	-.23063	313.044	140.691	96.000
1	6	22	.16133	-.09811	.23063	328.696	39.309	143.000
2	6	22	.16133	-.09811	-.23063	328.696	140.691	70.000
1	6	23	.18182	-.05094	.23063	344.348	39.309	117.000
2	6	23	.18182	-.05094	-.23063	344.348	140.691	164.000
1	7	1	.14713	0.00000	.25922	0.000	29.579	91.000

Table 2. (Cont.)

HEMISPHERE	RING	RETRO	X	Y	Z	THETA	PHI	ALPHA
2	7	1	.14713	0.00000	-.25922	0.000	150.421	138.000
1	7	2	.13825	.05032	.25922	20.000	29.579	65.000
2	7	2	.13825	.05032	-.25922	20.000	150.421	112.000
1	7	3	.11271	.09458	.25922	40.000	29.579	159.000
2	7	3	.11271	.09458	-.25922	40.000	150.421	86.000
1	7	4	.07356	.12741	.25922	60.000	29.579	133.000
2	7	4	.07356	.12741	-.25922	60.000	150.421	180.000
1	7	5	.02554	.14489	.25922	80.000	29.579	107.000
2	7	5	.02554	.14489	-.25922	80.000	150.421	154.000
1	7	6	-.02554	.14489	.25922	100.000	29.579	81.000
2	7	6	-.02554	.14489	-.25922	100.000	150.421	128.000
1	7	7	-.07356	.12741	.25922	120.000	29.579	175.000
2	7	7	-.07356	.12741	-.25922	120.000	150.421	102.000
1	7	8	-.11271	.09458	.25922	140.000	29.579	149.000
2	7	8	-.11271	.09458	-.25922	140.000	150.421	76.000
1	7	9	-.13825	.05032	.25922	160.000	29.579	123.000
2	7	9	-.13825	.05032	-.25922	160.000	150.421	170.000
1	7	10	-.14713	0.00000	.25922	180.000	29.579	97.000
2	7	10	-.14713	0.00000	-.25922	180.000	150.421	144.000
1	7	11	-.13825	-.05032	.25922	200.000	29.579	71.000
2	7	11	-.13825	-.05032	-.25922	200.000	150.421	118.000
1	7	12	-.11271	-.09458	.25922	220.000	29.579	165.000
2	7	12	-.11271	-.09458	-.25922	220.000	150.421	92.000
1	7	13	-.07356	-.12741	.25922	240.000	29.579	139.000
2	7	13	-.07356	-.12741	-.25922	240.000	150.421	66.000
1	7	14	-.02554	-.14489	.25922	260.000	29.579	113.000
2	7	14	-.02554	-.14489	-.25922	260.000	150.421	160.000
1	7	15	.02554	-.14489	.25922	280.000	29.579	87.000
2	7	15	.02554	-.14489	-.25922	280.000	150.421	134.000
1	7	16	.07356	-.12741	.25922	300.000	29.579	61.000
2	7	16	.07356	-.12741	-.25922	300.000	150.421	108.000
1	7	17	.11271	-.09458	.25922	320.000	29.579	155.000
2	7	17	.11271	-.09458	-.25922	320.000	150.421	82.000
1	7	18	.13825	-.05032	.25922	340.000	29.579	129.000
2	7	18	.13825	-.05032	-.25922	340.000	150.421	176.000
1	8	1	.10120	0.00000	.28036	0.000	19.848	103.000
2	8	1	.10120	0.00000	-.28036	0.000	160.151	150.000
1	8	2	.08764	.05060	.28036	30.000	19.848	77.000
2	8	2	.08764	.05060	-.28036	30.000	160.151	124.000
1	8	3	.05060	.08764	.28036	60.000	19.848	171.000
2	8	3	.05060	.08764	-.28036	60.000	160.151	98.000
1	8	4	0.00000	.10120	.28036	90.000	19.848	145.000
2	8	4	0.00000	.10120	-.28036	90.000	160.151	72.000
1	8	5	-.05060	.08764	.28036	120.000	19.848	119.000
2	8	5	-.05060	.08764	-.28036	120.000	160.151	166.000
1	8	6	-.08764	.05060	.28036	150.000	19.848	93.000
2	8	6	-.08764	.05060	-.28036	150.000	160.151	140.000
1	8	7	-.10120	0.00000	.28036	180.000	19.848	67.000
2	8	7	-.10120	0.00000	-.28036	180.000	160.151	114.000
1	8	8	-.08764	-.05060	.28036	210.000	19.848	161.000

Table 2. (Cont.)

HEMISPHERE	RING	RETRO	X	Y	Z	THETA	PHI	ALPHA
2	8	8	-.08764	-.05060	-.28036	210.000	160.151	88.000
1	8	9	-.05060	-.08764	.28036	240.000	19.848	135.000
2	8	9	-.05060	-.08764	-.28036	240.000	160.151	62.000
1	8	10	0.00000	-.10120	.28036	270.000	19.848	109.000
2	8	10	0.00000	-.10120	-.28036	270.000	160.151	156.000
1	8	11	.05060	-.08764	.28036	300.000	19.848	83.000
2	8	11	.05060	-.08764	-.28036	300.000	160.151	130.000
1	8	12	.08764	-.05060	.28036	330.000	19.848	177.000
2	8	12	.08764	-.05060	-.28036	330.000	160.151	104.000
1	9	1	.05236	0.00000	.29343	0.000	10.118	151.000
2	9	1	.05236	0.00000	-.29343	0.000	169.881	78.000
1	9	2	.02618	.04535	.29343	60.000	10.118	125.000
2	9	2	.02618	.04535	-.29343	60.000	169.881	172.000
1	9	3	-.02618	.04535	.29343	120.000	10.118	99.000
2	9	3	-.02618	.04535	-.29343	120.000	169.881	146.000
1	9	4	-.05236	0.00000	.29343	180.000	10.118	73.000
2	9	4	-.05236	0.00000	-.29343	180.000	169.881	120.000
1	9	5	-.02618	-.04535	.29343	240.000	10.118	167.000
2	9	5	-.02618	-.04535	-.29343	240.000	169.881	94.000
1	9	6	.02618	-.04535	.29343	300.000	10.118	141.000
2	9	6	.02618	-.04535	-.29343	300.000	169.881	68.000
2	10	1	0.00000	0.00000	-.29807	0.000	180.000	162.000



#### 4. METHOD OF COMPUTING THE TRANSFER FUNCTION

In computing the reflectivity of the Lageos retroreflector array, the cube corners have been modeled as isothermal, geometrically perfect reflectors (except for the dihedral-angle offset) with no reflecting coatings on the back faces. The change in phase and amplitude on reflection from the back faces is computed for either ordinary reflection or total internal reflection, depending on the incidence angle at each face. The changes on transmission through the front face are also computed.

Computation of the range correction includes a correction for the optical path length of the ray within the cube corner. The range correction is the difference between the centroid of the actual return signal and the centroid of the return signal that would be received from a point reflector at the center of gravity of the satellite. The correction listed is the one-way correction.

The reflectivities and range corrections presented in all the tables are for the incoherent case; that is, the intensities of the reflections are added without taking into account coherent interference among the reflected signals from the individual cube corners.

The variation of the range correction due to optical coherence has been derived by statistical analysis of a set of coherent returns, which was constructed by assigning random phases to the reflection from each cube corner by means of a pseudo random-number generator. Since the computer time required to compute a coherent return increases as the square of the number of cube corners, the calculations were done with a reduced array obtained by omitting about a third of the cube corners. The total contribution of the omitted cubes is about 0.2% of the return energy because they reflect by ordinary reflection rather than total internal reflection and are at large incidence angles, and thus have small effective apertures. Reduced arrays have also been used in diffraction calculations. Except when the calculations have been performed for specific values of velocity aberration, the curves in Figure 6 (Section 6), giving the average reflectivity of the cube corners between velocity aberrations of 32 and 41  $\mu\text{rad}$ , have been used to compute the strength of the reflection from each cube corner. The curve for 5320  $\text{\AA}$  is used unless runs have been made for both wavelengths.



## 5. SIGNAL-STRENGTH COMPUTATION

The data contained in the tables presented later can be used to estimate signal strengths for laser ranging by use of the following equation:

$$N = \frac{E}{h\nu} G_T A_S G_S A_R \frac{T^2}{R^4} \eta \quad ,$$

where

- N = number of photoelectrons,
- E = transmitted energy,
- h = Planck's constant,
- $\nu$  = frequency of laser light,
- $G_T$  = "gain" of transmitter,
- $A_S$  = active reflecting area of satellite,
- $G_S$  = "gain" of satellite array,
- $A_R$  = area of receiving telescope,
- T = atmospheric-transmission factor,
- R = range from station to satellite,
- $\eta$  = constant, which includes the quantum efficiency of the photomultiplier and the optical transmission factors of the transmitter, the satellite, and the receiver.

If the transmitted beam is a uniform spot of solid angle  $\Omega_T$ , the "gain" function of the transmitter is

$$G_T = \frac{1}{\Omega_T} \quad .$$

The gain functions in this equation do not contain the factor of  $4\pi$  used in the standard definition of gain. Those given in later sections can be converted to the standard definition by multiplying by  $4\pi$ . The signal-strength equation above can be converted to the standard definition of gain by adding the factor  $1/(4\pi)^2$ .



## 6. OPTICAL CUBE-CORNER REFLECTIVITY

The reflectivity of the Lageos optical cube corners is given below as a function of incidence angle. The angle  $\phi$  is measured from the normal to the front face, and the angle  $\theta$  is the angle to the projection of the incident beam onto the front face; both these angles are shown in Figure 4. In each graph of Figure 6, the upper curve is the total reflectivity and the lower curve is the average reflectivity in the annulus between 32 and 41  $\mu$ rad from the center of the reflected beam in the far field, which is approximately that region of the far field observed during laser ranging because of velocity aberration. All curves are normalized to unity at normal incidence. The total reflectivity at normal incidence is proportional to the area of the front face, which is 11.4009  $\text{cm}^2$  for a circular cube corner of radius 1.905 cm. For a perfect reflector of the same aperture, the gain at the center of the far-field pattern would be  $G = A/\lambda^2$ , where  $A$  is the area,  $\lambda$  the wavelength of the incident beam, and  $G$  the gain as defined in Section 5. (The standard expression for gain in this case is  $4\pi A/\lambda^2$ .) The program used to compute the reflectivity of the Lageos cube corners is normalized such that  $A/\lambda^2$  is unity. The average intensity computed by this program between 32 and 41  $\mu$ rad is 0.0262 at 5320  $\text{\AA}$  and 0.0291 at 6943  $\text{\AA}$ . To convert the reflectivities in the annulus to gain, values from Figure 6 are multiplied by  $G_{5320}$  or  $G_{6943}$ , where

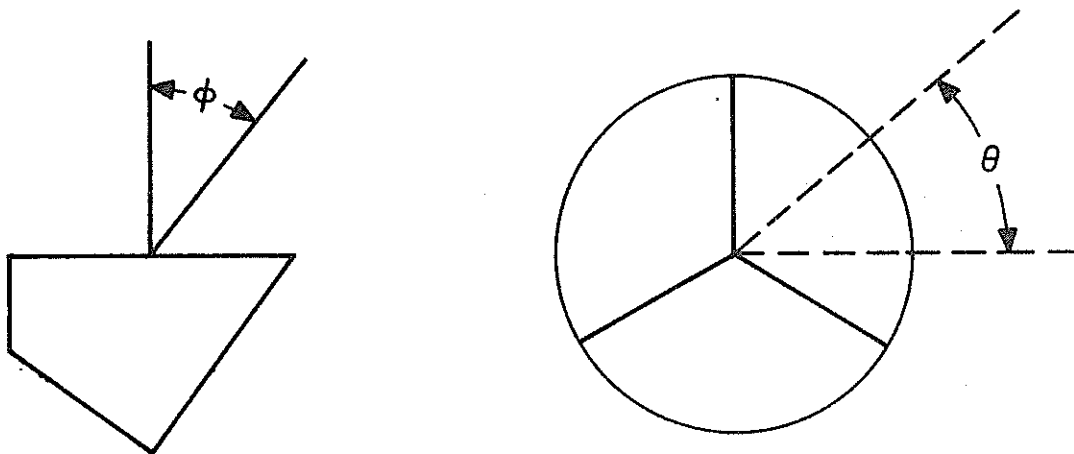


Figure 4. Direction of incident beam.

$$G_{5320} = 0.0262 (A/\lambda_{5320}^2) = 1.0554 \times 10^8$$

and

$$G_{6943} = 0.0291 (A/\lambda_{6943}^2) = 6.882 \times 10^7 .$$

The reflectivity of a cube corner depends on the polarization of the input beam. The reflection losses on entering and leaving the front face are different for the components of the radiation parallel and perpendicular to the plane of incidence. When the light is reflected from each of the back faces there is a change in phase for the parallel and perpendicular components of the radiation if the incidence angle is large enough to give total internal reflection, and a change in amplitude for each component if the incidence angle is less than the critical angle. It is possible for only one of the three back faces to lose total internal reflection at a time. The total reflectivity curve was generated by computing the active reflecting area and then correcting for all reflection losses assuming that the light is unpolarized at each encounter with a surface. The reflectivity in the annulus was computed for a circularly polarized input beam and all reflections and transmissions are treated rigorously. In general, the reflectivity in the annulus falls off more rapidly than the total reflectivity because diffraction spreads the beam more as the effective reflecting area decreases.

Since the front face of the cube corner is circular, the active reflecting area is independent of the azimuth angle  $\theta$ . However, the reflectivity depends on  $\theta$  primarily because of loss of total reflection, and to a lesser extent because of polarization effects. The reflectivity repeats exactly every  $120^\circ$  in  $\theta$  starting at any of the three real back edges, which are at  $\theta = -30^\circ, 90^\circ,$  and  $210^\circ$ . The cutoff angle for total internal reflection is symmetrical about the centers of each  $120^\circ$  interval, which are at  $\theta = +30^\circ, 120^\circ,$  and  $240^\circ$ . The cutoff angle  $\phi_c$  for total internal reflection is given from  $\theta = -30^\circ$  to  $+90^\circ$  in Table 3, for  $n = 1.461$  and  $1.455$ , the refractive indices at  $5320$  and  $6943 \text{ \AA}$ , respectively. The cube corner never loses total internal reflection at  $\theta = 30^\circ$ . The cutoff angle listed for this azimuth is the angle where the active reflecting area goes to zero. This angle is computed from the formula

$$\phi_c(\theta = 30^\circ) = \sin^{-1} (n \sin \phi'_c) ,$$

where

$$\phi'_c = \tan^{-1} \frac{r}{\ell} ,$$

$r$  = the radius of the front face (1.905 cm),

$\ell$  = the length of the cube corner (2.7838 cm),

$n$  = the index of refraction.

When the incidence angle is past the limit for total reflection, the cube corner reflects by ordinary reflection at one of the back faces. Figure 6-15 shows a detailed plot of the total reflectivity as a function of  $\phi$  in the vicinity of the cutoff angle  $\phi_c$ , which is  $16^\circ.595$  for this case. The curve shows a discontinuity in slope at the cutoff angle, and the reflectivity decreases rapidly just past the cutoff. One degree past cutoff, the reflectivity is down to 42% of the value before cutoff, and two degrees past, it is down to 28%.

Table 3. Cutoff angle for total internal reflection.

$\theta$	$\phi_c(5320 \text{ \AA})$	$\phi_c(6943 \text{ \AA})$
-30°	16.998	16.595
-20	17.315	16.903
-10	18.340	17.899
0	20.347	19.844
+10	24.079	23.446
+20	32.215	31.204
+30	55.597	55.255
+40	32.215	31.204
+50	24.079	23.446
+60	20.347	19.844
+70	18.340	17.899
+80	17.315	16.903
+90	16.998	16.595

The reflectivities listed in Table 4 are nearly symmetric about  $\theta = 30^\circ$  because the total reflection cutoff is symmetric about this azimuth. The slight asymmetry is due to an asymmetry in the input polarization. The circular polarization vector used as input has components of equal magnitude perpendicular and parallel to the plane of incidence and a phase difference of  $90^\circ$  between the components. Figure 5 shows the input polarization vectors just before and just after  $\theta = 30^\circ$ . It is apparent that to obtain polarization symmetry about  $\theta = 30^\circ$ , the direction (or sign) of  $\vec{E}_\perp$  should be reversed when the symmetry angle is crossed. Some computer runs have been done reversing the sign, and exact symmetry is obtained. Since the polarization asymmetry is small, only the curves for  $\theta = -30^\circ$  to  $+30^\circ$  have been plotted in Figure 6.

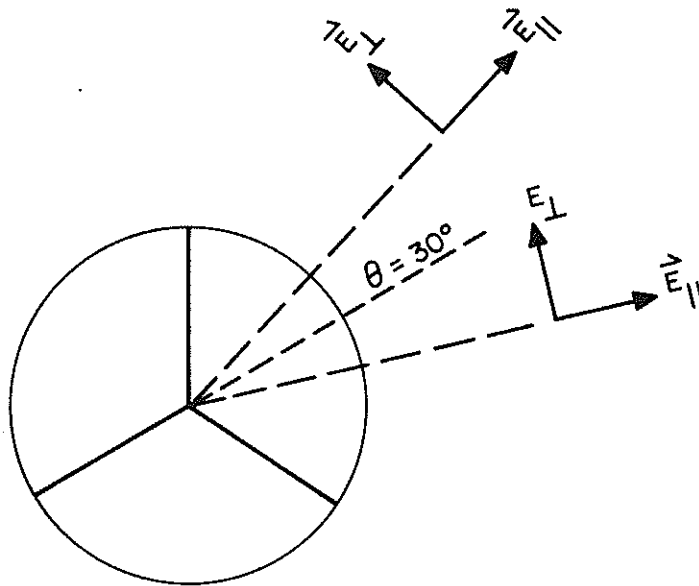


Figure 5. Asymmetry of the input polarization vector with respect to  $\theta = 30^\circ$ .



Table 4. Average reflectivity of a Lageos optical cube corner in the 32- to 41- $\mu$ rad annulus of the far-field diffraction pattern. The angles  $\theta$  and  $\phi$  are defined in Figure 4.

$\lambda = 5320 \text{ \AA}$

	-30	-20	-10	0	10	20	30	40	50	60	70	80	90	$\theta$
0	1.00000	1.00000	1.00000	1.00000	1.00000	1.00000	1.00000	1.00000	1.00000	1.00000	1.00000	1.00000	1.00000	1.00000
5	.84198	.83617	.84629	.84871	.85854	.86205	.85690	.86266	.87030	.85462	.84939	.85048	.84198	
10	.64899	.63828	.64989	.65020	.65551	.67307	.66814	.67917	.69342	.66777	.65883	.66000	.64899	
15	.49886	.47880	.47712	.46654	.46492	.48740	.48756	.50136	.52601	.51443	.50754	.51275	.49886	
20	.09065	.09184	.11770	.36279	.35001	.36616	.37029	.38399	.40637	.41819	.13598	.10329	.09065	
25	.03306	.03258	.03789	.05321	.12504	.29511	.29568	.30312	.14256	.06562	.04562	.03751	.03306	
30	.01451	.01383	.01526	.01977	.03582	.20427	.20948	.21923	.04711	.02765	.02011	.01663	.01451	
35	.00739	.00680	.00684	.00788	.01263	.04142	.12344	.05201	.02004	.01284	.00983	.00845	.00739	
40	.00411	.00382	.00380	.00415	.00601	.01564	.07214	.01929	.00858	.00617	.00506	.00453	.00411	
45	.00179	.00170	.00177	.00202	.00287	.00672	.03634	.00738	.00357	.00251	.00208	.00192	.00179	
50	.00038	.00038	.00042	.00050	.00072	.00165	.01047	.00163	.00077	.00053	.00045	.00042	.00038	
55	0.00000	0.00000	0.00000	.00004	.00004	.00008	.00053	.00008	.00004	.00004	.00004	0.00000	0.00000	
60	0.00000	0.00000	0.00000	0.00000	0.00000	0.00000	0.00000	0.00000	0.00000	0.00000	0.00000	0.00000	0.00000	

$\lambda = 6943 \text{ \AA}$

	-30	-20	-10	0	10	20	30	40	50	60	70	80	90	$\theta$
0	1.00000	1.00000	1.00000	1.00000	1.00000	1.00000	1.00000	1.00000	1.00000	1.00000	1.00000	1.00000	1.00000	1.00000
5	.86265	.84987	.84522	.85573	.86285	.87386	.87438	.87022	.86810	.86660	.87019	.87151	.86265	
10	.77398	.75196	.73903	.75055	.76309	.78050	.78933	.78051	.78768	.78141	.79153	.79065	.77398	
15	.65893	.64083	.63247	.64606	.67000	.69407	.70599	.68984	.68950	.68783	.68602	.68021	.65893	
20	.10528	.10954	.14476	.36574	.53615	.56948	.58395	.57953	.56734	.40972	.16854	.12116	.10528	
25	.03626	.03537	.04074	.06025	.14821	.39284	.41295	.42854	.18711	.08302	.05436	.04187	.03626	
30	.01738	.01599	.01640	.02058	.03732	.22720	.25083	.27610	.05792	.03382	.02454	.01994	.01738	
35	.00967	.00895	.00882	.01001	.01533	.06696	.14816	.06053	.02380	.01586	.01451	.01076	.00967	
40	.00506	.00484	.00498	.00571	.00832	.02030	.09063	.02314	.01053	.00740	.00607	.00541	.00506	
45	.00196	.00196	.00206	.00248	.00364	.00838	.04604	.00858	.00394	.00275	.00230	.00206	.00196	
50	.00045	.00045	.00048	.00058	.00089	.00203	.01314	.00196	.00089	.00065	.00051	.00045	.00045	
55	0.00000	0.00000	0.00000	.00003	.00007	.00007	.00052	.00007	.00003	.00003	.00003	.00003	0.00000	
60	0.00000	0.00000	0.00000	0.00000	0.00000	0.00000	0.00000	0.00000	0.00000	0.00000	0.00000	0.00000	0.00000	

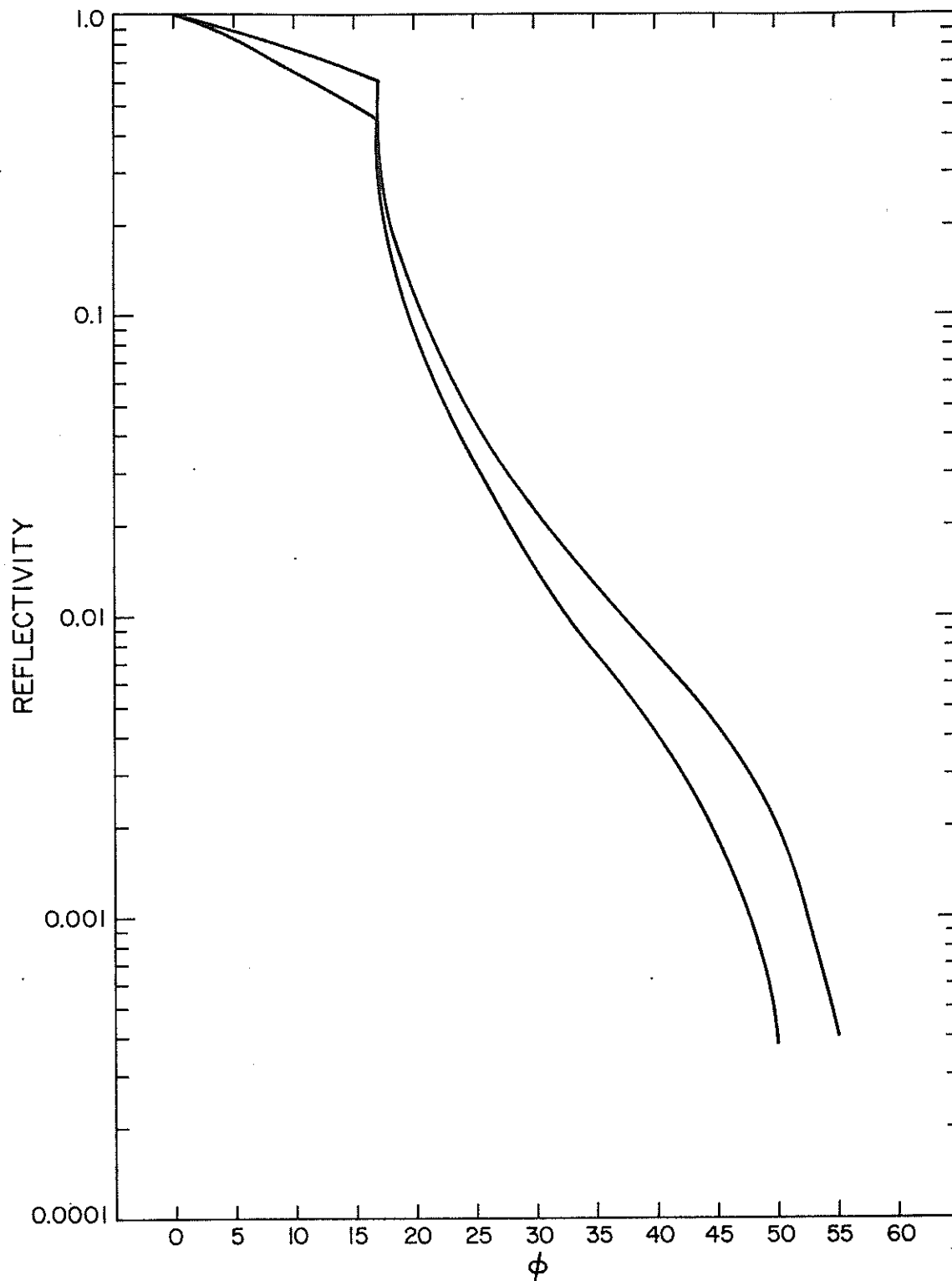


Figure 6(1-15). Total reflectivity (upper curve) and average reflectivity in the 32- to 41- $\mu$ rad annulus of the far-field pattern for a Lageos optical cube corner. The angles  $\theta$  and  $\phi$  are defined in Figure 4; the angle  $\theta$  and the wavelength  $\lambda$  are listed for each set of curves. Figure 6-1.  $\theta = -30^\circ$ ,  $\lambda = 5320 \text{ \AA}$ .

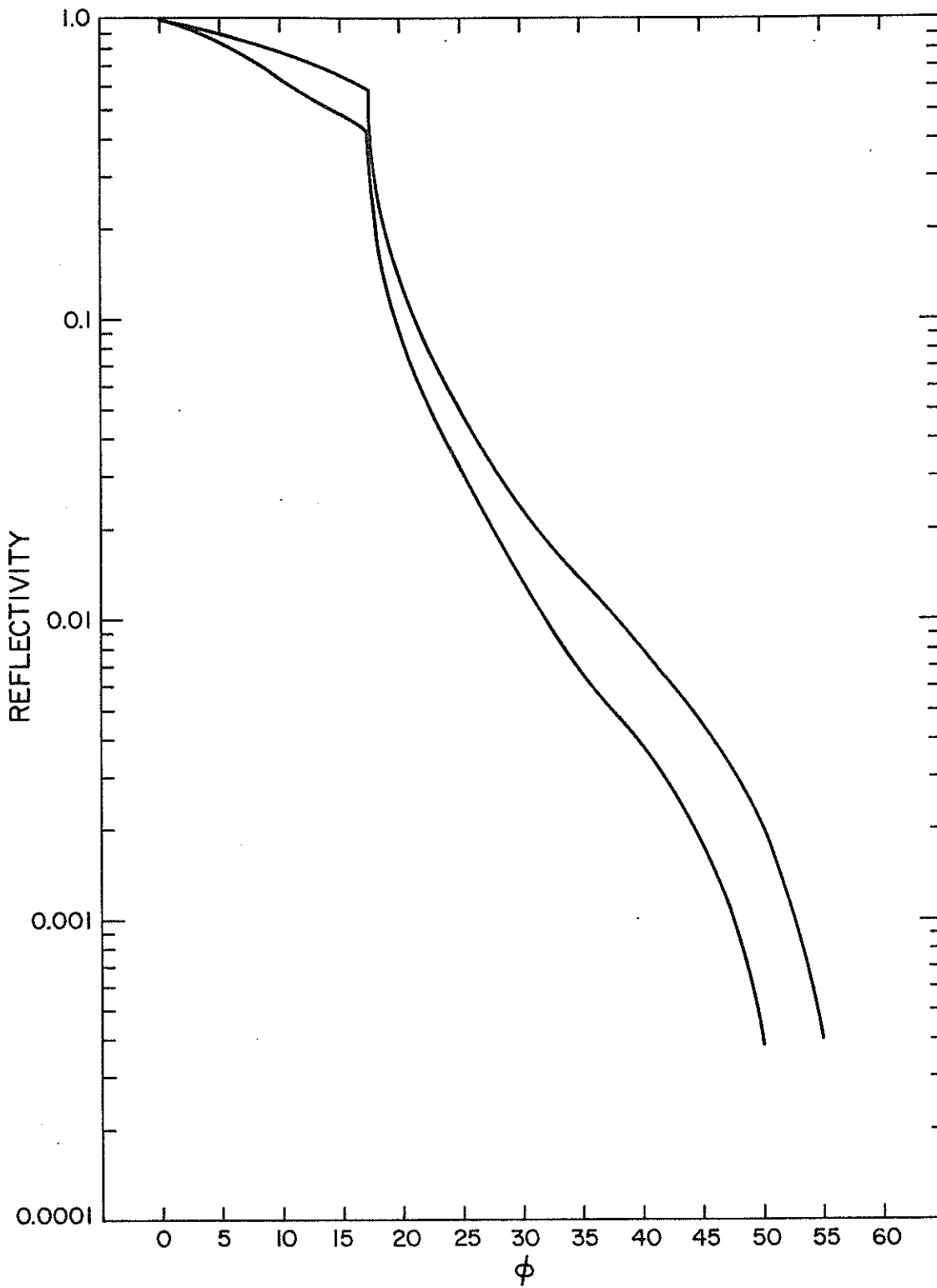


Figure 6-2.  $\theta = -20^\circ$ ,  $\lambda = 5320 \text{ \AA}$ .

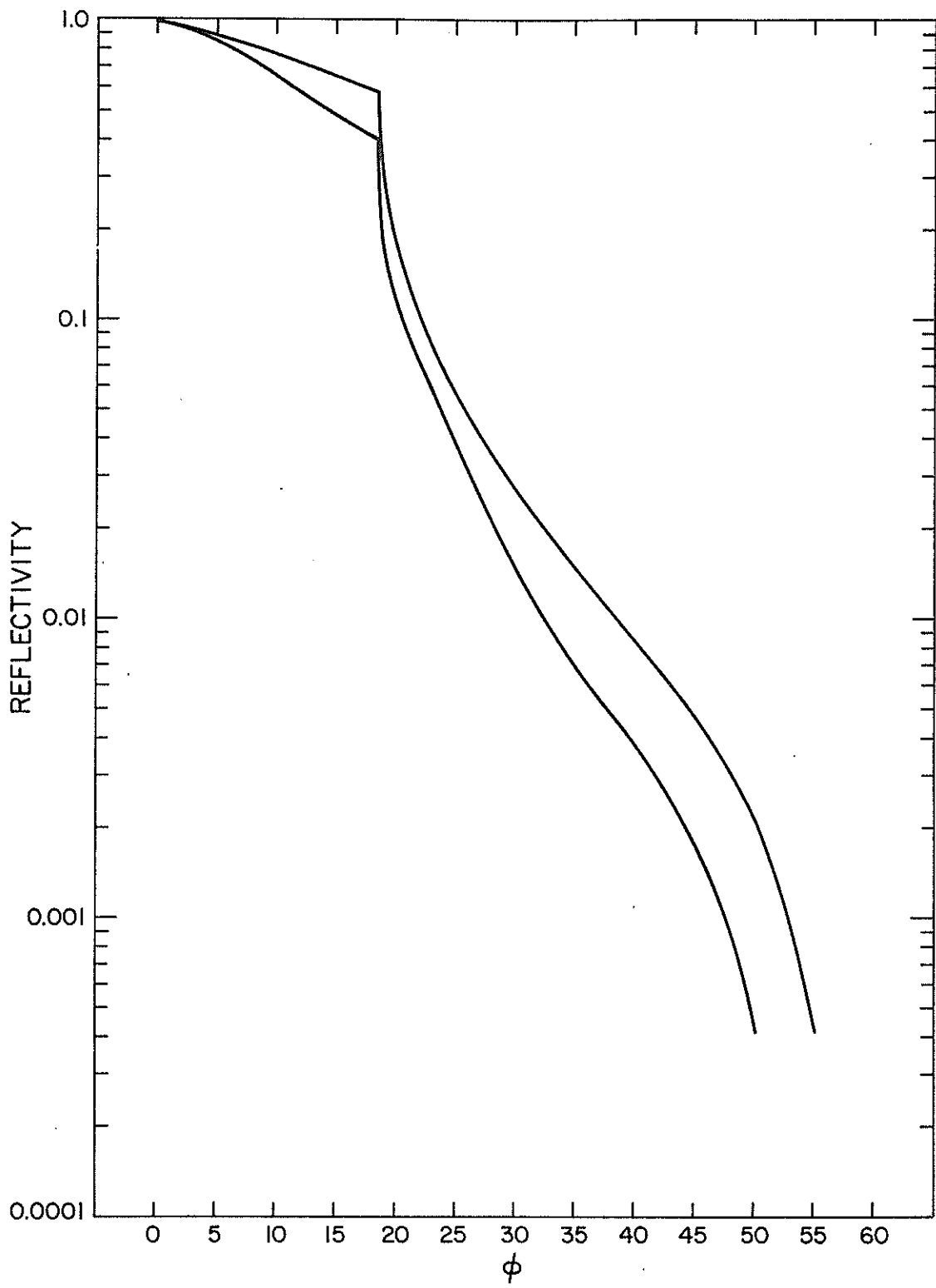


Figure 6-3.  $\theta = -10^\circ$ ,  $\lambda = 5320 \text{ \AA}$ .

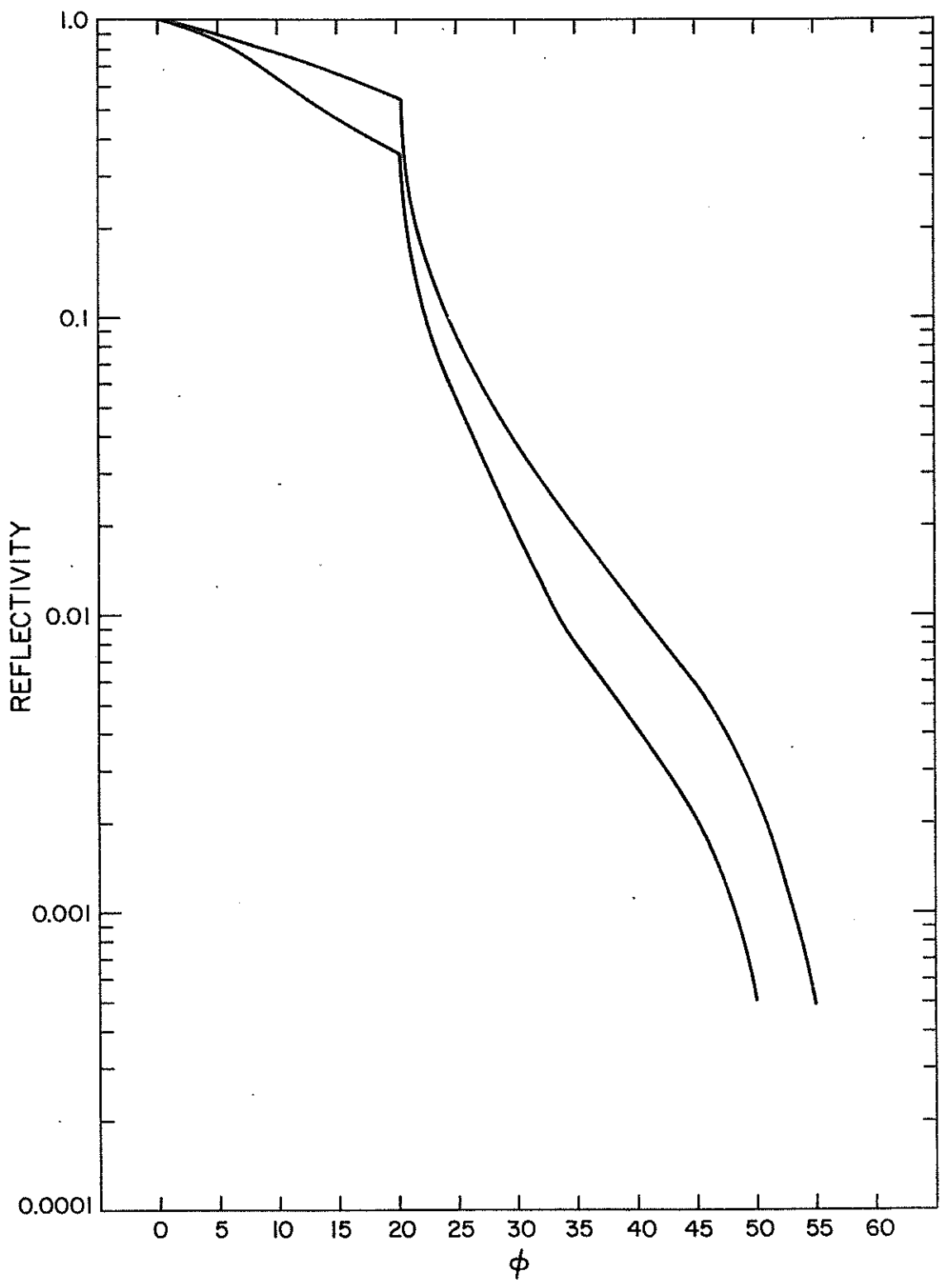


Figure 6-4.  $\theta = 0^\circ$ ,  $\lambda = 5320 \text{ \AA}$ .

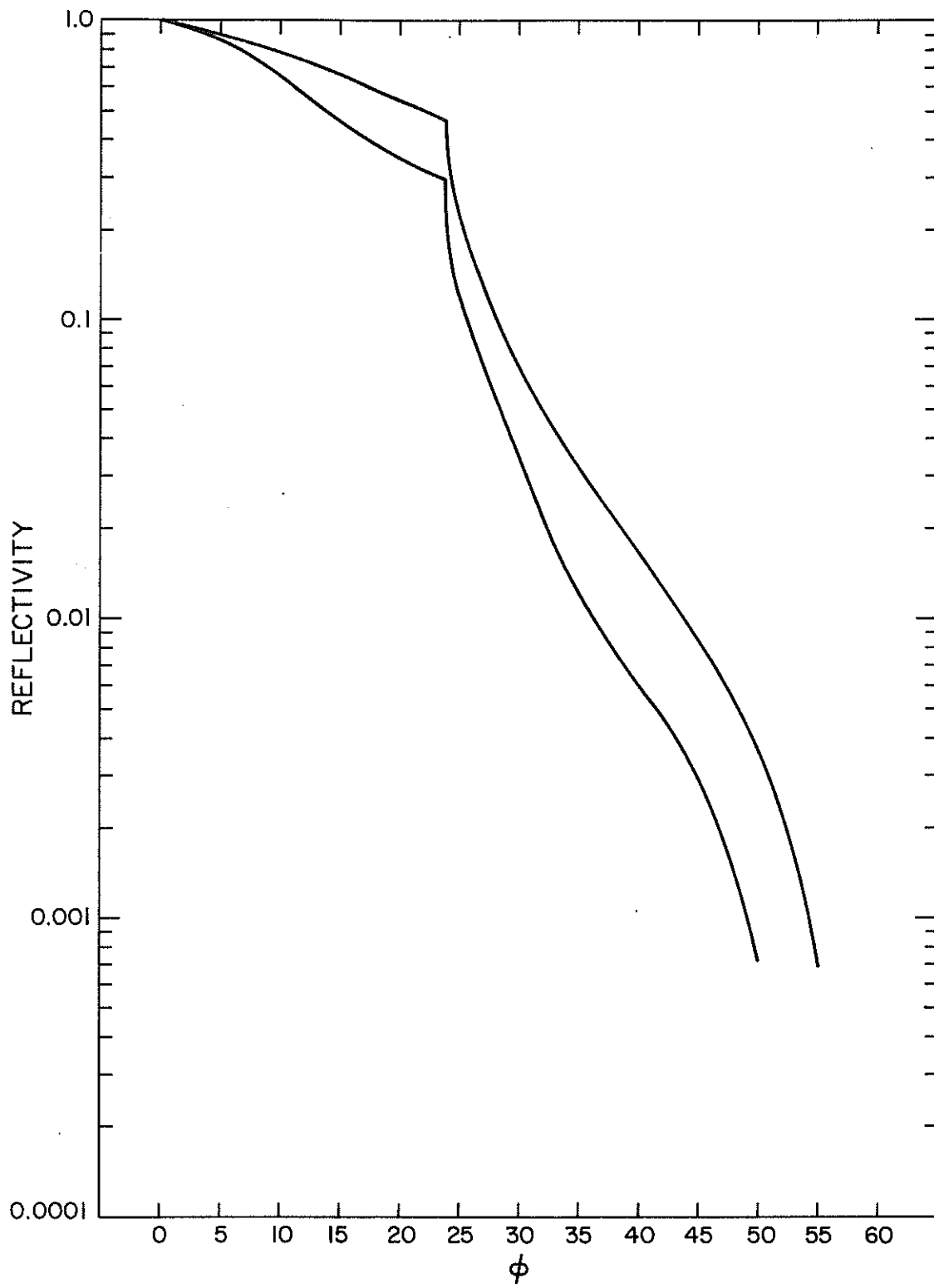


Figure 6-5.  $\theta = 10^\circ$ ,  $\lambda = 5320 \text{ \AA}$ .

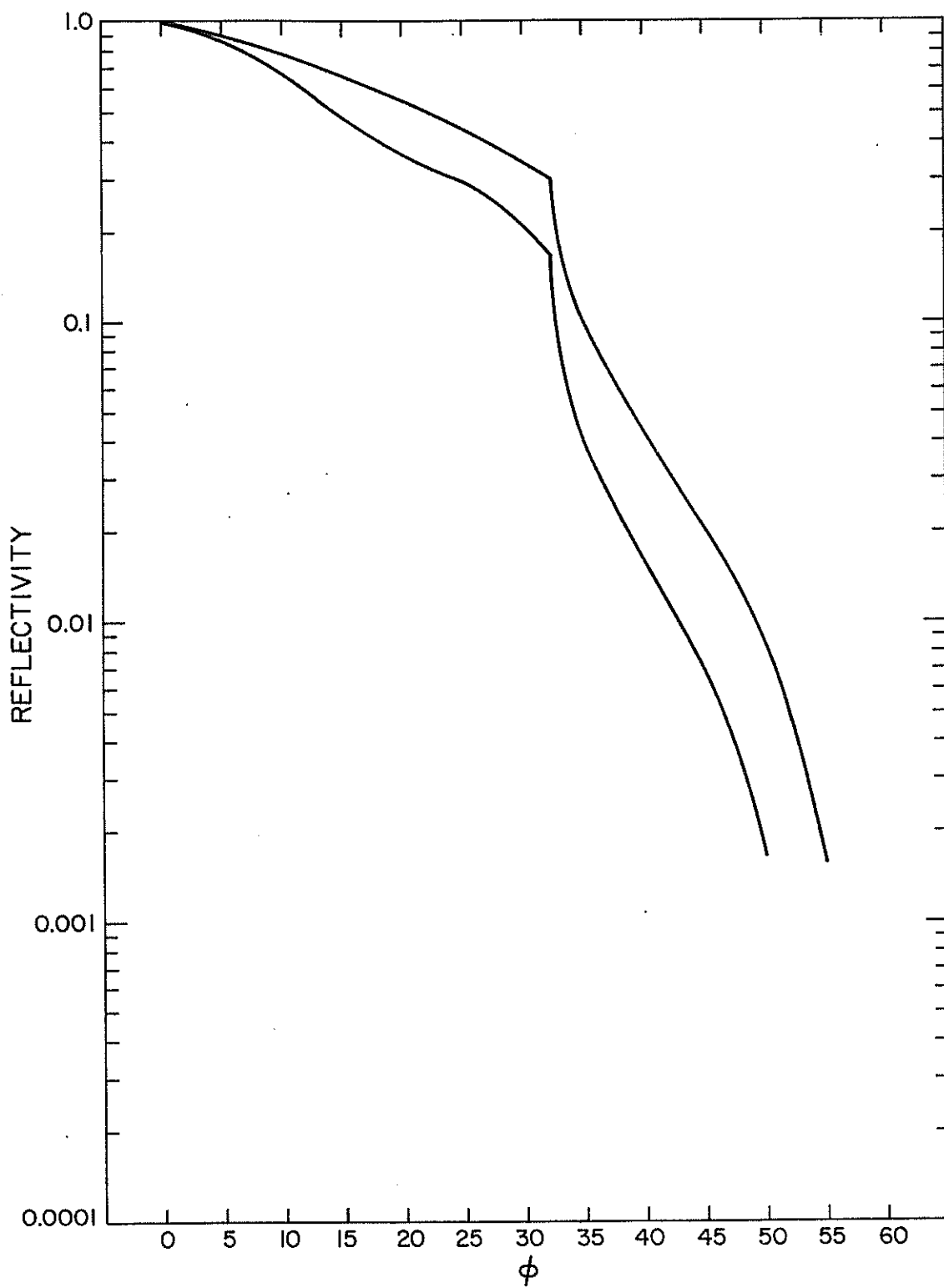


Figure 6-6.  $\theta = 20^\circ$ ,  $\lambda = 5320 \text{ \AA}$ .

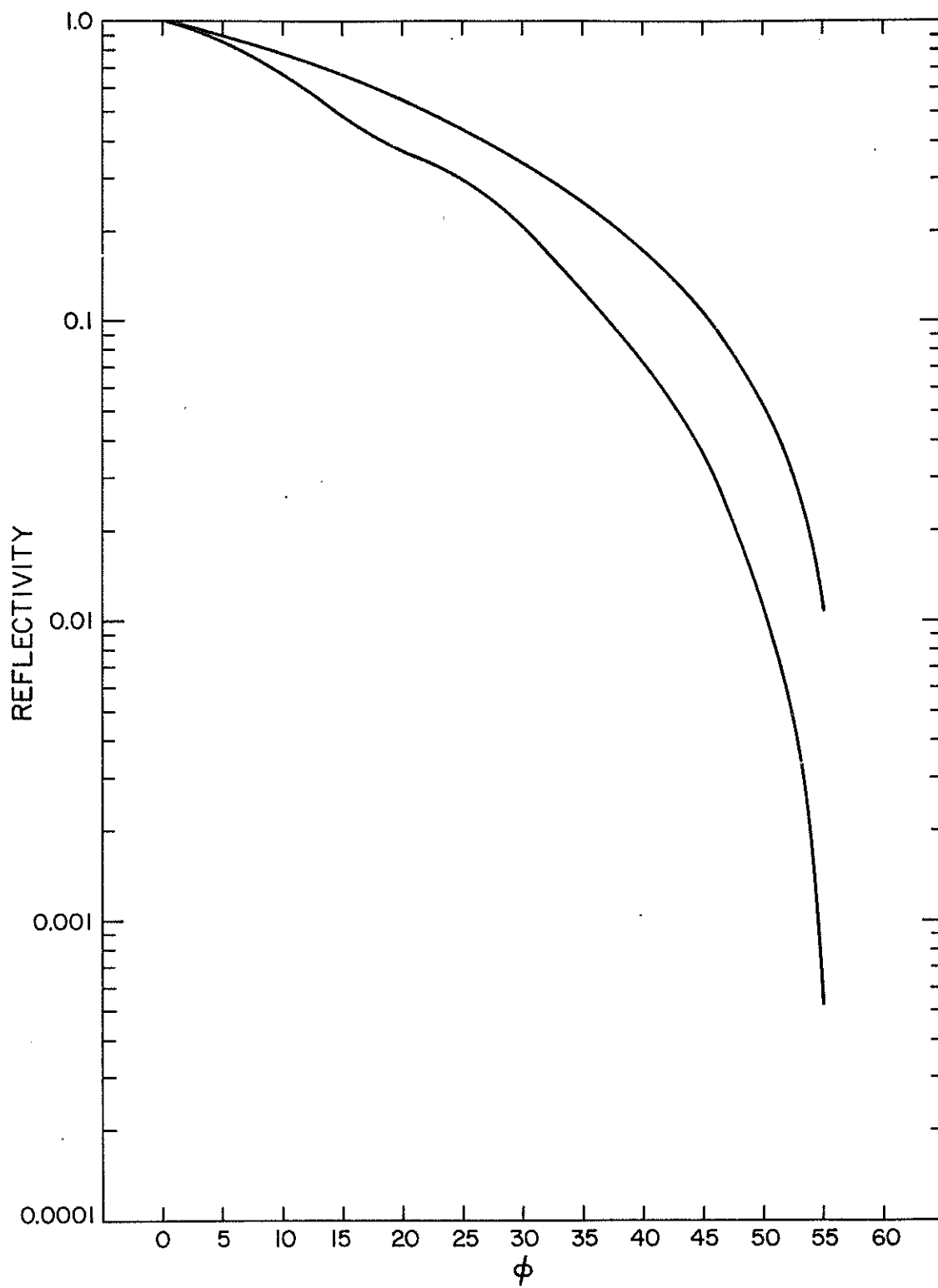


Figure 6-7.  $\theta = 30^\circ$ ,  $\lambda = 5320 \text{ \AA}$ .



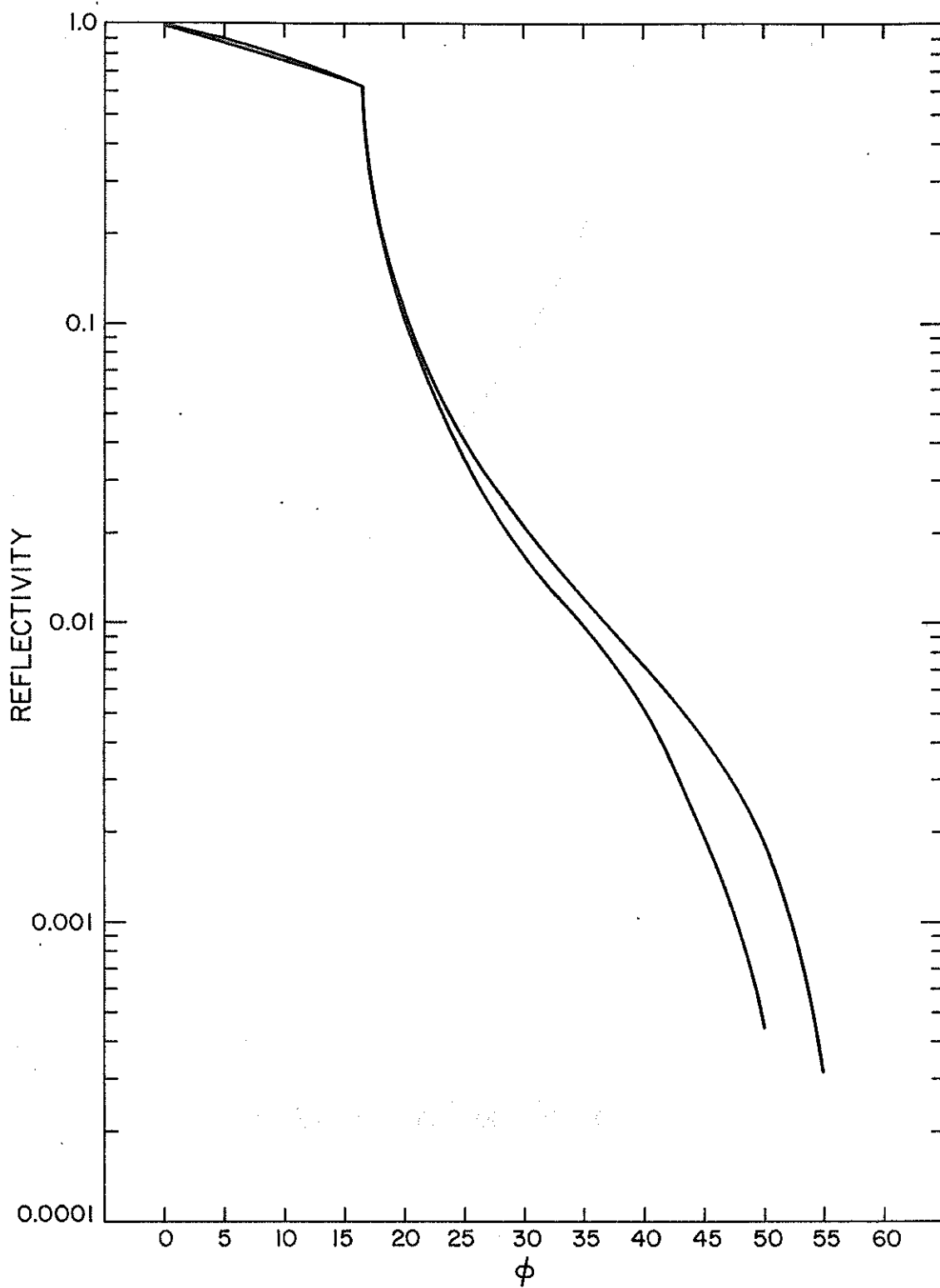


Figure 6-8.  $\theta = -30^\circ$ ,  $\lambda = 6943 \text{ \AA}$ .

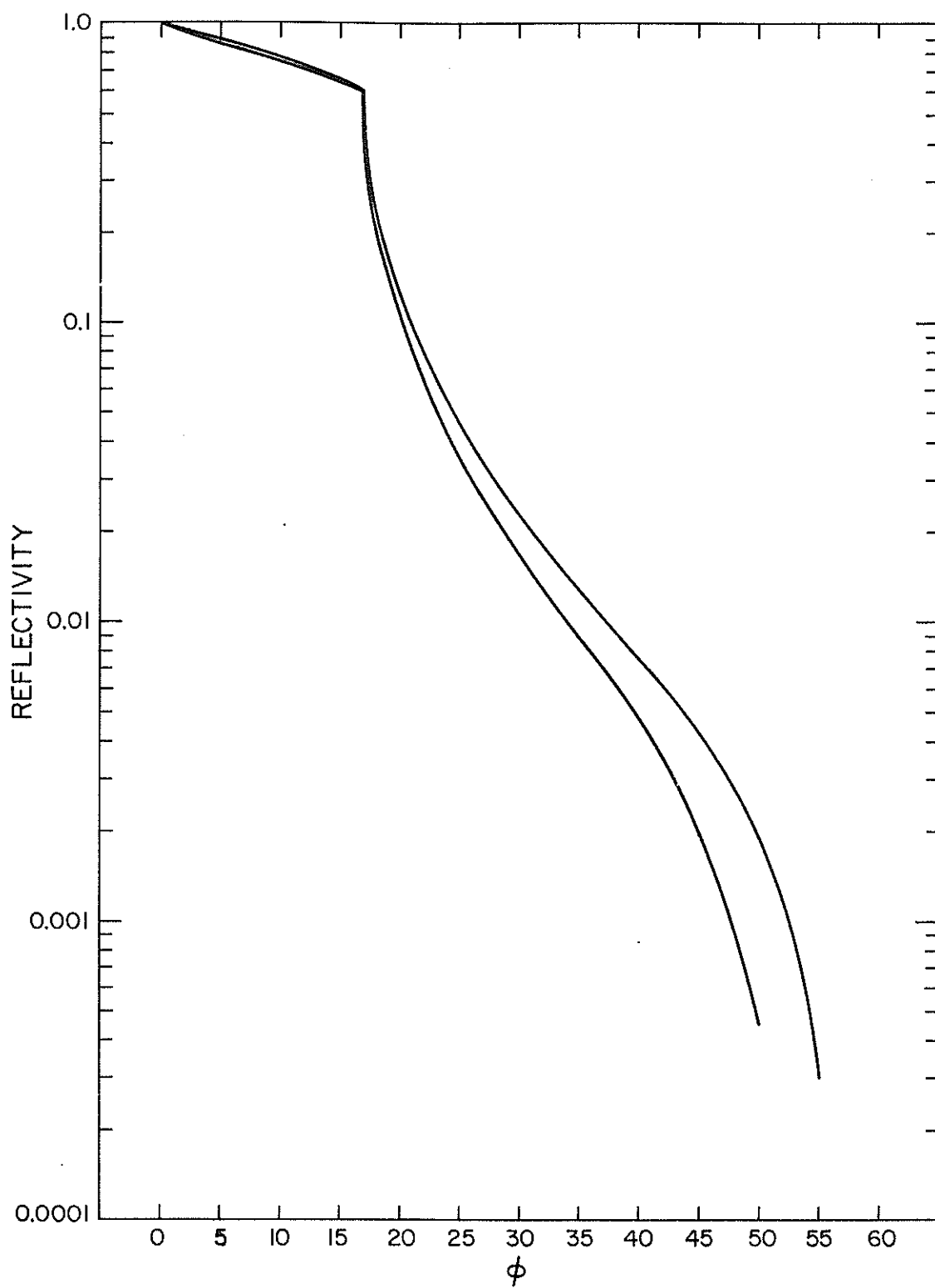


Figure 6-9.  $\theta = -20^\circ$ ,  $\lambda = 6943 \text{ \AA}$ .

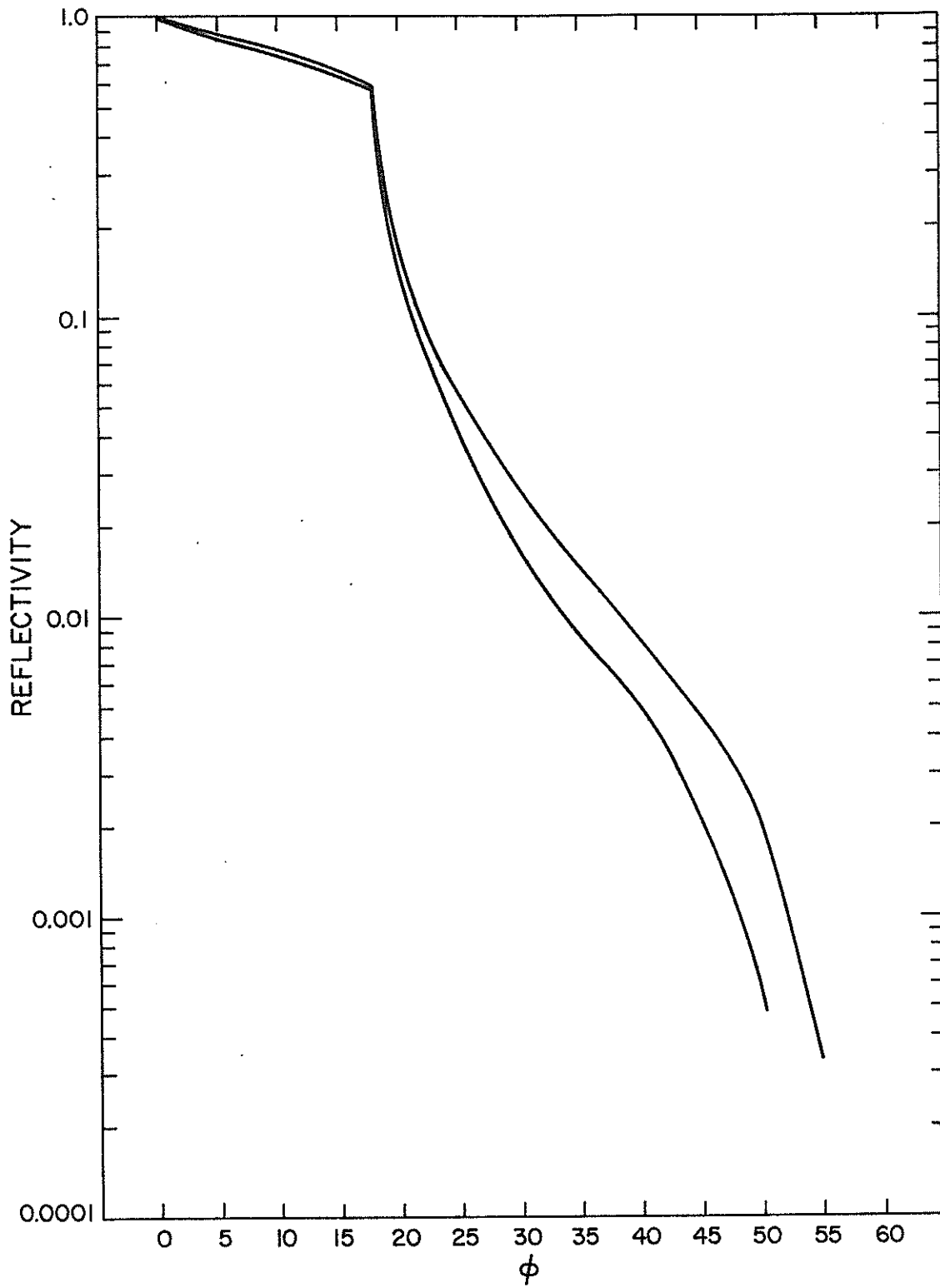


Figure 6-10.  $\theta = -10^\circ$ ,  $\lambda = 6943 \text{ \AA}$ .

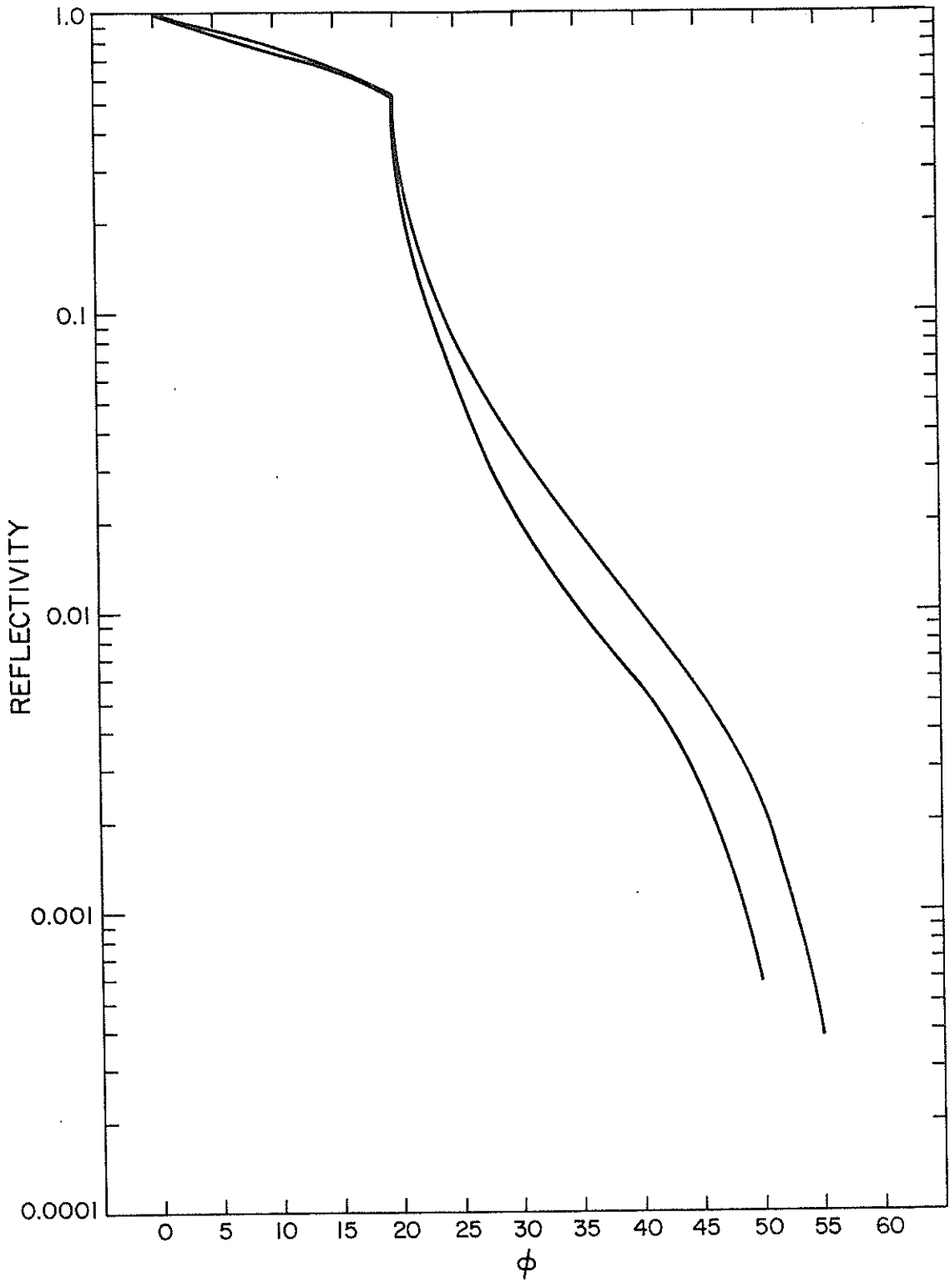


Figure 6-11.  $\theta = 0^\circ$ ,  $\lambda = 6943 \text{ \AA}$ .

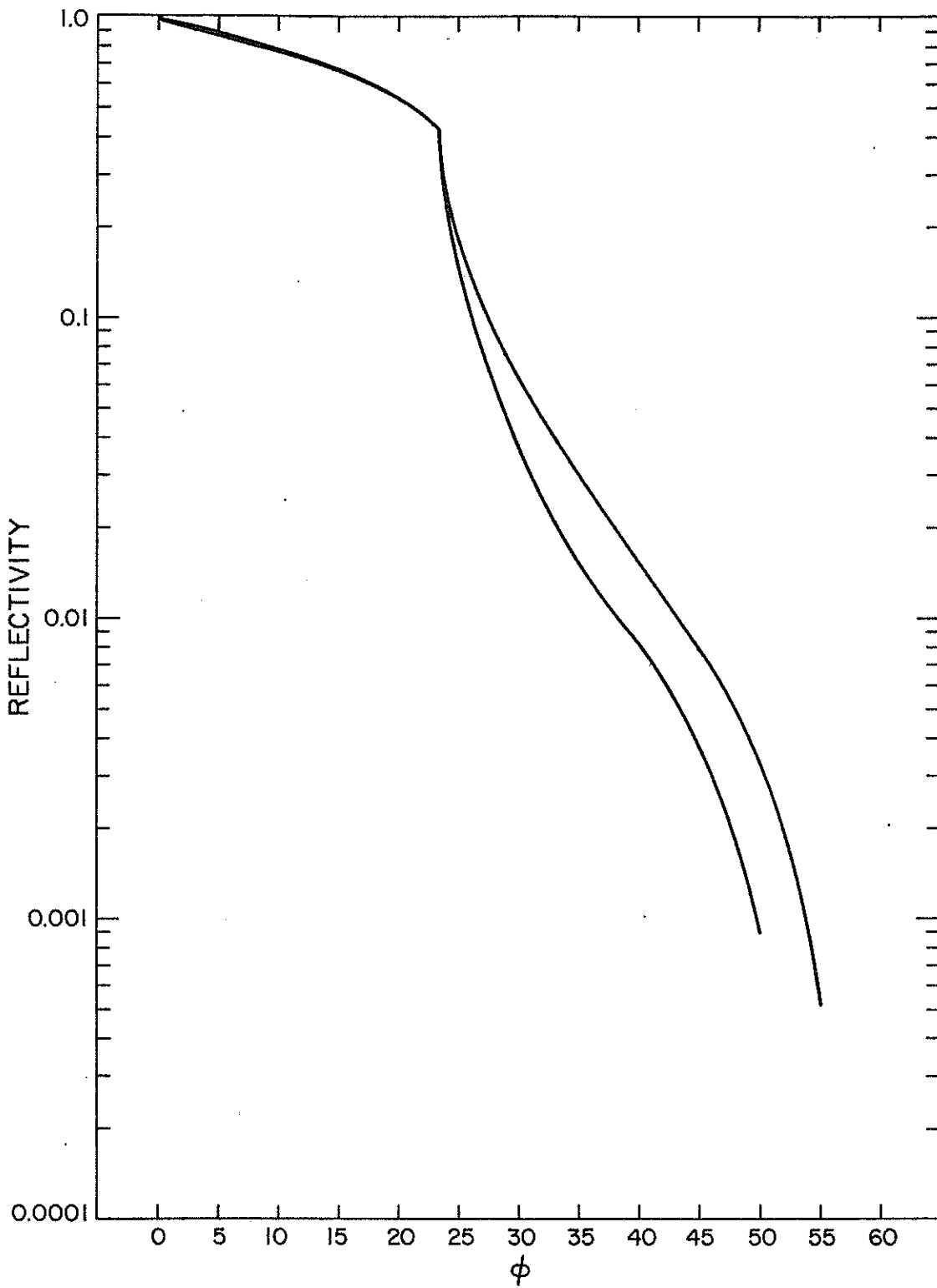


Figure 6-12.  $\theta = 10^\circ$ ,  $\lambda = 6943 \text{ \AA}$ .

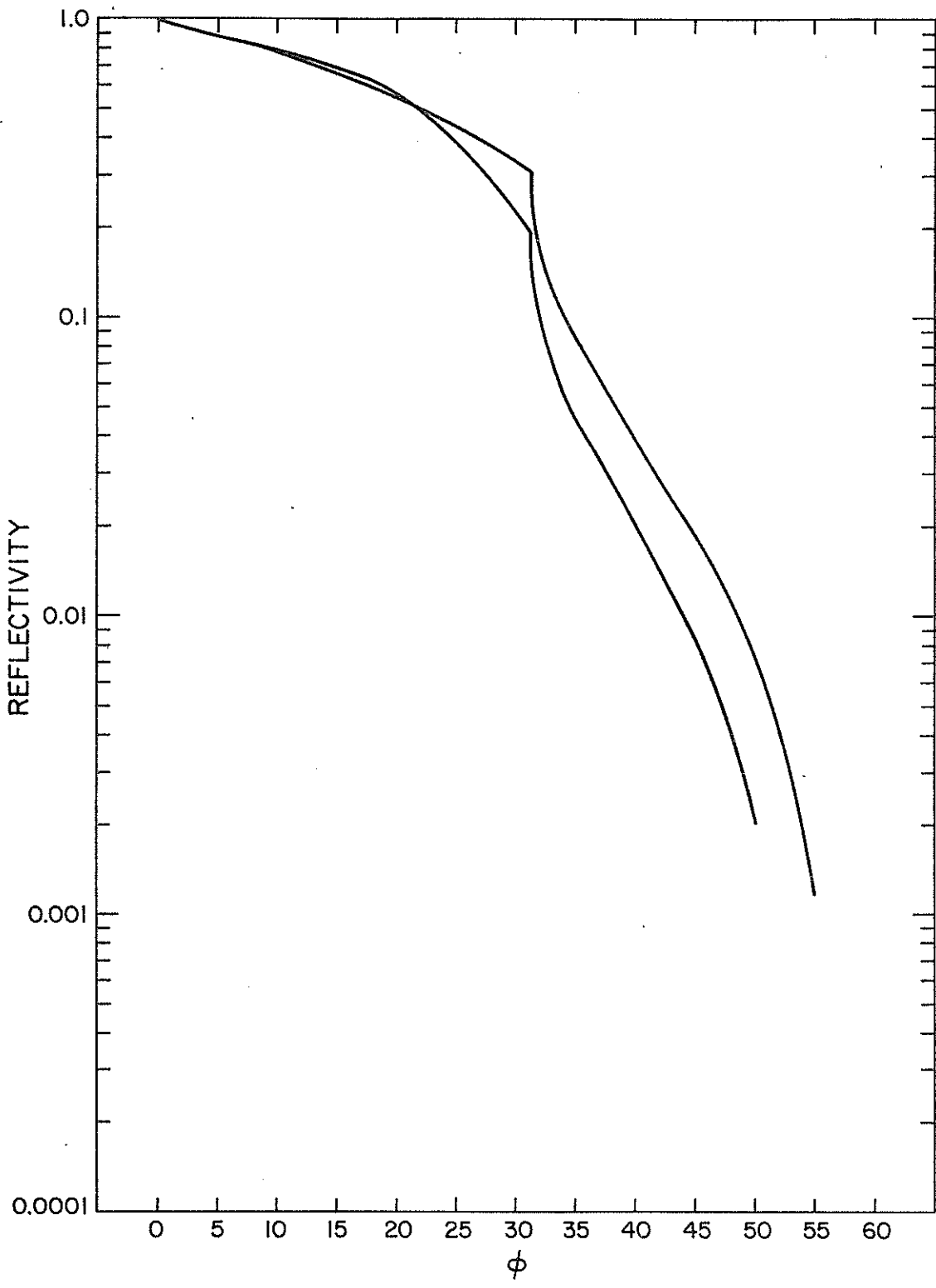


Figure 6-13.  $\theta = 20^\circ$ ,  $\lambda = 6943 \text{ \AA}$ .

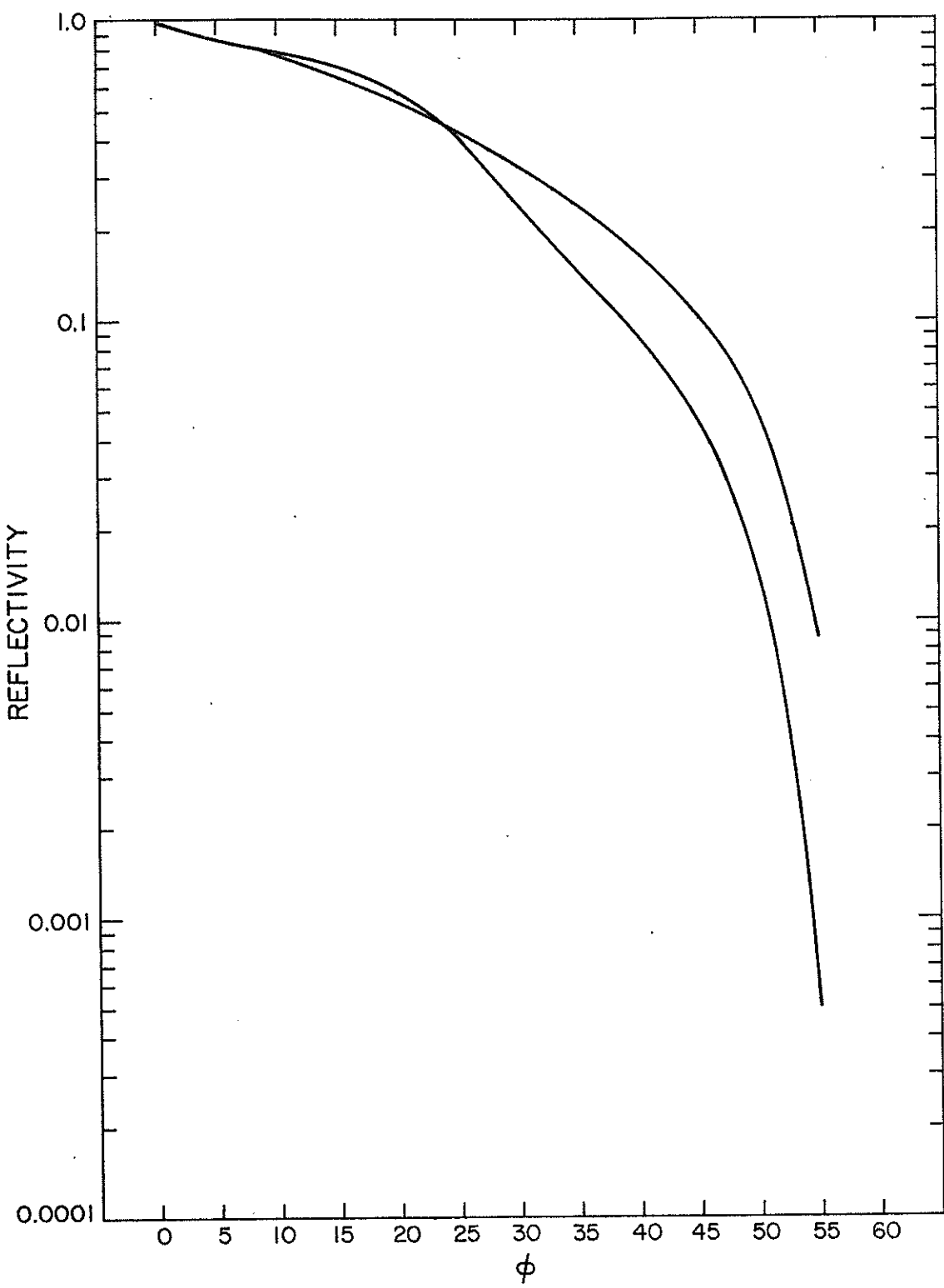


Figure 6-14.  $\theta = 30^\circ$ ,  $\lambda = 6943 \text{ \AA}$ .

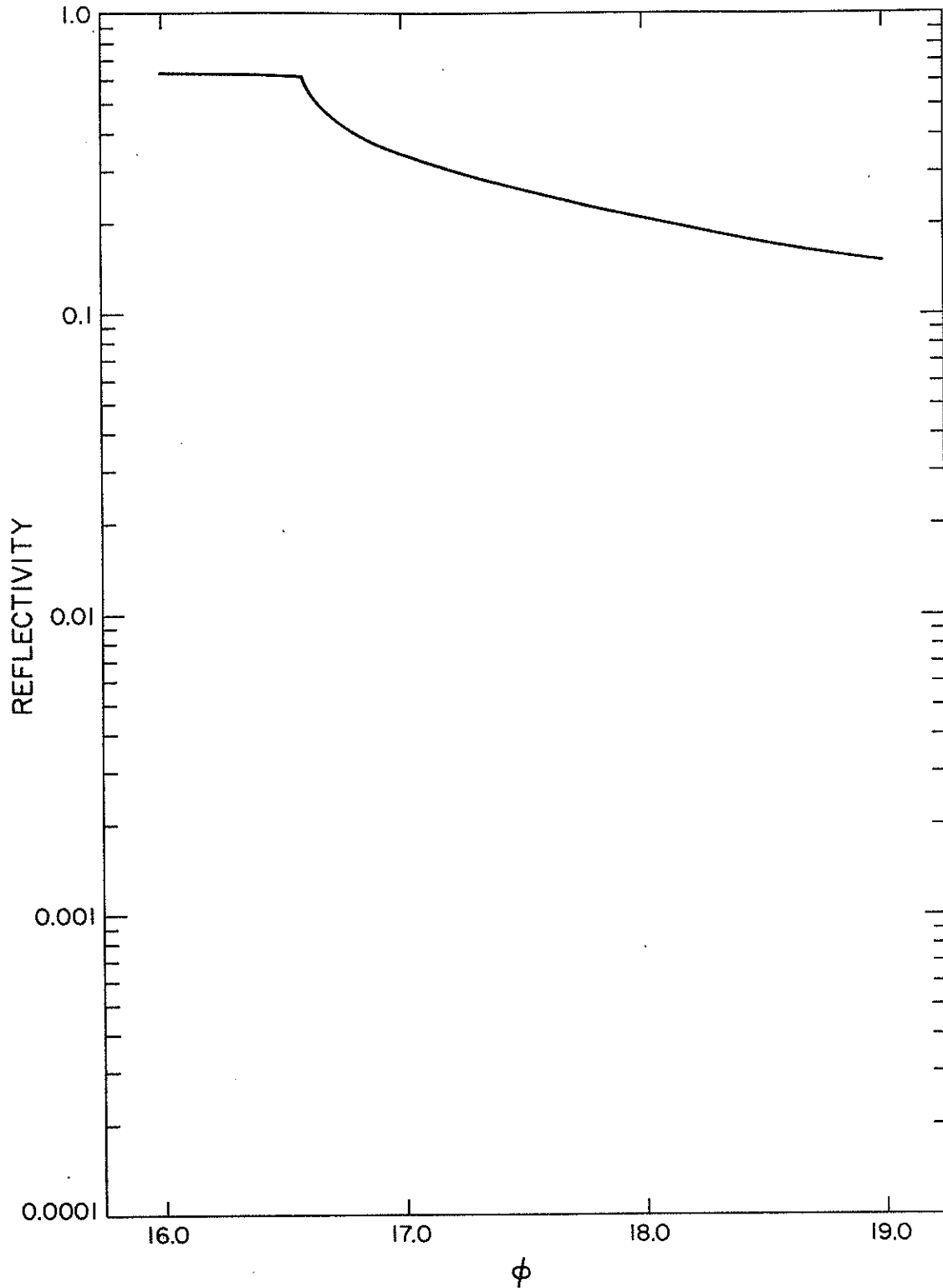


Figure 6-15. Total reflectivity for a Lageos optical cube corner in the vicinity of the cutoff for total internal reflection ( $\theta = -30^\circ$ ,  $\lambda = 6943 \text{ \AA}$ ).



## 7. VARIATION OF TRANSFER FUNCTION WITH SATELLITE ORIENTATION

The surface of the Lageos satellite is covered as uniformly as possible with cube corners to make the reflecting properties nearly independent of satellite orientation. Four of the cube corner locations have germanium reflectors for use by infrared lasers. Replacing an optical cube with a germanium cube, which is opaque to visible light, reduces the range correction by about 1.6 to 1.7 mm for a beam incident perpendicular to the face of the cube corner. The change in range was calculated by using the reflectivity curves for 5320 Å, with a 0.2-nsec incident pulse, and by computing the range correction for centroid, half-area, half-maximum, and peak detection methods.

A set of 138 sampling points was distributed over the surface of the sphere to study the variation of the transfer function with satellite orientation. The reflectivity curves for 5320 and 6943 Å were used to compute the reflectivity (in equivalent number of cube corners) and centroid range correction at each point. The rms variation of the centroid range correction is 0.85 mm and the variation of the reflected energy is about 6 or 7% over all satellite orientations. The difference between the maximum and minimum range corrections is 4.5 mm. The average range correction at each latitude has also been computed to look for systematic effects. Except at the north pole where there is an infrared cube corner, the average range corrections at all latitudes are contained within a 1-mm interval. The variation of the transfer function at points other than the location of germanium reflectors is due mainly to cube corners going in and out of total internal reflection, and, to a lesser extent, to differences in the configuration of the cube corners from different viewing angles. For the purpose of making more detailed studies of the transfer function, the sampling points have been looked at individually to find one whose properties are close to the average for all orientations. The point at  $\theta = 20^\circ$ ,  $\phi = 150^\circ$  has nearly the average reflectivity, range correction, and pulse spread, so it has been used for all the calculations in the following sections.



## 8. REFLECTIVITY HISTOGRAM

An important factor affecting the range accuracy obtainable from a retroreflector array is the spread in range along the line of sight of the cube corners contributing to the reflected signal. The return from Lageos comes from a spherical cap whose angular radius is the cutoff angle of the cube corners. In addition to the angle where the active reflecting area goes to zero, there is a sharp decrease in reflectivity when the incidence angle on a cube corner goes past the cutoff for total internal reflection. Table 5 below lists the apparent reflection points along the line of sight measured from the center of the satellite for three cases: the earliest possible reflection point (a cube corner whose face is normal to the incident beam); the earliest point where a cube corner can lose total internal reflection; and the last possible reflection point where the active reflecting area goes to zero. The apparent reflection point as a function of the angle  $\phi$  between the incident beam and the normal to the front face of the cube corner is given by the expression

$$R \cos \phi - \ell \sqrt{n^2 - \sin^2 \phi} ,$$

where

- R = the distance from the center of the satellite to the front face of the cube corner (29.807 cm),
- $\phi$  = the incidence angle on the cube corner,
- $\ell$  = the length of the cube corner (2.7838 cm),
- n = the index of refraction.

The cutoff angles ( $\phi$ ) for the cases listed are from Table 3 in Section 6.

The total range spread is a little over 12 cm. Total internal reflection is guaranteed for a little more than the first centimeter. Since the cube corners are spaced about  $10^\circ$  from each other on the surface, a beam incident in the center of a square of reflectors could be up to about  $7^\circ$  from the nearest cube corner. The apparent reflection point for  $\phi = 7^\circ$  and  $n = 1.461$  is 0.2553 m. Therefore, the maximum variation of the earliest reflection point is about 2 mm.

Table 5. Apparent reflection points for various incidence angles.

$\phi$	$\lambda$	n	Apparent reflection point (m)	Description
0	6943	1.455	0.2576	Earliest reflection point
0	5320	1.461	0.2574	Earliest reflection point
16°595	6943	1.455	0.2459	Earliest T.I.R. cutoff
16°998	5320	1.461	0.2452	Earliest T.I.R. cutoff
55°255	6943	1.455	0.13645	Latest reflection point
55°597	5320	1.461	0.13485	Latest reflection point

Figures 7(a-c), are histograms of the contribution to the reflected signal from each 1-cm interval along the line of sight starting from the earliest reflection point. The origin of the distance scale is the center of the satellite. Table 6 lists the data used to plot the histograms. The calculations were done using the reflectivity curves of Figure 6. Over half the return energy comes from the first 1-cm interval, and over 90% comes from the first 4-cm interval. The centroid of the first two histograms is at 24.25 cm, which is 1.50 cm in back of the first reflection point. The effect of loss of total internal reflection in concentrating the energy toward the earliest reflection point can be seen by comparing the second histogram with the third, which is the energy distribution that would be obtained by coating the back reflecting faces of the cube corners. The centroid, if the cubes were coated, would be at 0.2314 m, which is a little over 2.50 cm from the earliest reflection point.

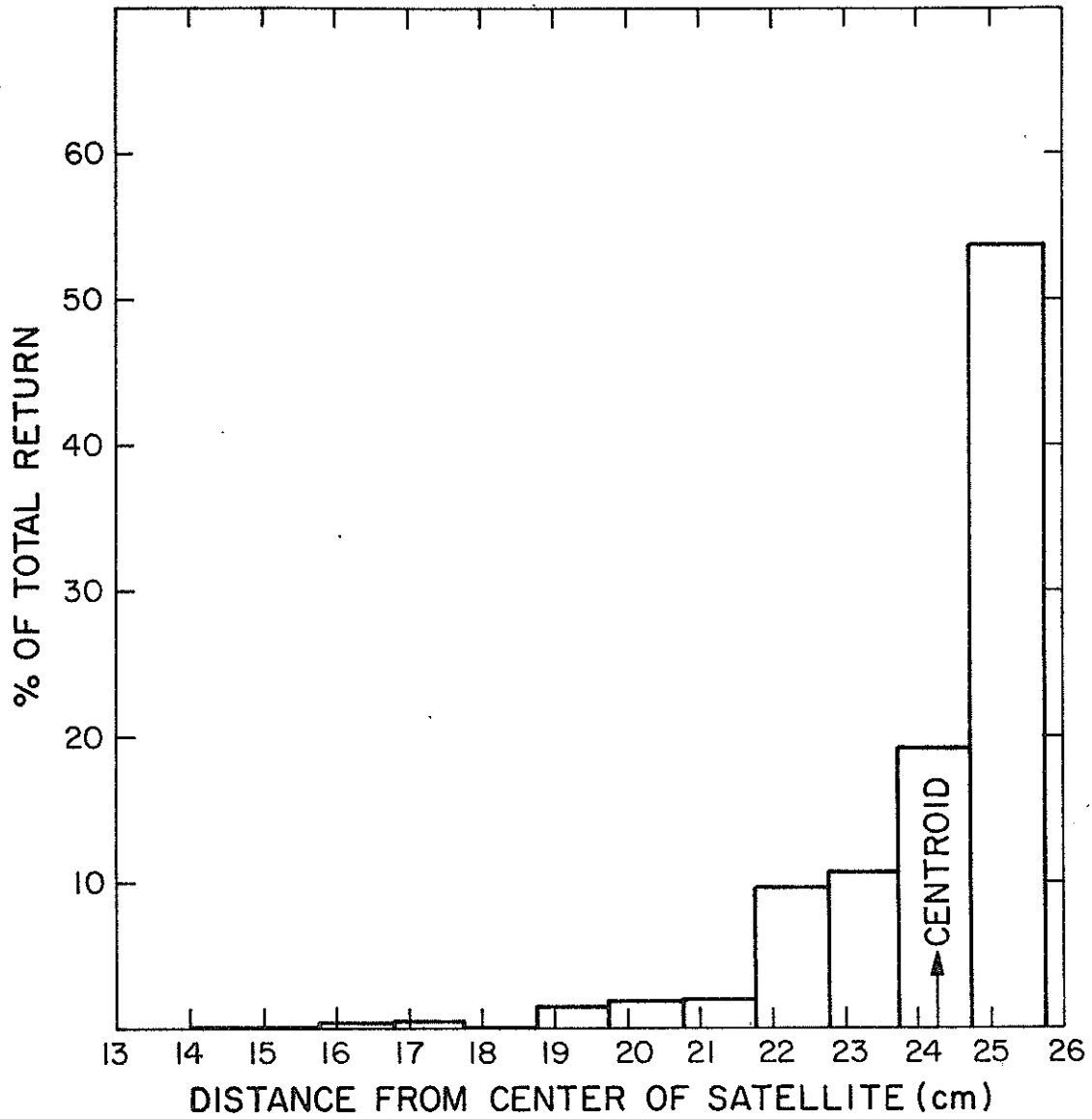


Figure 7a. Reflectivity histogram of Lageos using the reflectivity curve of Figure 6 for  $\lambda = 5320 \text{ \AA}$  (uncoated cube corners).

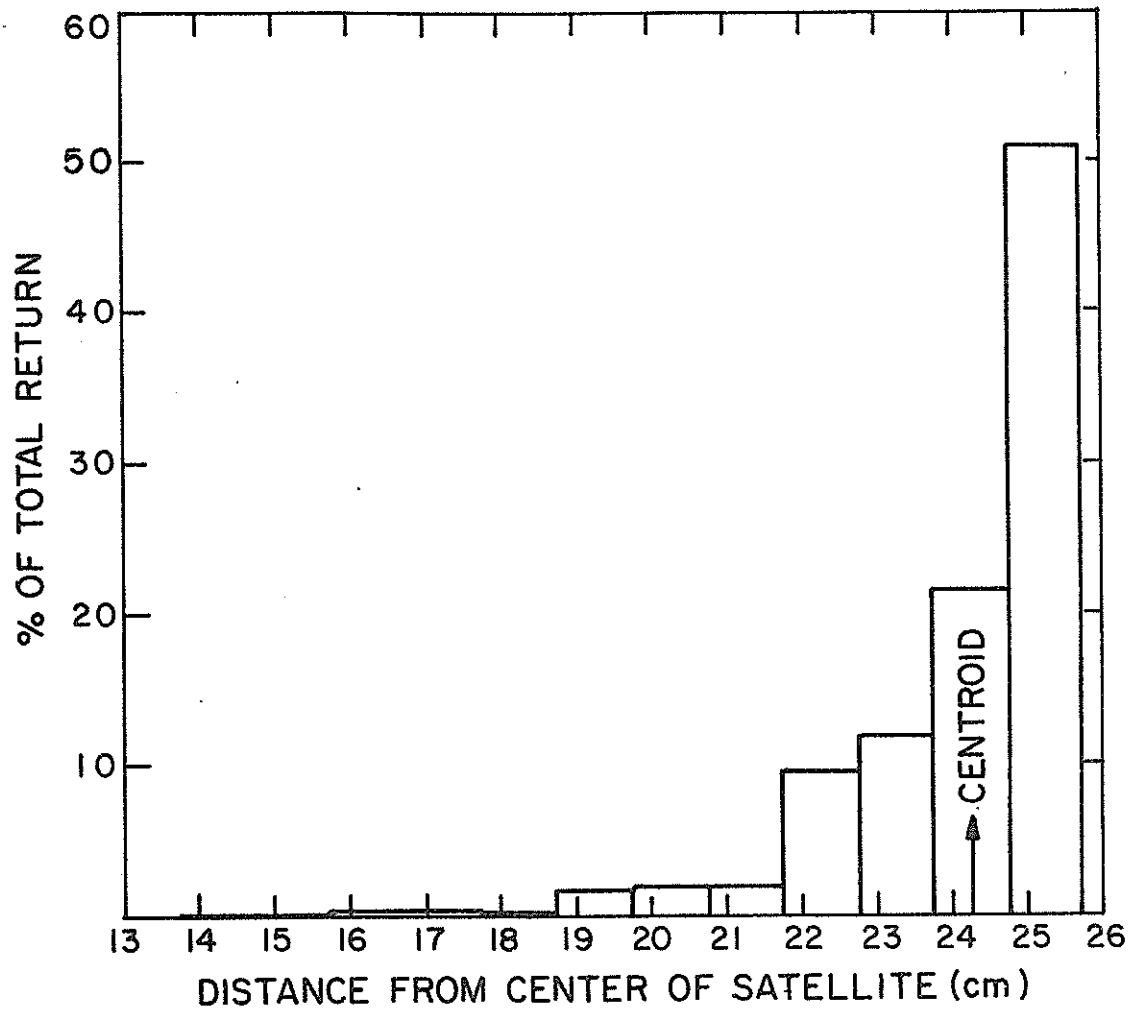


Figure 7b. Reflectivity histogram of Lageos using the reflectivity curve of Figure 6 for  $\lambda = 6943 \text{ \AA}$  (uncoated cube corners).

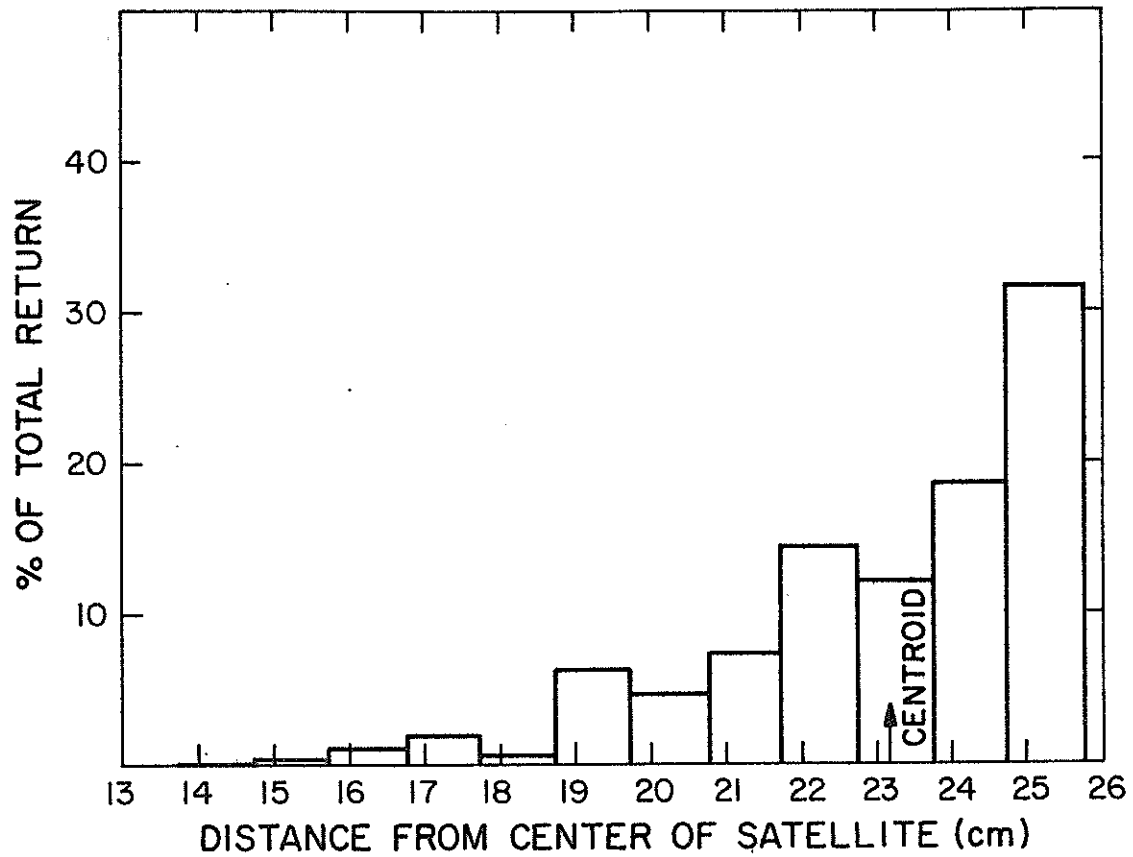


Figure 7c. Reflectivity histogram of Lageos using the reflectivity curve for cube corners with reflective coatings on the back faces ( $\lambda = 6943 \text{ \AA}$ ).

Table 6a. Percentage of total return in each 1-cm interval starting from the earliest apparent reflection point ( $\lambda = 5320$ , uncoated cube corners).

Interval	% of total return	Cumulative %
1	53.89	53.89
2	19.35	73.24
3	10.76	84.00
4	9.72	93.72
5	2.01	95.73
6	1.88	97.60
7	1.57	99.17
8	0.07	99.24
9	0.35	99.59
10	0.31	99.90
11	0.09	99.99
12	0.01	100.00

Table 6b. Percentage of total return in each 1-cm interval starting from the earliest apparent reflection point ( $\lambda = 6943$ , uncoated cube corners).

Interval	% of total return	Cumulative %
1	51.10	51.10
2	21.57	72.67
3	11.70	84.37
4	9.45	93.82
5	1.95	95.77
6	1.85	97.62
7	1.57	99.19
8	0.06	99.26
9	0.34	99.60
10	0.30	99.90
11	0.09	99.99
12	0.01	100.00



Table 6c. Percentage of total return in each 1-cm interval starting from the earliest apparent reflection point ( $\lambda = 6943$ , coated cube corners).

Interval	% of total return	Cumulative %
1	31.86	31.86
2	18.77	50.63
3	12.29	62.91
4	14.62	77.54
5	7.32	84.86
6	4.73	89.59
7	6.39	95.97
8	0.69	96.66
9	1.93	98.59
10	1.02	99.61
11	0.30	99.91
12	0.08	100.00



## 9. ARRAY REFLECTIVITY

This section presents information on the reflectivity of the Lageos array that can be used to estimate signal strengths by use of the formula given in Section 5. The array reflectivity is given by the cross section, which is the product of the reflecting area and the gain. In computing the diffraction pattern of the array, it is essentially the cross section that is computed. The gain can be computed by dividing the cross section by the reflecting area, which must be determined separately. The reflecting area can be computed by multiplying the area of one cube corner ( $11.4009 \text{ cm}^2$ ) by the equivalent number of cube corners, which can be obtained using a reflectivity curve normalized to unity at normal incidence. The total reflected energy is equivalent to 12.60 cube corners at  $\lambda = 5320 \text{ \AA}$  and 12.33 cube corners at  $\lambda = 6943$ . Multiplying these by the area of one cube gives  $0.014361$  and  $0.014052 \text{ m}^2$  at 5320 and  $6943 \text{ \AA}$ , respectively. These are the areas to be used with the gain matrices of this section for computing signal strength. The effective number of cube corners can also be computed from the reflectivity curves in Section 6. The average effective number of cube corners over all orientations using these curves are 9.88 and 12.21 at 5320 and  $6943 \text{ \AA}$ , respectively. Multiplying these values by the area and gain of one cube corner at normal incidence gives cross sections of  $1.198 \times 10^6 \text{ m}^2$  and  $0.958 \times 10^6 \text{ m}^2$  at 5320 and  $6943 \text{ \AA}$ . (In standard units of gain and cross section,  $15 \times 10^6 \text{ m}^2$  and  $12 \times 10^6 \text{ m}^2$  are obtained, respectively, because of the factor of  $4\pi$  in the standard definition.)

The gain matrix of the Lageos array has been computed for 5320 and  $6943 \text{ \AA}$ , with dihedral angle offsets of 0.75, 1.25, and 1.75 arcsec, and linear and circular polarization of the incident beam. In addition, an equal mixture of 0.75-, 1.25-, and 1.75-arcsec offsets has been used in an attempt to simulate the mixture of offsets present in the actual cube corners. The gain matrices are given in Table 7. The angles  $\theta_1$  and  $\theta_2$ , in microradians, are defined in Figure 8. The angle  $\theta_2$  is in the direction of decreasing  $\phi$  in the plane containing the Z axis and the direction toward the illuminating laser (the vector  $\vec{V}$ ). The angle  $\theta_1$  is normal to the plane in the direction of  $\hat{Z} \times \vec{V}$ .

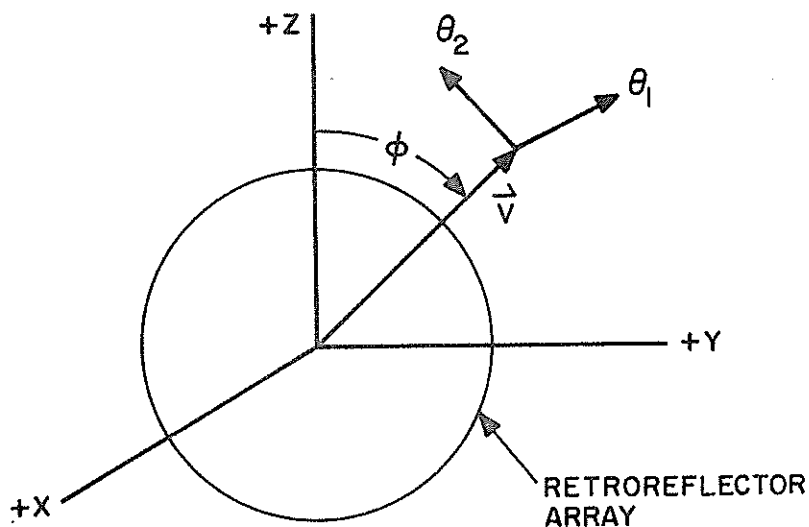


Figure 8. Diffraction-pattern coordinate system.

Table 8 shows how the array gain function varies with velocity aberration. The first column is the magnitude of the velocity aberration in microradians, and the second is the array gain function in units of  $10^7$ . In the computer-plotted graph, the gain function increases to the right and the velocity aberration, down the page. The gain function is the average value around a circle in the far field with radius equal to the velocity aberration. The second part of each table gives the root-mean-square (rms) variation of the gain around the circle.

Figure 9 consists of contour plots of the gain-function matrices given in Table 7. Circles have been drawn with radii of 32 and 41  $\mu\text{rad}$  to mark the minimum and maximum values of velocity aberration. The contour levels plotted are 8, 4, 2, and  $1 \times 10^7$ . The position of peaks in the pattern is indicated by asterisks. The contour plots for linearly polarized illumination show an asymmetry consisting of dumbbell-shaped contours aligned with the electric vector of the incident illumination. At 35  $\mu\text{rad}$  from the center of the pattern, the intensity in the bright lobes is about a factor of 2 higher than at points  $90^\circ$  away from the bright lobes. The asymmetry disappears if circularly polarized illumination is used. Test runs show that the asymmetry also disappears if there is no dihedral angle offset or if the back faces have metal coatings.



Table 7-2. Linear polarization.

$\theta_2$	DIHEDRAL ANGLE 1.25 WAVELENGTH 5320																				
	GAIN FUNCTION (1.E+7)																				
50	.69	.83	1.08	1.51	2.04	2.53	3.02	3.56	4.06	4.34	4.33	3.98	3.44	3.01	2.75	2.41	1.92	1.43	1.07	.80	.60
45	.78	1.03	1.45	2.07	2.85	3.74	4.78	5.87	6.88	6.98	6.79	6.16	5.27	4.56	4.22	3.86	3.17	2.33	1.63	1.12	.77
40	1.06	1.44	1.98	2.72	3.71	5.09	6.80	8.46	9.55	9.87	9.59	8.90	7.86	6.83	6.12	5.50	4.57	3.37	2.27	1.46	.94
35	1.51	1.99	2.63	3.49	4.71	6.43	8.48	10.37	11.56	11.87	11.52	10.88	10.05	9.00	7.91	6.85	5.64	4.24	2.91	1.90	1.25
30	1.96	2.58	3.42	4.53	5.89	7.57	9.52	11.43	12.80	12.23	12.77	11.97	11.23	10.35	9.12	7.75	6.34	4.89	3.55	2.52	1.80
25	2.38	3.21	4.27	5.52	6.68	7.98	9.90	12.25	14.24	15.22	14.93	13.79	12.57	11.36	9.89	8.30	6.85	5.47	4.22	3.22	2.43
20	2.81	3.76	4.89	5.98	6.61	7.58	9.70	12.80	15.00	16.30	16.50	15.37	13.67	12.01	10.19	8.41	7.09	6.01	4.88	3.83	2.92
15	3.15	4.09	5.14	5.96	6.17	7.12	9.70	12.01	12.94	13.85	14.59	13.76	12.16	11.02	9.70	8.02	6.92	6.31	5.43	4.28	3.20
10	3.30	4.19	5.14	5.76	5.80	6.78	8.81	9.37	8.88	10.27	11.96	10.68	8.54	8.42	8.60	7.49	6.52	6.25	5.66	4.51	3.31
5	3.37	4.25	5.09	5.47	5.35	6.12	7.13	6.21	5.92	9.68	12.84	10.07	5.91	4.84	7.44	7.04	6.11	5.93	5.54	4.53	3.37
0	3.45	4.39	5.15	5.28	5.02	5.64	6.07	4.64	5.06	10.48	14.34	10.59	5.14	4.84	6.70	6.55	5.69	5.56	5.31	4.51	3.46
-5	3.40	4.41	5.27	5.45	5.34	6.17	6.88	5.76	5.87	9.97	12.88	9.98	6.11	6.08	7.05	6.24	5.35	5.35	5.23	4.58	3.50
-10	3.19	4.23	5.30	5.89	6.19	7.26	8.57	8.58	8.66	10.66	12.14	10.91	9.53	9.49	8.59	6.50	5.34	5.31	5.17	4.57	3.59
-15	3.02	4.01	5.23	6.30	7.06	8.07	9.47	10.74	12.13	13.89	14.77	14.27	13.59	12.59	10.11	7.24	5.77	5.32	4.84	4.16	3.24
-20	2.92	3.82	4.96	6.28	7.50	8.50	9.55	11.15	13.51	15.80	16.63	15.94	14.77	13.15	10.64	8.11	6.46	5.32	4.28	3.42	2.63
-25	2.62	3.43	4.36	5.58	7.06	8.42	9.47	10.74	12.67	14.55	15.19	14.52	13.41	12.15	10.49	8.63	6.88	5.24	3.80	2.78	2.09
-30	2.04	2.76	3.53	4.50	5.87	7.50	9.00	10.29	11.80	13.73	13.19	12.87	12.14	11.14	9.78	8.15	6.49	4.89	3.49	2.45	1.75
-35	1.42	2.04	2.76	3.58	4.64	6.07	7.69	9.24	10.55	11.51	11.96	11.79	11.02	9.75	8.21	6.69	5.36	4.17	3.07	2.15	1.47
-40	1.00	1.47	2.10	2.83	3.68	4.69	5.90	7.28	8.63	9.64	10.07	9.80	8.87	7.53	6.13	4.94	3.97	3.13	2.37	1.70	1.16
-45	.77	1.09	1.49	2.02	2.70	3.43	4.20	5.13	6.16	6.96	7.24	6.91	6.11	5.12	4.19	3.38	2.67	2.06	1.60	1.22	.92
-50	.61	.81	1.03	1.34	1.79	2.32	2.85	3.40	3.99	4.43	4.54	4.29	3.80	3.24	2.72	2.22	1.73	1.33	1.08	.90	.76

Table 7-3. Linear polarization.

DIHEDRAL ANGLE 1.75 WAVELENGTH 5320

GAIN FUNCTION (1.E+7)

$\theta_2$	-50	-45	-40	-35	-30	-25	-20	-15	-10	-5	0	5	10	15	20	25	30	35	40	45	50 $\theta_1$
50	1.13	1.52	2.14	3.05	4.13	5.14	5.95	6.57	6.97	7.07	6.87	6.44	5.95	5.55	5.18	4.66	3.97	3.24	2.52	1.82	1.22
45	1.49	2.08	2.92	3.99	5.16	6.30	7.35	8.25	8.79	8.84	8.44	7.74	7.02	6.62	6.49	6.17	5.40	4.39	3.39	2.47	1.67
40	2.07	2.80	3.70	4.71	5.83	7.09	8.43	9.59	10.21	10.19	9.59	8.90	8.06	7.55	7.48	7.35	6.66	5.49	4.23	3.09	2.16
35	2.77	3.48	4.26	5.12	6.14	7.40	8.73	9.79	10.30	10.21	9.54	9.13	8.51	8.05	7.88	7.75	7.20	6.13	4.86	3.68	2.70
30	3.37	4.00	4.65	5.44	6.38	7.36	8.22	8.84	9.08	8.87	8.46	7.94	7.77	7.67	7.55	7.40	7.00	6.21	5.24	4.27	3.34
25	3.81	4.40	4.98	5.73	6.43	6.84	7.19	7.60	7.86	7.67	7.12	6.69	6.59	6.85	6.84	6.73	6.50	6.01	5.38	4.72	3.93
20	4.16	4.71	5.17	5.73	5.92	5.78	6.08	6.76	7.10	6.93	6.48	6.09	6.07	6.21	6.15	6.05	6.02	5.81	5.40	4.92	4.28
15	4.40	4.85	5.16	5.47	5.21	4.86	5.41	6.07	5.82	5.30	5.06	4.89	5.05	5.52	5.61	5.44	5.56	5.65	5.39	4.94	4.38
10	4.43	4.80	5.04	5.21	4.77	4.51	5.08	5.03	3.89	3.44	3.27	3.30	3.49	3.70	4.90	5.02	5.09	5.42	5.33	4.91	4.39
5	4.38	4.75	4.98	5.03	4.53	4.35	4.65	3.82	2.55	3.20	4.27	3.30	2.45	3.70	4.90	4.76	4.70	5.12	5.19	4.86	4.39
0	4.37	4.74	5.05	4.95	4.37	4.25	4.37	3.21	2.16	3.65	5.14	3.68	2.18	3.28	4.60	4.51	4.47	4.94	5.12	4.90	4.47
-5	4.31	4.77	5.10	5.02	4.51	4.48	4.70	3.66	2.46	3.29	4.31	3.34	2.62	3.74	4.59	4.31	4.41	5.01	5.24	5.08	4.61
-10	4.16	4.62	5.07	5.23	4.97	4.96	5.23	4.65	3.58	3.47	3.84	3.79	4.23	5.14	5.06	4.41	4.56	5.14	5.33	5.17	4.62
-15	4.10	4.58	5.11	5.54	5.62	5.52	5.50	5.32	5.01	5.02	5.21	5.49	6.10	6.39	5.71	4.95	4.97	5.20	5.14	4.90	4.35
-20	4.14	4.75	5.28	5.82	6.23	6.25	5.95	5.71	5.85	6.26	6.53	6.66	6.89	6.92	6.45	5.97	5.71	5.32	4.82	4.40	3.88
-25	3.97	4.79	5.38	5.91	6.51	6.92	6.85	6.57	6.57	6.90	7.18	7.30	7.46	7.60	7.47	7.08	6.46	5.59	4.72	4.04	3.44
-30	3.43	4.42	5.25	5.86	6.50	7.18	7.62	7.74	8.84	8.13	8.48	8.73	8.85	8.74	8.31	7.63	6.78	5.80	4.79	3.87	3.07
-35	2.69	3.72	4.81	5.70	6.42	7.11	7.76	8.33	8.87	9.43	9.93	10.16	9.98	9.36	8.45	7.49	6.58	5.65	4.62	3.56	2.62
-40	2.02	2.93	4.05	5.14	6.06	6.79	7.40	8.04	8.78	9.50	10.00	10.10	9.72	8.93	7.93	6.92	5.94	4.97	3.96	2.98	2.12
-45	1.52	2.25	3.15	4.13	5.12	5.97	6.62	7.20	7.82	8.40	8.76	8.79	8.45	7.81	6.96	5.96	4.90	3.89	3.01	2.27	1.67
-50	1.13	1.68	2.34	3.07	3.88	4.71	5.43	5.98	6.41	6.76	6.99	7.04	6.85	6.40	5.70	4.78	3.77	2.86	2.16	1.64	1.28





Table 7-5. Linear polarization.

$\theta_2$	DIHEDRAL ANGLE .75		WAVELENGTH 6943		GAIN FUNCTION (1.E+7)														
	0	180	0	180	5	10	15	20	25	30	35	40	45	50	60				
50	.62	1.20	1.59	2.06	2.50	2.80	2.90	2.85	2.73	2.62	2.51	2.36	2.14	1.88	1.60	1.31	1.03	.79	.62
45	.77	1.67	2.23	2.86	3.47	3.97	4.27	4.31	4.13	3.86	3.61	3.37	3.06	2.75	2.48	2.21	1.93	1.66	.98
40	.99	2.29	3.03	3.90	4.82	5.72	6.44	6.79	6.64	6.11	5.48	4.90	4.36	3.74	3.02	2.32	1.72	1.26	.93
35	1.28	2.91	3.90	5.16	6.57	8.05	9.41	10.32	10.41	9.67	8.48	7.28	6.22	5.20	4.14	3.13	2.28	1.55	1.20
30	1.59	3.45	4.80	6.55	8.43	10.31	12.16	13.67	14.22	13.47	11.81	9.96	8.29	6.78	5.31	3.96	2.87	2.09	1.53
25	1.88	3.99	5.74	7.84	9.75	11.42	13.24	15.11	16.16	15.62	13.77	11.58	9.66	7.94	6.21	4.60	3.35	2.50	1.89
20	2.13	4.58	6.57	8.60	9.93	10.84	12.34	14.53	16.06	15.64	13.58	11.31	9.63	8.26	6.67	5.00	3.68	2.83	2.23
15	2.30	4.99	6.91	8.43	8.92	9.29	11.12	14.25	16.38	15.59	12.62	9.83	8.48	7.44	6.00	4.54	3.26	2.50	1.89
10	2.36	4.94	6.49	7.33	7.28	8.05	11.48	16.54	19.47	17.70	12.80	8.60	7.07	6.09	4.80	3.50	2.28	1.66	1.20
5	2.36	4.54	5.66	5.96	5.84	7.68	13.28	20.49	24.16	21.22	14.13	8.15	6.01	5.36	4.20	3.00	1.93	1.26	.93
0	2.39	4.31	5.21	5.29	5.26	7.78	14.48	22.62	26.45	22.87	14.79	8.00	5.50	5.80	4.60	3.35	2.21	1.50	.88
-5	2.48	4.58	5.61	5.81	5.80	8.00	13.87	20.96	24.18	20.89	13.80	7.98	5.83	5.91	4.60	3.35	2.21	1.50	.88
-10	2.57	3.07	3.83	5.11	6.46	7.08	8.64	12.59	17.43	19.57	17.27	12.52	8.77	7.32	6.00	4.63	3.40	2.63	2.12
-15	2.56	3.17	4.03	5.37	6.94	8.07	9.94	12.46	15.35	16.55	15.20	12.62	10.63	9.51	8.31	6.46	4.50	3.13	2.41
-20	2.42	3.10	3.94	5.13	6.58	8.03	9.42	11.18	13.47	15.52	16.20	15.28	13.71	12.35	11.04	9.13	6.68	4.44	1.98
-25	2.15	2.83	3.60	4.51	5.61	6.98	8.80	11.20	13.84	15.79	16.24	15.28	13.77	12.32	10.75	8.69	6.31	4.25	1.82
-30	1.75	2.36	3.04	3.74	4.50	5.55	7.23	9.63	12.24	14.06	13.30	11.72	10.24	8.83	7.21	5.44	3.87	2.90	1.71
-35	1.29	1.76	2.33	2.92	3.51	4.26	5.48	7.27	9.23	10.56	10.69	9.78	8.48	7.35	6.41	5.43	4.34	3.29	1.94
-40	.88	1.19	1.61	2.12	2.66	3.27	4.08	5.14	6.35	6.98	7.01	6.42	5.62	4.95	4.42	3.87	3.23	2.55	1.44
-45	.83	1.10	1.48	1.95	2.48	3.04	3.84	4.45	4.45	4.45	4.18	3.78	3.40	3.05	2.67	2.24	1.81	1.44	1.03
-50	.58	.69	.86	1.11	1.44	1.82	2.21	2.54	2.78	2.92	2.94	2.85	2.65	2.39	2.10	1.79	1.50	1.24	.84

Table 7-6. Linear polarization.

$\theta_2$	DIHEDRAL ANGLE		WAVELENGTH		GAIN FUNCTION (1.E+7)																							
	1.25	1.25	6943	6943	-50	-45	-40	-35	-30	-25	-20	-15	-10	-5	0	5	10	15	20	25	30	35	40	45	50	$\theta_1$		
50	1.17	1.52	2.03	2.70	3.46	4.17	4.69	4.94	4.95	4.83	4.62	4.34	3.95	3.52	3.11	2.74	2.36	1.92	1.46	1.06								
45	1.54	2.00	2.64	3.45	4.34	5.18	5.81	6.15	6.19	6.01	5.74	5.44	5.07	4.60	4.04	3.46	2.89	2.33	1.78	1.30								
40	2.05	2.60	3.31	4.18	5.17	6.17	7.03	7.61	7.79	7.58	7.14	6.67	6.19	5.64	4.95	4.20	3.45	2.75	2.13	1.58								
35	2.59	3.15	3.83	4.75	5.93	7.25	8.52	9.52	10.03	9.92	9.30	8.46	7.63	6.80	5.89	4.93	4.02	3.21	2.51	1.92								
30	2.44	2.99	3.47	4.08	5.13	6.33	8.33	11.36	12.28	12.43	11.75	10.55	9.24	8.00	6.77	5.57	4.50	3.63	2.92	2.31								
25	2.73	3.21	3.56	4.15	5.39	7.18	9.00	10.56	11.96	13.13	13.62	13.05	11.68	10.11	8.66	7.28	5.93	4.77	3.91	3.27	2.70							
20	2.90	3.31	3.59	4.22	5.60	7.36	8.77	10.75	12.06	12.88	12.44	11.00	9.45	8.26	7.16	5.94	4.80	4.01	3.51	3.03								
15	2.96	3.33	3.59	4.25	5.57	6.92	7.54	8.72	10.51	11.72	11.13	9.24	7.62	6.91	6.50	5.72	4.73	4.01	3.62	3.23								
10	2.95	3.25	3.46	4.06	5.10	5.81	5.71	7.46	10.39	12.14	10.98	7.99	5.74	5.30	5.61	5.41	4.64	3.97	3.61	3.28								
5	2.91	3.01	3.07	3.68	4.00	4.38	4.55	4.08	4.51	4.73	4.99	4.20	4.60	4.06	4.82	5.06	4.51	3.87	3.50	3.19								
0	2.91	3.01	3.07	3.68	4.00	4.38	4.55	4.08	4.51	4.73	4.99	4.20	4.60	4.06	4.82	5.06	4.51	3.87	3.50	3.19								
-5	2.98	3.09	3.19	3.68	4.31	4.35	3.88	4.23	7.68	11.98	14.01	11.93	7.67	7.83	4.21	3.54	4.27	3.67	3.32	3.03								
-10	3.08	3.30	3.55	4.20	5.08	5.51	5.38	5.82	7.94	10.86	12.21	10.81	8.03	6.13	5.68	5.56	4.87	3.88	3.23	2.97	2.79							
-15	3.12	3.53	3.94	4.68	5.71	6.58	7.06	7.73	9.23	11.04	11.84	11.06	9.57	8.51	7.86	6.88	5.38	3.97	3.19	2.90	2.70							
-20	3.07	3.64	4.18	4.90	5.86	6.95	8.05	9.38	11.01	12.46	11.99	12.44	11.44	10.51	9.42	7.78	5.80	4.19	3.29	2.87	2.55							
-25	2.87	3.54	4.19	4.86	5.63	6.64	8.01	9.83	11.81	13.59	13.70	13.09	12.03	10.91	9.52	7.81	5.92	4.40	3.44	2.83	2.10							
-30	2.49	3.16	3.88	4.57	5.22	6.04	7.27	9.01	10.91	12.27	12.58	11.92	10.84	9.72	8.53	7.16	5.72	4.48	3.52	2.75	2.10							
-35	1.98	2.55	3.26	4.00	4.69	5.41	6.36	7.64	9.02	10.00	10.19	9.66	8.81	7.97	7.16	6.25	5.24	4.26	3.37	2.58	1.89							
-40	1.48	1.90	2.49	3.22	3.98	4.73	5.51	6.38	7.22	7.80	7.92	7.61	7.08	6.52	5.93	5.25	4.48	3.69	2.96	2.28	1.69							
-45	1.12	1.42	1.85	2.45	3.16	3.91	4.64	5.31	5.86	6.22	6.33	6.18	5.84	5.38	4.82	4.19	3.53	2.91	2.36	1.88	1.45							
-50	.91	1.13	1.44	1.86	2.40	3.02	3.65	4.23	4.69	4.99	5.10	5.00	4.71	4.25	3.69	3.12	2.58	2.13	1.76	1.44	1.16							



Table 7-8. Linear polarization, mixed dihedral angles.

$\theta_2$	GAIN FUNCTION (1.E+7)																					
	-50	-45	-40	-35	-30	-25	-20	-15	-10	-5	0	5	10	15	20	25	30	35	40	45	50	$\theta_1$
DIHEDRAL ANGLE 1.25 WAVELENGTH 6943																						
50	1.07	1.28	1.57	1.98	2.56	3.23	3.85	4.29	4.49	4.51	4.48	4.43	4.29	4.01	3.61	3.21	2.84	2.46	2.04	1.59	1.18	
45	1.39	1.67	2.05	2.59	3.32	4.11	4.81	5.28	5.46	5.44	5.36	5.30	5.24	5.03	4.60	4.02	3.42	2.85	2.30	1.78	1.31	
40	1.78	2.17	2.65	3.29	4.12	5.04	5.88	6.49	6.80	6.83	6.71	6.55	6.38	6.11	5.61	4.88	4.05	3.27	2.57	1.95	1.45	
35	2.21	2.68	3.18	3.84	4.77	5.94	7.22	8.09	8.76	9.07	9.02	8.67	8.17	7.55	6.77	5.79	4.73	3.73	2.88	2.18	1.64	
30	2.58	3.04	3.44	4.04	5.12	6.65	8.27	9.67	10.76	11.48	11.66	11.18	10.25	9.13	7.94	6.66	5.35	4.17	3.20	2.46	1.92	
25	2.93	3.20	3.44	3.96	5.20	7.02	8.83	10.29	11.51	12.55	13.04	12.59	11.38	9.96	8.59	7.21	5.78	4.47	3.47	2.77	2.24	
20	2.92	3.22	3.35	3.84	5.15	6.92	8.38	9.37	10.22	11.72	12.54	12.14	10.78	9.35	8.28	7.25	5.97	4.67	3.68	3.04	2.58	
15	2.86	3.17	3.32	3.79	4.99	6.31	7.03	7.44	8.57	10.47	11.72	11.11	9.24	7.70	7.13	6.81	5.99	4.82	3.85	3.27	2.84	
10	2.74	3.09	3.29	3.74	4.38	5.37	5.37	4.72	7.92	12.47	14.82	12.87	8.41	5.09	4.50	5.23	5.42	4.74	3.92	3.39	2.98	
5	2.78	3.03	3.29	3.80	4.32	4.17	3.59	4.47	8.31	13.52	16.07	13.74	8.62	4.75	3.87	4.57	4.86	4.34	3.66	3.23	2.88	
0	2.74	3.04	3.38	4.01	4.65	4.57	3.98	4.65	8.00	12.60	14.87	12.86	8.46	5.14	4.28	4.61	4.55	3.91	3.33	3.03	2.77	
-5	2.75	3.08	3.51	4.27	5.12	5.39	5.09	5.50	7.77	10.99	12.66	11.45	8.68	6.63	5.96	5.63	4.80	3.77	3.12	2.87	2.68	
-10	2.73	3.14	3.62	4.42	5.42	6.16	6.50	7.13	8.72	10.75	11.81	11.27	9.95	8.94	8.23	7.12	5.47	3.96	3.12	2.80	2.60	
-15	2.67	3.17	3.75	4.45	5.44	6.51	7.50	8.90	10.51	11.97	12.55	12.15	11.40	10.72	9.78	8.13	6.04	4.28	3.27	2.79	2.46	
-20	2.54	3.12	3.75	4.45	5.32	6.45	7.92	9.73	11.54	12.76	12.95	12.32	11.50	10.73	9.70	8.09	6.16	4.52	3.45	2.78	2.27	
-25	2.28	2.89	3.60	4.33	5.12	6.11	7.49	9.20	10.82	11.72	11.60	10.78	9.87	9.14	8.36	7.22	5.84	4.54	3.53	2.73	2.08	
-30	1.91	2.46	3.17	3.94	4.73	5.58	6.63	7.84	8.90	9.38	9.12	8.38	7.66	7.17	6.73	6.08	5.20	4.25	3.37	2.59	1.93	
-35	1.54	1.98	2.59	3.31	4.09	4.88	5.66	6.40	6.96	7.15	6.93	6.47	6.03	5.72	5.42	4.96	4.33	3.63	2.95	2.33	1.77	
-40	1.25	1.60	2.07	2.66	3.34	4.04	4.69	5.22	5.56	5.68	5.60	5.39	5.11	4.79	4.39	3.89	3.35	2.82	2.36	1.94	1.54	
-45	1.06	1.35	1.71	2.15	2.65	3.19	3.73	4.18	4.51	4.69	4.72	4.60	4.33	3.91	3.41	2.89	2.43	2.06	1.76	1.48	1.22	
-50																						

Table 7-9. Circular polarization.

DIPEDRAL ANGLE	WAVELENGTH 5320																				
	GAIN FUNCTION (1.E+7)																				
.75	0	5	10	15	20	25	30	35	40	45	50										
50	1.00	1.07	1.12	1.22	1.40	1.64	1.85	1.92	1.78	1.53	1.40	1.39	1.25	1.41	1.97	1.81	.84	.84	.97	.84	.70
45	1.27	1.42	1.61	1.96	2.48	3.00	3.31	3.33	3.08	2.72	2.45	2.24	1.89	1.41	1.97	1.38	1.06	.84	.90	.84	.76
40	1.68	1.94	2.36	3.10	4.03	4.87	5.30	5.21	4.82	4.41	4.04	3.55	2.80	1.97	1.81	1.38	1.06	.84	.90	.84	.70
35	2.33	2.81	3.48	4.44	5.61	6.74	7.41	7.23	6.51	5.84	5.48	4.99	4.01	2.78	2.77	2.27	1.81	1.27	.97	.97	.72
30	3.34	4.15	5.01	6.12	7.52	9.13	10.39	10.38	9.03	7.54	6.84	6.53	5.70	4.22	4.20	3.42	2.76	1.82	1.27	.97	.72
25	4.57	5.67	6.88	8.62	10.66	12.74	14.52	14.87	13.20	10.86	9.40	8.69	7.70	6.04	6.04	5.43	4.20	2.76	1.82	1.27	.97
20	5.65	7.08	9.17	12.16	14.53	15.75	16.75	17.16	16.05	14.32	13.05	11.70	9.71	7.48	7.48	6.63	5.43	3.67	2.32	1.46	.72
15	6.31	8.34	11.70	15.59	16.92	15.91	15.71	16.25	15.79	15.38	15.71	14.65	11.55	8.33	8.33	7.66	6.06	4.28	2.71	1.63	.72
10	6.49	9.19	13.55	17.35	17.13	15.64	17.53	19.74	18.06	15.89	16.43	16.25	12.90	8.92	8.92	8.34	6.34	4.59	3.09	1.93	.72
5	6.38	9.44	14.17	17.47	16.87	18.17	25.67	30.75	25.87	18.28	16.23	16.27	13.43	9.33	9.33	8.46	6.46	4.66	3.32	2.24	.72
0	6.38	9.36	14.07	17.18	16.95	20.35	30.80	36.86	28.88	19.32	15.74	15.82	13.48	9.56	9.56	8.49	6.49	4.50	3.22	2.25	.72
-5	6.53	9.22	13.74	16.95	16.60	18.22	25.19	28.96	23.46	16.60	15.52	16.02	13.51	9.62	9.62	8.53	6.53	4.34	2.96	2.03	.72
-10	6.52	8.95	13.03	16.27	15.86	14.91	15.76	17.93	15.65	14.56	16.29	16.35	13.05	9.27	9.27	8.47	6.47	4.29	2.78	1.82	.72
-15	8.41	11.78	14.63	14.89	14.17	14.79	15.45	15.17	15.76	16.71	15.13	11.46	8.33	8.33	6.11	6.11	4.12	2.57	1.62	1.34	.72
-20	5.36	7.48	10.08	12.11	12.79	13.53	15.45	16.99	16.80	15.85	14.51	12.06	9.21	7.11	7.11	5.41	3.63	2.19	1.34	1.11	.72
-25	4.19	6.05	8.06	9.34	9.74	10.62	12.70	14.41	14.12	12.62	10.49	8.65	7.06	5.77	5.77	4.41	2.94	1.78	1.11	.99	.72
-30	2.94	4.38	5.97	6.99	7.21	7.50	8.57	9.72	9.73	8.62	7.25	6.10	5.14	4.24	4.24	3.28	2.28	1.48	.99	.84	.72
-35	2.01	3.02	4.20	5.09	5.46	5.66	6.20	6.92	7.11	6.46	5.35	4.28	3.48	2.87	2.87	2.32	1.75	1.22	.84	.84	.72
-40	1.42	2.09	2.88	3.46	3.78	4.13	4.69	5.24	5.33	4.74	3.75	2.87	2.32	1.97	1.97	1.64	1.29	.92	.63	.63	.72
-45	.98	1.39	1.93	2.22	2.30	2.56	3.06	3.44	3.39	2.92	2.30	1.84	1.58	1.38	1.38	1.16	.94	.71	.51	.51	.72
-50	.68	.90	1.29	1.48	1.45	1.54	1.81	1.98	1.91	1.67	1.42	1.25	1.13	1.00	1.00	.89	.79	.67	.45	.45	.72

Table 7-10. Circular polarization.

$\theta_2$	DIHEDRAL ANGLE		WAVELENGTH		GAIN FUNCTION		WAVELENGTH		GAIN FUNCTION		WAVELENGTH		GAIN FUNCTION		WAVELENGTH		GAIN FUNCTION		WAVELENGTH		GAIN FUNCTION		
	1.25	1.25	1.25	1.25	1.25	1.25	1.25	1.25	1.25	1.25	1.25	1.25	1.25	1.25	1.25	1.25	1.25	1.25	1.25	1.25	1.25	1.25	
50	1.05	1.42	1.70	1.94	2.22	2.57	2.98	3.42	3.78	3.90	3.67	3.26	2.99	2.79	2.41	1.85	1.40	1.14	0.90	0.66			
45	1.28	1.84	2.33	2.77	3.26	3.87	4.56	5.22	5.67	5.73	5.37	4.82	4.39	4.05	3.50	2.75	2.07	1.56	1.10	0.75			
40	1.74	2.42	3.03	3.64	4.44	5.45	6.50	7.33	7.72	7.53	7.21	6.70	6.22	5.64	4.79	3.79	2.90	2.13	1.43	0.93			
35	2.40	3.19	3.91	4.67	5.66	6.83	7.95	8.76	9.05	8.75	8.20	7.82	7.61	7.14	6.15	4.88	3.77	2.86	2.03	1.38			
30	2.11	3.12	4.20	5.21	6.06	7.49	8.68	9.52	9.91	9.49	8.58	7.98	7.61	7.14	6.15	4.88	3.77	2.86	2.03	1.38			
25	2.47	3.84	5.40	6.76	7.49	8.79	9.63	10.74	11.43	11.08	9.79	8.67	8.52	8.90	8.84	7.90	6.41	4.95	3.70	2.64			
20	2.80	4.48	6.48	8.04	8.52	9.88	11.24	11.99	12.21	11.81	10.77	9.92	9.77	9.82	9.58	8.86	7.53	5.82	4.18	2.89			
15	3.05	4.85	7.04	8.65	9.09	9.77	11.44	12.21	11.24	10.20	9.43	9.84	10.77	10.80	9.90	9.00	7.94	6.29	4.46	3.00			
10	3.19	4.87	6.99	8.58	9.28	10.57	12.24	11.58	9.19	8.39	8.74	8.36	8.74	10.56	11.26	10.09	8.84	7.55	4.84	3.33			
5	3.35	4.86	6.76	8.26	9.16	10.78	12.04	10.41	8.55	10.32	12.32	10.53	8.57	9.75	11.06	10.20	8.79	7.81	6.68	5.26			
0	3.60	5.05	6.82	8.16	9.02	10.60	11.60	9.88	8.93	12.32	14.97	12.12	8.68	9.33	10.90	10.33	8.91	7.80	6.69	5.44			
-5	3.70	5.20	7.04	8.34	9.02	10.40	11.46	9.96	8.77	10.25	11.78	9.79	8.24	9.89	11.34	10.51	9.09	7.94	6.72	5.40			
-10	3.51	5.03	6.97	8.40	9.07	10.36	10.33	9.30	7.91	8.30	8.11	9.14	11.32	11.78	10.36	8.11	6.77	5.26	3.68				
-15	3.25	4.66	6.54	8.09	8.97	9.96	10.93	10.53	9.30	9.07	9.66	10.30	11.37	12.12	11.24	9.69	8.82	8.00	6.56	4.91			
-20	3.04	4.26	5.84	7.37	8.55	9.55	10.17	9.96	9.09	10.46	11.82	12.05	11.09	9.92	8.94	8.37	7.45	5.91	4.29	2.86			
-25	2.66	3.67	4.92	6.28	7.64	8.79	9.30	8.98	8.73	9.43	10.46	10.68	10.08	9.32	8.71	8.21	7.55	6.42	4.97	3.59			
-30	2.04	2.84	3.88	5.10	6.43	7.67	8.35	8.26	7.97	8.22	8.86	9.12	8.81	8.28	7.75	7.10	6.22	5.15	4.03	2.98			
-35	1.39	2.03	2.96	4.07	5.27	6.38	7.10	7.37	7.52	7.94	8.51	8.71	8.28	7.45	6.54	5.67	4.84	4.03	3.20	2.37			
-40	0.95	1.46	2.22	3.13	4.16	5.06	5.55	5.81	6.28	7.04	7.67	7.66	6.95	5.93	5.02	4.32	3.71	3.10	2.43	1.73			
-45	0.73	1.11	1.60	2.18	2.96	3.71	4.04	4.13	4.53	5.28	5.79	5.63	4.92	4.12	3.51	3.07	2.66	2.22	1.74	1.23			
-50	0.62	0.87	1.13	1.43	1.93	2.52	2.82	2.87	3.09	3.59	3.92	3.77	3.31	2.80	2.39	2.05	1.75	1.51	1.27	0.96			







Table 7-13. Circular polarization.

θ <sub>2</sub>	GAIN FUNCTION (1.E+7)																				
	DIHEDRAL ANGLE °75					DIHEDRAL ANGLE °75					DIHEDRAL ANGLE °75					WAVELENGTH 6943					
50	.82	.93	1.03	1.17	1.40	1.74	2.13	2.51	2.80	2.91	2.84	2.64	2.44	2.30	2.18	2.00	1.71	1.34	.99	.75	.60
45	1.00	1.19	1.38	1.61	1.93	2.34	2.81	3.32	3.76	4.00	3.91	3.56	3.16	2.88	2.73	2.56	2.24	1.77	1.28	.91	.68
40	1.24	1.57	1.89	2.24	2.67	3.18	3.77	4.46	5.17	5.64	5.62	5.07	4.31	3.71	3.40	3.23	2.94	2.43	1.81	1.26	.89
35	1.53	2.02	2.48	2.99	3.64	4.42	5.27	6.19	7.16	7.90	8.01	7.35	6.23	5.21	4.58	4.24	3.87	3.28	2.53	1.80	1.26
30	1.85	2.46	3.07	3.84	4.92	6.15	7.26	8.20	9.12	9.91	10.14	9.35	8.39	7.22	6.37	5.74	5.05	4.19	3.25	2.38	1.70
25	2.13	2.85	3.64	4.81	6.46	8.14	9.23	9.69	10.05	10.56	10.83	10.48	9.68	8.22	7.30	6.53	5.89	4.96	3.83	2.84	2.07
20	2.30	3.15	4.20	5.64	8.01	9.85	10.49	10.17	9.95	10.32	10.69	10.47	9.94	9.73	9.71	9.16	8.78	7.73	6.48	5.13	3.83
15	2.35	3.32	4.65	6.71	9.17	10.83	10.90	10.23	10.38	11.59	12.42	11.84	10.61	10.11	10.38	10.20	9.31	8.61	7.10	5.65	4.49
10	2.34	3.37	4.91	7.23	9.74	11.10	10.94	10.48	12.82	16.07	17.77	16.23	13.02	10.89	10.58	10.36	9.35	8.70	7.00	5.49	4.58
5	2.44	3.41	5.01	7.43	9.85	11.05	11.15	12.17	16.32	21.81	24.32	21.63	16.11	11.90	10.54	10.36	9.22	8.70	7.30	5.15	4.50
0	2.44	3.41	5.01	7.43	9.85	10.97	11.15	12.90	18.01	24.29	28.93	23.61	17.10	12.07	10.31	10.09	9.22	8.70	7.32	5.22	4.42
-5	2.58	3.46	4.97	7.33	9.74	10.89	10.96	12.18	16.21	21.23	23.14	20.13	14.79	11.03	10.07	10.08	9.19	8.71	7.28	5.22	4.42
-10	2.65	3.48	4.86	7.08	9.44	10.63	10.47	10.59	12.50	15.21	16.08	14.10	11.20	9.83	10.13	10.31	9.17	8.71	7.11	5.09	4.38
-15	2.68	3.47	4.86	6.63	8.81	10.03	9.89	9.42	9.83	10.82	11.05	10.13	9.28	9.80	10.45	10.34	8.79	8.63	6.63	4.76	4.33
-20	2.68	3.47	4.86	6.01	7.86	9.02	8.95	8.95	9.20	9.81	10.04	9.71	9.57	10.03	10.37	9.08	7.82	7.82	5.81	4.25	4.21
-25	2.68	3.47	4.86	5.25	6.67	7.63	8.02	8.36	9.15	10.15	10.68	10.21	10.09	9.77	9.25	8.03	6.41	6.41	4.84	3.67	3.00
-30	1.70	2.36	3.27	4.37	5.40	6.06	6.44	6.99	8.06	9.32	10.05	9.88	9.11	8.21	7.25	6.14	4.94	3.90	3.09	2.39	1.72
-35	1.31	1.83	2.56	3.43	4.18	4.63	4.84	5.22	6.05	7.08	7.75	6.94	6.04	5.19	4.41	3.68	3.04	2.49	1.89	1.53	1.43
-40	.96	1.33	1.88	2.54	3.14	3.50	3.63	3.79	4.20	4.81	5.29	5.32	4.90	4.28	3.67	3.14	2.67	2.26	1.89	1.53	1.18
-45	.72	.97	1.35	1.84	2.31	2.64	2.79	2.87	3.05	3.38	3.71	3.82	3.62	3.20	2.71	2.26	1.90	1.62	1.39	1.18	.97
-50	.60	.75	1.02	1.36	1.70	1.95	2.09	2.19	2.33	2.56	2.80	2.91	2.78	2.44	2.02	1.63	1.35	1.17	1.04	.92	.79

Table 7-14. Circular polarization.

$\theta_2$	DIHEDRAL ANGLE 1.25		WAVELENGTH 6943		GAIN FUNCTION (1.E+7)		WAVELENGTH 6943		DIHEDRAL ANGLE 1.25		$\theta_1$										
50	1.20	1.40	1.61	1.90	2.30	2.79	3.32	3.80	4.13	4.25	4.15	3.92	3.68	3.47	3.27	3.00	2.61	2.11	1.62	1.23	0.94
45	1.52	1.81	2.11	2.47	2.92	3.45	4.02	4.55	4.94	5.07	4.91	4.57	4.23	4.02	3.89	3.70	3.50	2.71	2.08	1.56	1.18
40	1.96	2.39	2.77	3.15	3.59	4.10	4.67	5.28	5.81	6.05	5.87	5.35	4.79	4.44	4.35	4.30	4.04	3.48	2.76	2.09	1.57
35	2.49	3.07	3.50	3.87	4.30	4.88	5.57	6.33	7.04	7.45	7.31	6.65	5.80	5.20	4.98	4.96	4.81	4.33	3.60	2.80	2.13
30	3.03	3.72	4.17	4.57	5.15	5.97	6.85	7.66	8.35	8.78	8.70	8.05	7.13	6.41	6.04	5.86	5.59	5.09	4.36	3.52	2.71
25	3.46	4.22	4.72	5.27	6.19	7.32	8.21	8.65	8.88	9.04	8.97	8.52	7.93	7.51	7.28	6.95	6.37	5.63	4.84	4.01	3.16
20	3.70	4.52	5.14	5.98	7.29	8.57	9.08	8.76	8.29	8.16	7.93	7.48	6.76	6.41	6.17	5.84	5.09	4.25	3.43	2.58	1.72
15	3.72	4.80	5.41	6.57	8.15	9.30	9.19	8.22	7.59	7.78	8.06	7.81	7.48	7.74	8.30	8.64	7.90	6.49	5.21	4.32	3.60
10	3.63	4.53	5.49	6.90	8.56	9.41	8.85	7.89	8.10	9.52	10.41	9.65	8.22	7.94	8.92	9.45	8.63	6.62	5.30	4.33	3.58
5	3.56	4.43	5.44	6.94	8.57	9.21	8.55	8.12	9.67	12.55	14.02	12.55	9.66	7.94	8.82	8.45	7.94	6.71	5.39	4.35	3.53
0	3.62	4.40	5.36	6.84	8.43	9.00	8.42	8.37	10.56	14.01	15.59	13.70	10.15	7.93	7.82	8.32	8.03	6.79	5.47	4.40	3.51
-5	3.75	4.46	5.32	6.71	8.26	8.90	8.34	8.08	9.66	12.31	13.42	11.75	8.97	7.55	7.89	8.46	8.07	6.73	5.47	4.45	3.54
-10	3.82	4.51	5.28	6.54	8.04	8.77	8.25	7.51	7.87	9.10	9.59	8.63	7.64	7.43	8.34	8.78	8.07	6.42	5.32	4.43	3.55
-15	3.74	4.46	5.20	6.33	7.69	8.48	8.14	7.28	6.95	7.27	7.47	7.23	7.25	8.02	8.90	8.87	7.79	6.42	5.32	4.43	3.55
-20	3.52	4.28	5.04	6.04	7.18	7.91	7.84	7.37	7.22	7.55	7.90	8.04	8.28	8.77	8.97	8.34	7.09	5.88	5.02	4.29	3.45
-25	3.16	3.93	4.73	5.64	6.53	7.09	7.16	7.13	7.50	8.24	8.86	9.04	8.92	8.67	8.16	7.24	6.15	5.27	4.64	4.00	3.20
-30	2.70	3.43	4.23	5.07	5.78	6.14	6.18	6.28	6.84	7.74	8.45	8.57	8.16	7.50	6.75	5.96	5.24	4.67	4.17	3.57	2.81
-35	2.17	2.81	3.56	4.35	4.98	5.26	5.23	5.23	5.60	6.29	6.88	7.00	6.82	6.01	5.40	4.87	4.42	4.00	3.55	3.00	2.35
-40	1.68	2.21	2.86	3.57	4.16	4.47	4.50	4.46	4.61	5.02	5.45	5.60	5.39	4.96	4.48	4.04	3.64	3.25	2.84	2.38	1.90
-45	1.29	1.73	2.26	2.85	3.37	3.70	3.84	3.90	4.05	4.35	4.68	4.83	4.59	4.30	3.80	3.31	2.88	2.50	2.17	1.85	1.52
-50	1.01	1.35	1.78	2.24	2.64	2.91	3.08	3.24	3.49	3.82	4.12	4.21	4.03	3.60	3.08	2.59	2.19	1.90	1.66	1.43	1.20





Table 8(1-16). Gain function vs. velocity aberration. The average and rms fluctuations are computed around a circle in the far field whose radius is the velocity aberration listed in the first column in microradians. Table 8-1. Linear polarization.

DIHEDRAL ANGLE .75 WAVELENGTH 5320

AVERAGE GAIN FUNCTION (1.E+7)

0	36.03	*	*
5	28.27	*	*
10	19.18	*	*
15	16.16	*	*
20	16.40	*	*
25	14.15	*	*
30	10.17	*	*
35	7.12	*	*
40	5.02	*	*
45	3.28	*	*
50	2.03	*	*

R.M.S. FLUCTUATION

0	0.00	*	*
5	1.39	*	*
10	4.24	*	*
15	6.17	*	*
20	5.98	*	*
25	4.35	*	*
30	2.59	*	*
35	1.32	*	*
40	.56	*	*
45	.22	*	*
50	.16	*	*

Table 8-2. Linear polarization.

DIHEDRAL ANGLE 1.25 WAVELENGTH 5320

AVERAGE GAIN FUNCTION (1.E+7)

0	14.34	*
5	11.25	*
10	8.70	*
15	9.66	*
20	11.26	*
25	10.70	*
30	9.36	*
35	8.43	*
40	7.19	*
45	5.47	*
50	3.84	*

R.M.S. FLUCTUATION

0	0.00	*
5	.74	*
10	2.33	*
15	3.36	*
20	3.49	*
25	3.17	*
30	2.78	*
35	2.28	*
40	1.62	*
45	.92	*
50	.39	*

Table 8-3. Linear polarization.

DIHEDRAL ANGLE 1.75 WAVELENGTH 5320

AVERAGE GAIN FUNCTION (1.E+7)

0	5.14
5	3.81
10	3.09
15	4.22
20	5.49
25	5.88
30	6.37
35	7.05
40	7.09
45	6.49
50	5.60

*
*
*
*
*
*
*
*
*
*
*

R.M.S. FLUCTUATION

0	0.00
5	.21
10	.54
15	.66
20	.76
25	1.05
30	1.47
35	1.76
40	1.73
45	1.43
50	1.01

*
*
*
*
*
*
*
*
*
*
*

Table 8-4. Linear polarization, mixed dihedral angles.

DIHEDRAL ANGLE  $\overline{1.25}$  WAVELENGTH 5320

AVERAGE GAIN FUNCTION (1.E+7)

0	18.12
5	14.22
10	10.35
15	10.22
20	11.27
25	10.38
30	8.70
35	7.54
40	6.40
45	5.02
50	3.77

\*

\*

\*

\*

\*

\*

\*

R.M.S. FLUCTUATION

0	0.00
5	.82
10	2.51
15	3.58
20	3.54
25	2.96
30	2.37
35	1.85
40	1.36
45	.84
50	.46

\*

\*

\*

\*

\*

\*

\*

\*

\*







Table 8-7. Linear polarization.

DIHEDRAL ANGLE 1.75 WAVELENGTH 6943

AVERAGE GAIN FUNCTION (1.E+7)

0	6.93	*
5	5.92	*
10	4.62	*
15	4.29	*
20	5.09	*
25	5.95	*
30	6.04	*
35	5.60	*
40	5.22	*
45	4.99	*
50	4.62	*

R.M.S. FLUCTUATION

0	0.00	*
5	.23	*
10	.79	*
15	1.34	*
20	1.65	*
25	1.72	*
30	1.68	*
35	1.62	*
40	1.54	*
45	1.40	*
50	1.16	*





Table 8-10. Circular polarization.

DIHEDRAL ANGLE 1.25 WAVELENGTH 5320

AVERAGE GAIN FUNCTION (1.E+7)

0	14.97	*
5	11.66	*
10	8.79	*
15	9.58	*
20	11.15	*
25	10.57	*
30	9.25	*
35	8.38	*
40	7.19	*
45	5.46	*
50	3.83	*

R.M.S. FLUCTUATION

0	0.00	*
5	.29	*
10	.25	*
15	.39	*
20	.67	*
25	.59	*
30	.45	*
35	.37	*
40	.35	*
45	.29	*
50	.22	*

Table 8-11. Circular polarization.

DIHEDRAL ANGLE 1.75 WAVELENGTH 5320

AVERAGE GAIN FUNCTION (1.E+7)

0	5.52	*
5	4.05	*
10	3.15	*
15	4.20	*
20	5.45	*
25	5.82	*
30	6.32	*
35	7.02	*
40	7.06	*
45	6.44	*
50	5.55	*

R.M.S. FLUCTUATION

0	0.00	*
5	.10	*
10	.10	*
15	.27	*
20	.39	*
25	.33	*
30	.23	*
35	.22	*
40	.24	*
45	.22	*
50	.19	*

Table 8-12. Circular polarization, mixed dihedral angles.

DIHEDRAL ANGLE  $\overline{1.25}$  WAVELENGTH 5320

AVERAGE GAIN FUNCTION (1.E+7)

0 19.26  
 5 15.02  
 10 10.62  
 15 10.08  
 20 11.00  
 25 10.18  
 30 8.63  
 35 7.56  
 40 6.40  
 45 4.98  
 50 3.72

\*  
 \*  
 \*  
 \*  
 \*  
 \*  
 \*  
 \*  
 \*  
 \*

R.M.S. FLUCTUATION

0 0.00 \*  
 5 .61 \*  
 10 .53 \*  
 15 .47 \*  
 20 .58 \*  
 25 .50 \*  
 30 .37 \*  
 35 .35 \*  
 40 .41 \*  
 45 .30 \*  
 50 .27 \*







Table 8-15. Circular polarization.

DIHEDRAL ANGLE 1.75 WAVELENGTH 6943

AVERAGE GAIN FUNCTION (1.E+7)

0	7.31	*
5	6.22	*
10	4.77	*
15	4.31	*
20	5.06	*
25	5.90	*
30	5.98	*
35	5.53	*
40	5.16	*
45	4.95	*
50	4.60	*

R.M.S. FLUCTUATION

0	0.00	*
5	.12	*
10	.12	*
15	.11	*
20	.26	*
25	.39	*
30	.39	*
35	.31	*
40	.24	*
45	.20	*
50	.21	*



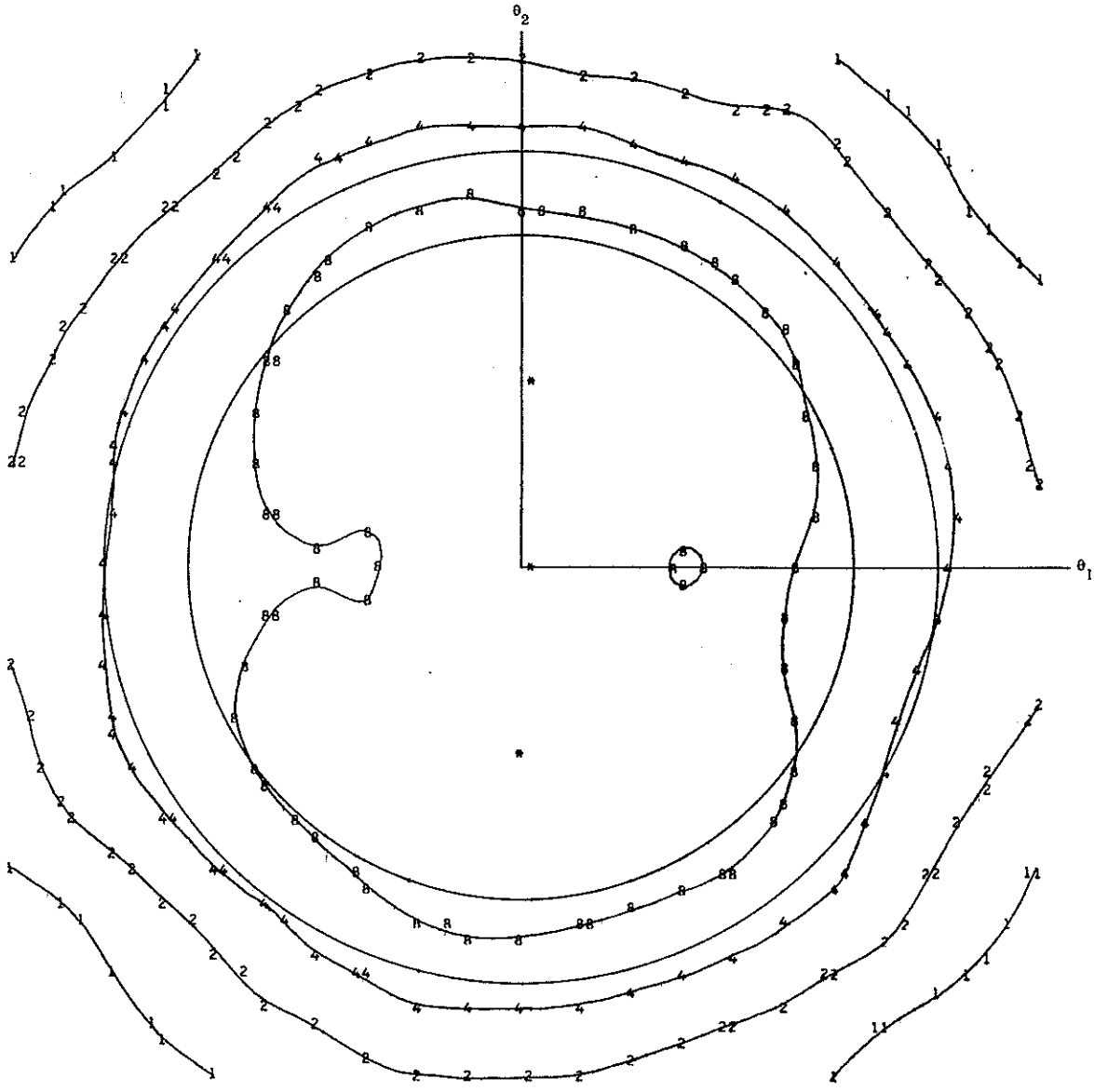


Figure 9(1-16). Contour plots of the gain-function matrices given in Table 7. Circles 32 and 41  $\mu$ rad in radius are shown to mark the minimum and maximum values of velocity aberration. The numbers are the gain in units of  $10^4$ . The dihedral-angle offset  $\delta$  and the wavelength  $\lambda$  are given for each figure. Figure 9-1. Linear polarization,  $\delta = 0^\circ 75$ ,  $\lambda = 5320 \text{ \AA}$ .

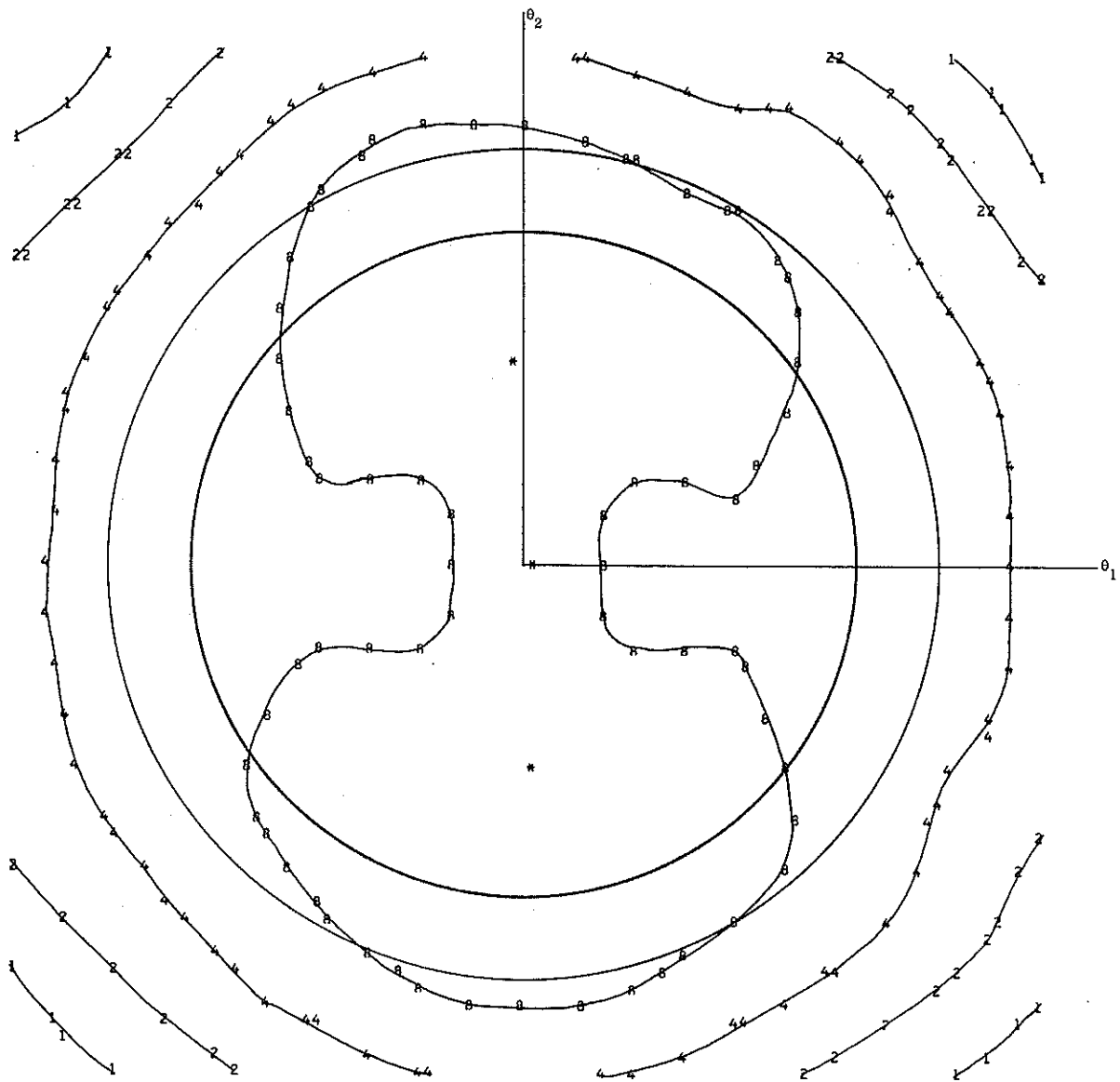


Figure 9-2. Linear polarization,  $\delta = 1''25$ ,  $\lambda = 5320 \text{ \AA}$ .

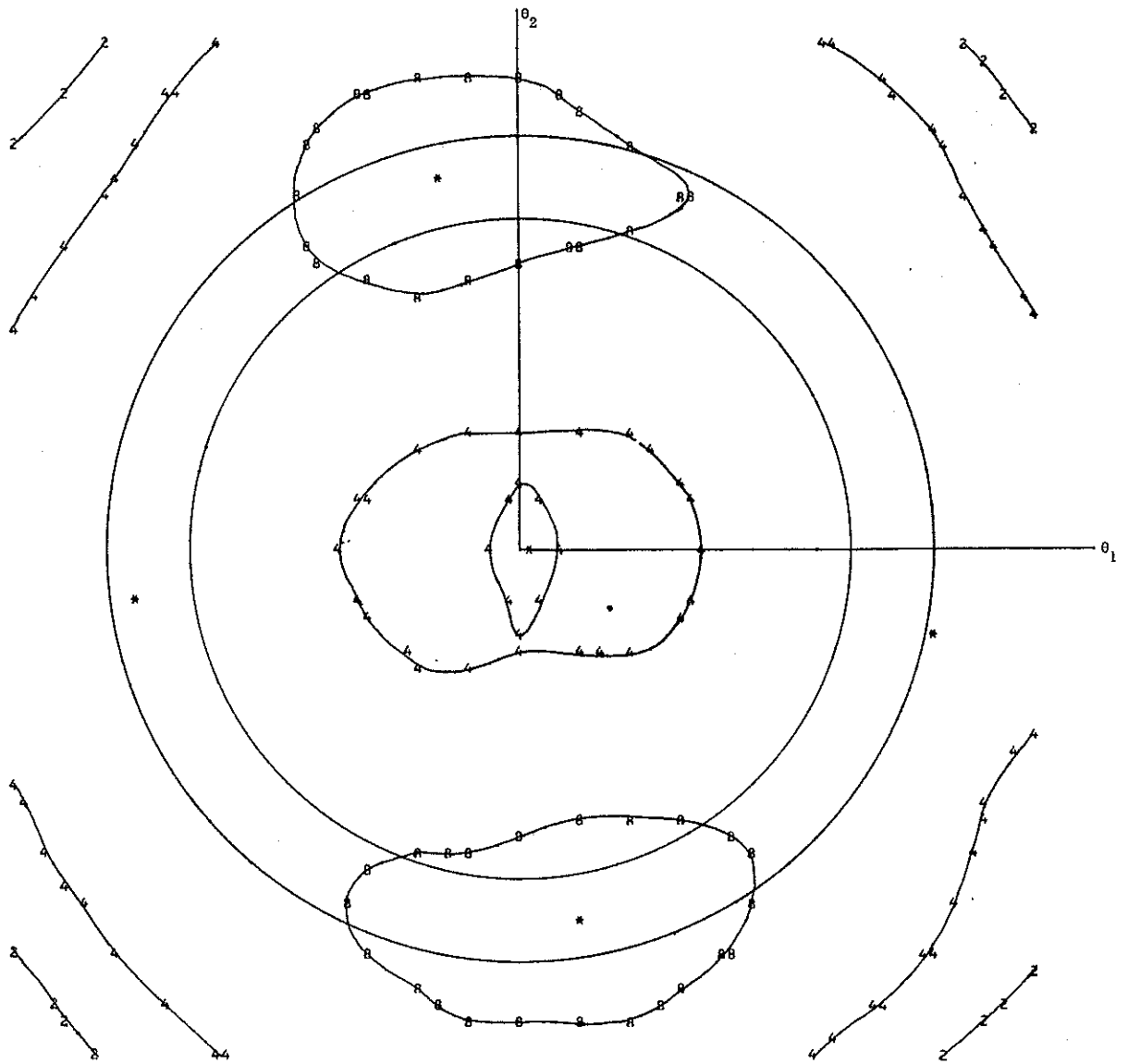


Figure 9-3. Linear polarization,  $\delta = 1''75$ ,  $\lambda = 5320 \text{ \AA}$ .

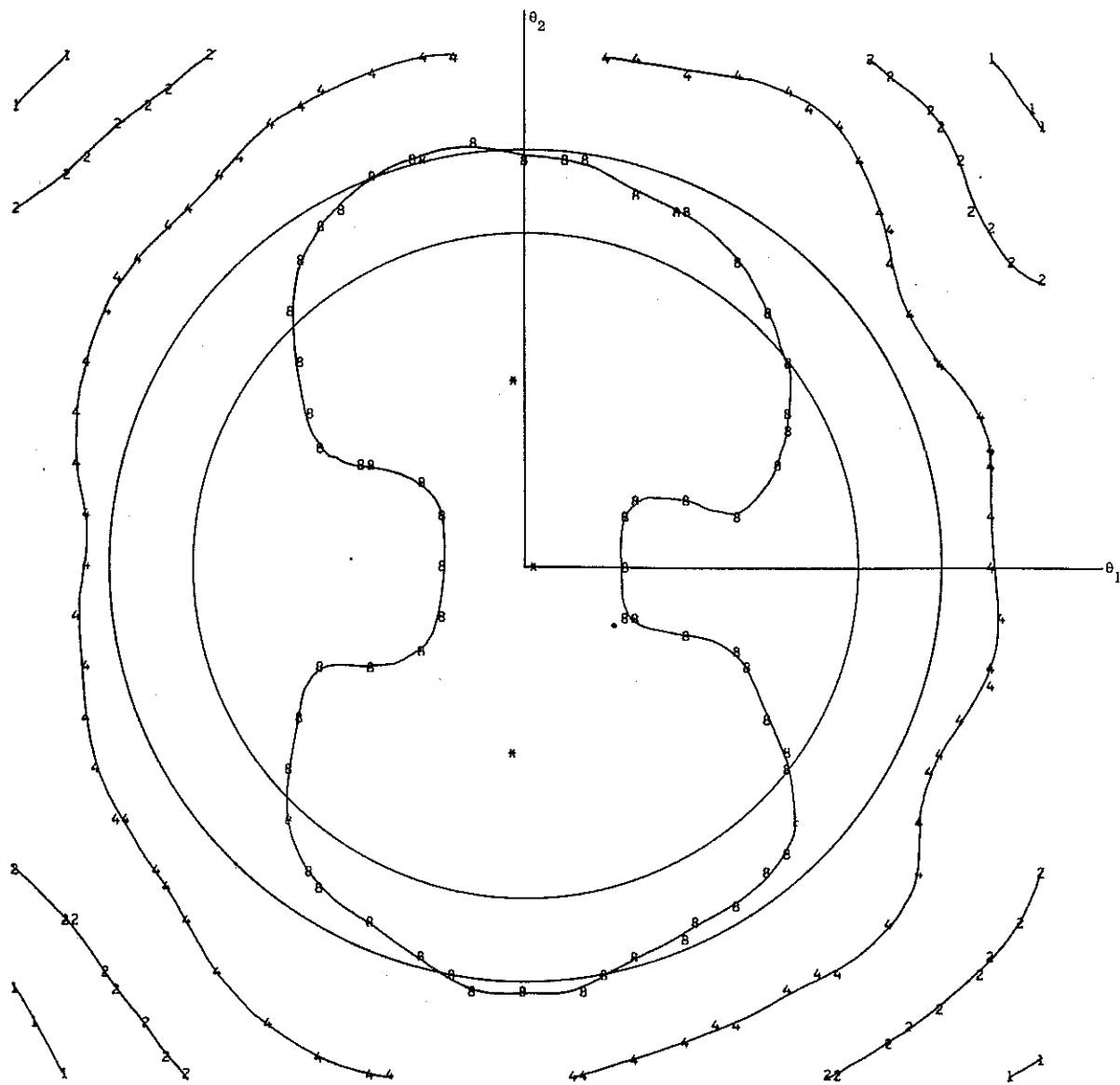


Figure 9-4. Linear polarization,  $\bar{\delta} = 1^{\circ}25'$  (mixed dihedral angles),  $\lambda = 5320 \text{ \AA}$ .



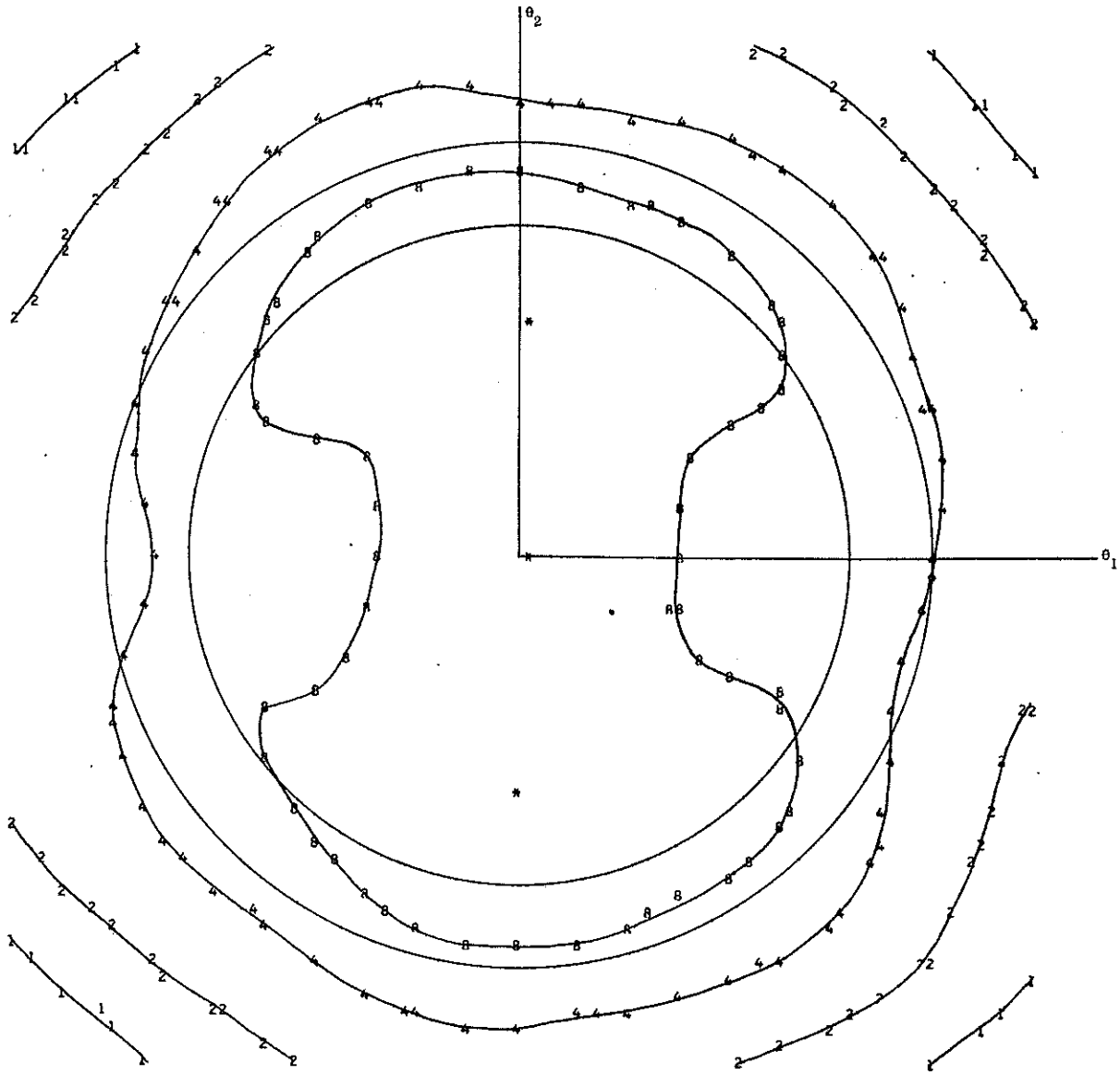


Figure 9-5. Linear polarization,  $\delta = 0.75$ ,  $\lambda = 6943 \text{ \AA}$ .

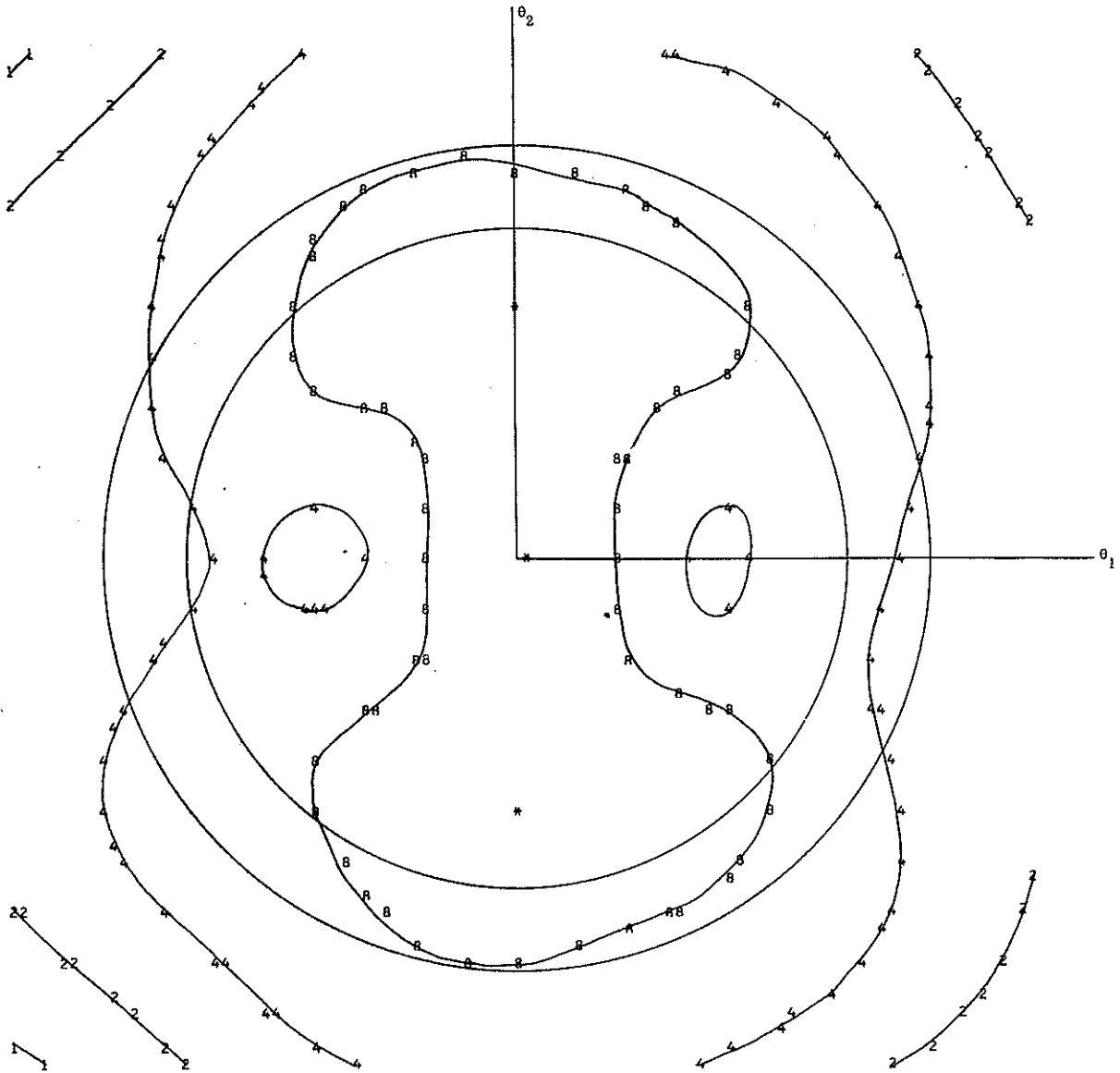


Figure 9-6. Linear polarization,  $\delta = 1''25$ ,  $\lambda = 6943 \text{ \AA}$ .

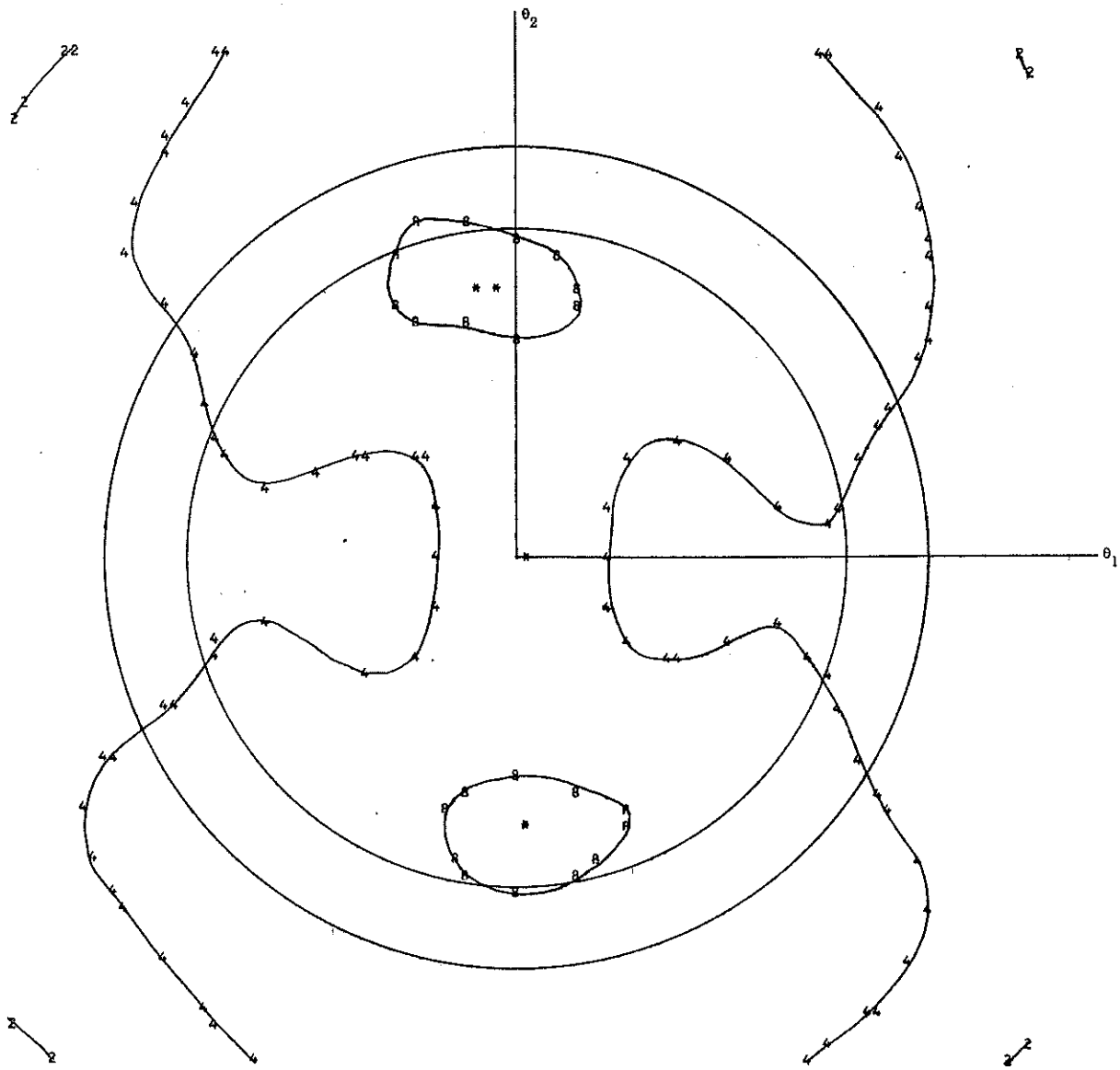


Figure 9-7. Linear polarization,  $\delta = 1.175$ ,  $\lambda = 6943 \text{ \AA}$ .

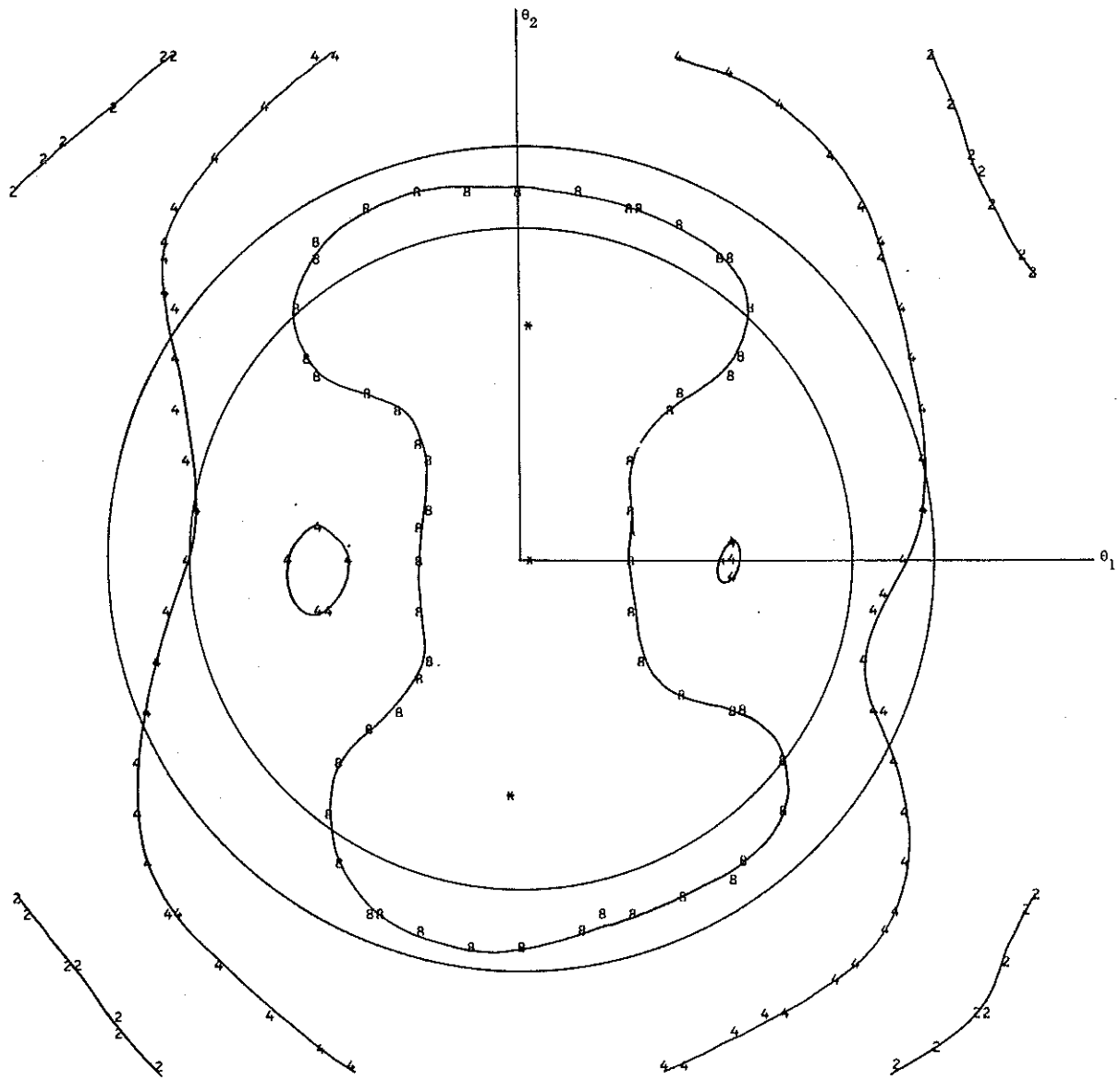


Figure 9-8. Linear polarization,  $\bar{\delta} = 1'25$  (mixed dihedral angles),  $\lambda = 6943 \text{ \AA}$ .

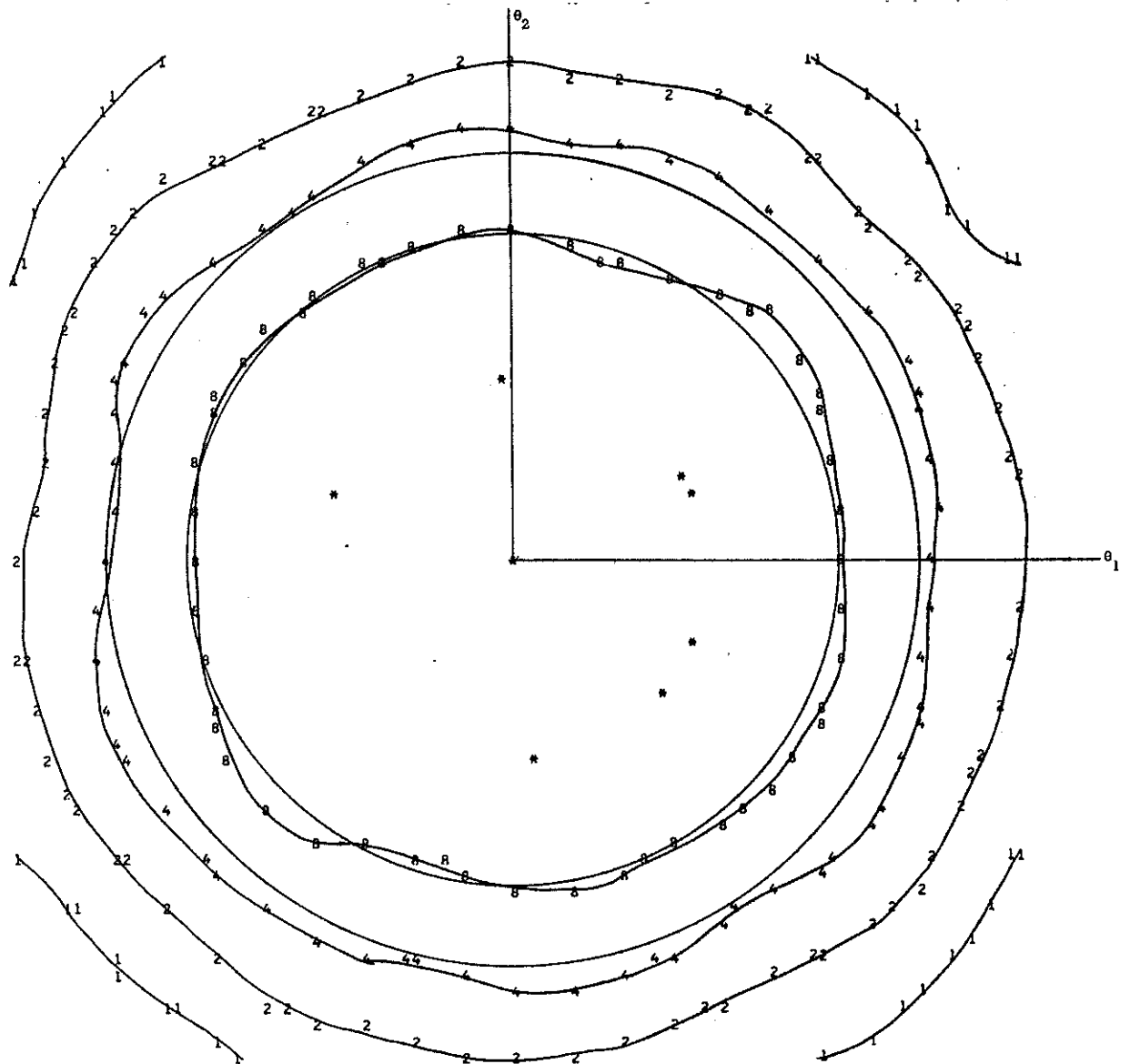


Figure 9-9. Circular polarization,  $\delta = 0''75$ ,  $\lambda = 5320 \text{ \AA}$ .

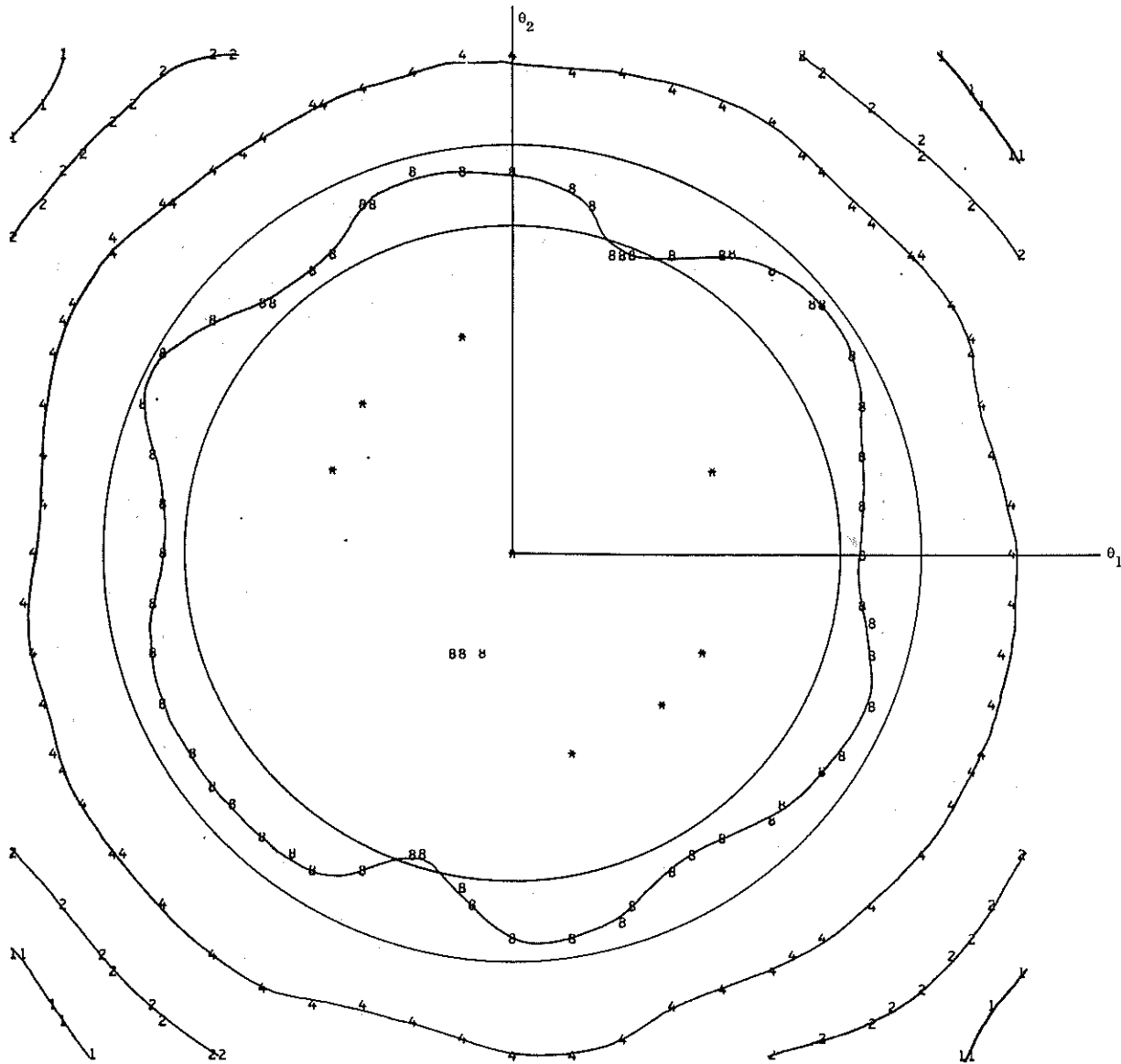


Figure 9-10. Circular polarization,  $\delta = 1'25$ ,  $\lambda = 5320 \text{ \AA}$ .

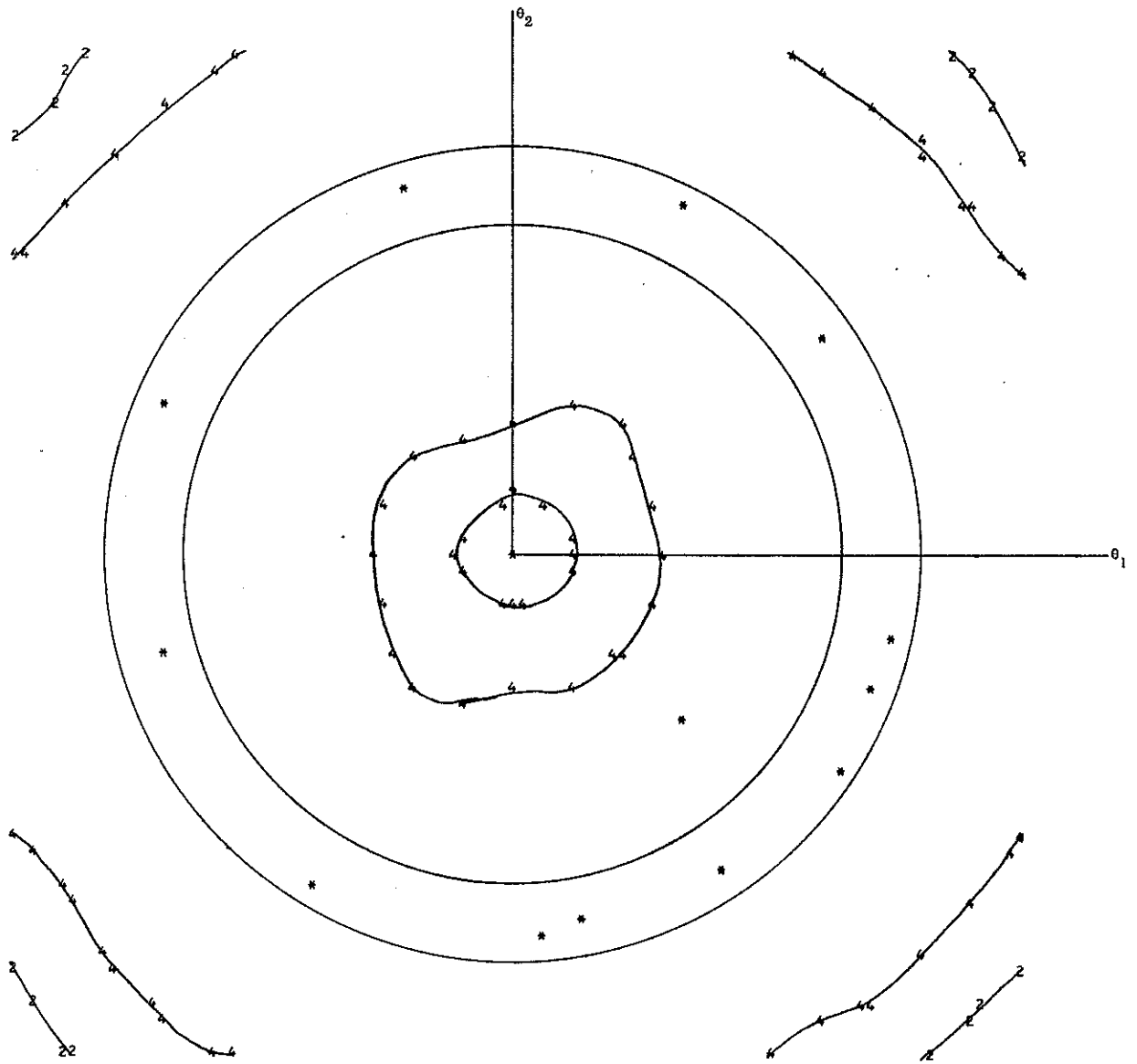


Figure 9-11. Circular polarization,  $\delta = 1.775$ ,  $\lambda = 5320 \text{ \AA}$ .

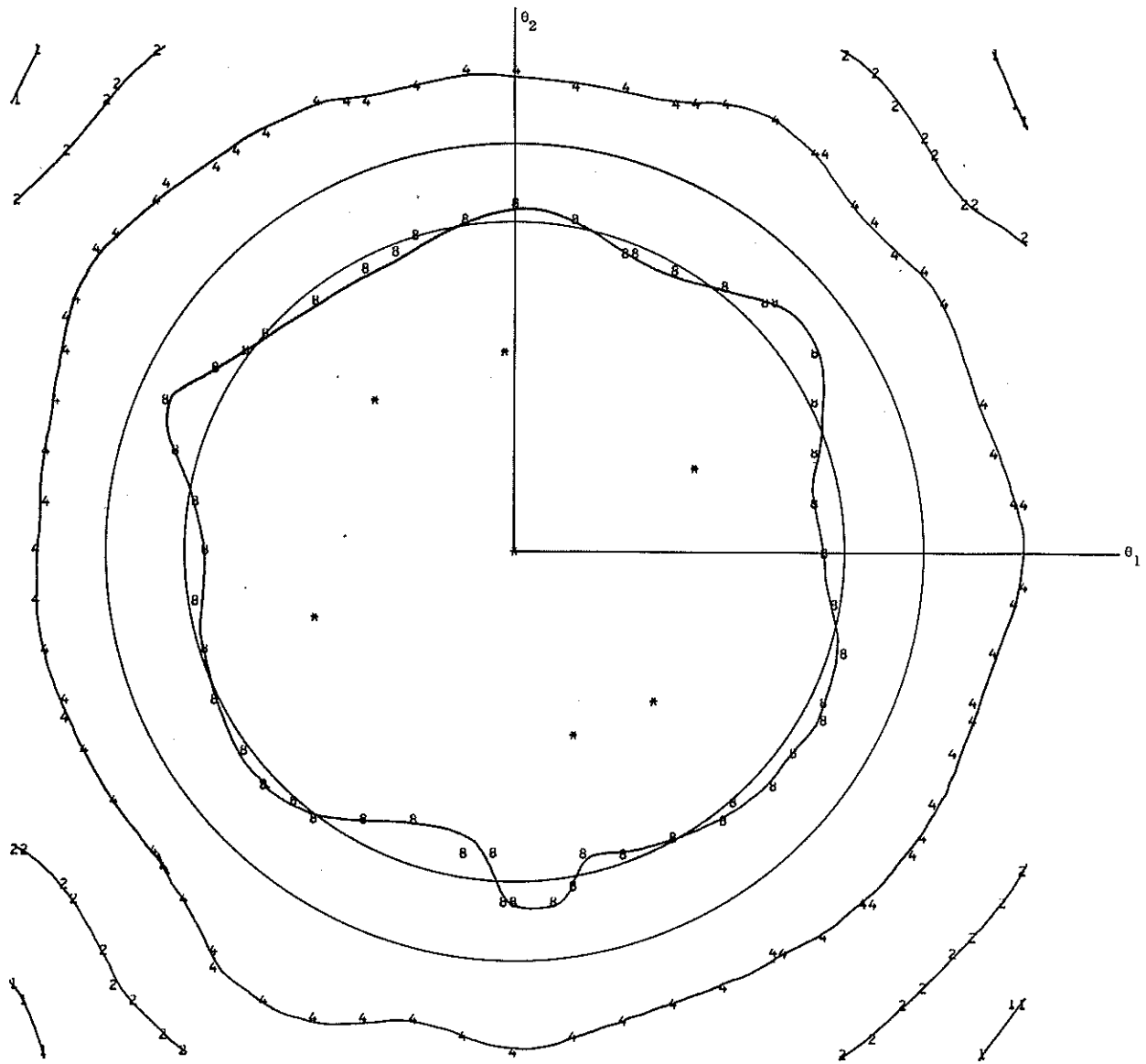


Figure 9-12. Circular polarization,  $\bar{\delta} = 1'25$  (mixed dihedral angles),  $\lambda = 5320 \text{ \AA}$ .



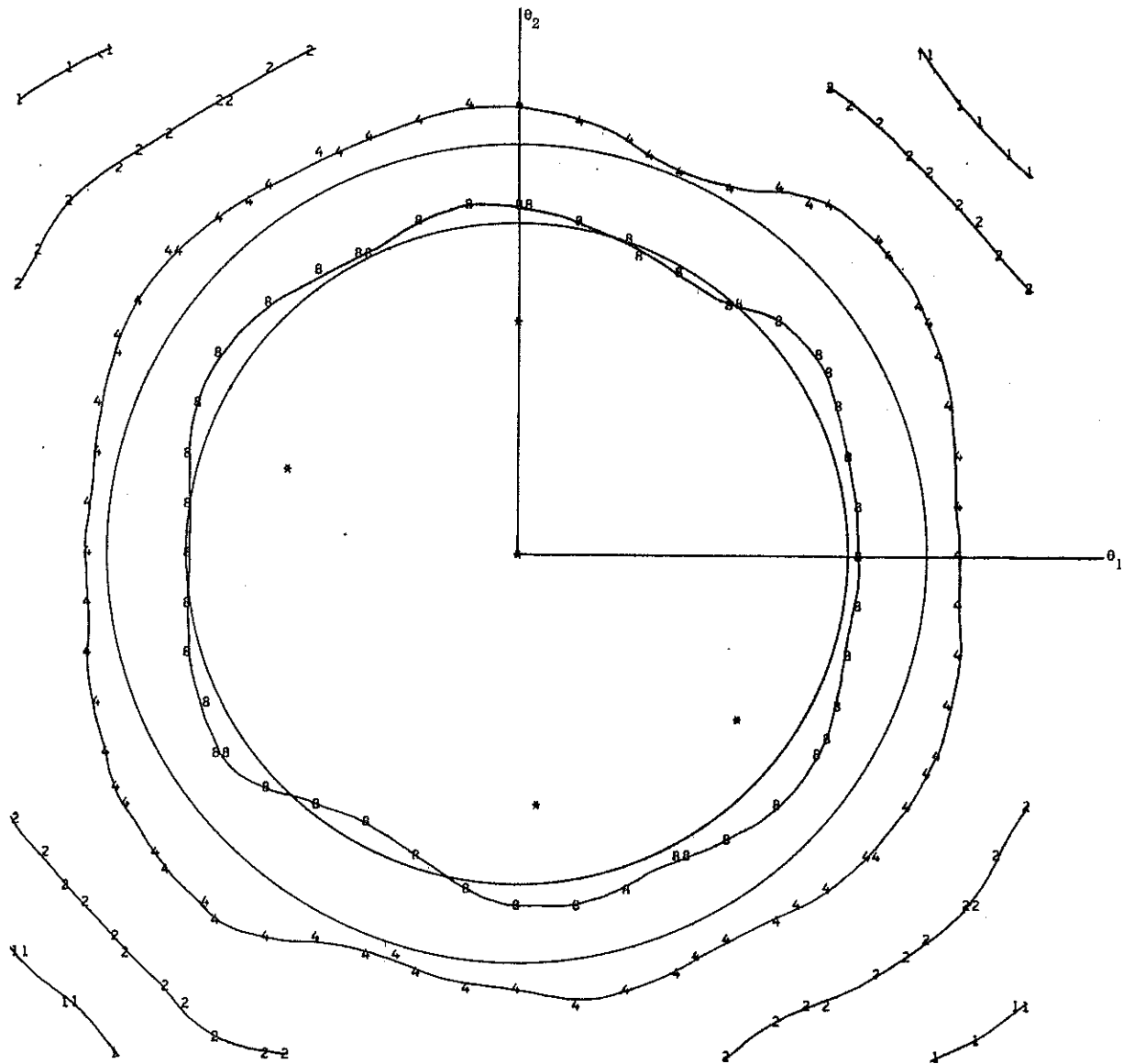


Figure 9-13. Circular polarization,  $\delta = 0.75$ ,  $\lambda = 6943 \text{ \AA}$ .

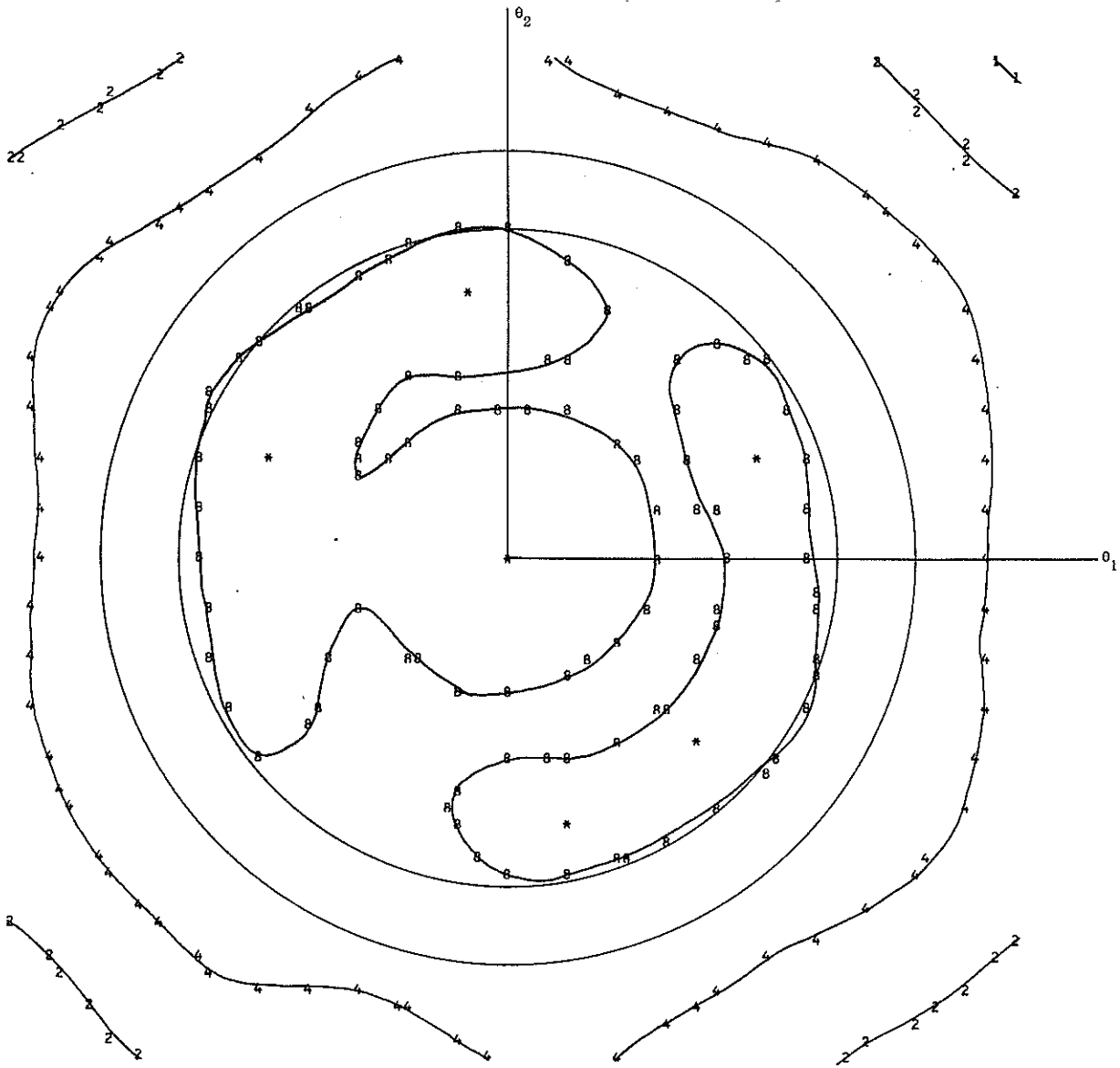


Figure 9-14. Circular polarization,  $\delta = 1''25$ ,  $\lambda = 6943 \text{ \AA}$ .

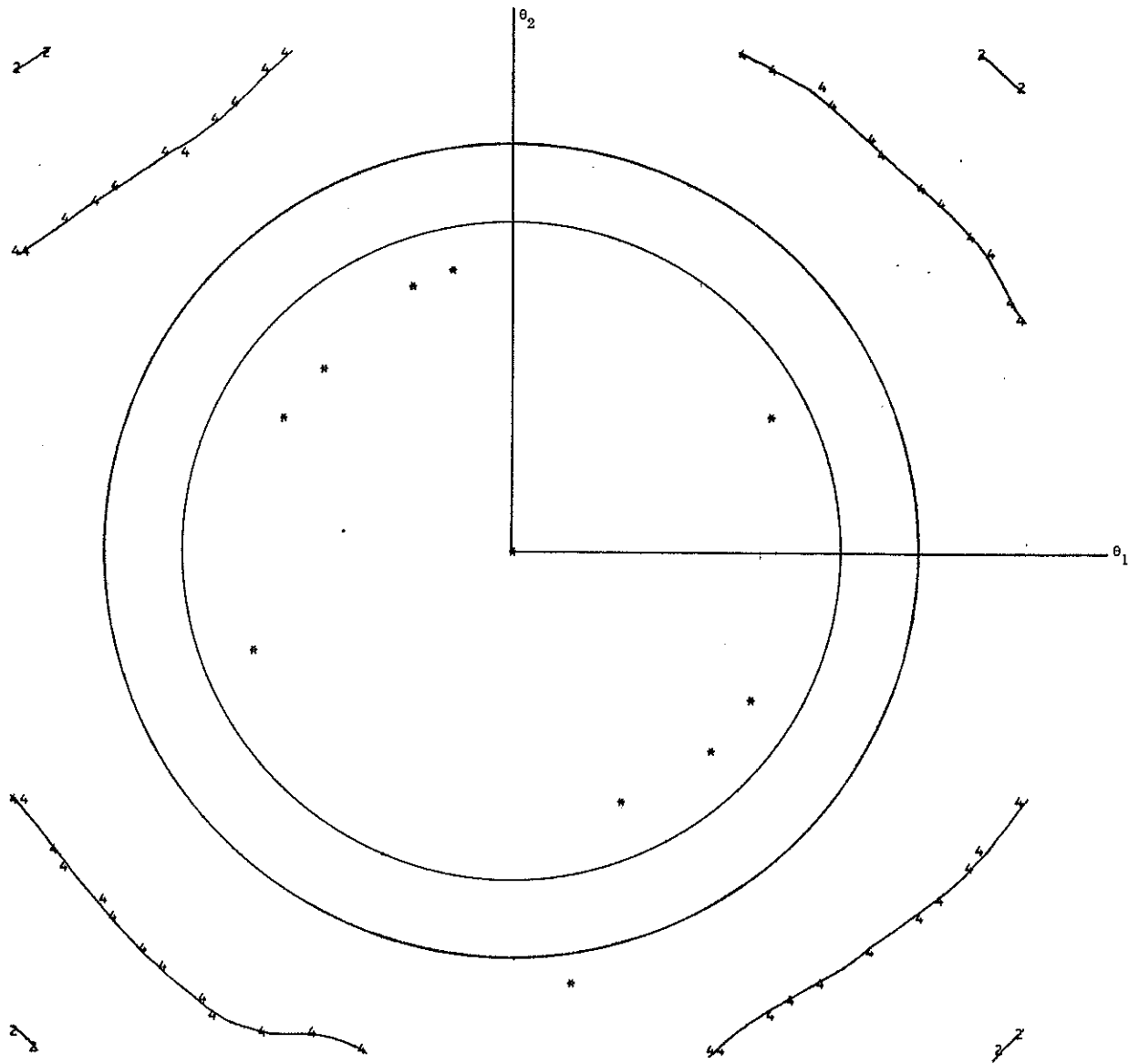


Figure 9-15. Circular polarization,  $\delta = 1^{\circ}75$ ,  $\lambda = 6943 \text{ \AA}$ .

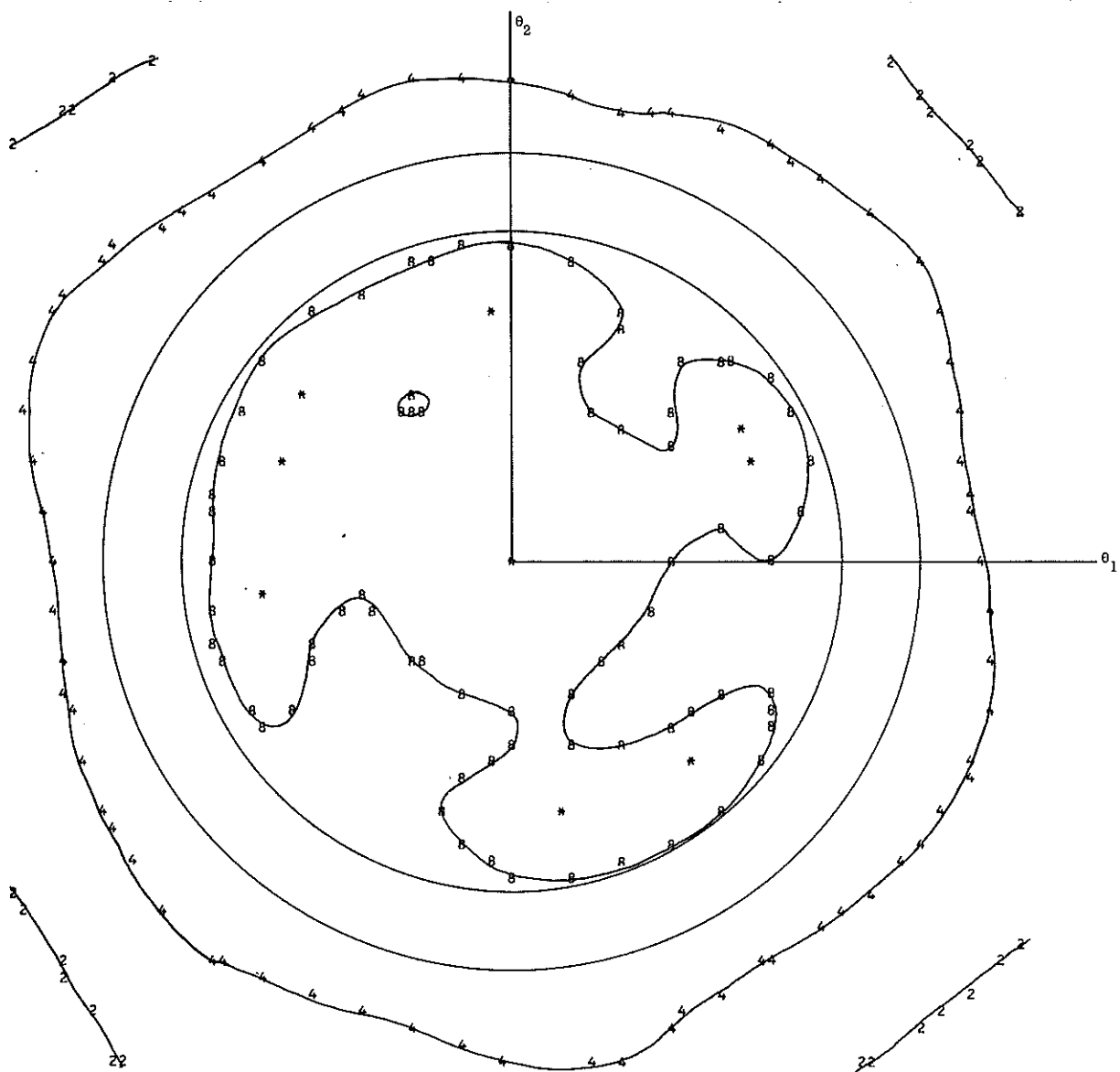


Figure 9-16. Circular polarization,  $\bar{\sigma} = 1.125$  (mixed dihedral angles),  $\lambda = 6943 \text{ \AA}$ .

Table 9 gives the average gain in the 32- to 41- $\mu$ rad annulus for each of the array diffraction patterns computed. At 5320 Å the strongest signal is obtained with the 1.25-arcsec dihedral angle offset. At 6943 Å the intensity is slightly higher at the 0.75-arcsec offset. As can be seen from Table 8, the energy is concentrated in the center of the pattern for small dihedral angle offsets and shifts outward as the offset is increased. At 6943 Å the pattern is wider than at 5320 Å due to diffraction effects, and, in fact, the dihedral angle offset is not really essential at 6943 Å. The phase changes due to total internal reflection at the back faces also help to widen the pattern at both wavelengths. At 5320 Å, the diffraction pattern is sharper than at 6943 Å, and it is possible to obtain a better concentration of energy in the desired range of velocity aberration. Using a mixture of dihedral angle offsets with an average of 1.25 arcsec reduces the gain in the annulus compared to having all the offsets 1.25 arcsec. The effect is greater at 5320 Å because the pattern is sharper at this wavelength. The results for a mixture of offsets are probably more representative of the behavior of the actual array. Multiplication of the gains for linear polarization and mixed offsets by the area for each wavelength gives cross sections of  $1.03 \times 10^6 \text{ m}^2$  and  $0.90 \times 10^6 \text{ m}^2$  at 5320 Å and 6943 Å, respectively ( $13.0 \times 10^6 \text{ m}^2$  and  $11.3 \times 10^6 \text{ m}^2$  in standard cross section units).

Table 9. Average gain in the 32-41  $\mu$ rad annulus for the gain matrices in Table 7.

Polarization	$\lambda$	$\delta$	$G(10^7)$
Linear	5320	0.75	6.4086
		1.25	8.0338
		1.75	7.079134
		$\overline{1.25}$	7.191611
	6943	0.75	6.95308
		1.25	6.6090
		1.75	5.47506
		$\overline{1.25}$	6.3981
Circular	5320	0.75	6.4418
		1.25	8.01035
		1.75	7.06848
		$\overline{1.25}$	7.1942
	6943	0.75	6.8869
		1.25	6.522986
		1.75	5.39929
		$\overline{1.25}$	6.295369

## 10. RANGE CORRECTION

The range corrections presented in this section give the difference between the range that would be measured to a point reflector at the center of the satellite and the range measured to the retroreflector array. All values are for the incoherent case. The effect of coherent interference is discussed in Section 11. The centroid of the total reflected energy (which can be measured only in the laboratory) is 0.2394 m from the center of the satellite. When diffraction is taken into account, the centroid moves to about 0.2425 m. For long incident pulses, the range correction is the same for all pulse detection methods because there is negligible pulse distortion. For short pulses, the range correction is a function of pulse length for methods other than centroid detection. The table below gives range corrections (m) computed for three pulse lengths using the reflectivity curve for 5320 Å in Figure 6 (Section 6).

Table 10. Variation of range correction with pulse length.

Pulse length (nanosecs)	Centroid	Half area	Peak	Half maximum
20.0	0.2427	0.2427	0.2427	0.2428
5.0	0.2427	0.2427	0.2428	0.2431
0.2	0.2427	0.2451	0.2483	0.2506

Tables 14 and 15, and Figure 10 give the centroid range correction matrices, the range correction vs velocity aberration, and contour plots of the range correction matrices. The information is for the same conditions and in the same formats as the gain information in Section 9. The range correction vs velocity aberration in Table 15 is plotted at a scale of one millimeter per horizontal print position. The contour plots of Figure 10 are plotted using the codes in Table 11 below.

Circles of radius 32 and 41  $\mu$ rad are drawn to mark the minimum and maximum velocity aberration. The average value of the range correction in the 32- to 41- $\mu$ rad annulus is listed for each case in Table 12.

Table 11. Codes for range contour plots in Figure 10.

Range correction (m)	Plot code
0.2380	8
0.2400	0
0.2410	1
0.2420	2
0.2430	3
0.2440	4
0.2450	5

Table 12. Average range correction in the 32-41  $\mu$ rad annulus for various cases.

Polarization	Wavelength ( $\text{\AA}$ )	Dihedral angle offset (arcsecs)	Range correction (m)
Linear	5320	0.75	0.2411
		1.25	0.2426
		1.75	0.2421
		$\overline{1.25}$	0.2424
	6943	0.75	0.2425
		1.25	0.2421
		1.75	0.2412
		$\overline{1.25}$	0.2424
Circular	5320	0.75	0.2412
		1.25	0.2428
		1.75	0.2424
		$\overline{1.25}$	0.2426
	6943	0.75	0.2427
		1.25	0.2426
		1.75	0.2418
		$\overline{1.25}$	0.2427



The range corrections for pulse detection methods other than centroid have been computed at selected points in the far field to see how much these corrections vary with velocity aberration. The results are given in Table 13. The standard deviation of the corrections computed (excluding the point at the center of the diffraction pattern) was 1.2 mm for centroid detection, 1.0 mm for half area, 0.9 mm for peak, and 0.7 mm for half maximum detection, and the average values were 0.2429, 0.2456, 0.2490, and 0.2509 m, respectively. A single dihedral angle of 1.25 arcsecs was used.

In summary, the range correction for Lageos for centroid detection is about 0.2425 m for all pulse lengths and wavelengths. For other pulse detection methods, the range correction varies with pulse length and is different for each method.

Table 13. Range correction for four pulse detection techniques at selected points in the far field.

Polarization	Wavelength (Å)	$\theta_1$	$\theta_2$	Centroid	Half area	Peak	Half maximum
Linear	5320	0	0	0.2353	0.2388	0.2458	0.2497
		0	30	0.2428	0.2455	0.2489	0.2508
		0	35	0.2437	0.2464	0.2496	0.2513
		0	40	0.2441	0.2467	0.2497	0.2513
		30	0	0.2391	0.2425	0.2475	0.2502
		35	0	0.2410	0.2444	0.2490	0.2512
		40	0	0.2425	0.2457	0.2496	0.2512
		21.2	21.2	0.2424	0.2446	0.2475	0.2501
		24.7	24.7	0.2431	0.2454	0.2483	0.2506
28.3	28.3	0.2431	0.2454	0.2482	0.2504		
Linear	9643	0	0	0.2389	0.2423	0.2477	0.2503
		0	30	0.2449	0.2472	0.2499	0.2515
		0	35	0.2440	0.2464	0.2494	0.2512
		0	40	0.2432	0.2459	0.2493	0.2511
		30	0	0.2420	0.2457	0.2496	0.2512
		35	0	0.2414	0.2449	0.2489	0.2507
		40	0	0.2410	0.2444	0.2488	0.2510
		21.2	21.2	0.2425	0.2447	0.2473	0.2496
		24.7	24.7	0.2425	0.2446	0.2470	0.2493
28.3	28.3	0.2427	0.2447	0.2472	0.2497		
Circular	5320	0	0	0.2357	0.2391	0.2463	0.2495
		0	30	0.2429	0.2457	0.2490	0.2509
		0	35	0.2442	0.2469	0.2498	0.2514
		0	40	0.2449	0.2474	0.2500	0.2513
		30	0	0.2410	0.2441	0.2482	0.2504
		35	0	0.2417	0.2448	0.2489	0.2508
		40	0	0.2426	0.2456	0.2493	0.2508
		21.2	21.2	0.2428	0.2456	0.2495	0.2517
		24.7	24.7	0.2438	0.2465	0.2502	0.2522
28.3	28.3	0.2434	0.2461	0.2497	0.2517		

Table 13. (Cont.)

Polarization	Wavelength (Å)	$\theta_1$	$\theta_2$	Centroid	Half area	Peak	Half maximum
Circular	6943	0	0	0.2392	0.2426	0.2481	0.2505
		0	30	0.2440	0.2465	0.2495	0.2512
		0	35	0.2438	0.2463	0.2493	0.2510
		0	40	0.2438	0.2465	0.2496	0.2513
		30	0	0.2433	0.2462	0.2492	0.2507
		35	0	0.2424	0.2453	0.2485	0.2502
		40	0	0.2416	0.2446	0.2482	0.2502
		21.2	21.2	0.2438	0.2466	0.2501	0.2519
		24.7	24.7	0.2435	0.2461	0.2496	0.2516
28.3	28.3	0.2434	0.2460	0.2497	0.2518		

Table 14. Centroid range correction matrices. The angles  $\theta_1$  and  $\theta_2$ , in microradians, are defined in Figure 8. Table 14-1. Linear polarization.

	DIPEDRAL ANGLE .75 WAVELENGTH 5320																				
	RANGE CORRECTION (METERS)																				
9 <sub>2</sub>																					
50	2388	2370	2348	2347	2346	2330	2319	2330	2348	2359	2361	2368	2367	2362	2347	2368	2357	2340	2361	2394	2401
45	2366	2353	2340	2341	2341	2338	2348	2367	2382	2388	2385	2374	2354	2363	2362	2383	2379	2359	2365	2389	2391
40	2356	2351	2343	2341	2344	2357	2375	2392	2403	2405	2402	2397	2392	2386	2388	2393	2390	2373	2359	2386	2390
35	2348	2354	2358	2362	2367	2378	2392	2405	2414	2415	2410	2407	2410	2413	2411	2405	2398	2383	2357	2387	2313
30	2337	2362	2386	2395	2393	2393	2400	2411	2423	2428	2426	2421	2421	2424	2423	2417	2408	2394	2367	2393	2320
25	2346	2382	2411	2417	2404	2395	2403	2417	2432	2442	2445	2440	2433	2429	2425	2420	2415	2407	2386	2387	2342
20	2374	2401	2426	2428	2407	2397	2411	2425	2435	2445	2451	2447	2437	2428	2420	2413	2411	2413	2406	2384	2362
15	2389	2406	2429	2432	2413	2412	2426	2428	2423	2427	2434	2431	2423	2419	2418	2408	2403	2412	2418	2405	2379
10	2386	2399	2422	2429	2418	2424	2432	2412	2382	2391	2404	2398	2384	2399	2421	2416	2403	2410	2421	2416	2394
5	2383	2390	2407	2412	2405	2417	2416	2360	2334	2380	2399	2385	2342	2360	2424	2429	2413	2413	2421	2417	2402
0	2388	2390	2395	2389	2381	2400	2392	2309	2321	2384	2403	2386	2326	2351	2411	2427	2417	2417	2419	2412	2400
-5	2388	2392	2393	2382	2379	2404	2408	2354	2341	2384	2399	2384	2340	2347	2401	2411	2408	2415	2415	2406	2395
-10	2378	2394	2401	2396	2395	2416	2427	2410	2390	2398	2405	2399	2394	2408	2414	2402	2397	2412	2415	2406	2396
-15	2369	2394	2411	2414	2413	2419	2427	2429	2429	2431	2433	2432	2434	2435	2424	2404	2397	2411	2413	2406	2397
-20	2368	2391	2413	2425	2426	2420	2418	2427	2440	2448	2449	2445	2440	2435	2423	2408	2404	2410	2403	2390	2381
-25	2364	2376	2397	2417	2427	2422	2415	2421	2435	2445	2445	2438	2429	2423	2417	2411	2411	2410	2388	2361	2347
-30	2351	2350	2364	2386	2407	2416	2417	2419	2427	2434	2433	2425	2416	2412	2411	2410	2410	2405	2384	2352	2336
-35	2348	2338	2341	2355	2373	2394	2408	2416	2420	2423	2421	2416	2409	2402	2396	2393	2395	2396	2384	2365	2353
-40	2379	2365	2352	2351	2359	2370	2384	2397	2407	2412	2412	2407	2396	2379	2364	2361	2367	2373	2372	2370	2368
-45	2407	2394	2364	2351	2357	2356	2353	2365	2383	2394	2396	2388	2370	2344	2330	2334	2340	2339	2347	2367	2378
-50	2405	2399	2364	2335	2337	2337	2328	2334	2356	2371	2372	2360	2335	2311	2313	2330	2335	2330	2344	2372	2386

Table 14-2. Linear polarization.

$\theta_2$	DIHEDRAL ANGLE		1.25		WAVELENGTH		5320		RANGE CORRECTION (METERS)													
	-50	-45	-40	-35	-30	-25	-20	-15	-10	-5	0	5	10	15	20	25	30	35	40	45	50	$\theta_1$
50	2359	2339	2331	2347	2366	2375	2381	2392	2405	2416	2420	2416	2404	2398	2404	2405	2390	2368	2358	2358	2347	2347
45	2352	2348	2354	2370	2385	2395	2404	2414	2424	2432	2434	2429	2417	2410	2416	2423	2416	2397	2388	2369	2369	2347
40	2364	2367	2374	2384	2396	2407	2417	2426	2433	2438	2441	2439	2432	2425	2426	2430	2427	2412	2391	2368	2368	2340
35	2378	2383	2391	2399	2407	2416	2423	2429	2434	2437	2437	2438	2438	2436	2434	2433	2429	2416	2394	2368	2368	2345
30	2386	2397	2409	2418	2421	2422	2423	2426	2429	2430	2428	2428	2428	2438	2438	2434	2428	2416	2397	2377	2368	2345
25	2397	2411	2425	2433	2428	2422	2417	2420	2426	2429	2428	2426	2425	2432	2433	2431	2428	2419	2402	2392	2389	2368
20	2411	2420	2433	2437	2422	2403	2406	2418	2425	2430	2432	2429	2425	2424	2421	2419	2421	2415	2407	2402	2392	2389
15	2420	2423	2432	2434	2412	2394	2408	2418	2425	2433	2435	2433	2429	2413	2410	2403	2407	2420	2424	2419	2411	2411
10	2420	2419	2425	2425	2403	2385	2413	2408	2373	2361	2370	2365	2365	2396	2409	2396	2394	2414	2427	2427	2417	2417
5	2419	2414	2415	2409	2387	2388	2404	2367	2288	2321	2349	2326	2285	2363	2412	2400	2390	2410	2427	2430	2423	2423
0	2418	2412	2406	2391	2364	2373	2388	2318	2233	2319	2352	2321	2237	2327	2404	2399	2391	2410	2426	2429	2426	2426
-5	2412	2409	2403	2384	2360	2375	2396	2354	2282	2323	2348	2324	2286	2352	2395	2388	2389	2412	2424	2428	2428	2428
-10	2399	2404	2405	2396	2381	2391	2410	2401	2370	2363	2369	2366	2377	2400	2400	2384	2390	2414	2423	2427	2429	2429
-15	2392	2403	2413	2416	2410	2408	2414	2416	2414	2412	2412	2413	2419	2420	2408	2382	2400	2415	2418	2422	2425	2425
-20	2395	2405	2417	2428	2432	2427	2420	2420	2426	2430	2430	2427	2424	2421	2413	2409	2415	2418	2419	2422	2425	2425
-25	2398	2405	2413	2426	2438	2440	2434	2429	2430	2432	2431	2426	2422	2421	2422	2425	2429	2422	2404	2387	2379	2379
-30	2391	2398	2405	2416	2430	2440	2443	2441	2439	2437	2435	2431	2429	2428	2429	2432	2433	2427	2409	2385	2366	2366
-35	2372	2386	2398	2409	2421	2431	2439	2443	2445	2443	2440	2435	2429	2429	2425	2425	2427	2426	2414	2393	2371	2371
-40	2352	2370	2388	2404	2416	2423	2428	2435	2442	2446	2445	2441	2432	2420	2411	2409	2413	2414	2407	2394	2378	2378
-45	2346	2357	2368	2387	2405	2413	2416	2423	2432	2439	2440	2433	2421	2404	2391	2386	2384	2381	2380	2383	2383	2383
-50	2343	2348	2345	2355	2377	2393	2400	2408	2419	2427	2427	2420	2404	2383	2366	2354	2341	2331	2338	2361	2381	2381

Table 14-3. Linear polarization.

$\theta_2$	DIHEDRAL ANGLE 1.75 WAVELENGTH 5320																					$\theta_1$
	RANGE CORRECTION (METERS)																					
50	2372	2395	2414	2425	2430	2432	2435	2438	2440	2439	2439	2441	2445	2442	2433	2423	2415	2402	2373			
45	2380	2411	2423	2430	2433	2435	2437	2441	2442	2440	2437	2439	2446	2448	2442	2430	2420	2408	2384			
40	2390	2418	2425	2430	2432	2435	2437	2440	2441	2439	2435	2435	2442	2446	2432	2420	2410	2400	2391			
35	2404	2412	2419	2424	2428	2429	2430	2432	2433	2433	2432	2433	2436	2440	2429	2417	2406	2396				
30	2412	2415	2421	2425	2427	2428	2429	2431	2431	2431	2430	2431	2432	2433	2422	2412	2406	2403				
25	2418	2419	2426	2427	2428	2429	2430	2431	2431	2431	2430	2431	2432	2433	2422	2412	2406	2403				
20	2427	2422	2427	2428	2429	2430	2431	2431	2431	2431	2430	2431	2432	2433	2422	2412	2406	2403				
15	2434	2424	2422	2422	2422	2422	2422	2422	2422	2422	2422	2422	2422	2422	2422	2422	2422	2422				
10	2434	2422	2415	2413	2380	2386	2381	2365	2359	2370	2386	2397	2403	2409	2414	2410	2411	2413				
5	2432	2419	2409	2402	2378	2378	2362	2294	2295	2325	2378	2385	2386	2387	2401	2412	2415	2416				
0	2427	2416	2405	2391	2361	2352	2337	2266	2254	2251	2351	2353	2352	2370	2374	2402	2418	2424				
-5	2418	2411	2402	2386	2379	2376	2361	2297	2290	2254	2344	2378	2373	2362	2379	2407	2419	2428				
-10	2405	2402	2392	2385	2383	2380	2369	2309	2288	2252	2344	2381	2377	2376	2396	2410	2415	2424				
-15	2399	2399	2392	2385	2383	2382	2370	2358	2354	2363	2381	2387	2390	2400	2411	2411	2408	2413				
-20	2403	2405	2408	2416	2420	2420	2415	2401	2378	2378	2383	2387	2399	2420	2424	2418	2408	2403				
-25	2408	2413	2415	2420	2422	2422	2418	2404	2380	2378	2391	2399	2409	2420	2424	2418	2408	2403				
-30	2408	2417	2422	2426	2428	2432	2437	2441	2436	2434	2436	2427	2427	2427	2427	2427	2427	2427				
-35	2399	2414	2426	2435	2440	2439	2438	2438	2436	2434	2436	2427	2427	2427	2427	2427	2427	2427				
-40	2385	2406	2424	2438	2447	2442	2442	2444	2444	2441	2436	2431	2429	2431	2433	2430	2422	2410				
-45	2374	2399	2417	2432	2445	2445	2447	2447	2447	2444	2439	2434	2430	2427	2423	2415	2407	2402				
-50	2364	2392	2408	2421	2444	2445	2446	2446	2445	2443	2438	2432	2425	2417	2405	2378	2378	2378				



Table 14-5. Linear polarization.

$\theta_2$	DIHEDRAL ANGLE .75 WAVELENGTH 6943																					
	RANGE CORRECTION (METERS)																					
	-50	-45	-40	-35	-30	-25	-20	-15	-10	-5	0	5	10	15	20	25	30	35	40	45	50	
50	2354	2385	2339	2341	2352	2367	2381	2391	2394	2390	2382	2376	2379	2379	2381	2382	2383	2382	2382	2377	2368	2363
45	2359	2386	2355	2360	2370	2382	2394	2404	2408	2407	2400	2393	2398	2398	2403	2403	2398	2403	2384	2375	2364	
40	2377	2379	2377	2377	2382	2392	2403	2415	2424	2426	2423	2417	2414	2414	2417	2417	2413	2417	2396	2386	2371	
35	2398	2399	2391	2385	2389	2399	2412	2425	2437	2443	2444	2440	2433	2438	2425	2423	2419	2413	2407	2399	2383	
30	2415	2412	2398	2390	2396	2409	2421	2433	2444	2452	2456	2453	2445	2436	2429	2424	2419	2414	2407	2397		
25	2426	2422	2406	2400	2410	2422	2429	2435	2442	2450	2455	2453	2445	2436	2428	2423	2417	2410	2407	2409	2407	
20	2431	2429	2418	2417	2427	2435	2433	2427	2427	2434	2440	2439	2432	2423	2423	2423	2418	2409	2403	2406	2411	
15	2428	2431	2426	2430	2440	2441	2427	2405	2399	2409	2418	2416	2407	2402	2413	2426	2427	2416	2405	2405	2413	
10	2418	2424	2424	2432	2441	2436	2405	2370	2377	2399	2409	2404	2387	2373	2397	2430	2439	2429	2414	2410	2414	
5	2402	2406	2409	2422	2431	2416	2367	2343	2375	2404	2414	2406	2382	2351	2374	2427	2445	2438	2424	2416	2415	
0	2389	2388	2392	2409	2420	2400	2344	2335	2379	2408	2417	2409	2381	2350	2353	2414	2439	2437	2427	2420	2415	
-5	2385	2381	2388	2409	2424	2411	2364	2348	2380	2406	2414	2406	2380	2346	2358	2405	2426	2426	2420	2417	2413	
-10	2391	2387	2395	2417	2433	2431	2403	2379	2388	2404	2410	2404	2388	2378	2394	2414	2419	2413	2410	2413	2411	
-15	2401	2400	2406	2421	2436	2439	2428	2413	2411	2416	2418	2416	2414	2418	2427	2428	2420	2406	2402	2410	2412	
-20	2411	2414	2415	2422	2430	2435	2435	2434	2435	2438	2439	2438	2438	2438	2441	2435	2421	2405	2400	2408	2411	
-25	2416	2422	2423	2421	2420	2423	2430	2440	2448	2452	2452	2450	2447	2445	2442	2433	2419	2405	2401	2406	2405	
-30	2410	2421	2424	2419	2412	2411	2421	2436	2448	2454	2454	2449	2443	2437	2431	2424	2413	2405	2403	2403	2394	
-35	2388	2406	2415	2414	2408	2404	2412	2427	2441	2447	2446	2439	2429	2421	2416	2412	2408	2404	2403	2399	2385	
-40	2358	2375	2391	2399	2401	2401	2407	2418	2428	2433	2431	2423	2413	2405	2402	2400	2399	2398	2397	2394	2382	
-45	2342	2349	2361	2374	2386	2394	2401	2407	2413	2415	2414	2408	2399	2392	2387	2383	2381	2381	2381	2383	2385	
-50	2355	2352	2353	2358	2367	2377	2386	2392	2396	2398	2398	2395	2389	2378	2367	2358	2355	2357	2364	2370	2371	



Table 14-6. Linear polarization.

$\theta_2$	DIHEDRAL ANGLE 1.25		WAVELENGTH 6943		RANGE CORRECTION (METERS)																					
					-50	-45	-40	-35	-30	-25	-20	-15	-10	-5	0	5	10	15	20	25	30	35	40	45	50	
50	2360	2364	2373	2384	2397	2408	2418	2425	2430	2431	2431	2430	2427	2424	2419	2417	2417	2418	2413	2401	2383					
45	2380	2385	2391	2399	2407	2415	2423	2429	2432	2432	2431	2429	2430	2432	2432	2430	2426	2423	2417	2406	2388					
40	2404	2409	2410	2413	2418	2424	2429	2430	2434	2434	2432	2430	2431	2434	2437	2436	2433	2428	2421	2411	2393					
35	2423	2426	2420	2414	2412	2416	2424	2431	2437	2440	2440	2437	2435	2436	2437	2436	2433	2430	2425	2417	2402					
30	2435	2435	2423	2410	2407	2414	2425	2434	2441	2447	2448	2446	2442	2437	2434	2431	2428	2426	2425	2422	2413					
25	2441	2438	2422	2406	2406	2418	2428	2434	2441	2446	2449	2447	2442	2436	2430	2425	2420	2418	2420	2424	2422					
20	2442	2438	2421	2407	2413	2425	2429	2428	2428	2432	2436	2435	2430	2425	2423	2420	2414	2408	2411	2421	2427					
15	2438	2435	2421	2413	2422	2430	2424	2407	2397	2403	2410	2408	2401	2400	2411	2419	2414	2405	2404	2417	2428					
10	2429	2427	2414	2412	2422	2424	2400	2361	2356	2377	2389	2383	2363	2356	2389	2419	2410	2404	2404	2415	2428					
5	2416	2411	2398	2399	2411	2404	2352	2299	2332	2373	2387	2376	2340	2304	2355	2414	2426	2416	2409	2416	2428					
0	2405	2393	2379	2384	2399	2385	2312	2268	2329	2375	2389	2377	2333	2275	2325	2402	2421	2415	2411	2418	2427					
5	2400	2385	2372	2383	2402	2395	2341	2298	2337	2375	2387	2375	2337	2299	2340	2395	2410	2406	2407	2418	2426					
10	2403	2391	2382	2394	2413	2417	2393	2361	2363	2381	2389	2382	2365	2369	2387	2405	2404	2397	2402	2418	2426					
-5	2412	2406	2400	2406	2420	2427	2421	2408	2403	2407	2409	2408	2407	2413	2420	2418	2406	2395	2401	2418	2425					
-15	2421	2422	2418	2417	2422	2427	2430	2431	2432	2434	2434	2434	2434	2435	2434	2425	2410	2400	2406	2418	2423					
-20	2426	2432	2433	2429	2425	2425	2430	2437	2444	2447	2447	2445	2442	2439	2434	2425	2414	2409	2414	2420	2418					
-25	2422	2433	2439	2437	2431	2427	2429	2437	2445	2449	2448	2444	2439	2434	2430	2424	2420	2419	2422	2422	2412					
-30	2408	2423	2434	2439	2437	2433	2433	2437	2442	2445	2443	2439	2433	2429	2426	2424	2424	2426	2427	2423	2410					
-35	2388	2403	2419	2430	2436	2437	2438	2439	2440	2441	2440	2436	2431	2428	2426	2425	2425	2426	2426	2423	2410					
-40	2373	2384	2400	2415	2426	2433	2437	2439	2440	2441	2439	2437	2433	2428	2422	2418	2416	2416	2418	2417	2409					
-45	2367	2376	2388	2400	2411	2420	2428	2434	2438	2439	2439	2436	2430	2421	2411	2402	2397	2398	2402	2405	2401					
-50																										

Table 14-7. Linear polarization.

$\theta_2$	DIHEDRAL ANGLE 1.75		WAVELENGTH 6943		RANGE CORRECTION (METERS)																				
					-50	-45	-40	-35	-30	-25	-20	-15	-10	-5	0	5	10	15	20	25	30	35	40	45	50
50	2393	2400	2408	2415	2422	2428	2434	2439	2443	2446	2447	2444	2440	2436	2435	2438	2439	2435	2438	2439	2435	2435	2435	2425	2410
45	2404	2410	2416	2421	2426	2430	2434	2438	2440	2441	2442	2442	2443	2442	2442	2442	2443	2440	2442	2443	2440	2438	2435	2426	2411
40	2417	2422	2425	2427	2428	2429	2431	2433	2434	2434	2433	2433	2433	2433	2433	2433	2433	2433	2433	2433	2433	2433	2433	2424	2411
35	2428	2433	2433	2428	2425	2424	2425	2428	2430	2429	2427	2426	2426	2426	2426	2426	2426	2426	2426	2426	2426	2426	2426	2424	2413
30	2436	2439	2434	2423	2415	2415	2420	2425	2428	2430	2429	2427	2426	2426	2426	2426	2426	2426	2426	2426	2426	2426	2426	2425	2417
25	2439	2440	2428	2411	2403	2409	2418	2423	2426	2428	2429	2427	2424	2423	2423	2423	2423	2423	2423	2423	2423	2423	2424	2423	2423
20	2438	2436	2421	2400	2398	2410	2418	2418	2414	2414	2415	2414	2412	2413	2415	2413	2407	2406	2406	2406	2406	2406	2413	2423	2427
15	2433	2430	2413	2395	2401	2414	2416	2400	2380	2377	2380	2379	2378	2389	2405	2402	2394	2401	2402	2394	2401	2401	2417	2428	
10	2425	2420	2403	2391	2402	2413	2401	2356	2322	2334	2346	2339	2323	2342	2391	2411	2404	2391	2391	2394	2401	2412	2412	2427	
5	2415	2407	2387	2380	2395	2402	2368	2284	2273	2322	2342	2326	2278	2279	2369	2411	2408	2392	2392	2392	2410	2410	2426	2426	
0	2407	2392	2370	2366	2386	2391	2340	2256	2260	2324	2345	2325	2262	2240	2348	2403	2405	2392	2392	2393	2411	2426	2426	2426	
-5	2403	2386	2364	2364	2387	2395	2356	2272	2273	2323	2341	2323	2276	2276	2355	2396	2396	2386	2386	2394	2413	2426	2426	2426	
-10	2404	2390	2374	2375	2395	2407	2391	2354	2321	2335	2345	2338	2279	2371	2386	2398	2390	2382	2382	2395	2415	2426	2426	2426	
-15	2410	2404	2394	2392	2403	2413	2410	2354	2321	2335	2345	2338	2279	2371	2386	2398	2390	2382	2382	2395	2415	2426	2426	2426	
-20	2418	2420	2416	2411	2412	2415	2416	2415	2413	2412	2412	2412	2412	2412	2419	2410	2405	2391	2385	2399	2417	2425	2425	2425	
-25	2424	2431	2433	2430	2424	2420	2419	2422	2425	2427	2426	2425	2425	2425	2419	2410	2405	2396	2396	2408	2419	2422	2422	2418	
-30	2424	2433	2441	2442	2438	2431	2427	2427	2429	2431	2429	2426	2423	2422	2421	2420	2420	2421	2426	2429	2436	2436	2426	2416	
-35	2420	2429	2440	2446	2447	2443	2438	2435	2434	2434	2432	2429	2426	2425	2426	2426	2426	2426	2426	2431	2435	2436	2431	2418	
-40	2416	2424	2434	2443	2448	2449	2447	2445	2443	2441	2439	2437	2435	2433	2433	2433	2433	2433	2433	2437	2438	2434	2434	2423	
-45	2413	2421	2429	2437	2443	2447	2449	2449	2449	2449	2448	2446	2442	2438	2434	2434	2434	2434	2433	2431	2433	2435	2434	2426	
-50	2409	2420	2428	2434	2438	2441	2445	2448	2451	2452	2451	2449	2444	2437	2430	2424	2422	2422	2425	2428	2428	2428	2428	2423	

Table 14-8. Linear polarization, mixed dihedral angles.

$\theta_2$	DIHEDRAL ANGLE 1.25 WAVELENGTH 6943																					$\theta_1$
	RANGE CORRECTION (METERS)																					
	-50	-45	-40	-35	-30	-25	-20	-15	-10	-5	0	5	10	15	20	25	30	35	40	45	50	
50	2361	2380	2378	2381	2388	2398	2408	2416	2420	2422	2422	2421	2419	2416	2416	2415	2416	2418	2417	2408	2393	
45	2396	2397	2396	2398	2403	2410	2417	2422	2423	2422	2422	2420	2423	2427	2428	2425	2422	2419	2414	2403	2384	
40	2412	2415	2414	2412	2414	2418	2423	2426	2427	2425	2422	2421	2425	2430	2434	2432	2428	2421	2414	2401	2378	
35	2428	2431	2426	2419	2417	2421	2426	2431	2434	2434	2432	2430	2433	2433	2435	2434	2430	2424	2416	2403	2382	
30	2439	2440	2430	2417	2415	2422	2430	2435	2440	2443	2443	2441	2437	2435	2433	2431	2427	2423	2418	2410	2395	
25	2445	2444	2428	2413	2414	2425	2433	2437	2440	2444	2444	2442	2437	2432	2429	2425	2421	2417	2416	2416	2409	
20	2445	2443	2426	2412	2419	2431	2435	2431	2428	2429	2431	2430	2425	2421	2422	2422	2418	2413	2413	2418	2419	
15	2440	2440	2425	2416	2426	2435	2429	2410	2399	2402	2407	2404	2397	2397	2412	2424	2416	2416	2412	2419	2425	
10	2430	2431	2421	2418	2429	2432	2408	2369	2364	2382	2391	2384	2365	2360	2396	2428	2424	2424	2417	2421	2427	
5	2418	2418	2411	2413	2424	2418	2370	2323	2349	2382	2393	2383	2350	2322	2371	2426	2438	2430	2422	2424	2429	
0	2408	2406	2400	2407	2419	2406	2341	2329	2347	2385	2397	2385	2349	2303	2347	2414	2432	2427	2421	2425	2428	
-5	2403	2399	2395	2405	2418	2409	2354	2309	2346	2382	2394	2384	2355	2326	2360	2407	2420	2415	2415	2422	2427	
-10	2404	2400	2397	2407	2420	2418	2387	2352	2359	2381	2392	2388	2378	2381	2403	2418	2415	2405	2407	2419	2426	
-15	2410	2409	2405	2409	2419	2421	2411	2396	2394	2401	2406	2409	2414	2425	2434	2432	2418	2404	2405	2418	2424	
-20	2416	2421	2417	2415	2416	2420	2422	2423	2425	2428	2430	2432	2437	2443	2444	2437	2422	2408	2408	2417	2420	
-25	2419	2428	2429	2424	2424	2420	2425	2433	2440	2442	2442	2441	2442	2444	2442	2437	2422	2408	2414	2417	2414	
-30	2413	2427	2433	2432	2427	2424	2428	2436	2442	2444	2443	2438	2436	2435	2434	2435	2424	2415	2414	2418	2408	
-35	2399	2416	2428	2433	2433	2432	2433	2436	2440	2440	2436	2430	2425	2425	2426	2427	2426	2426	2426	2421	2407	
-40	2384	2400	2416	2427	2433	2436	2437	2437	2437	2434	2436	2430	2425	2421	2422	2422	2423	2424	2425	2422	2411	
-45	2378	2391	2404	2417	2426	2432	2436	2436	2435	2433	2430	2427	2423	2419	2415	2412	2411	2413	2418	2419	2412	
-50	2379	2391	2402	2410	2417	2423	2428	2431	2433	2433	2431	2428	2422	2413	2402	2392	2388	2393	2402	2408	2406	

Table 14-9. Circular polarization.

$\theta_2$	DIHEDRAL ANGLE		WAVELENGTH 5320		RANGE CORRECTION (METERS)																				$\theta_1$
	.75	.75	.75	5320	-50	-45	-40	-35	-30	-25	-20	-15	-10	-5	0	5	10	15	20	25	30	35	40	45	
50	2373	2382	2370	2350	2329	2309	2305	2330	2369	2400	2412	2400	2368	2348	2356	2358	2333	2321	2364	2402	2404				
45	2362	2374	2367	2353	2337	2329	2343	2375	2407	2427	2429	2415	2389	2372	2373	2373	2336	2341	2363	2392	2393				
40	2355	2365	2361	2350	2340	2346	2370	2401	2426	2439	2436	2422	2405	2394	2390	2381	2356	2344	2342	2346	2346				
35	2348	2361	2362	2360	2354	2359	2379	2405	2427	2437	2434	2419	2406	2403	2403	2396	2376	2348	2323	2304	2302				
30	2331	2362	2382	2386	2377	2371	2379	2398	2419	2433	2433	2421	2405	2403	2412	2416	2405	2379	2345	2317	2312				
25	2326	2375	2407	2413	2399	2384	2387	2402	2420	2435	2440	2433	2418	2412	2419	2427	2426	2411	2382	2349	2332				
20	2345	2392	2426	2433	2417	2406	2411	2418	2424	2432	2437	2433	2427	2427	2429	2429	2426	2419	2401	2370	2339				
15	2362	2398	2433	2442	2433	2430	2435	2430	2445	2455	2454	2450	2447	2435	2440	2429	2414	2408	2400	2380	2351				
10	2368	2393	2426	2438	2438	2444	2446	2427	2389	2376	2380	2377	2392	2430	2444	2430	2404	2392	2392	2389	2379				
5	2384	2389	2410	2422	2402	2445	2445	2414	2376	2386	2396	2387	2381	2415	2440	2430	2404	2399	2390	2399	2405				
0	2400	2394	2396	2392	2405	2405	2442	2418	2382	2387	2393	2394	2371	2407	2433	2433	2413	2400	2396	2403	2411				
-5	2397	2396	2396	2395	2405	2429	2429	2425	2388	2374	2374	2380	2371	2407	2433	2433	2425	2420	2396	2403	2400				
-10	2374	2389	2398	2395	2409	2425	2435	2424	2406	2402	2406	2409	2421	2432	2430	2434	2423	2435	2423	2402	2385				
-15	2350	2380	2401	2405	2411	2425	2423	2414	2414	2428	2440	2440	2421	2432	2430	2424	2429	2438	2428	2400	2373				
-20	2342	2370	2398	2411	2418	2423	2423	2414	2406	2427	2442	2441	2427	2408	2430	2424	2419	2431	2421	2390	2353				
-25	2340	2355	2382	2404	2418	2415	2415	2401	2398	2415	2431	2434	2421	2401	2387	2384	2390	2416	2406	2374	2333				
-30	2328	2352	2356	2383	2405	2415	2412	2401	2400	2415	2433	2438	2427	2404	2380	2384	2394	2407	2386	2364	2335				
-35	2320	2351	2356	2364	2388	2401	2402	2398	2400	2419	2439	2442	2426	2396	2367	2367	2370	2370	2370	2361	2344				
-40	2348	2350	2344	2353	2378	2389	2385	2381	2394	2419	2439	2442	2426	2396	2348	2348	2350	2355	2358	2357	2345				
-45	2385	2385	2351	2331	2362	2381	2369	2353	2373	2410	2432	2431	2408	2371	2341	2336	2341	2346	2356	2364	2354				
-50	2397	2392	2344	2292	2326	2366	2360	2338	2353	2393	2413	2406	2378	2344	2325	2325	2331	2344	2367	2382	2375				

Table 14-10. Circular polarization.

$\theta_2$	DIHEDRAL ANGLE 1.25 WAVELENGTH 5320																				
	RANGE CORRECTION (METERS)																				
50	2355	2367	2364	2353	2349	2356	2371	2393	2416	2435	2444	2439	2423	2412	2411	2405	2379	2347	2339	2342	2333
45	2353	2368	2372	2369	2370	2378	2392	2410	2429	2443	2449	2443	2429	2419	2418	2416	2401	2376	2356	2338	2311
40	2366	2374	2375	2374	2378	2390	2406	2422	2437	2447	2449	2443	2433	2426	2423	2420	2409	2392	2372	2343	2309
35	2382	2388	2387	2384	2386	2396	2410	2424	2436	2442	2442	2436	2430	2429	2428	2424	2414	2400	2385	2366	2345
30	2392	2403	2407	2406	2403	2401	2404	2413	2424	2430	2429	2421	2418	2423	2431	2438	2426	2413	2400	2388	2377
25	2400	2418	2428	2430	2419	2403	2396	2402	2413	2423	2425	2417	2410	2416	2429	2438	2428	2415	2404	2400	2389
20	2412	2430	2443	2446	2431	2408	2401	2406	2413	2420	2422	2417	2414	2418	2425	2433	2424	2411	2402	2404	2386
15	2423	2437	2451	2453	2439	2421	2419	2418	2406	2392	2386	2389	2406	2424	2426	2421	2424	2412	2401	2404	2383
10	2430	2438	2449	2451	2440	2432	2433	2419	2373	2332	2327	2332	2374	2419	2427	2413	2407	2415	2417	2411	2398
5	2434	2436	2441	2440	2431	2432	2435	2407	2338	2325	2340	2329	2342	2402	2423	2411	2402	2410	2419	2423	2421
0	2432	2432	2433	2427	2417	2424	2432	2399	2333	2340	2356	2339	2331	2389	2418	2414	2410	2417	2426	2434	2436
-5	2420	2425	2427	2420	2408	2416	2428	2405	2341	2328	2337	2336	2374	2419	2422	2414	2410	2417	2426	2434	2436
-10	2403	2415	2425	2421	2408	2412	2424	2412	2363	2327	2325	2336	2378	2416	2421	2422	2432	2442	2442	2439	2434
-15	2390	2407	2423	2426	2418	2415	2418	2411	2391	2383	2391	2403	2415	2421	2416	2417	2434	2445	2443	2439	2434
-20	2389	2403	2419	2427	2427	2423	2418	2407	2401	2411	2425	2428	2422	2413	2406	2414	2434	2445	2443	2439	2434
-25	2375	2397	2410	2421	2428	2429	2423	2410	2402	2411	2424	2428	2422	2413	2406	2414	2434	2445	2443	2439	2434
-30	2350	2384	2398	2411	2422	2427	2426	2418	2402	2412	2424	2428	2422	2413	2406	2414	2434	2445	2443	2439	2434
-35	2322	2366	2387	2406	2419	2423	2422	2420	2424	2417	2427	2431	2425	2417	2413	2414	2434	2445	2443	2439	2434
-40	2322	2351	2377	2400	2417	2423	2421	2420	2424	2417	2427	2431	2425	2417	2413	2414	2434	2445	2443	2439	2434
-45	2312	2343	2360	2381	2408	2420	2413	2404	2417	2441	2454	2453	2441	2422	2406	2396	2391	2389	2386	2381	2367
-50	2322	2336	2335	2347	2384	2409	2408	2401	2413	2437	2448	2441	2420	2394	2372	2356	2348	2352	2364	2369	2357

Table 14-11. Circular polarization.

$\theta_2$	DIHEDRAL ANGLE 1.75 WAVELENGTH 5320																					$\theta_1$
	RANGE CORRECTION (METERS)																					
50	2348	2366	2378	2386	2395	2406	2418	2427	2436	2443	2446	2445	2440	2440	2442	2443	2439	2426	2412	2401	2386	2355
45	2366	2382	2393	2400	2406	2412	2418	2424	2432	2440	2445	2443	2438	2438	2438	2443	2443	2435	2422	2409	2391	2360
40	2390	2395	2400	2403	2408	2413	2419	2424	2430	2436	2439	2438	2434	2434	2435	2439	2441	2436	2428	2416	2399	2374
35	2409	2409	2407	2405	2406	2411	2417	2422	2425	2428	2428	2427	2428	2428	2431	2434	2434	2431	2427	2421	2411	2397
30	2422	2421	2417	2413	2411	2411	2411	2411	2410	2409	2406	2403	2409	2420	2420	2428	2431	2428	2425	2420	2420	2413
25	2432	2432	2430	2427	2420	2408	2396	2390	2391	2393	2389	2380	2381	2398	2417	2428	2429	2431	2427	2424	2422	2417
20	2441	2441	2441	2440	2427	2401	2381	2381	2387	2391	2388	2377	2372	2383	2401	2418	2418	2428	2428	2419	2412	2412
15	2451	2448	2448	2446	2428	2395	2383	2388	2383	2368	2354	2349	2367	2385	2389	2398	2414	2422	2419	2413	2407	2407
10	2457	2451	2448	2443	2423	2395	2393	2389	2383	2368	2262	2264	2329	2382	2385	2380	2396	2413	2419	2419	2419	2416
5	2452	2445	2437	2434	2411	2391	2395	2395	2373	2278	2288	2263	2280	2365	2382	2374	2388	2410	2424	2432	2432	2433
0	2440	2436	2432	2425	2399	2383	2390	2361	2262	2287	2321	2286	2261	2350	2380	2379	2393	2416	2433	2444	2447	2453
-5	2426	2426	2427	2422	2401	2379	2382	2375	2277	2261	2285	2255	2281	2366	2386	2388	2406	2427	2440	2450	2450	2452
-10	2417	2419	2424	2424	2411	2392	2384	2376	2353	2343	2358	2375	2388	2391	2387	2398	2417	2435	2442	2448	2452	2452
-15	2415	2418	2421	2423	2419	2408	2396	2381	2357	2373	2388	2392	2388	2385	2391	2408	2425	2432	2442	2442	2445	2445
-20	2414	2417	2418	2420	2420	2418	2411	2397	2381	2378	2385	2387	2387	2393	2406	2418	2424	2424	2425	2426	2426	2426
-25	2408	2412	2415	2419	2422	2423	2421	2413	2405	2402	2404	2407	2409	2413	2418	2420	2420	2420	2419	2419	2420	2418
-30	2396	2406	2414	2422	2428	2430	2425	2420	2420	2426	2432	2432	2428	2423	2422	2422	2420	2418	2417	2416	2414	2409
-35	2382	2400	2412	2423	2433	2438	2431	2423	2425	2436	2444	2442	2434	2426	2423	2423	2423	2420	2417	2412	2404	2395
-40	2371	2397	2409	2418	2431	2440	2437	2429	2430	2442	2450	2447	2437	2428	2424	2424	2415	2409	2402	2392	2378	2378
-45	2363	2391	2402	2409	2423	2435	2437	2433	2436	2446	2452	2449	2440	2430	2421	2421	2409	2398	2390	2385	2376	2361
-50																						



Table 14-13. Circular polarization.

$\theta_2$	DIHEDRAL ANGLE .75 WAVELENGTH 6943																				
	RANGE CORRECTION (METERS)																				
	-50	-45	-40	-35	-30	-25	-20	-15	-10	-5	0	5	10	15	20	25	30	35	40	45	50
50	2364	2352	2338	2332	2342	2364	2391	2414	2429	2434	2427	2414	2399	2389	2385	2384	2379	2369	2355	2345	2347
45	2365	2357	2347	2343	2351	2369	2392	2413	2428	2434	2429	2416	2401	2391	2390	2393	2391	2382	2364	2344	2329
40	2375	2373	2365	2358	2361	2372	2390	2410	2427	2436	2435	2425	2409	2396	2394	2400	2405	2402	2390	2368	2341
35	2393	2394	2383	2374	2374	2383	2397	2414	2430	2441	2444	2438	2425	2410	2404	2408	2416	2418	2412	2396	2370
30	2412	2412	2400	2391	2393	2402	2412	2422	2434	2444	2448	2445	2436	2425	2420	2420	2423	2425	2421	2411	2392
25	2426	2427	2417	2411	2416	2424	2428	2429	2432	2437	2440	2448	2438	2432	2433	2433	2431	2425	2419	2411	2399
20	2432	2435	2430	2430	2437	2440	2437	2426	2416	2414	2415	2417	2439	2432	2439	2444	2439	2425	2410	2400	2394
15	2427	2435	2437	2442	2449	2448	2448	2442	2394	2393	2395	2414	2438	2414	2438	2450	2445	2427	2404	2388	2383
10	2413	2426	2435	2446	2453	2448	2426	2397	2387	2397	2402	2397	2390	2401	2431	2449	2447	2429	2403	2383	2377
5	2396	2410	2426	2444	2453	2445	2418	2391	2395	2409	2415	2409	2396	2395	2420	2443	2444	2430	2407	2387	2377
0	2384	2394	2415	2439	2451	2445	2417	2393	2400	2414	2419	2412	2397	2390	2412	2436	2441	2431	2415	2398	2385
-5	2380	2385	2406	2434	2451	2448	2423	2397	2397	2409	2413	2405	2389	2387	2413	2436	2441	2435	2424	2413	2398
-10	2382	2383	2401	2429	2448	2450	2430	2401	2390	2395	2396	2387	2378	2392	2422	2440	2442	2437	2432	2427	2414
-15	2387	2388	2402	2425	2443	2446	2433	2408	2392	2390	2388	2383	2388	2412	2434	2442	2440	2435	2434	2435	2425
-20	2393	2397	2407	2423	2435	2438	2429	2417	2411	2413	2415	2415	2420	2430	2438	2438	2431	2426	2429	2434	2427
-25	2396	2405	2414	2423	2428	2427	2421	2419	2426	2437	2443	2443	2439	2436	2432	2425	2416	2412	2418	2426	2421
-30	2399	2404	2416	2423	2423	2417	2410	2412	2427	2443	2451	2450	2442	2430	2418	2407	2398	2398	2406	2414	2409
-35	2372	2393	2409	2418	2418	2410	2400	2401	2416	2434	2445	2444	2435	2419	2403	2390	2383	2385	2393	2399	2393
-40	2351	2373	2393	2406	2409	2404	2395	2391	2402	2420	2433	2445	2435	2412	2394	2379	2371	2372	2377	2381	2378
-45	2340	2356	2375	2390	2396	2395	2389	2387	2395	2412	2427	2433	2428	2413	2392	2371	2357	2354	2358	2364	2367
-50	2347	2350	2366	2379	2383	2380	2377	2380	2393	2412	2428	2435	2430	2413	2387	2360	2343	2340	2347	2356	2360





Table 14-15. Circular polarization.

θ <sub>2</sub>	DIHEDRAL ANGLE 1.75		WAVELENGTH 6943		RANGE CORRECTION (METERS)		DIHEDRAL ANGLE 1.75														
	WAVELENGTH	6943	0	5	10	15	20	25	30	35	40	45	50	θ <sub>1</sub>							
2386	2385	2388	2388	2385	2406	2418	2429	2439	2447	2451	2452	2448	2442	2437	2433	2432	2430	2426	2419	2409	2397
2395	2393	2394	2394	2400	2408	2418	2428	2436	2442	2445	2444	2440	2436	2434	2434	2434	2433	2428	2421	2413	2405
2411	2408	2406	2406	2419	2427	2432	2439	2447	2452	2455	2454	2450	2446	2444	2444	2443	2438	2431	2423	2415	2407
2428	2426	2420	2420	2432	2440	2448	2456	2464	2470	2473	2472	2468	2464	2462	2462	2461	2456	2449	2441	2433	2425
2442	2441	2432	2432	2444	2452	2460	2468	2476	2482	2485	2484	2480	2476	2474	2474	2473	2468	2461	2453	2445	2437
2452	2451	2440	2440	2452	2460	2468	2476	2484	2490	2493	2492	2488	2484	2482	2482	2477	2470	2462	2454	2446	2438
2457	2456	2445	2445	2457	2465	2473	2481	2489	2495	2498	2497	2493	2489	2487	2487	2482	2475	2467	2459	2451	2443
2458	2456	2446	2446	2458	2466	2474	2482	2490	2496	2499	2498	2494	2490	2488	2488	2483	2476	2468	2460	2452	2444
2453	2451	2442	2442	2453	2461	2469	2477	2485	2491	2494	2493	2489	2485	2483	2483	2478	2471	2463	2455	2447	2439
2456	2441	2432	2432	2443	2451	2459	2467	2475	2481	2484	2483	2479	2475	2473	2473	2468	2461	2453	2445	2437	2429
2459	2432	2422	2422	2433	2441	2449	2457	2465	2471	2474	2473	2469	2465	2463	2463	2458	2451	2443	2435	2427	2419
2434	2426	2414	2414	2425	2433	2441	2449	2457	2463	2466	2465	2461	2457	2455	2455	2450	2443	2435	2427	2419	2411
2432	2425	2413	2413	2424	2432	2440	2448	2456	2462	2465	2464	2460	2456	2454	2454	2449	2442	2434	2426	2418	2410
2431	2427	2417	2417	2428	2436	2444	2452	2460	2466	2469	2468	2464	2460	2458	2458	2453	2446	2438	2430	2422	2414
2431	2431	2425	2425	2436	2444	2452	2460	2468	2474	2477	2476	2472	2468	2466	2466	2461	2454	2446	2438	2430	2422
2429	2433	2431	2431	2442	2450	2458	2466	2474	2480	2483	2482	2478	2474	2472	2472	2467	2460	2452	2444	2436	2428
2424	2431	2433	2433	2444	2452	2460	2468	2476	2482	2485	2484	2480	2476	2474	2474	2469	2462	2454	2446	2438	2430
2417	2425	2431	2431	2442	2450	2458	2466	2474	2480	2483	2482	2478	2474	2472	2472	2467	2460	2452	2444	2436	2428
2409	2419	2427	2427	2438	2446	2454	2462	2470	2476	2479	2478	2474	2470	2468	2468	2463	2456	2448	2440	2432	2424
2404	2416	2425	2425	2436	2444	2452	2460	2468	2474	2477	2476	2472	2468	2466	2466	2461	2454	2446	2438	2430	2422
2399	2414	2425	2425	2436	2444	2452	2460	2468	2474	2477	2476	2472	2468	2466	2466	2461	2454	2446	2438	2430	2422

Table 14-16. Circular polarization, mixed dihedral angles.

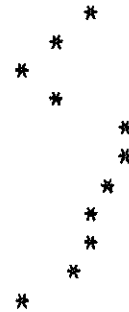
$\theta_2$	DIPEDRAL ANGLE 1.25		WAVELENGTH 69.3		RANGE CORRECTION (METERS)																																		
50	2370	2367	2365	2369	2378	2392	2409	2424	2435	2439	2436	2428	2419	2413	2410	2410	2410	2410	2410	2409	2405	2398	2388	2376															
45	2380	2378	2375	2376	2384	2396	2410	2424	2433	2435	2431	2423	2417	2414	2415	2415	2416	2416	2416	2415	2411	2402	2389	2373															
40	2396	2395	2390	2386	2387	2394	2405	2417	2426	2426	2427	2421	2414	2412	2412	2412	2412	2412	2412	2412	2412	2416	2402	2383															
35	2414	2415	2407	2395	2391	2394	2403	2413	2423	2423	2430	2426	2419	2415	2415	2417	2424	2424	2424	2431	2435	2432	2422	2403															
30	2433	2433	2422	2407	2399	2402	2409	2417	2425	2431	2434	2431	2426	2422	2423	2423	2428	2428	2435	2440	2440	2442	2435	2420															
25	2447	2448	2436	2420	2415	2418	2422	2424	2425	2426	2427	2426	2425	2427	2431	2434	2434	2438	2441	2441	2441	2441	2438	2427															
20	2456	2457	2446	2434	2432	2435	2433	2424	2413	2406	2404	2404	2410	2424	2437	2441	2441	2443	2443	2443	2443	2442	2431	2424															
15	2457	2459	2451	2445	2446	2446	2437	2415	2392	2381	2379	2377	2386	2412	2437	2447	2447	2447	2447	2447	2447	2447	2447	2447															
10	2451	2453	2449	2449	2453	2450	2432	2399	2378	2380	2382	2377	2376	2399	2432	2447	2447	2447	2447	2447	2447	2447	2447	2447															
5	2440	2442	2442	2448	2454	2450	2424	2387	2378	2390	2396	2389	2378	2388	2421	2442	2442	2442	2442	2442	2442	2442	2442	2442															
0	2428	2430	2433	2443	2453	2449	2421	2383	2378	2393	2399	2391	2376	2379	2411	2435	2435	2435	2435	2435	2435	2435	2435	2435															
-5	2420	2421	2425	2438	2451	2449	2423	2382	2369	2381	2386	2378	2364	2373	2409	2434	2434	2434	2434	2434	2434	2434	2434	2434															
-10	2417	2418	2421	2433	2446	2447	2426	2384	2357	2360	2364	2358	2358	2385	2420	2437	2437	2437	2437	2437	2437	2437	2437	2437															
-15	2417	2420	2425	2430	2440	2441	2425	2393	2367	2362	2365	2370	2385	2413	2433	2439	2439	2439	2439	2439	2439	2439	2439	2439															
-20	2418	2424	2429	2438	2448	2453	2431	2404	2395	2398	2405	2412	2422	2432	2437	2437	2437	2437	2437	2437	2437	2437	2437	2437															
-25	2415	2426	2429	2430	2429	2424	2415	2408	2412	2423	2432	2437	2437	2435	2431	2423	2423	2423	2423	2423	2423	2423	2423	2423															
-30	2406	2421	2429	2431	2428	2420	2410	2406	2413	2427	2437	2440	2436	2429	2420	2411	2407	2412	2422	2422	2422	2422	2422	2422															
-35	2393	2411	2422	2427	2426	2419	2409	2403	2408	2420	2431	2434	2430	2421	2411	2403	2401	2404	2410	2410	2410	2410	2410	2410															
-40	2381	2400	2413	2420	2422	2418	2411	2406	2408	2418	2428	2433	2430	2422	2411	2402	2396	2395	2396	2396	2396	2396	2396	2396															
-45	2379	2398	2410	2415	2416	2414	2411	2411	2411	2416	2426	2441	2439	2429	2414	2402	2389	2383	2382	2382	2382	2382	2382	2382															
-50	2385	2401	2412	2416	2413	2407	2405	2410	2421	2435	2445	2448	2443	2430	2411	2393	2380	2374	2372	2372	2372	2372	2372	2372															

Table 15. Centroid range correction vs. velocity aberration. The average and rms deviation are computed around a circle in the far field whose radius is the velocity aberration listed, in microradians, in the first column. Table 15-1. Linear polarization.

DIHEDRAL ANGLE .75 WAVELENGTH 5320

AVERAGE RANGE CORRECTION (METERS)

0	.2403
5	.2390
10	.2370
15	.2389
20	.2424
25	.2427
30	.2416
35	.2412
40	.2409
45	.2393
50	.2370



R.M.S. FLUCTUATION

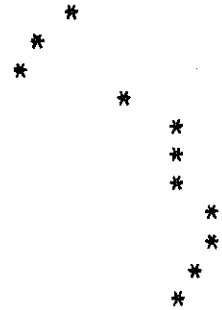
0	0.0000	*
5	.0004	*
10	.0028	*
15	.0036	*
20	.0016	*
25	.0011	*
30	.0012	*
35	.0009	*
40	.0010	*
45	.0015	*
50	.0020	*

Table 15-2. Linear polarization.

DIHEDRAL ANGLE 1.25 WAVELENGTH 5320

AVERAGE RANGE CORRECTION (METERS)

0	.2352
5	.2332
10	.2319
15	.2376
20	.2412
25	.2412
30	.2412
35	.2423
40	.2428
45	.2422
50	.2411



R.M.S. FLUCTUATION

0	0.0000	*
5	.0009	*
10	.0044	*
15	.0028	*
20	.0013	*
25	.0016	*
30	.0020	*
35	.0015	*
40	.0010	*
45	.0008	*
50	.0010	*

Table 15-3. Linear polarization.

DIHEDRAL ANGLE 1.75 WAVELENGTH 5320

AVERAGE RANGE CORRECTION (METERS)

0	.2314				*
5	.2273				
10	.2266		*		
15	.2348		*		
20	.2380			*	
25	.2381			*	*
30	.2396				*
35	.2417				*
40	.2425				*
45	.2428				*
50	.2429				*

R.M.S. FLUCTUATION

0	0.0000	*
5	.0008	*
10	.0027	*
15	.0007	*
20	.0004	*
25	.0012	*
30	.0017	*
35	.0014	*
40	.0012	*
45	.0012	*
50	.0013	*

Table 15-4. Linear polarization, mixed dihedral angles.

DIHEDRAL ANGLE  $\overline{1.25}$  WAVELENGTH 5320

AVERAGE RANGE CORRECTION (METERS)

0	.2372	*
5	.2355	*
10	.2341	*
15	.2383	*
20	.2418	*
25	.2418	*
30	.2416	*
35	.2422	*
40	.2424	*
45	.2417	*
50	.2409	*

R.M.S. FLUCTUATION

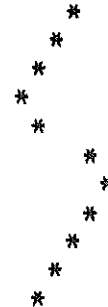
0	0.0000	*
5	.0006	*
10	.0031	*
15	.0024	*
20	.0010	*
25	.0009	*
30	.0011	*
35	.0008	*
40	.0008	*
45	.0010	*
50	.0015	*

Table 15-5. Linear polarization.

DIHEDRAL ANGLE .75 WAVELENGTH 6943

AVERAGE RANGE CORRECTION (METERS)

0	.2417
5	.2410
10	.2394
15	.2383
20	.2401
25	.2428
30	.2437
35	.2430
40	.2417
45	.2408
50	.2402



R.M.S. FLUCTUATION

0	0.0000	*
5	.0002	*
10	.0011	*
15	.0027	*
20	.0029	*
25	.0016	*
30	.0010	*
35	.0009	*
40	.0009	*
45	.0009	*
50	.0013	*



Table 15-6. Linear polarization.

DIHEDRAL ANGLE 1.25      WAVELENGTH 6943

AVERAGE RANGE CORRECTION (METERS)

0	.2389		
5	.2380		*
10	.2362		*
15	.2357		*
20	.2390		*
25	.2422		*
30	.2429		*
35	.2423		*
40	.2419		*
45	.2422		*
50	.2426		*

R.M.S. FLUCTUATION

0	0.0000	*	
5	.0004	*	
10	.0020	*	
15	.0045	*	*
20	.0037	*	*
25	.0019	*	
30	.0014	*	
35	.0015	*	
40	.0016	*	
45	.0013	*	
50	.0009	*	

Table 15-7. Linear polarization.

DIHEDRAL ANGLE 1.75      WAVELENGTH 6943

AVERAGE RANGE CORRECTION (METERS)

0	.2345								
5	.2331								
10	.2309								
15	.2326				*				
20	.2382				*				
25	.2411							*	
30	.2414								*
35	.2411								*
40	.2415								*
45	.2426								*
50	.2433								*

R.M.S. FLUCTUATION

0	0.0000	*		
5	.0005	*		
10	.0029		*	
15	.0045			*
20	.0023		*	
25	.0011	*		
30	.0012	*		
35	.0019	*		
40	.0021	*		
45	.0016	*		
50	.0012	*		

Table 15-8. Linear polarization, mixed dihedral angles.

DIHEDRAL ANGLE  $\overline{1.25}$  WAVELENGTH 6943

AVERAGE RANGE CORRECTION (METERS)

0	.2397	*
5	.2388	*
10	.2370	*
15	.2365	*
20	.2395	*
25	.2425	*
30	.2432	*
35	.2426	*
40	.2421	*
45	.2422	*
50	.2423	*

R.M.S. FLUCTUATION

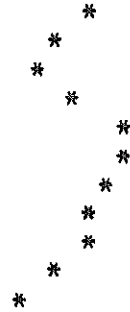
0	0.0000	*
5	.0003	*
10	.0016	*
15	.0035	*
20	.0029	*
25	.0013	*
30	.0009	*
35	.0009	*
40	.0010	*
45	.0008	*
50	.0008	*

Table 15-9. Circular polarization.

DIHEDRAL ANGLE .75 WAVELENGTH 5320

AVERAGE RANGE CORRECTION (METERS)

0	.2406
5	.2392
10	.2378
15	.2403
20	.2431
25	.2431
30	.2418
35	.2413
40	.2409
45	.2394
50	.2372



R.M.S. FLUCTUATION

0	0.0000	*
5	.0002	*
10	.0003	*
15	.0005	*
20	.0008	*
25	.0008	*
30	.0011	*
35	.0015	*
40	.0017	*
45	.0018	*
50	.0020	*

Table 15-10. Circular polarization

DIHEDRAL ANGLE  $\alpha = 1.25$  BY WAVELENGTH  $\lambda = 53200$

AVERAGE RANGE CORRECTION (METERS)

0	.2356	*	*	*	1585.	0
5	.2336		*	*	1585.	0
10	.2333			*	1585.	0
15	.2387			*	1585.	0
20	.2418	*		*	1585.	0
25	.2418	*		*	1585.	0
30	.2418	*		*	1585.	0
35	.2427	*		*	1585.	0
40	.2430	*		*	1585.	0
45	.2423	*		*	1585.	0
50	.2412	*		*	1585.	0

R.M.S. FLUCTUATION

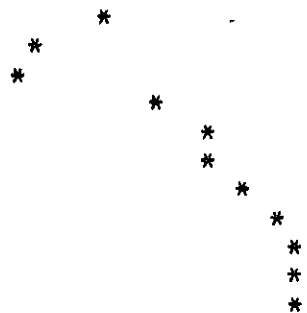
0	0.0000	*	*	*	0000.	0
5	.0002	*		*	0000.	0
10	.0004	*		*	0000.	0
15	.0007	*		*	0000.	0
20	.0008	*		*	0000.	0
25	.0007	*		*	0000.	0
30	.0009	*		*	0000.	0
35	.0011	*		*	0000.	0
40	.0012	*		*	0000.	0
45	.0014	*		*	0000.	0
50	.0017	*		*	0000.	0

Table 15-11. Circular polarization.

DIHEDRAL ANGLE 1.75 WAVELENGTH 5320

AVERAGE RANGE CORRECTION (METERS)

0	.2321
5	.2279
10	.2271
15	.2349
20	.2382
25	.2385
30	.2401
35	.2421
40	.2429
45	.2431
50	.2431



R.M.S. FLUCTUATION

0	0.0000	*
5	.0004	*
10	.0007	*
15	.0011	*
20	.0008	*
25	.0005	*
30	.0006	*
35	.0007	*
40	.0009	*
45	.0011	*
50	.0013	*

Table 15-12. Circular polarization, mixed dihedral angles.

DIHEDRAL ANGLE  $\overline{1.25}$  WAVELENGTH 5320

AVERAGE RANGE CORRECTION (METERS)

0	.2378
5	.2361
10	.2351
15	.2390
20	.2420
25	.2421
30	.2420
35	.2426
40	.2426
45	.2418
50	.2410

\*  
\*  
\*  
\*  
\*  
\*  
\*  
\*  
\*  
\*  
\*

R.M.S. FLUCTUATION

0	0.0000	*
5	.0006	*
10	.0009	*
15	.0011	*
20	.0012	*
25	.0011	*
30	.0011	*
35	.0013	*
40	.0014	*
45	.0015	*
50	.0018	*

Table 15-13. Circular polarization.

DIHEDRAL ANGLE .75 WAVELENGTH 6943

AVERAGE RANGE CORRECTION (METERS)

0	.2419
5	.2412
10	.2398
15	.2391
20	.2411
25	.2434
30	.2440
35	.2432
40	.2418
45	.2408
50	.2402

*
*
*
*
*
*
*
*
*
*
*
*

R.M.S. FLUCTUATION

0	0.0000	*
5	.0001	*
10	.0003	*
15	.0004	*
20	.0005	*
25	.0007	*
30	.0008	*
35	.0009	*
40	.0012	*
45	.0016	*
50	.0019	*



Table 15-14. Circular polarization.

DIHEDRAL ANGLE 1.25 WAVELENGTH 6943

AVERAGE RANGE CORRECTION (METERS)

0	.2392	*
5	.2383	*
10	.2368	*
15	.2372	*
20	.2405	*
25	.2430	*
30	.2434	*
35	.2428	*
40	.2423	*
45	.2425	*
50	.2427	*

R.M.S. FLUCTUATION

0	0.0000	*
5	.0001	*
10	.0003	*
15	.0004	*
20	.0006	*
25	.0008	*
30	.0008	*
35	.0009	*
40	.0011	*
45	.0014	*
50	.0016	*



Table 15-16. Circular polarization, mixed dihedral angles.

DIHEDRAL ANGLE  $\overline{1.25}$  WAVELENGTH 6943

AVERAGE RANGE CORRECTION (METERS)

0	.2399	*
5	.2390	*
10	.2374	*
15	.2376	*
20	.2405	*
25	.2430	*
30	.2435	*
35	.2429	*
40	.2424	*
45	.2424	*
50	.2425	*

R.M.S. FLUCTUATION

0	0.0000	*
5	.0004	*
10	.0007	*
15	.0008	*
20	.0010	*
25	.0011	*
30	.0011	*
35	.0010	*
40	.0011	*
45	.0014	*
50	.0016	*

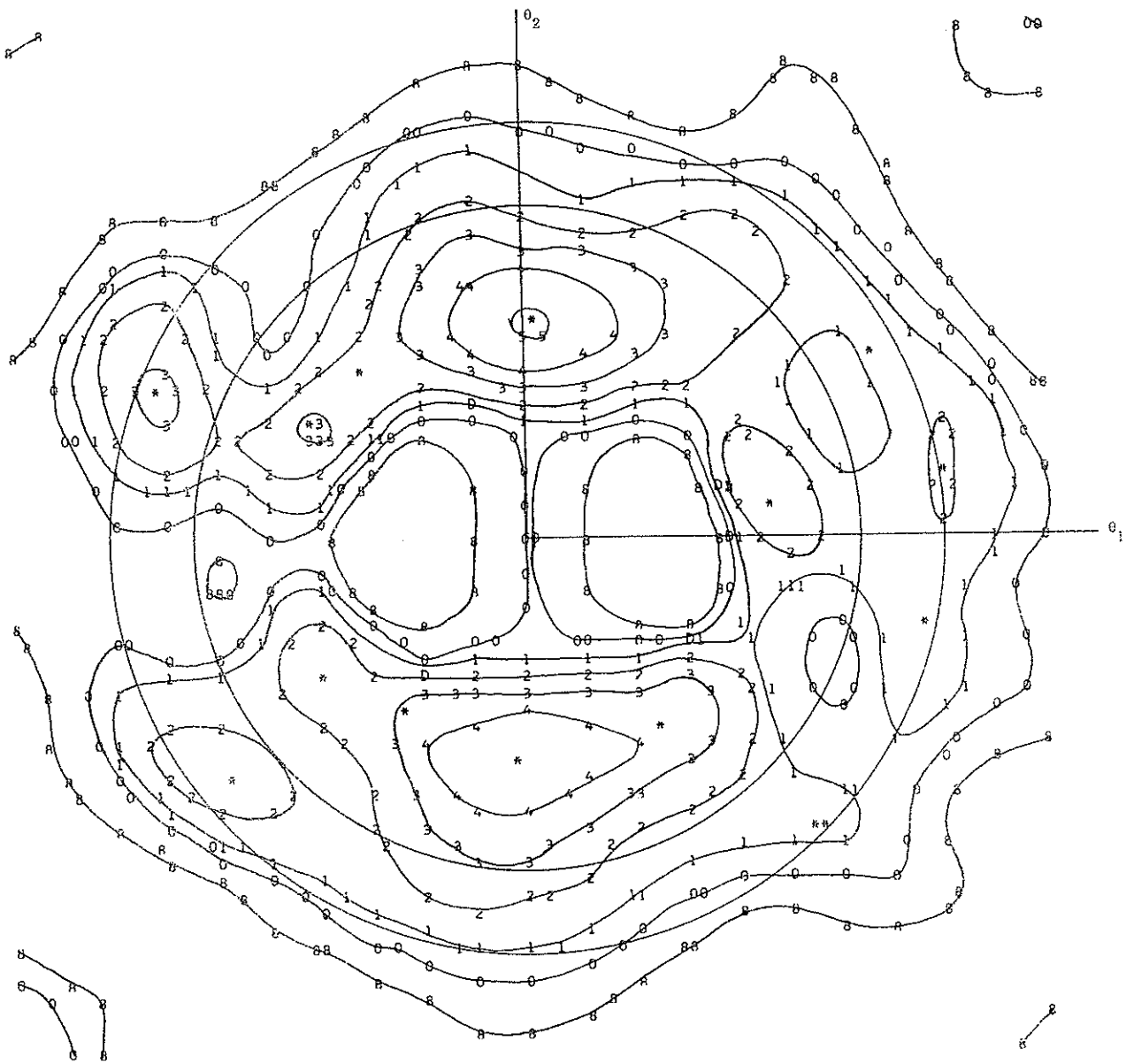


Figure 10. Contour plots of the centroid range correction matrices given in Table 14. Circles of radius 32 and 41  $\mu$ rad are shown to mark the minimum and maximum values of the velocity aberration. Table 11 lists the range correction corresponding to the numbers used to mark each contour. The polarization, dihedral angle offset  $\delta$ , and wavelength  $\lambda$  are given for each figure. Figure 10-1. Linear polarization,  $\delta=0^\circ 75$ ,  $\lambda = 5320 \text{ \AA}$ .

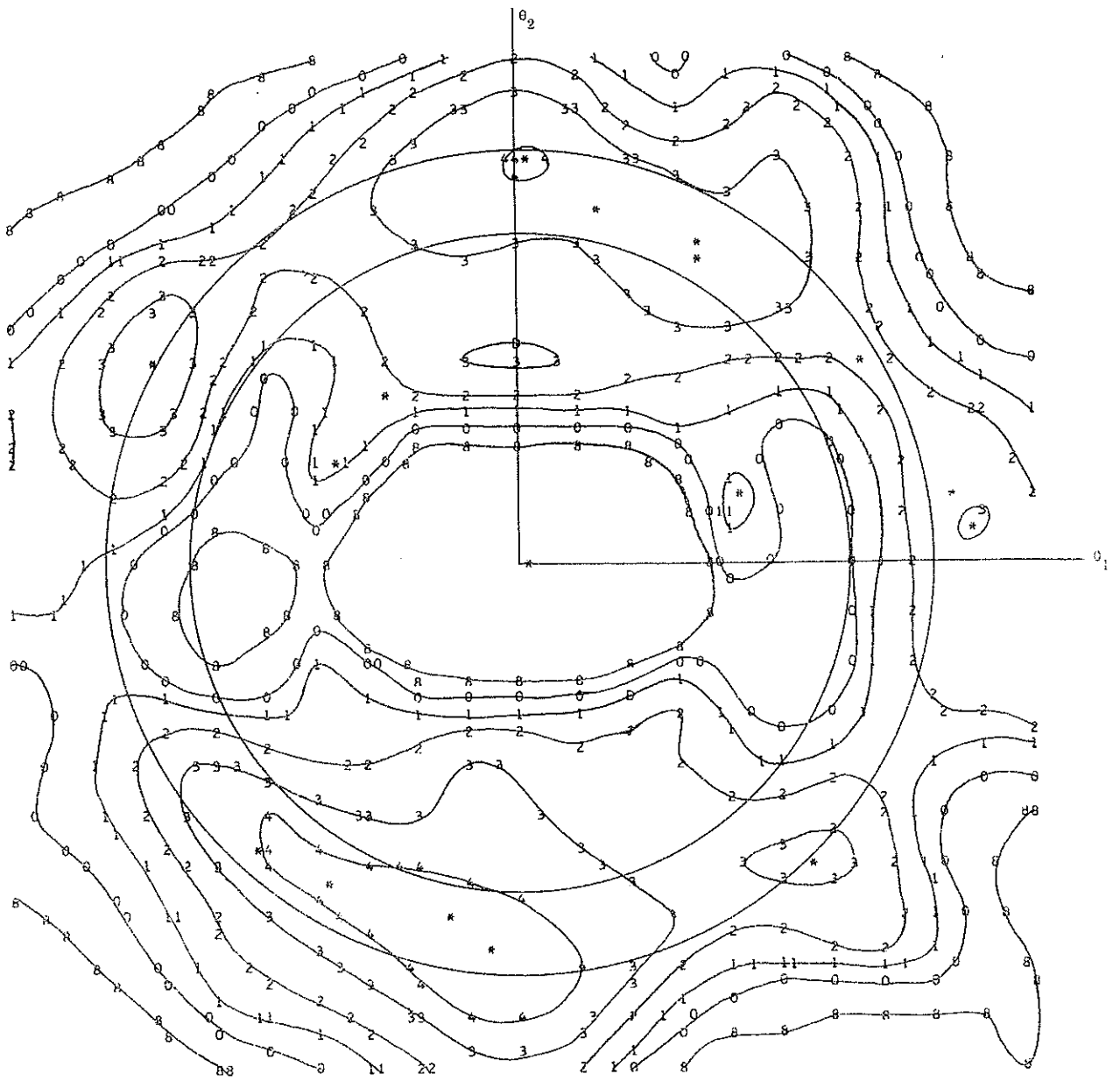


Figure 10-2. Linear polarization,  $\delta = 1''25$ ,  $\lambda = 5320 \text{ \AA}$ .

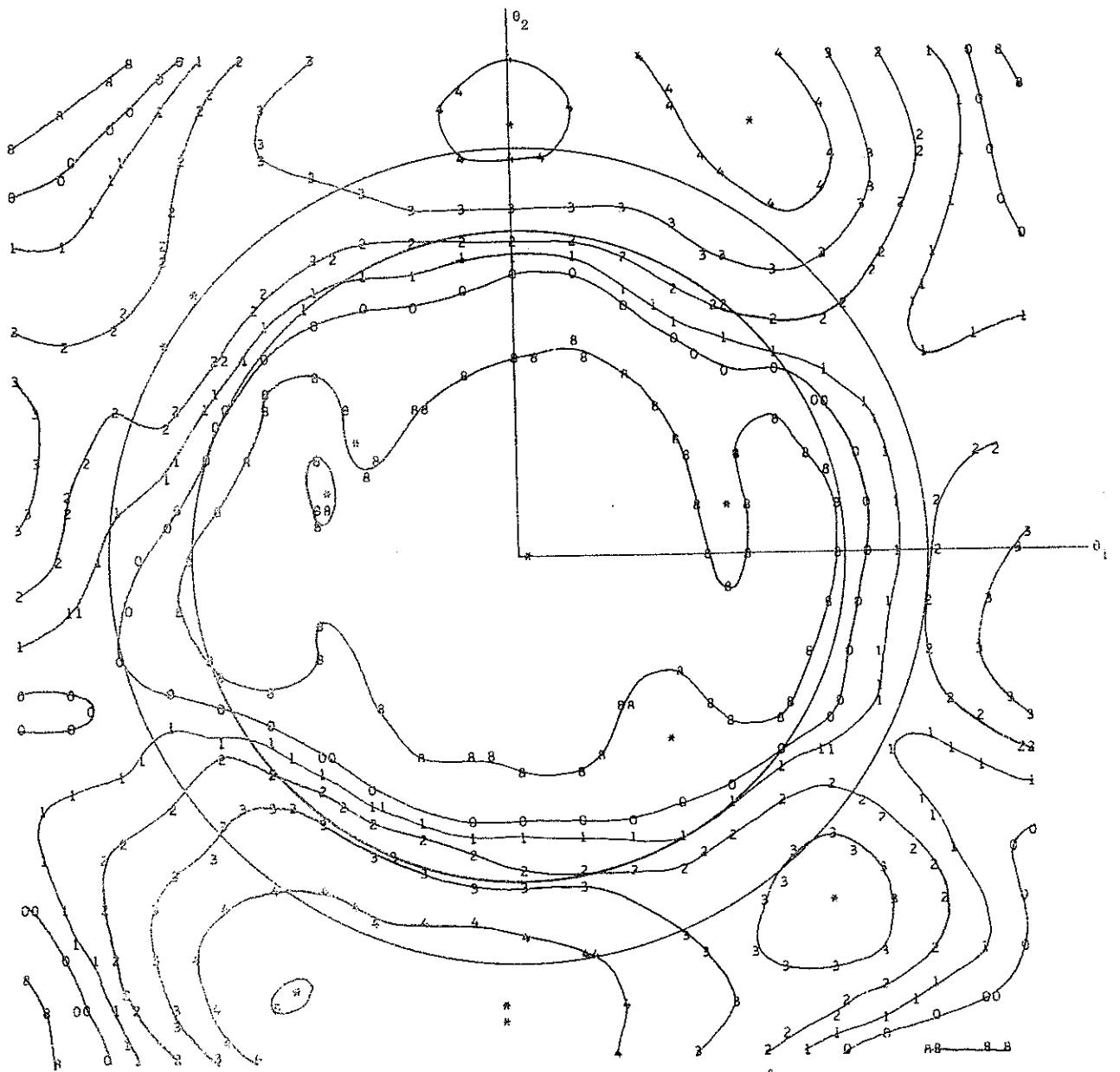


Figure 10-3. Linear polarization,  $\delta = 1.175$ ,  $\lambda = 5320 \text{ \AA}$ .

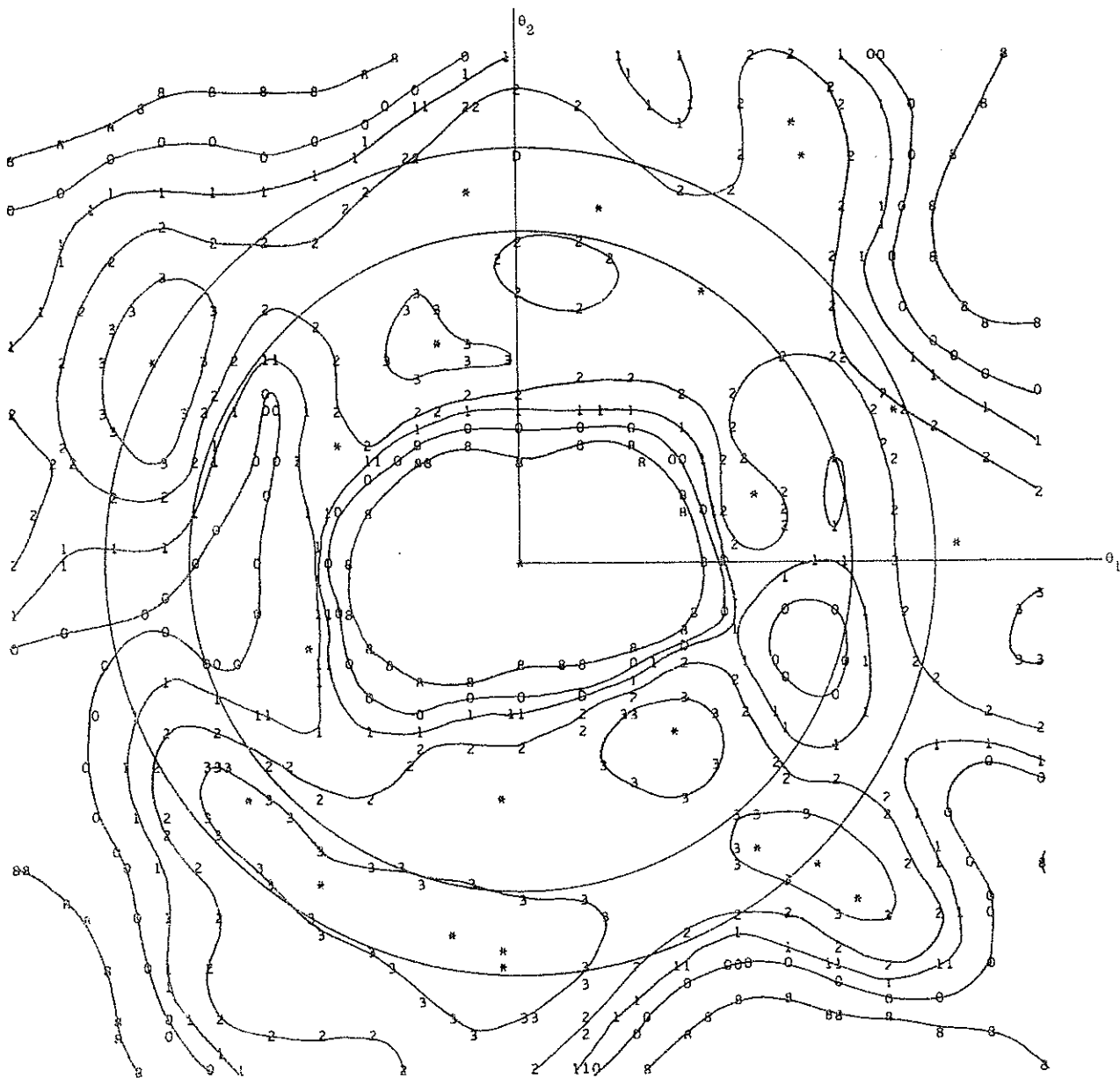


Figure 10-4. Linear polarization,  $\bar{\epsilon} = 1.25$  (mixed dihedral angles),  $\lambda = 5320 \text{ \AA}$ .

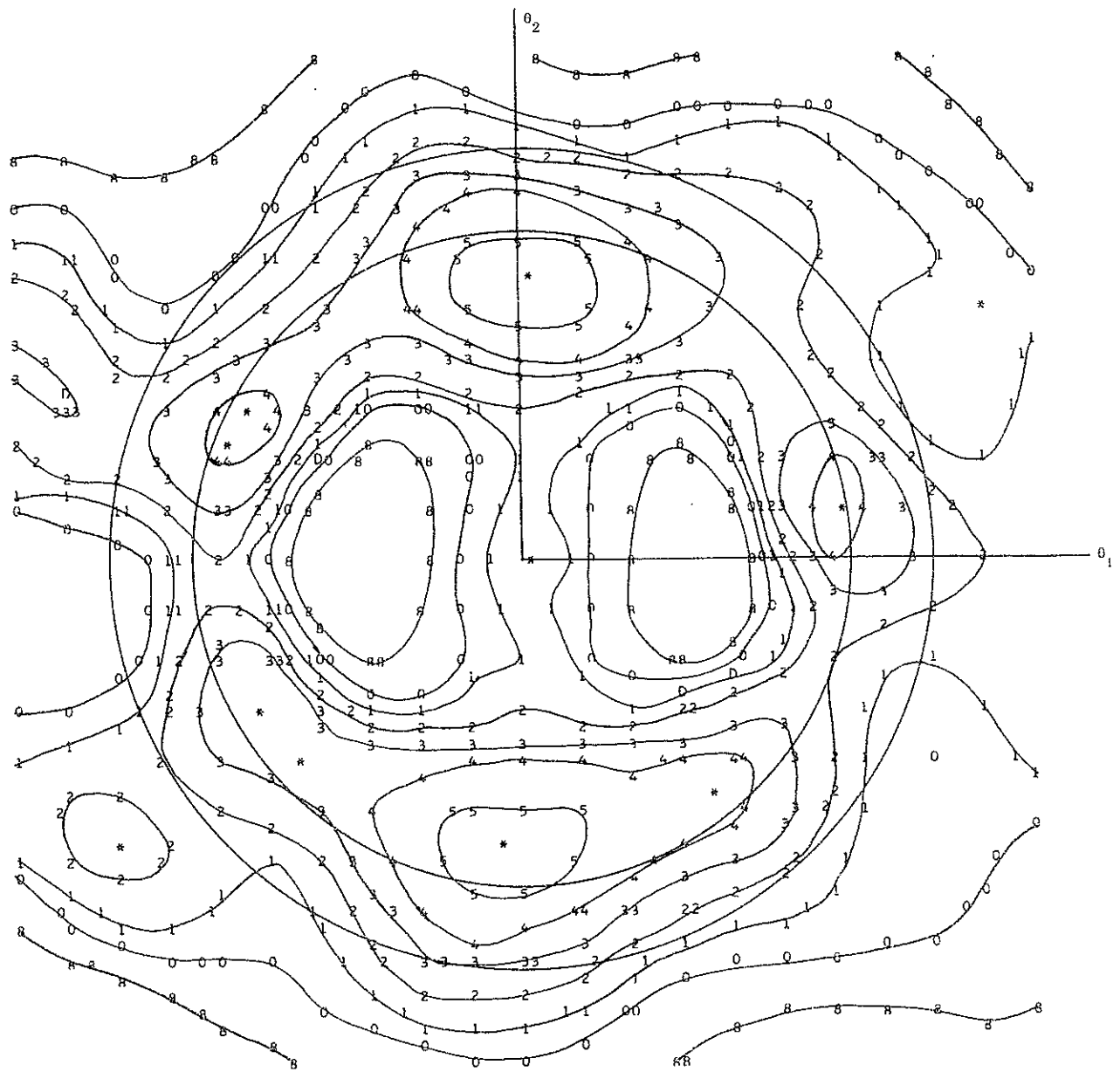


Figure 10-5. Linear polarization,  $\delta = 0^{\circ}75$ ,  $\lambda = 6943 \text{ \AA}$ .



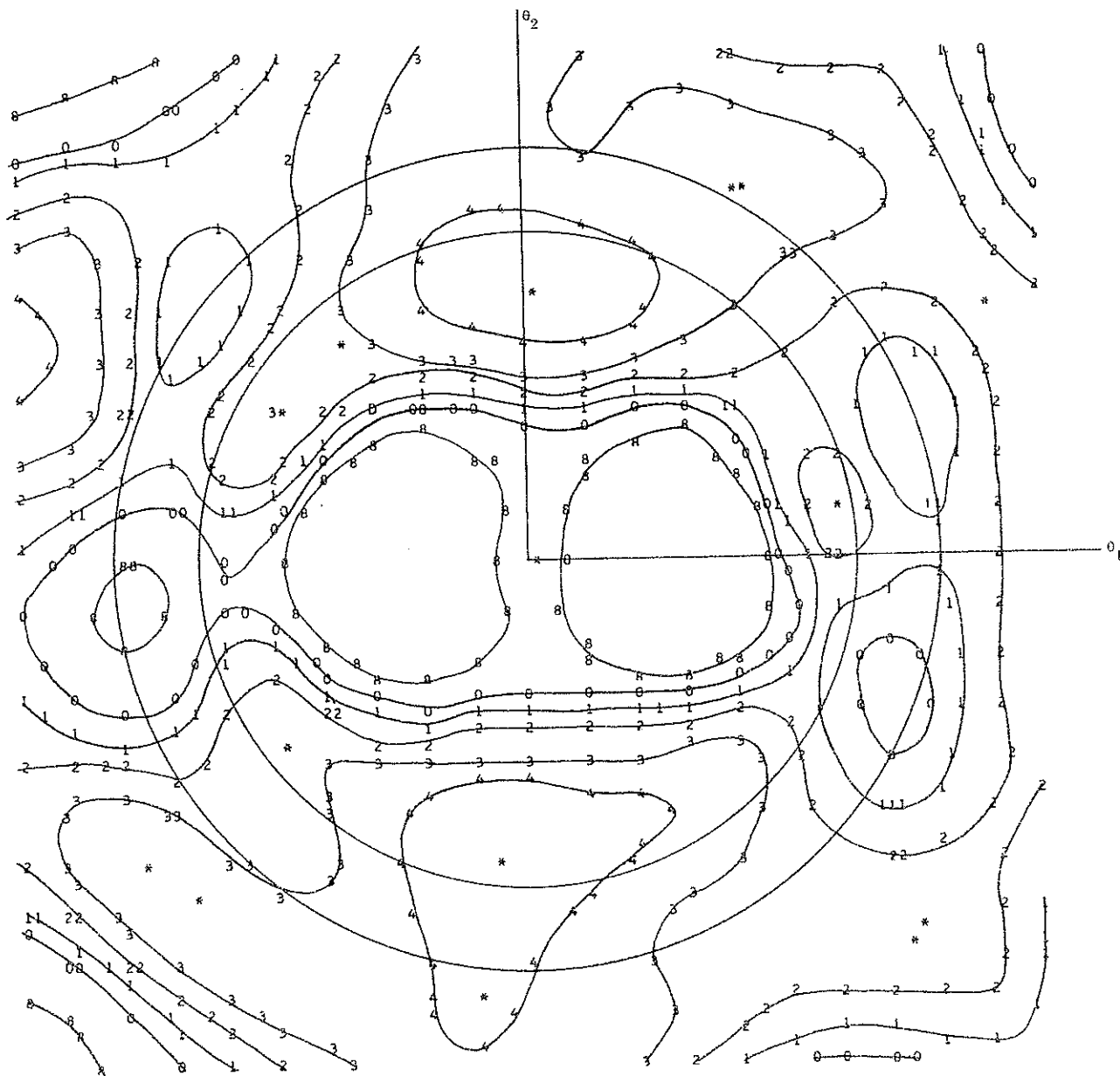


Figure 10-6. Linear polarization,  $\delta = 1''25$ ,  $\lambda = 6943 \text{ \AA}$ .

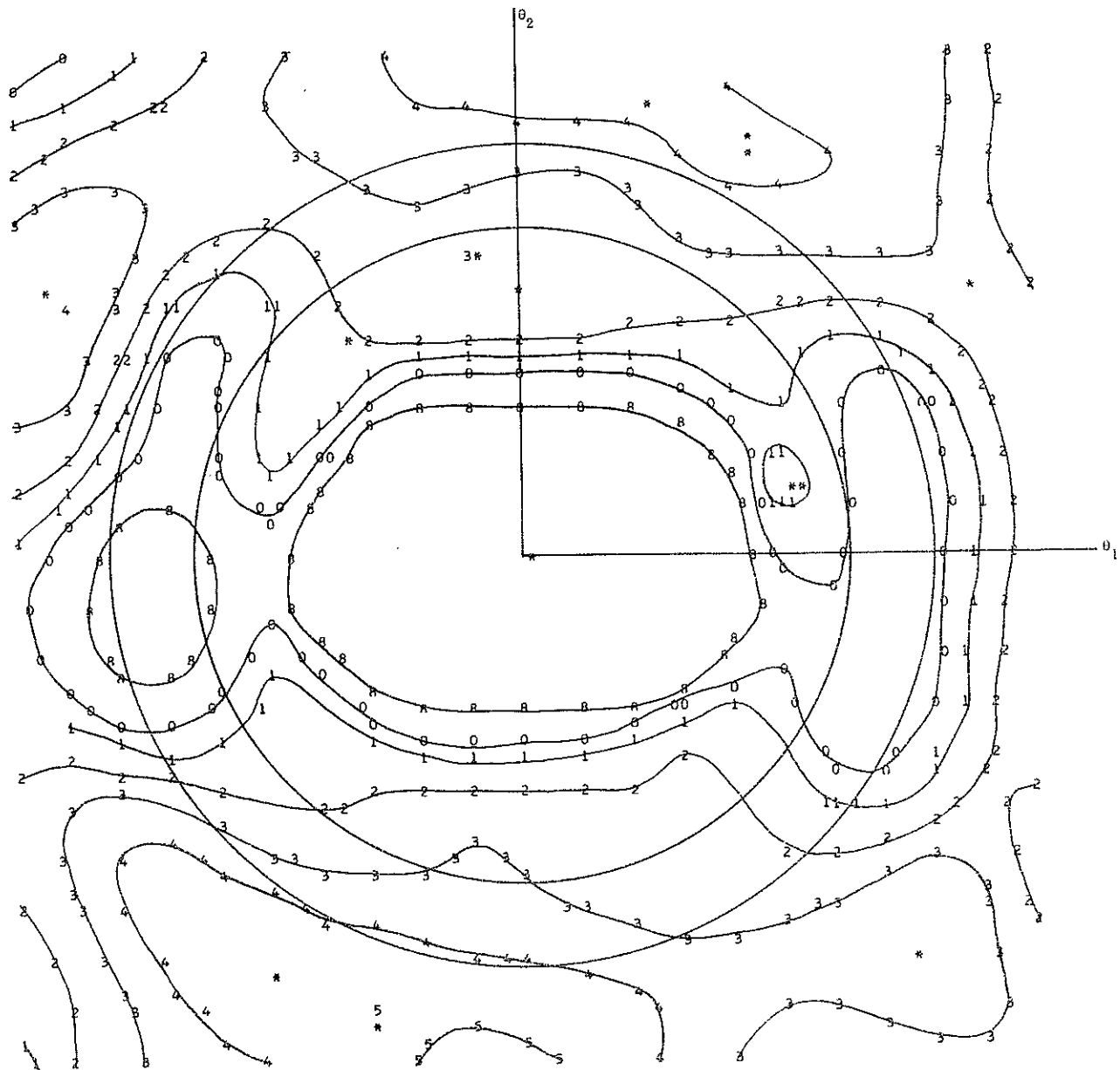


Figure 10-7. Linear polarization,  $\delta = 1^{\circ}75$ ,  $\lambda = 6943 \text{ \AA}$ .

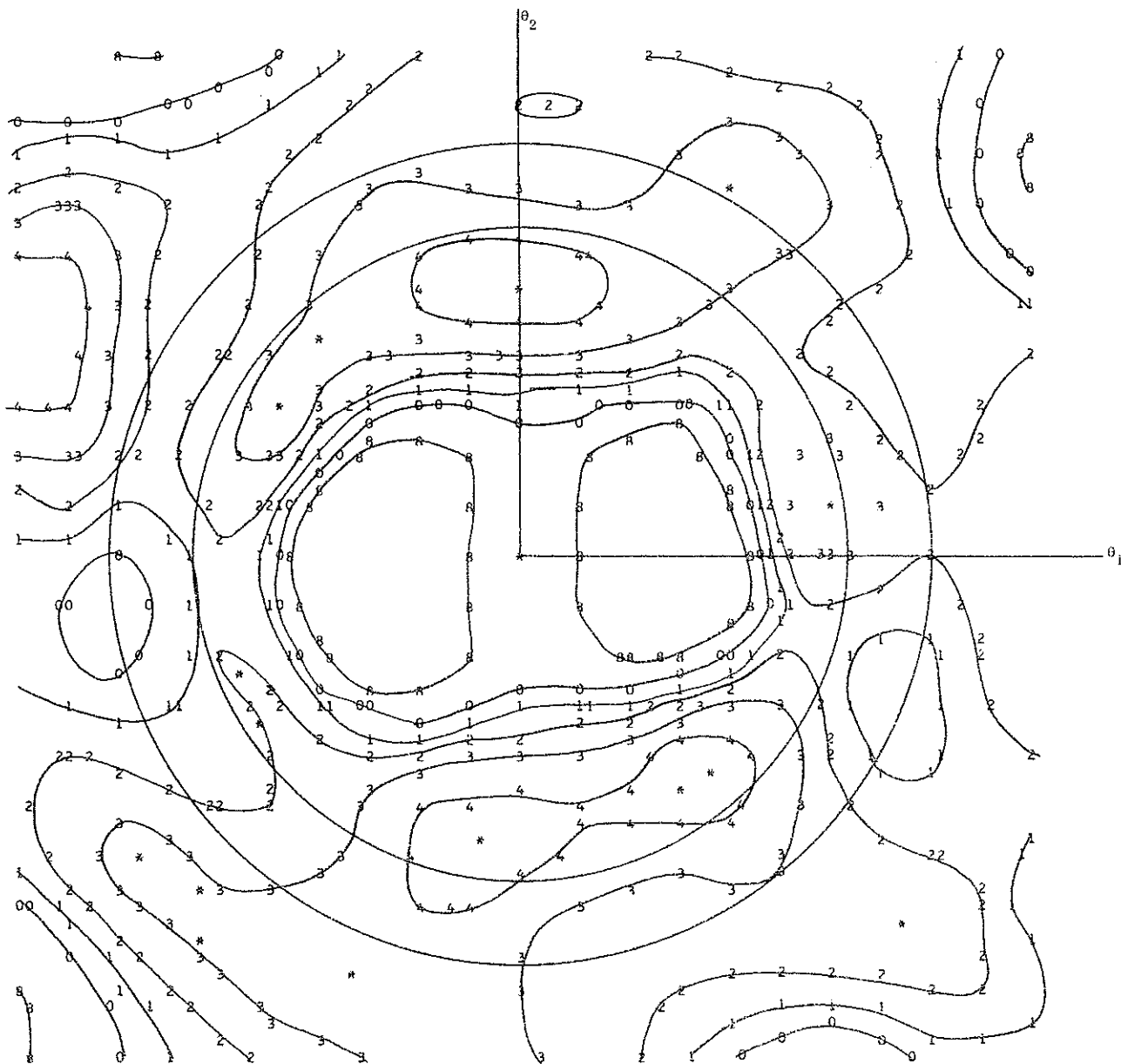


Figure 10-8. Linear polarization,  $\bar{\delta} = P25$  (mixed dihedral angles),  $\lambda = 6943 \text{ \AA}$ .

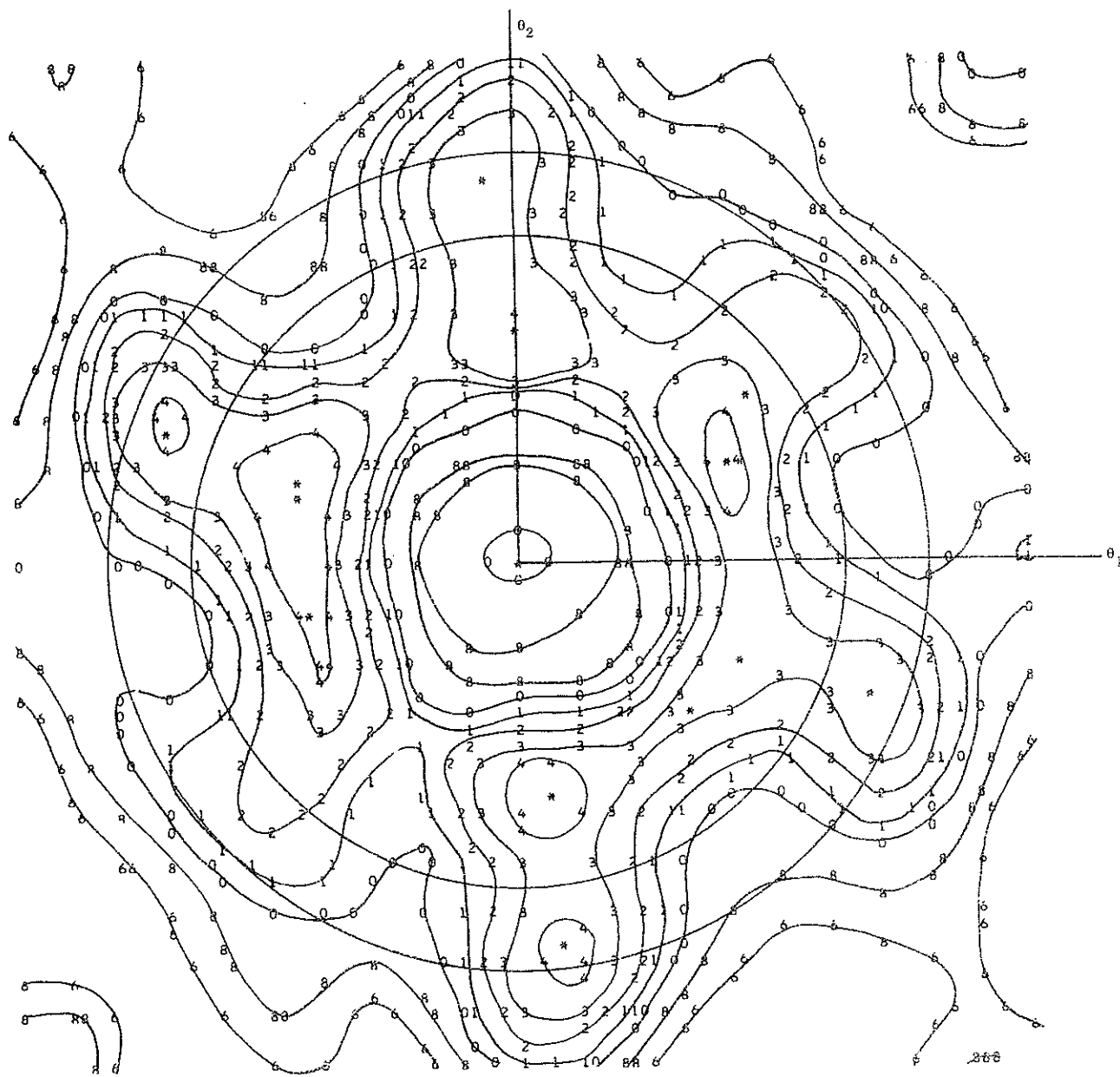


Figure 10-9. Circular polarization,  $\delta = 0^{\circ}75$ ,  $\lambda = 5320 \text{ \AA}$ .

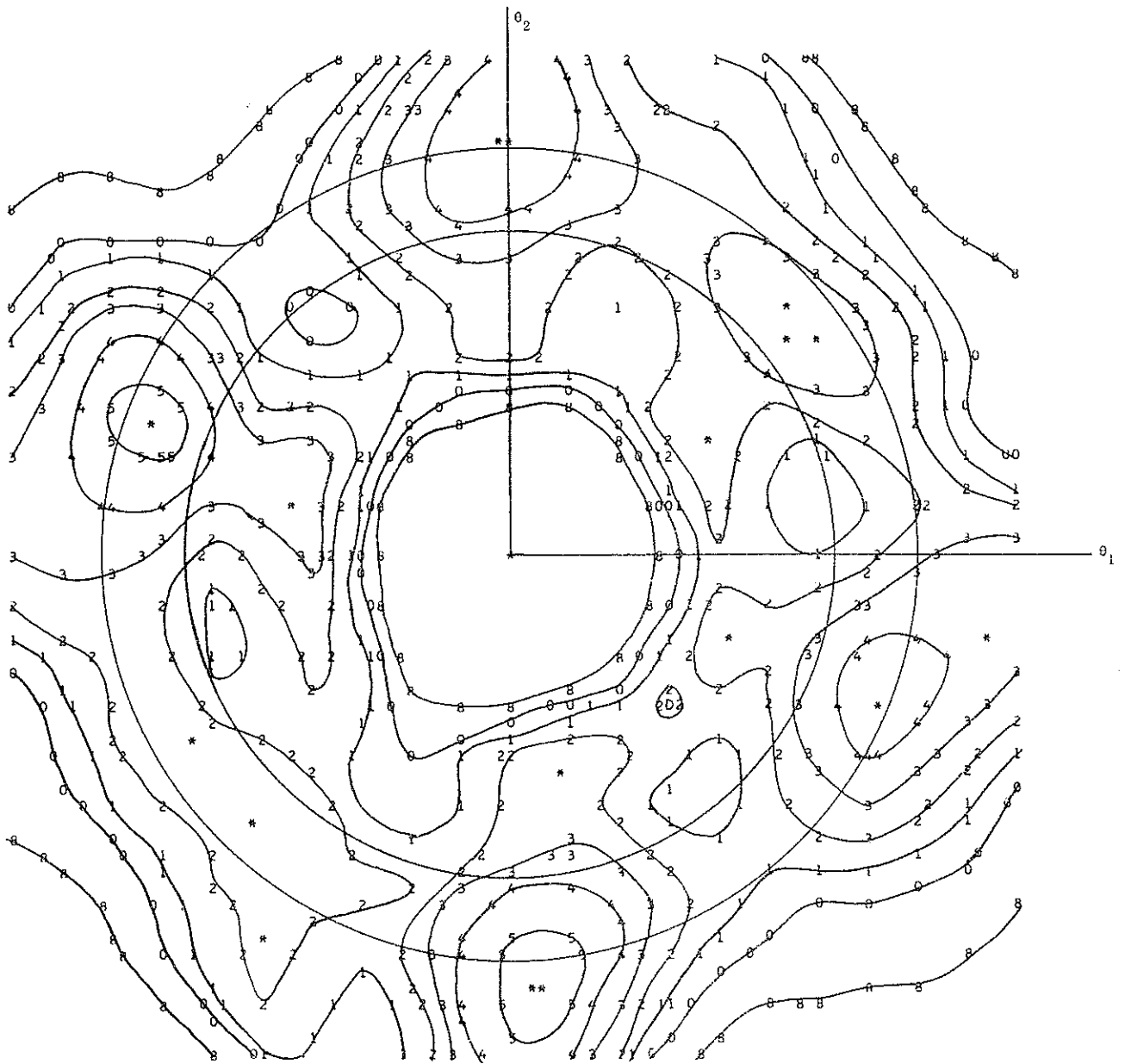


Figure 10-10. Circular polarization,  $\delta = 1''25$ ,  $\lambda = 5320 \text{ \AA}$ .

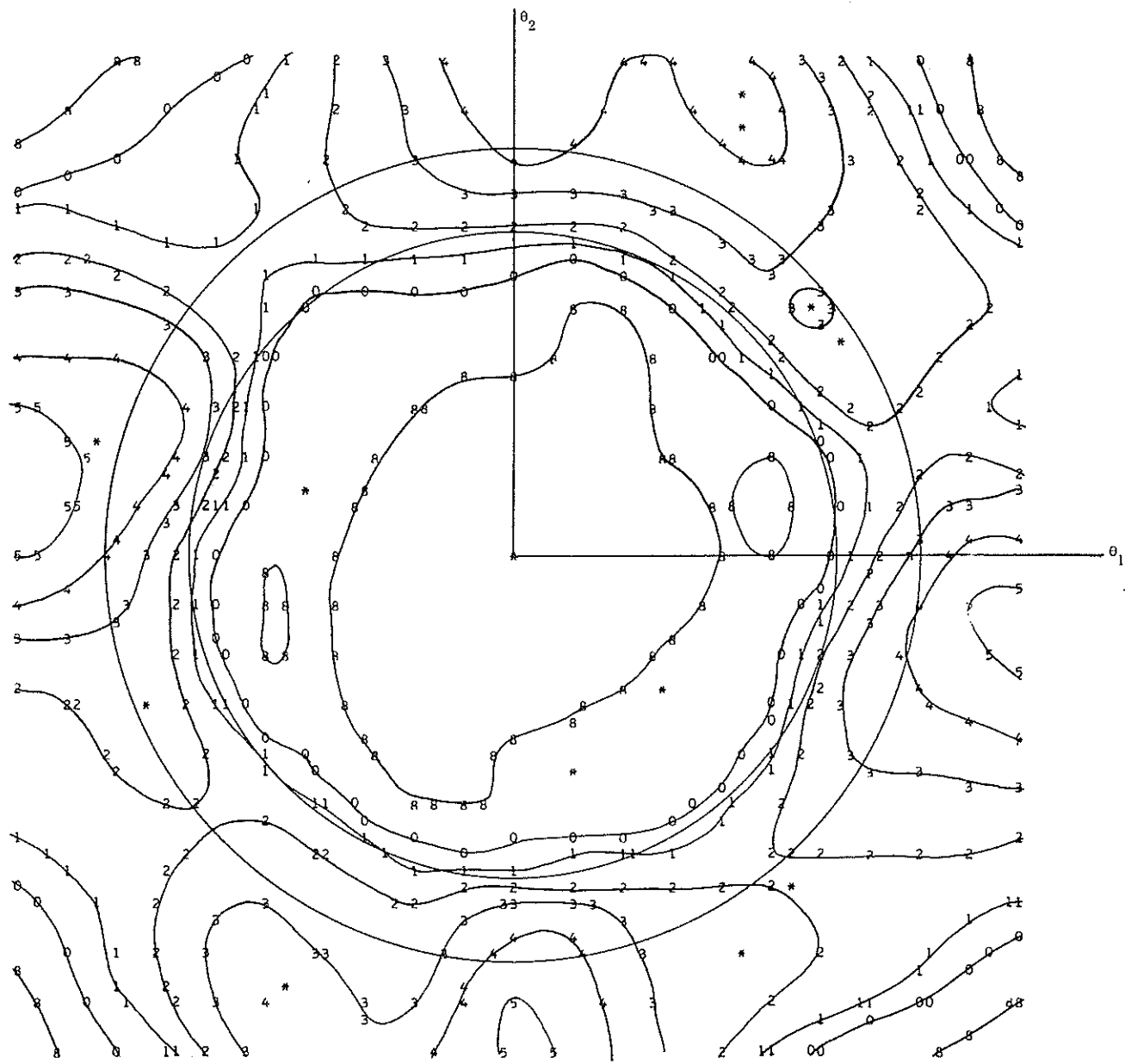


Figure 10-11. Circular polarization,  $\delta = 1''.75$ ,  $\lambda = 5320 \text{ \AA}$ .

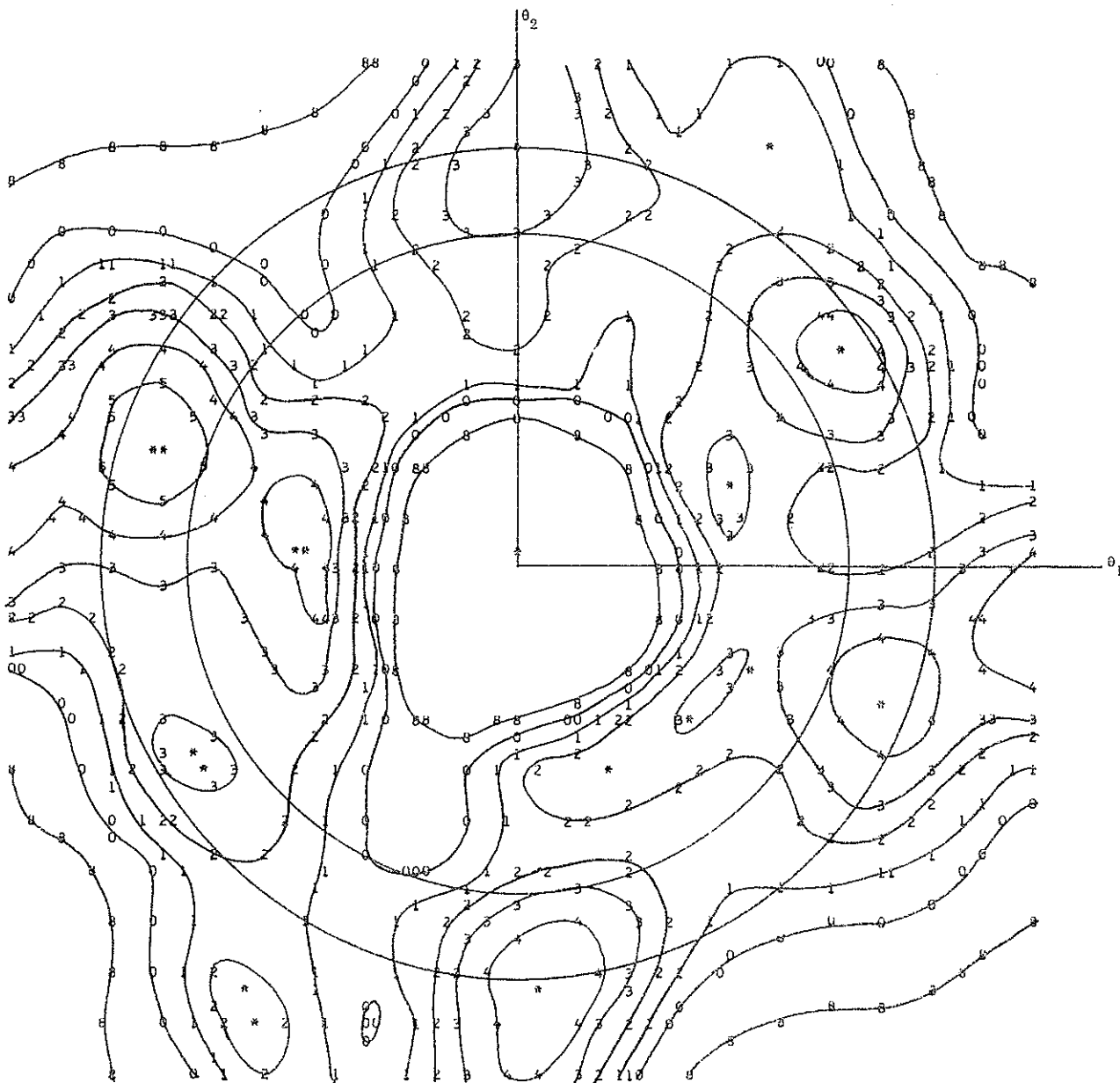


Figure 10-12. Circular polarization,  $\bar{\delta} = 1.125$  (mixed dihedral angles),  $\lambda = 5326 \text{ \AA}$ .

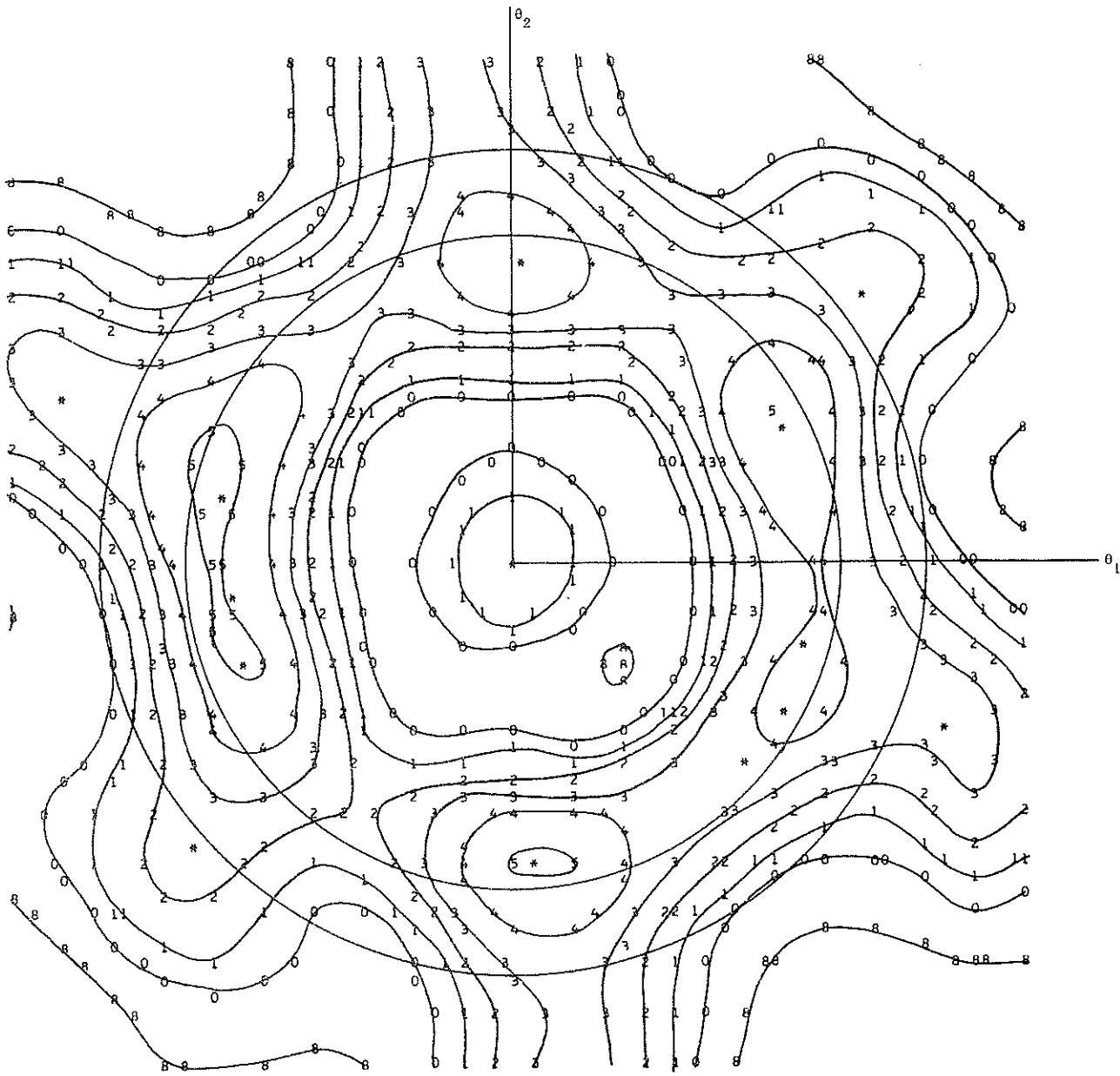


Figure 10-13. Circular polarization,  $\delta = 0''75$ ,  $\lambda = 6943 \text{ \AA}$ .



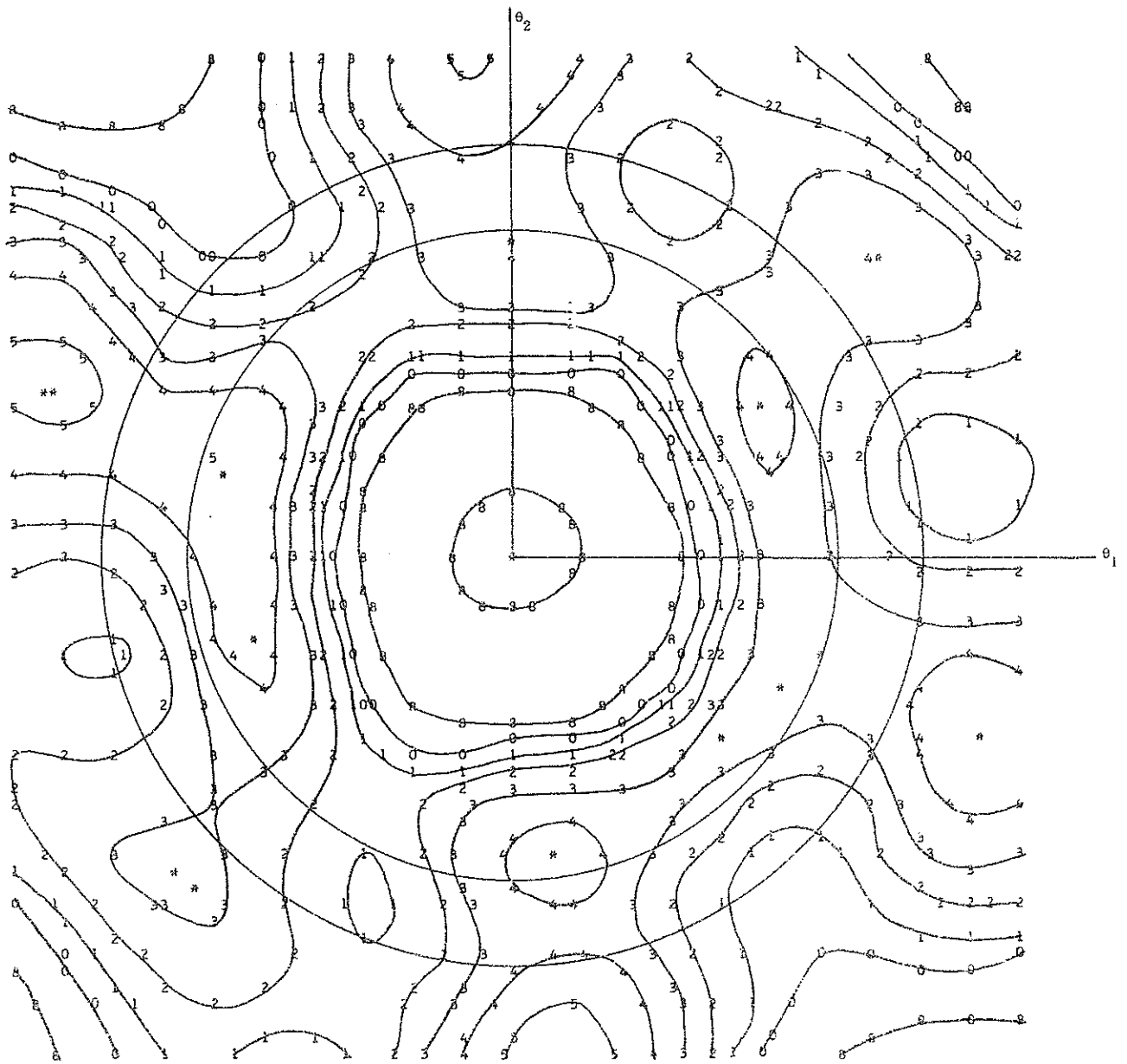


Figure 10-14. Circular polarization,  $\delta = 1^{\circ}25'$ ,  $\lambda = 6933 \text{ \AA}$ .

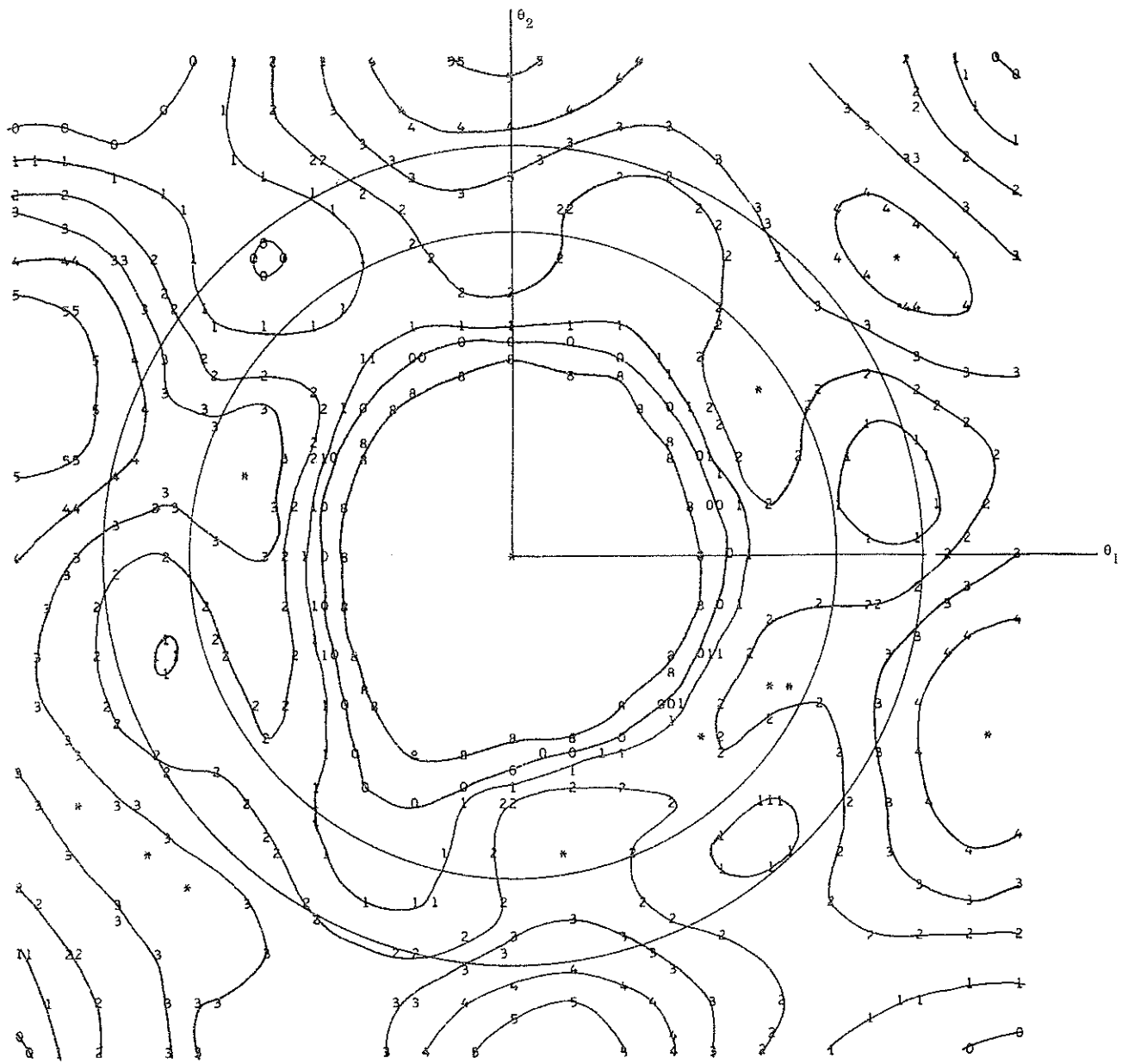


Figure 10-15. Circular polarization,  $\delta = 1^{\circ}75$ ,  $\lambda = 6943 \text{ \AA}$ .

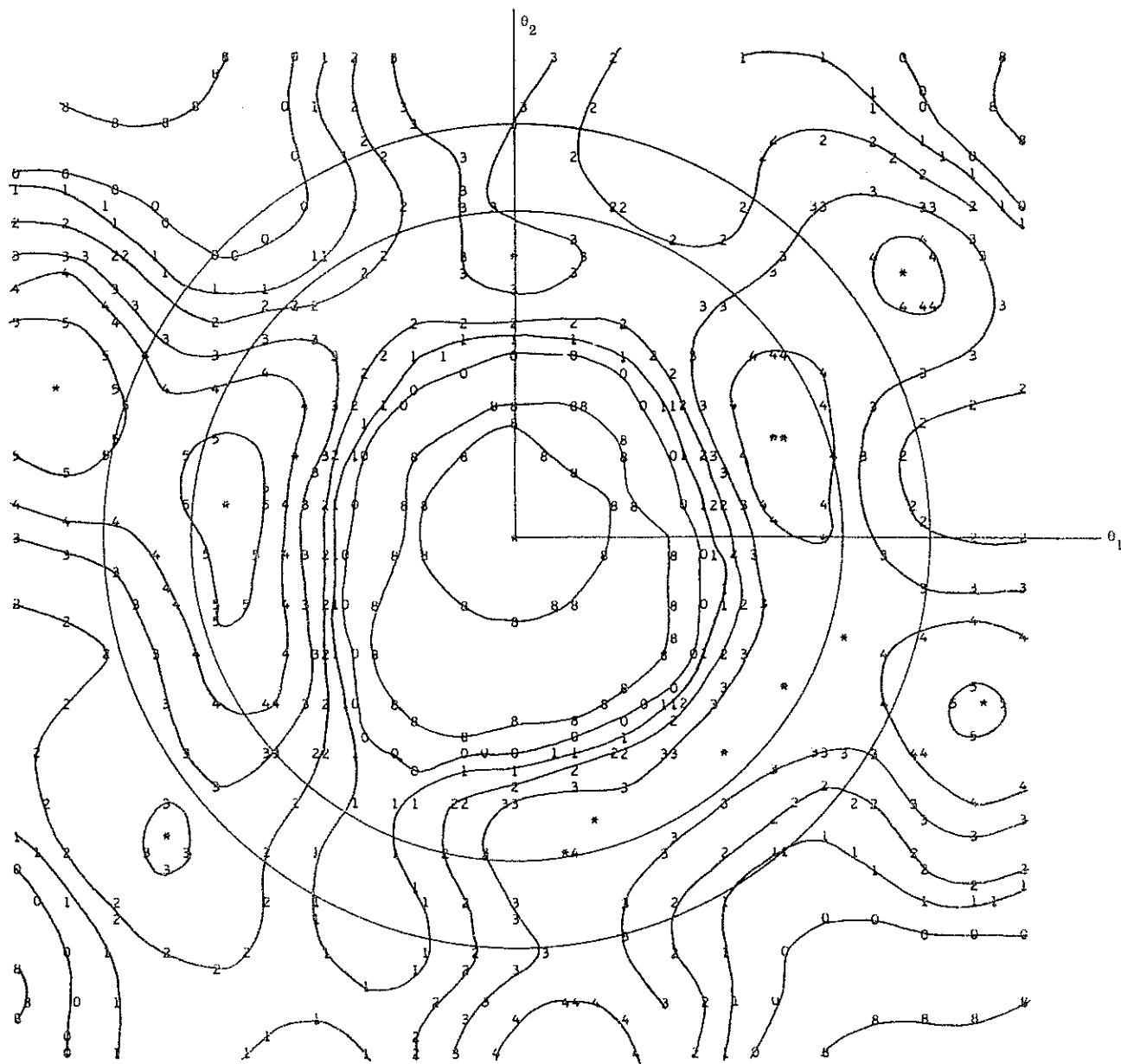


Figure 10-16. Circular polarization,  $\bar{\sigma} = 1.25$  (mixed dihedral angles),  $\lambda = 6943 \text{ \AA}$ .



## 11. EFFECT OF OPTICAL COHERENCE

The range corrections given in Section 10 were derived by adding the intensities of the reflections from each cube corner to construct the return pulse. Since slight changes in the direction of illumination of the satellite give different phase relationships among the reflections from individual cube corners, the shape and strength of the laser echo from Lageos varies from pulse to pulse when the individual reflections are added coherently. The variation of the return energy is described by the Rayleigh distribution. The effect on the range correction for various pulse lengths and pulse detection methods has been analyzed by constructing a set of coherent returns by using a pseudo random number generator to assign phases to the individual reflections. It can be shown mathematically that the incoherent centroid range correction is the average of the coherent centroid range corrections when each pulse is weighted by its intensity. This result is only approximately true for other pulse detection methods.

Table 16 gives a statistical summary of the set of coherent range corrections constructed for three different pulse lengths. The table lists the coherent average minus the incoherent value ( $\Delta$ ), the standard deviation of an individual pulse ( $\sigma$ ), the number of coherent returns in the sample ( $N$ ), the standard deviation of the average ( $\sigma_m = \sigma/\sqrt{N}$ ), and the ratio of the difference  $\Delta$  to the standard deviation of the mean ( $\sigma_m$ ). The last column is a measure of the statistical significance of  $\Delta$ . The variation of the range correction ( $\sigma$ ) due to coherent interference increases as the pulse length increases, and reaches a value of about 40 mm for the 20-nsec pulse length. The greatest variations occur for the weakest pulses. When each return is weighted by its intensity, the standard deviation of a pulse of average energy is found to be on the order of 10 mm. For long pulses, the return pulse shape is nearly the same as the transmitted pulse shape. As a result, there is no difference between the range correction for different pulse detection methods and no bias in the average coherent range correction. For the shortest pulse length (0.2 nsec), there is a small but statistically significant bias in the coherent average for all pulse detection methods, which is made possible by the asymmetry of the contributions to the return along the line of sight. Weighting by signal strength removes all the bias for centroid detection, most of the bias for half-area detection, and a little of the bias for half-maximum detection.

Table 16. Difference between the average range correction for a set of coherent returns and the range correction for the incoherent return. The pulse length is in nsecs;  $\Delta$ ,  $\sigma$ , and  $\sigma_m$  are in mm.

Pulse length	$\Delta$	$\sigma$	N	$\sigma_m$	$\Delta/\sigma_m$
Centroid, Equal Weighting					
0.2	-2.16	8.67	400	0.43	-4.98
5.0	0.09	26.07	1000	0.82	0.11
20.0	-2.01	37.17	1000	1.18	-1.71
Centroid, Weighted by Signal Strength					
0.2	0.04	7.08	400	0.35	0.11
5.0	0.02	10.81	1000	0.34	0.07
20.0	-0.23	11.34	1000	0.36	-0.65
Half-Area, Equal Weighting					
0.2	-2.55	10.07	400	0.50	-5.06
5.0	0.02	28.27	1000	0.89	0.02
20.0	-2.16	40.17	1000	1.27	-1.70
Half-Area, Weighted by Signal Strength					
0.2	-0.82	7.72	400	0.39	-2.12
5.0	-0.01	10.81	1000	0.34	-0.02
20.0	-0.24	11.32	1000	0.36	-0.68
Half-Maximum, Equal Weight					
0.2	-3.47	9.84	400	0.49	-7.06
5.0	0.34	26.78	1000	0.85	0.40
20.0	-2.43	44.82	1000	1.42	-1.72
Half-Maximum, Weighted by Signal Strength					
0.2	-2.54	6.93	400	0.35	-7.33
5.0	-0.16	10.51	1000	0.33	-0.48
20.0	-0.29	11.27	1000	0.36	-0.82

Figure 11 gives some sample coherent and incoherent pulse shapes for three pulse lengths. Only one coherent return is given for the 20- and 5-nsec pulse lengths since the effect of coherent interference is primarily a displacement of the pulse rather than a distortion of the shape for long pulses. Ten sample coherent pulses are given at 0.2 nsec. The position, in meters, listed in the first column of Figure 11, is measured with respect to the center of the pulse that would be received from a point reflector at the center of gravity of the satellite. The intensity in the second column is in normalized units such that the area under the curve is equal to the signal strength in equivalent number of cube corners at normal incidence.

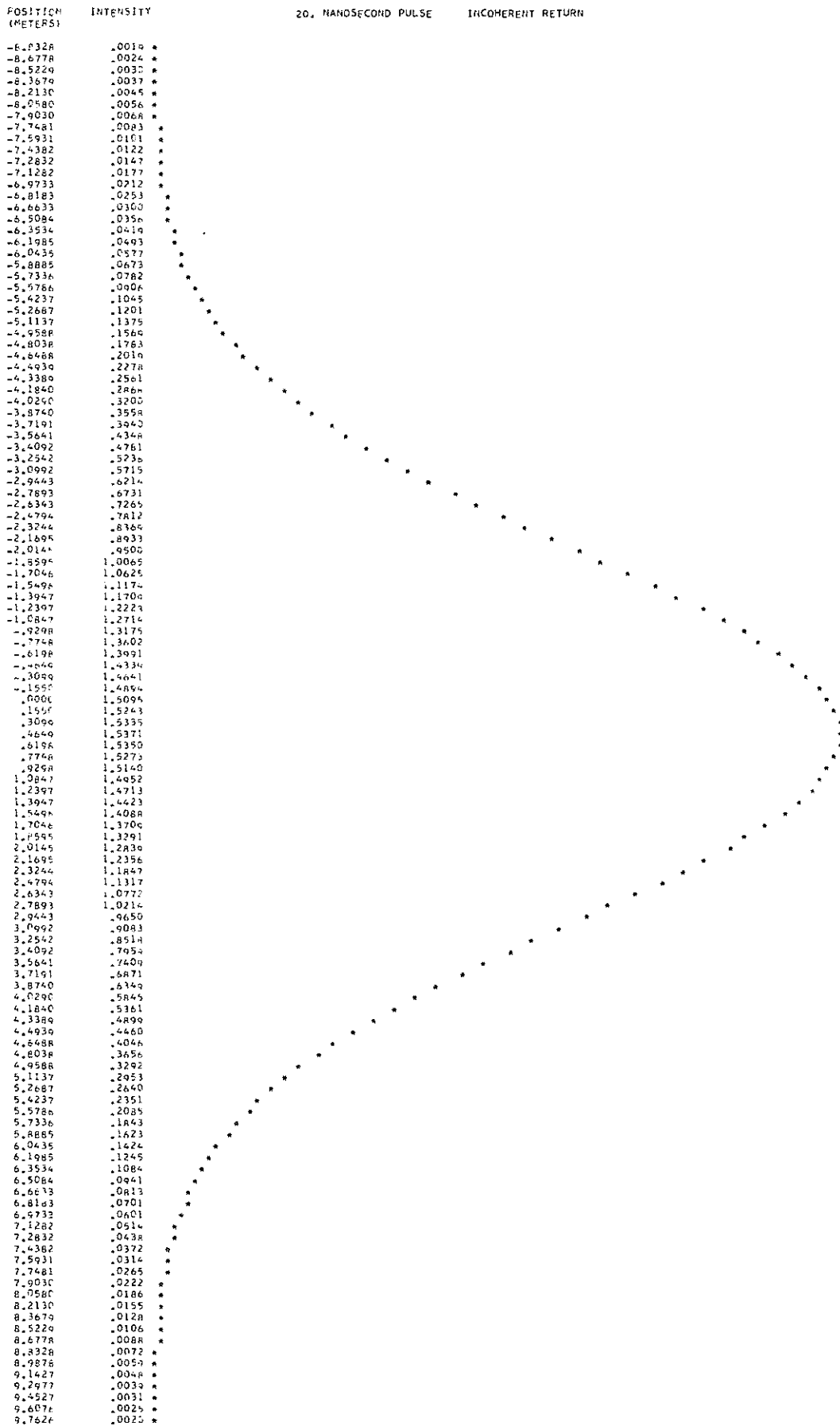


Figure 11. Sample incoherent and coherent reflected pulse shapes. The intensity is plotted vs. the distance along the line of sight Figure 11-1.



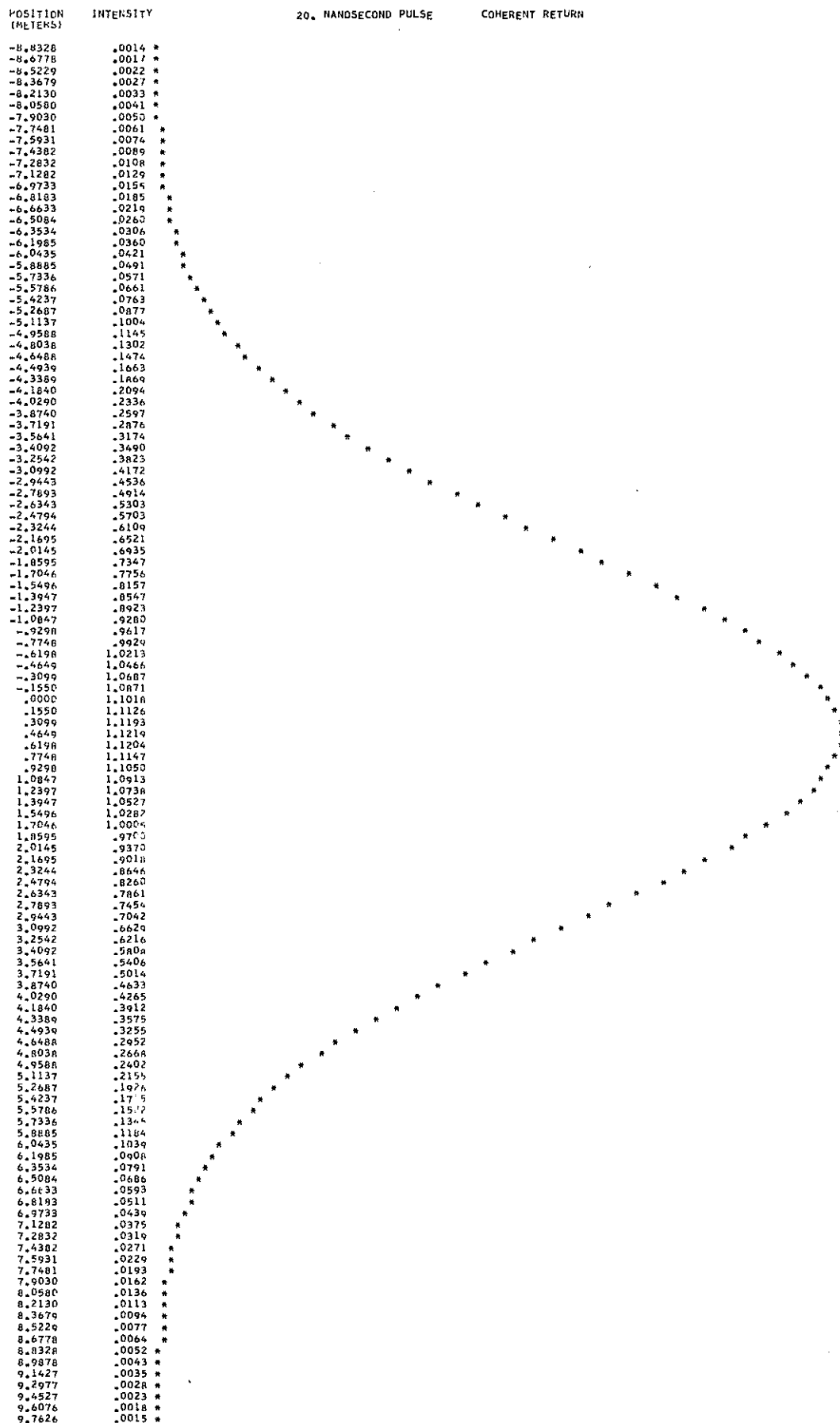


Figure 11-2.

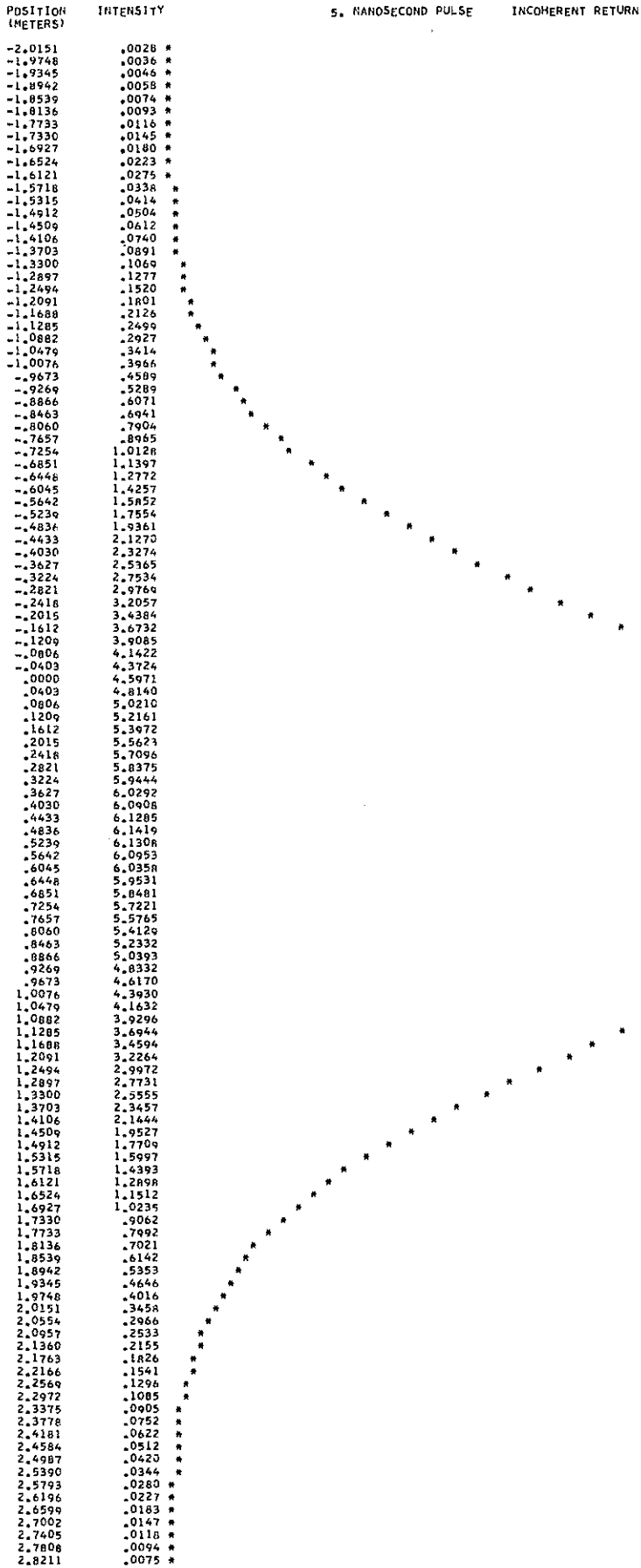


Figure 11-3.

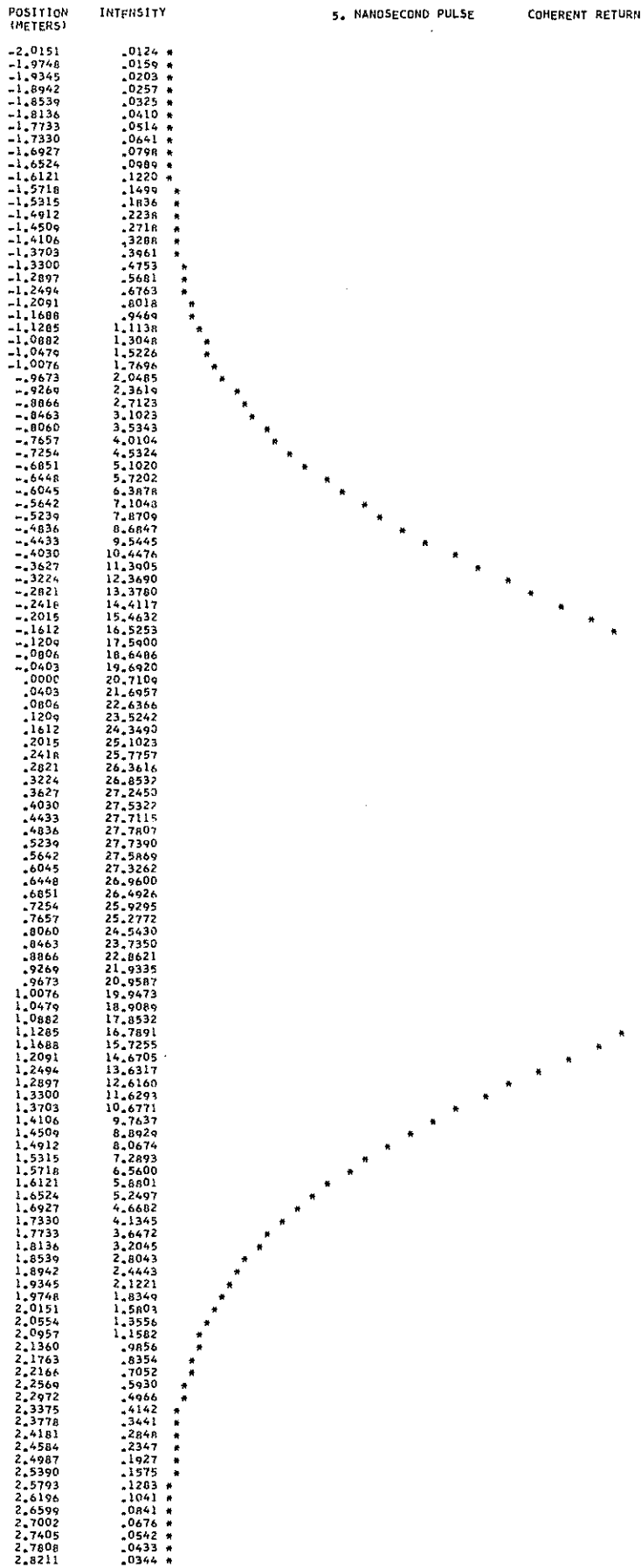


Figure 11-4.

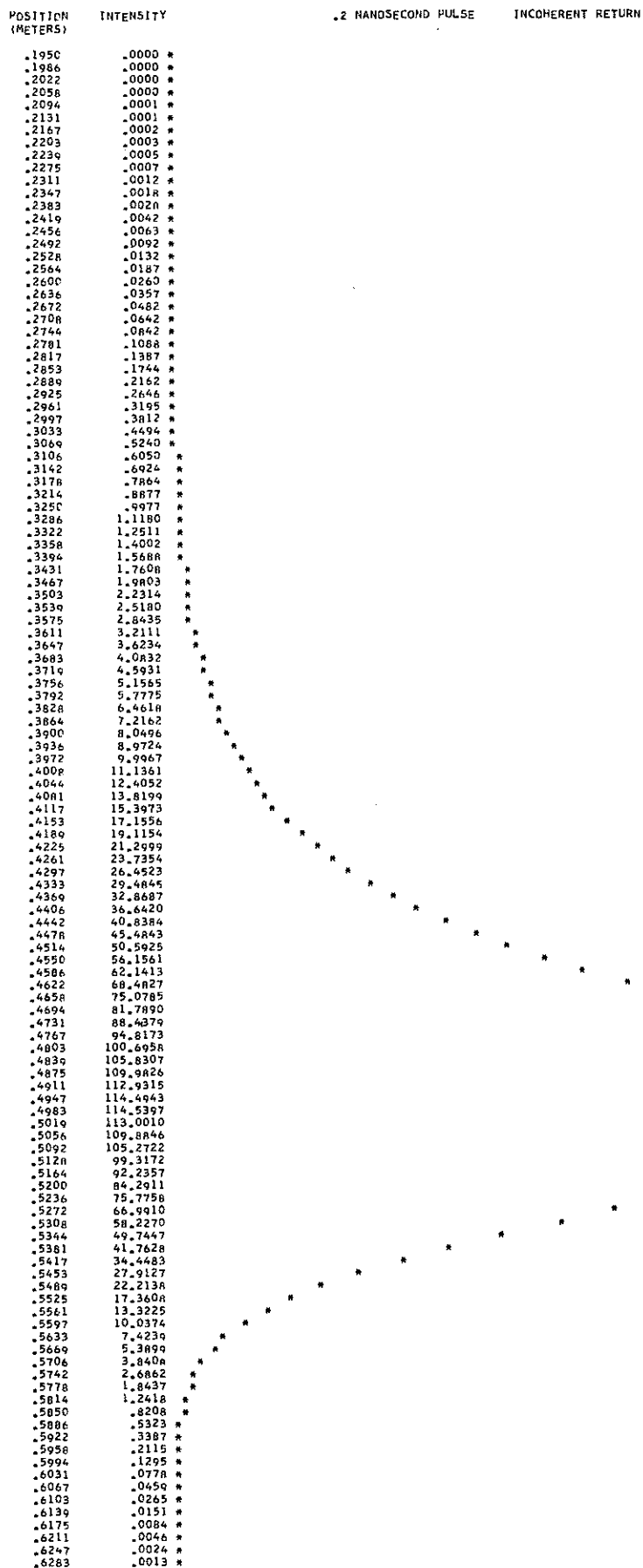


Figure 11-5.

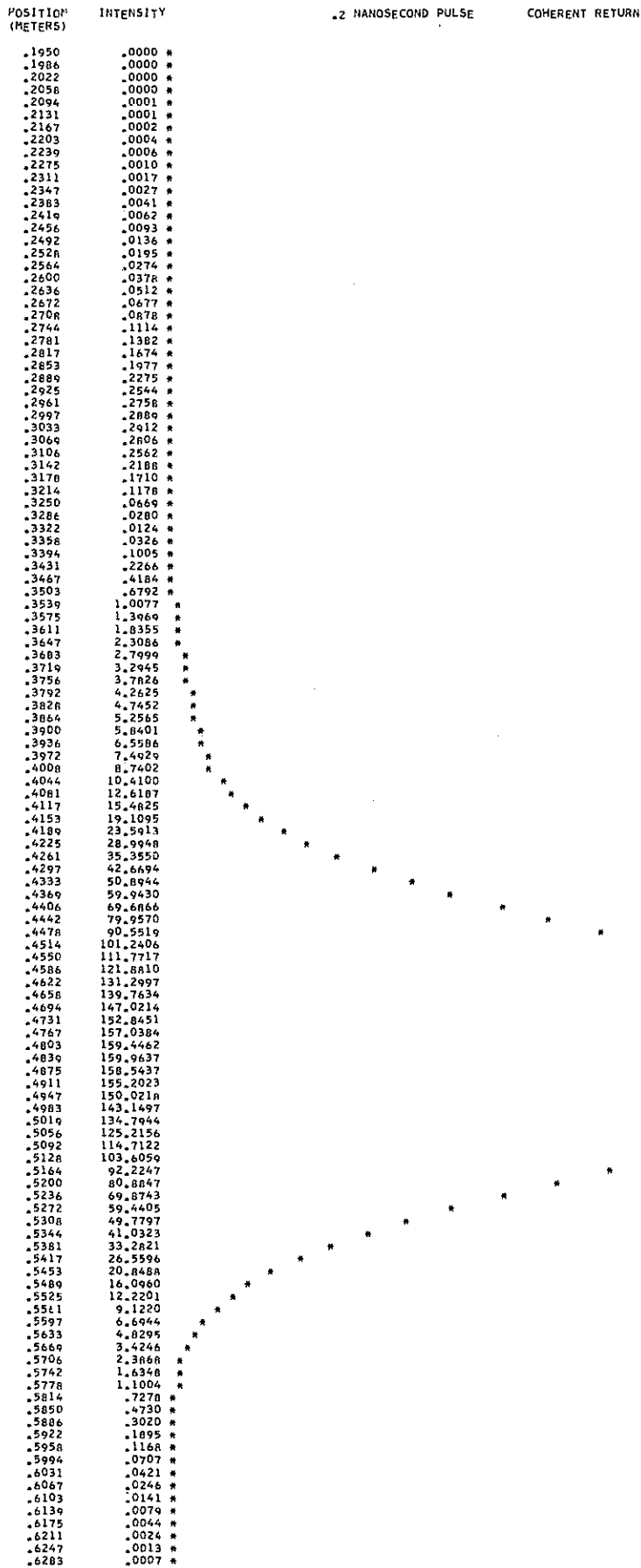


Figure 11-6.

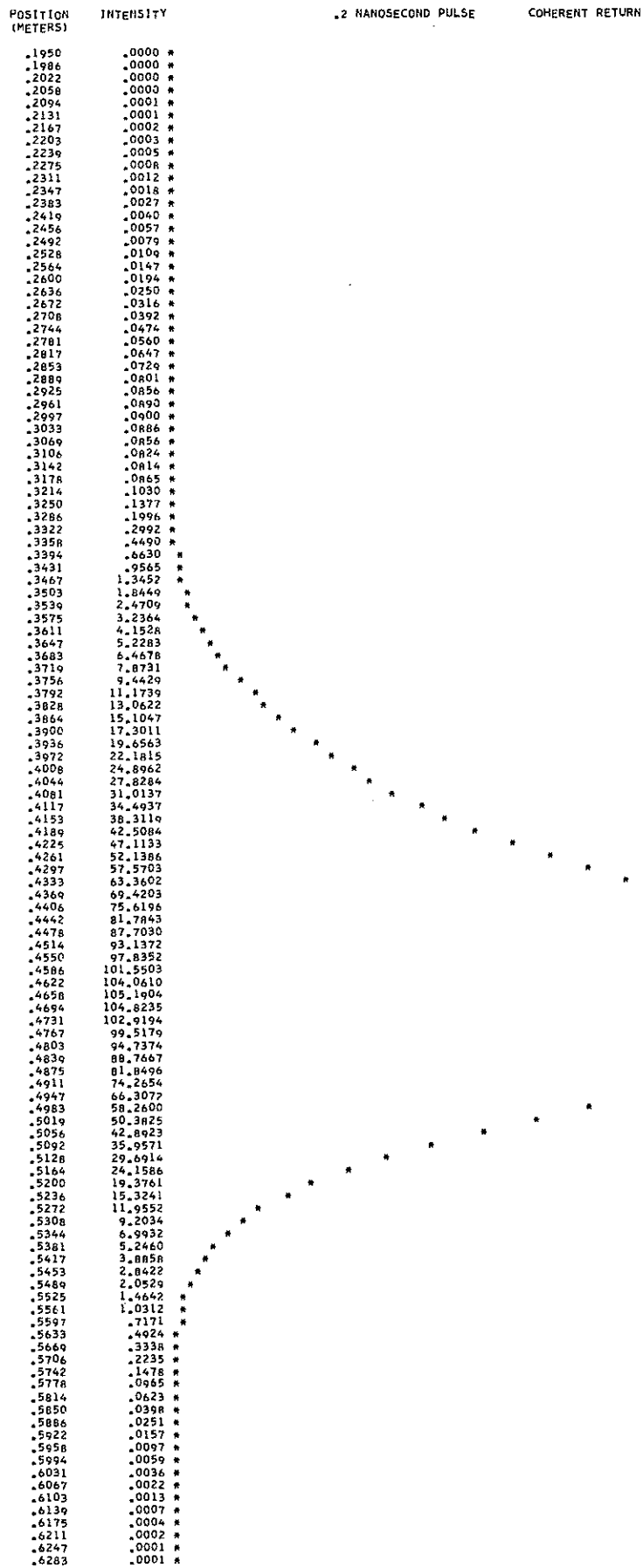


Figure 11-7.

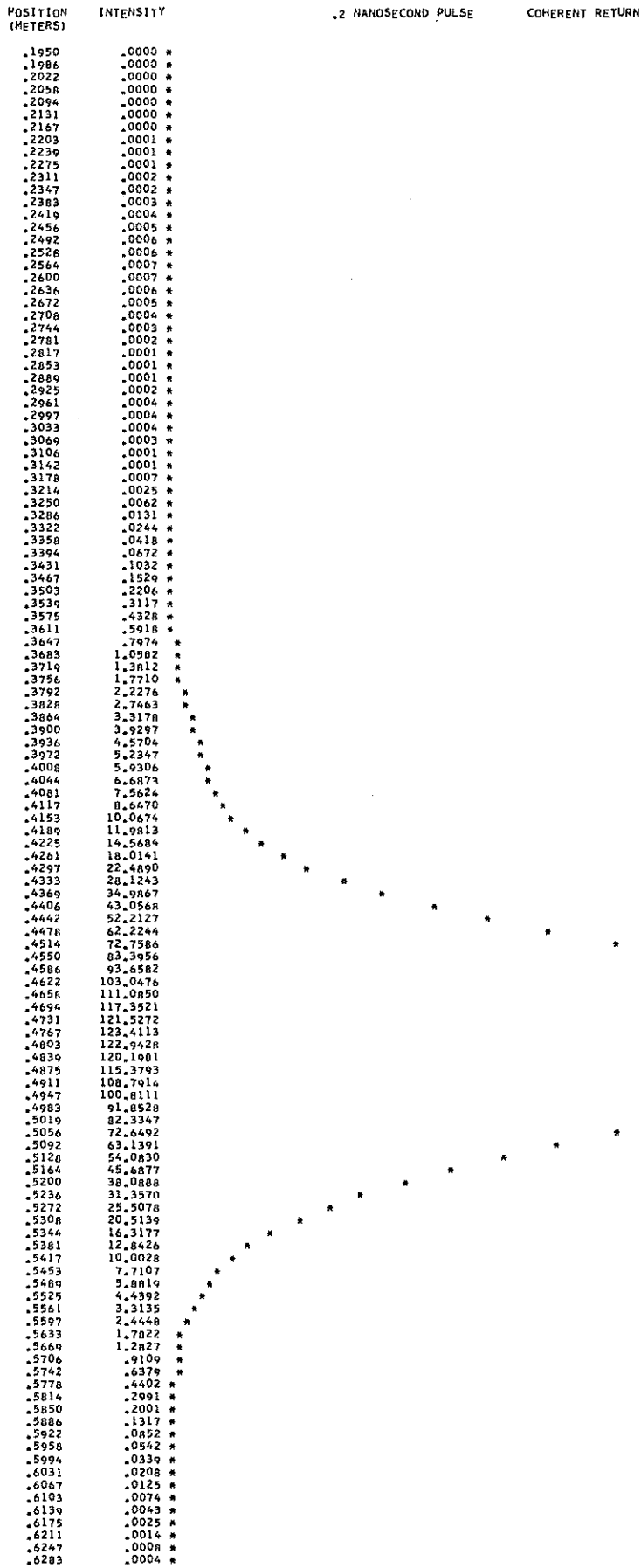


Figure 11-8.

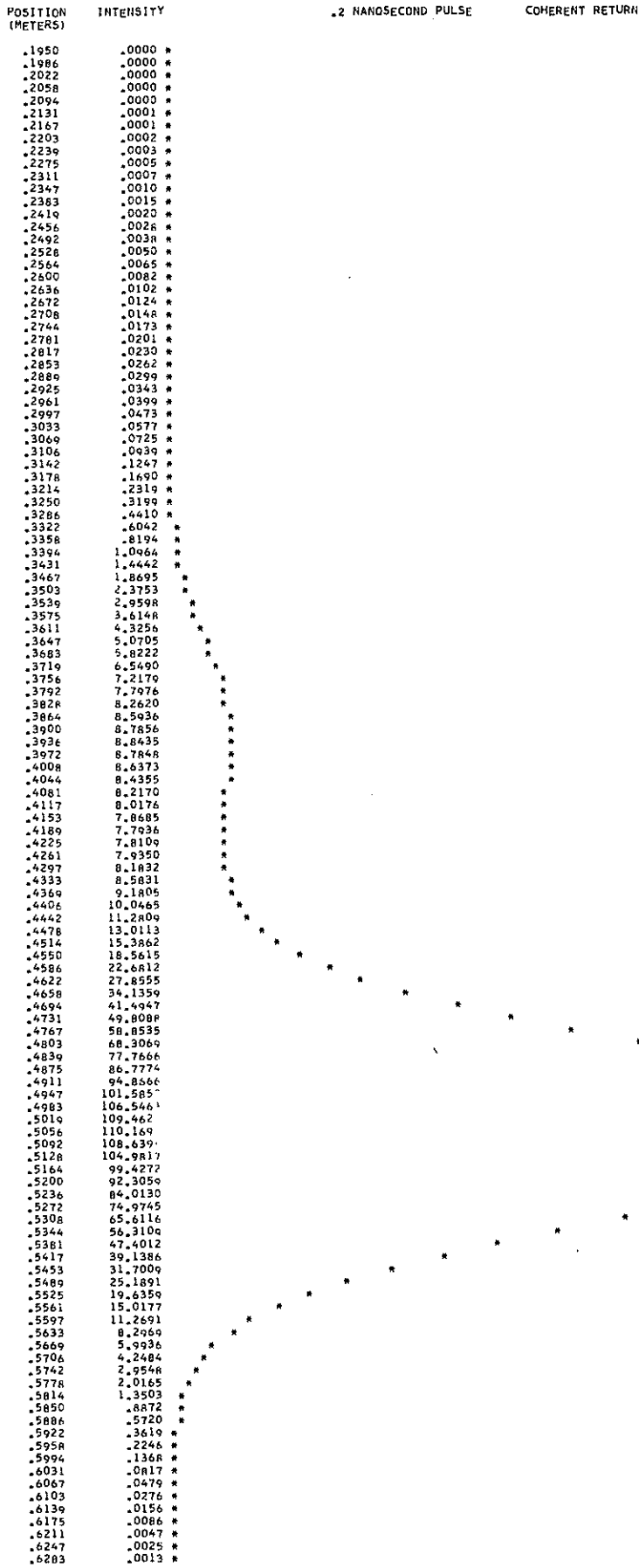


Figure 11-9.



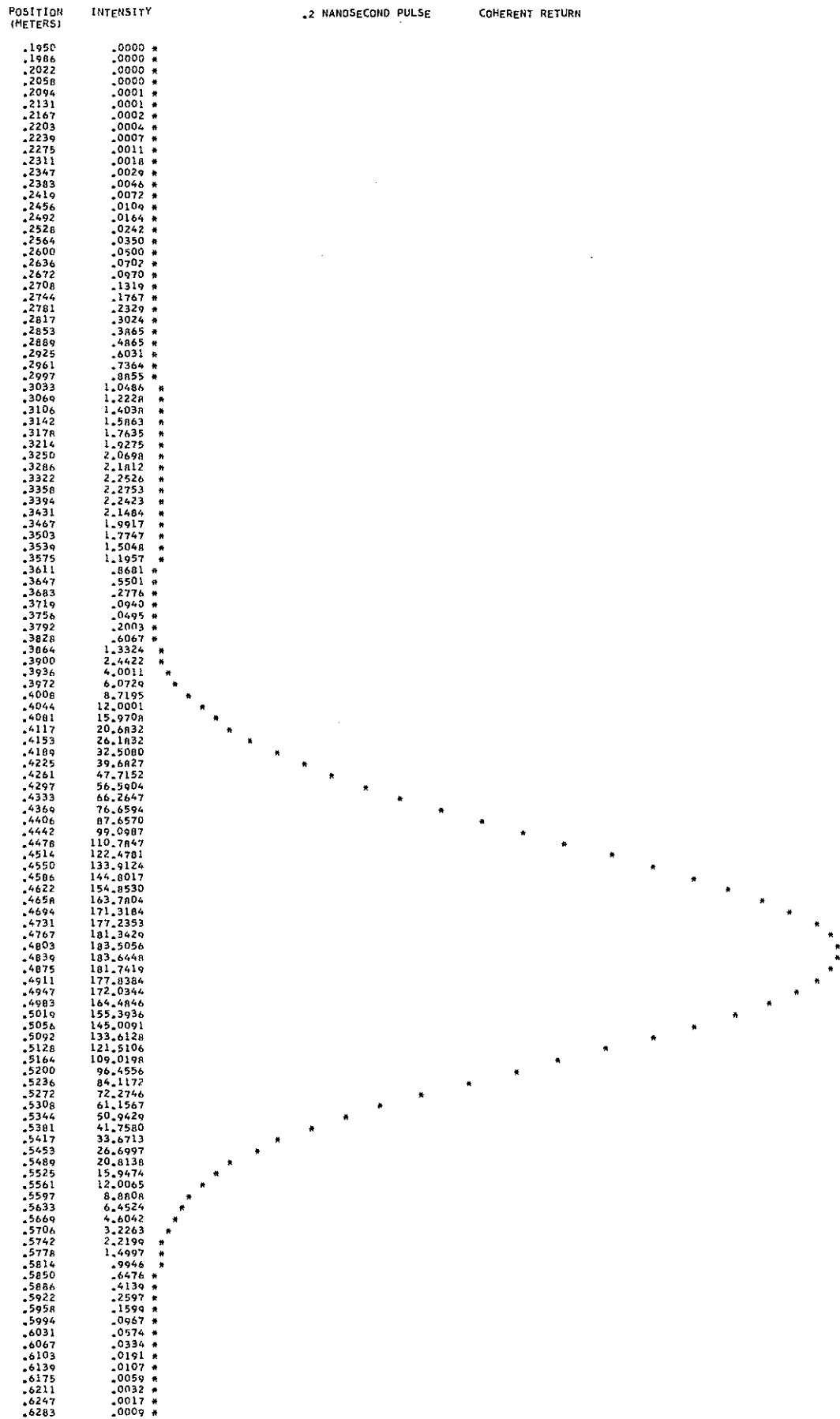


Figure 11-10.

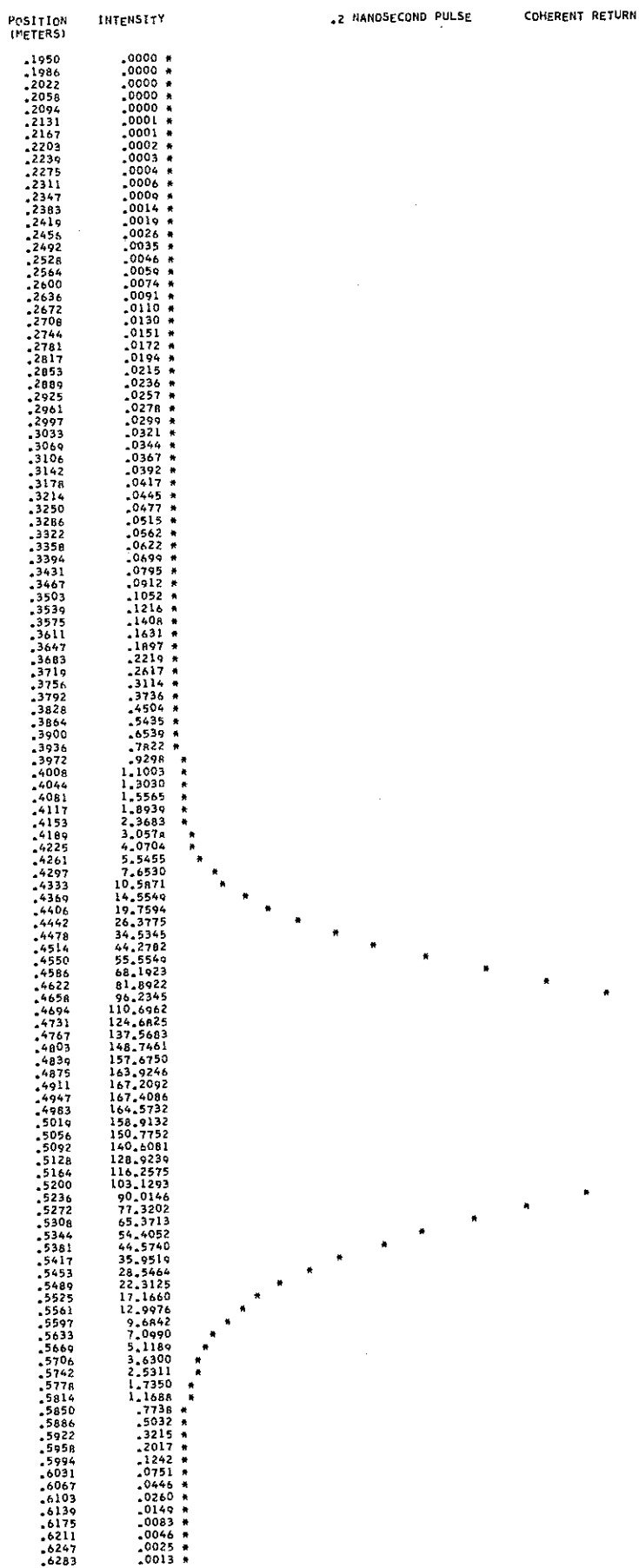


Figure 11-11.

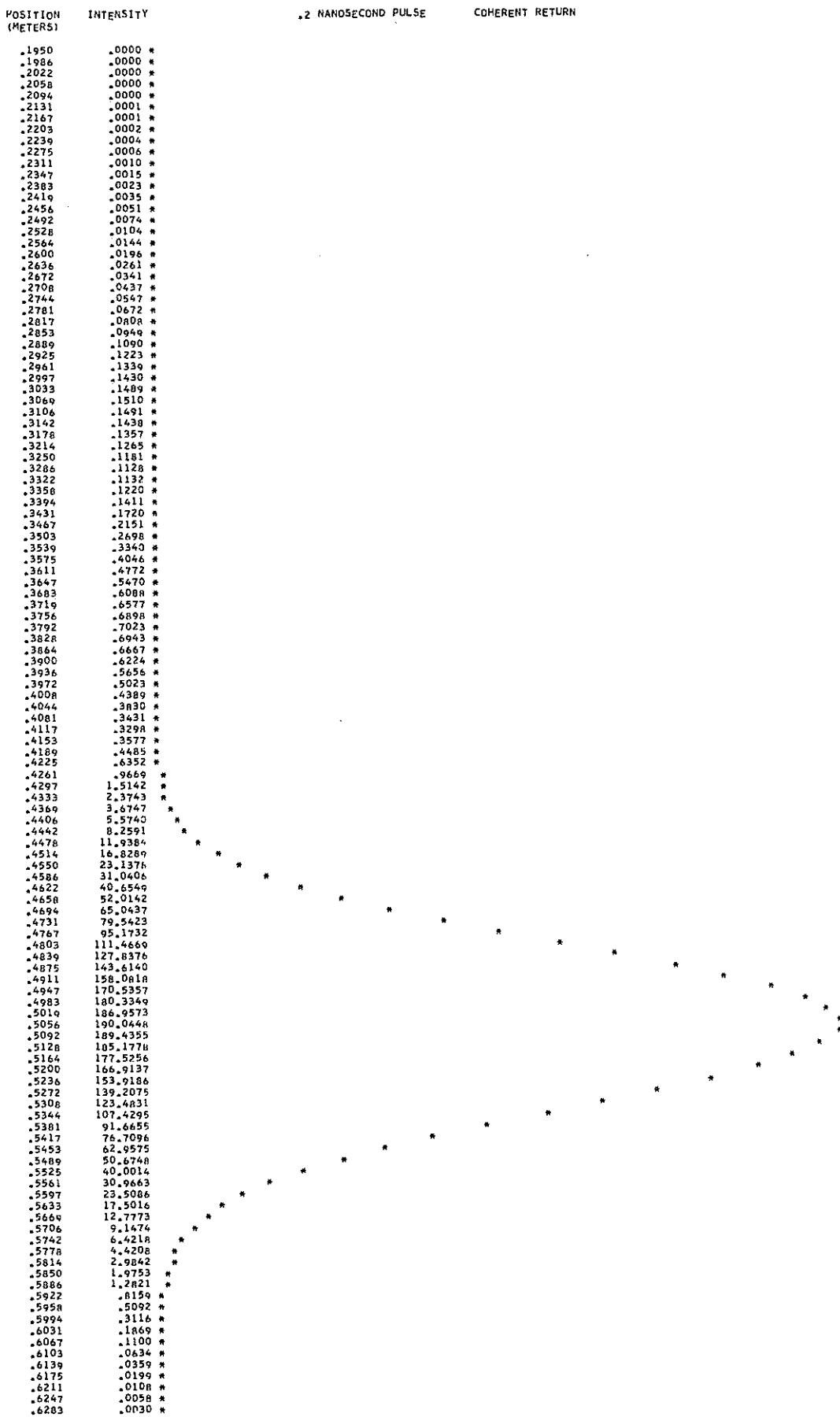


Figure 11-12.

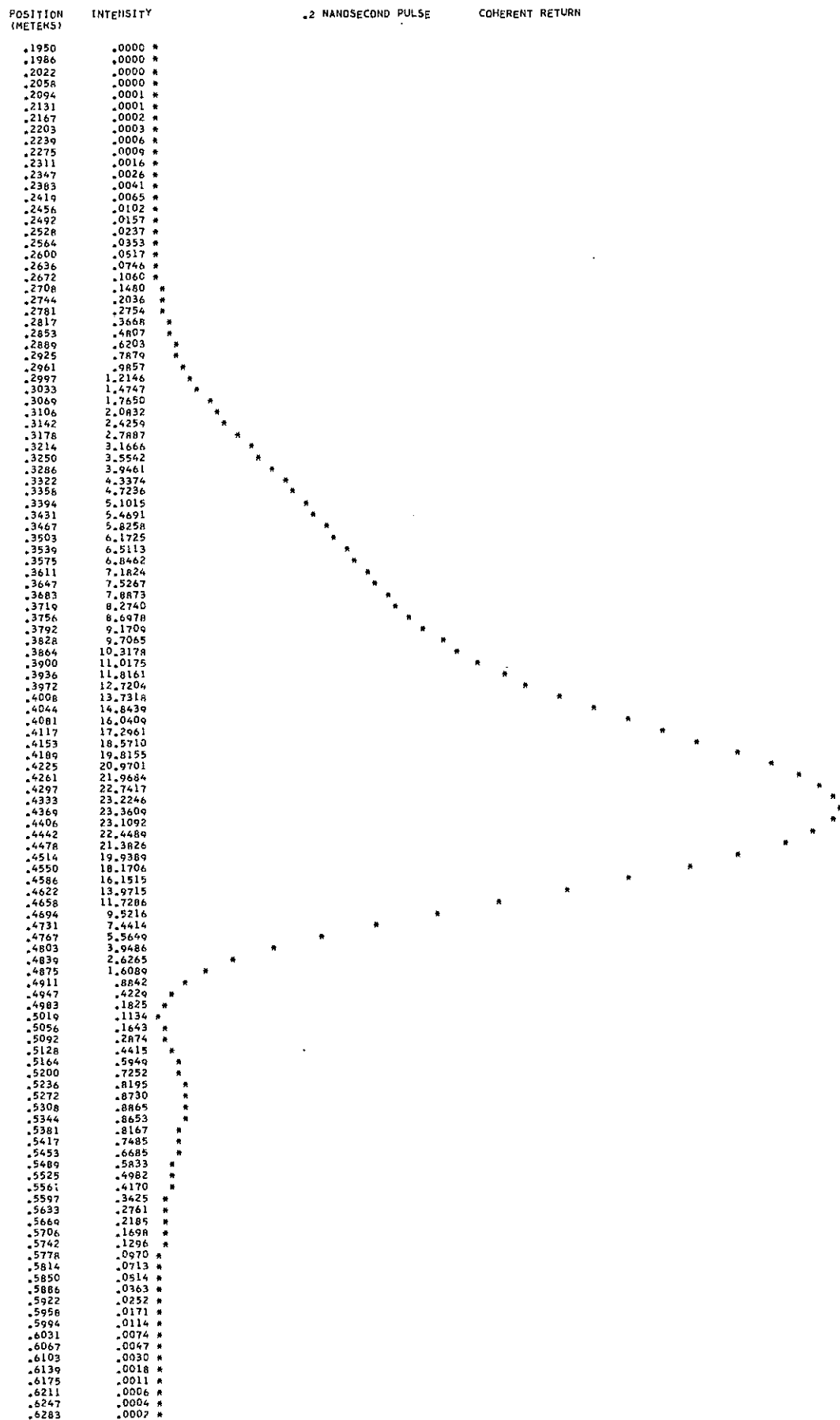


Figure 11-13.

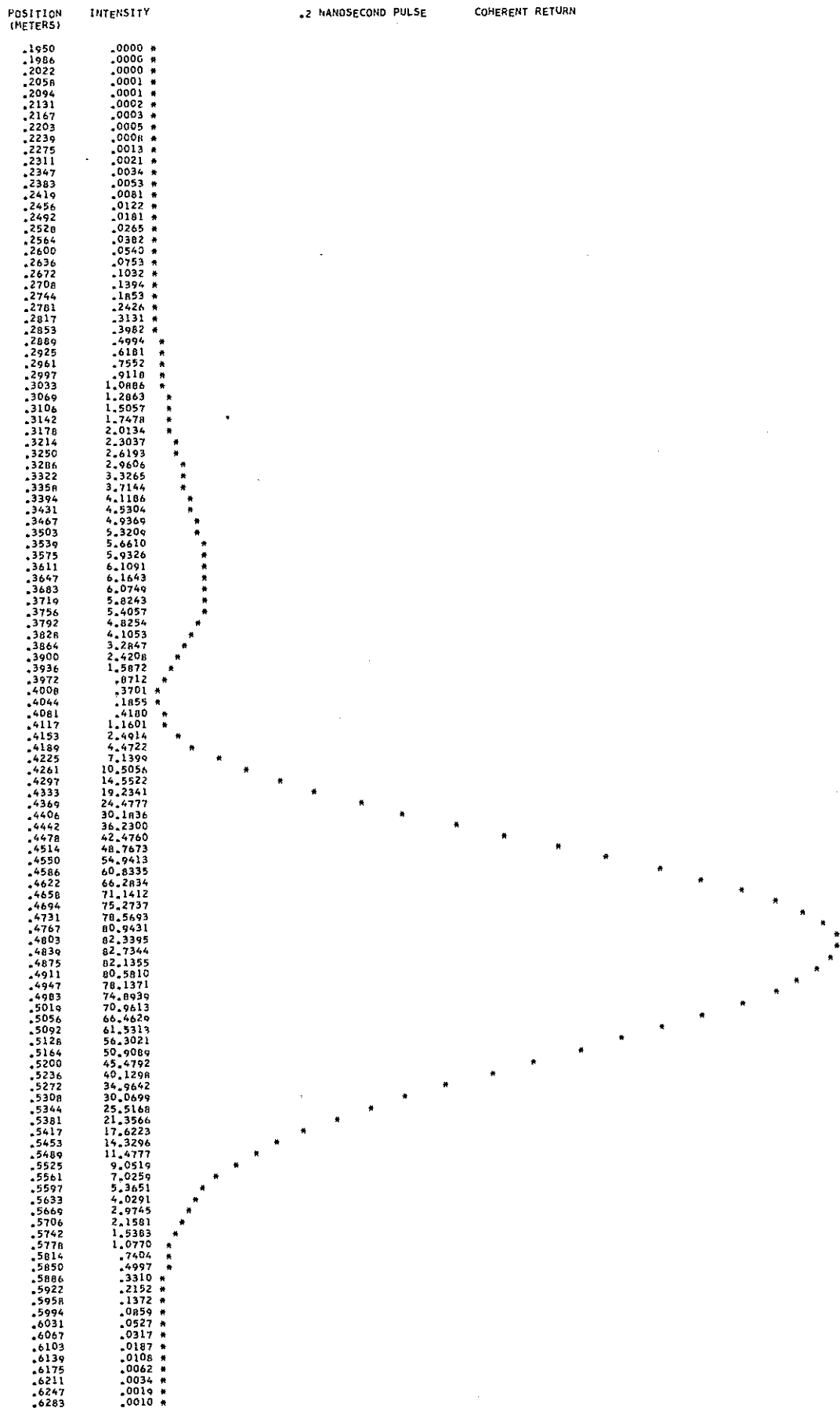


Figure 11-14.

POSITION (METERS)	INTENSITY	.2 NANOSECOND PULSE	COHERENT RETURN
.1950	.0000	*	*
.1986	.0000	*	*
.2022	.0000	*	*
.2058	.0000	*	*
.2094	.0001	*	*
.2131	.0002	*	*
.2167	.0003	*	*
.2203	.0005	*	*
.2239	.0008	*	*
.2275	.0013	*	*
.2311	.0020	*	*
.2347	.0032	*	*
.2383	.0050	*	*
.2419	.0076	*	*
.2456	.0114	*	*
.2492	.0168	*	*
.2528	.0242	*	*
.2564	.0343	*	*
.2600	.0477	*	*
.2636	.0651	*	*
.2672	.0870	*	*
.2708	.1140	*	*
.2744	.1465	*	*
.2781	.1846	*	*
.2817	.2278	*	*
.2853	.2755	*	*
.2889	.3284	*	*
.2925	.3789	*	*
.2961	.4312	*	*
.2997	.4813	*	*
.3033	.5275	*	*
.3069	.5688	*	*
.3106	.6053	*	*
.3142	.6383	*	*
.3178	.6710	*	*
.3214	.7079	*	*
.3250	.7553	*	*
.3286	.8201	*	*
.3322	.9096	*	*
.3358	1.0302	*	*
.3394	1.1865	*	*
.3431	1.3800	*	*
.3467	1.6087	*	*
.3503	1.8663	*	*
.3539	2.1427	*	*
.3575	2.4246	*	*
.3611	2.6967	*	*
.3647	2.9442	*	*
.3683	3.1530	*	*
.3719	3.3176	*	*
.3756	3.4332	*	*
.3792	3.5068	*	*
.3828	3.5535	*	*
.3864	3.5978	*	*
.3900	3.6740	*	*
.3936	3.8257	*	*
.3972	4.1057	*	*
.4008	4.5766	*	*
.4044	5.3121	*	*
.4081	6.3990	*	*
.4117	7.9407	*	*
.4153	10.0610	*	*
.4189	12.9091	*	*
.4225	16.6634	*	*
.4261	21.5348	*	*
.4297	27.7675	*	*
.4333	35.6366	*	*
.4369	45.4400	*	*
.4405	57.4852	*	*
.4442	72.0691	*	*
.4478	89.4498	*	*
.4514	109.8132	*	*
.4550	133.2338	*	*
.4586	159.6353	*	*
.4622	188.7532	*	*
.4658	220.1067	*	*
.4694	252.9848	*	*
.4731	286.4520	*	*
.4767	319.3767	*	*
.4803	350.4853	*	*
.4839	378.4370	*	*
.4875	401.9173	*	*
.4911	419.7386	*	*
.4947	430.9392	*	*
.4983	434.8683	*	*
.5019	431.2474	*	*
.5056	420.1994	*	*
.5092	402.2416	*	*
.5128	378.2434	*	*
.5164	349.3530	*	*
.5200	316.9075	*	*
.5236	282.3185	*	*
.5272	246.9776	*	*
.5308	212.1590	*	*
.5344	178.9486	*	*
.5381	148.1963	*	*
.5417	120.4951	*	*
.5453	96.1848	*	*
.5489	75.3758	*	*
.5525	57.9869	*	*
.5561	43.7910	*	*
.5597	32.4626	*	*
.5633	23.6216	*	*
.5669	16.8713	*	*
.5706	11.8274	*	*
.5742	8.1379	*	*
.5778	5.4955	*	*
.5814	3.6422	*	*
.5850	2.3690	*	*
.5886	1.5122	*	*
.5922	.9472	*	*
.5958	.5822	*	*
.5994	.3512	*	*
.6031	.2079	*	*
.6067	.1207	*	*
.6103	.0688	*	*
.6139	.0385	*	*
.6175	.0211	*	*
.6211	.0114	*	*
.6247	.0060	*	*
.6283	.0031	*	*

Figure 11-15.

## 12. ACCURACY OF RESULTS

Individual range measurements to the Lageos retroreflector array can vary due to a number of factors. Some variations are random and some systematic. The design goal accuracy of  $\pm 5$  mm refers to systematic errors since truly random errors can be averaged out in analysis. In practice, photon quantization at the detector is the largest single source of random noise and depends on signal level and pulse length. For example, a single photoelectron return gives an rms range variation of 1.3, 0.3, and 0.013 m at pulse lengths of 20, 5, and 0.2 nsec, respectively. The largest single source of noise due to the satellite itself is coherent interference among the reflections from individual cube corners, which produces a noise of about 1 cm at the pulse lengths considered if weighting by signal strength is used (Section 11). In principle, if the pulse length were shorter than the distance between cube corners along the line of sight, there would be no coherent interference. Calculating the return signal so that the range correction can be determined requires knowing the position and reflectivity of each cube corner contributing to the return. The range correction at a point in the far field pattern is a function of the intensity of the diffraction pattern of each cube corner at that point and the position of the cube corner along the line of sight. The positions of the cube corners on the satellite and the variation of the configuration of the cube corners from different viewing directions contribute an uncertainty of about 1 mm (Section 7). The primary source of systematic errors in computing the range correction is the variation of the range correction with position in the far field. The magnitude of the effect for Lageos can be seen from the range contour plots in Figure 10 of Section 10. In an attempt to estimate the effect of manufacturing tolerances on the range correction, calculations have been done for dihedral angle offsets of 0.75, 1.25, and 1.75 arcsec. The uncertainty in the offset is one of the primary manufacturing tolerances to be considered. Other factors affecting the far field pattern are surface curvature, material inhomogeneities, and thermal gradients that produce refractive index gradients. Optical testing of the cube corners under the expected thermal conditions showed that the variation in performance of an individual cube corner under different thermal conditions is in general less than the variation from one cube corner to another due to manufacturing differences. Looking at the range contour plots for

different dihedral angle offsets, wavelengths, and polarizations of the incident illumination shows that the extreme variations in the range correction within the annulus are from a high of about 0.2450 m to a low of about 0.2380, which gives peak-to-peak error limits of about plus 2 or 3 mm to minus 4 or 5 mm. Looking only at the plots for a mixture of angles whose mean is 1.25 arcsec, the extremes are from plus 2 or 3 mm to minus 2 or 3 mm. This is probably the best estimate of the range uncertainty since it should be a reasonable approximation for modeling the actual array.

The calculation of range corrections for other pulse detection methods at selected points in the far field shows that half-maximum and peak detection are more stable over the far field pattern than centroid or half-area detection for short pulses. The histogram in Figure 7 (Section 8) shows that the return energy is strongly peaked toward the front of the array. Half-maximum detection with a short pulse effectively detects the earliest part of the return whose location is well defined. In practice, strong signals would be required to take advantage of this fact, since the probability distribution for a single photoelectron is the energy distribution shown in the histogram, and the mean position of a photoelectron is the centroid.

In summary, the range corrections presented in this report are estimated to be accurate to 3 mm or better.



### 13. INFRARED TRANSFER FUNCTION

The infrared array carried by the Lageos satellite was designed to provide coverage from any direction of illumination with a minimum of interference between the reflections from different cube corners. Germanium was chosen for the material because its high index of refraction gives each cube corner a very large viewing angle so that only a small number of reflectors are required. The material has the disadvantage that it becomes opaque at around 100°C, which occurs if the cube corner faces the sun. An accurate range correction to the center of the satellite requires knowing the orientation of the satellite. In principle, the orientation can be determined from the infrared data.

The four infrared cube corners are positioned to form an approximate tetrahedron. One cube is at the north pole and the other three are in the third row below the equator in holes 1, 11, and 21. The coordinates of each cube are given in Section 3. For a perfect tetrahedron, the central angle between any pair of vertices is 109°47'12". The central angle between all pairs of infrared cube corners is listed in Table 17. The cubes are numbered starting with the pole cube as 1 and the cubes in holes 1, 11, and 21 of the third row below the equator as cubes 2, 3, and 4, respectively.

Table 17. Central angles between pairs of infrared cube corners.

Pair	Angle (°)
1-2	112.982
1-3	112.982
1-4	112.982
2-3	102.756
3-4	102.756
4-2	111.490

Since the back faces are uncoated, the infrared reflectors depend on total internal reflection. The minimum incidence angle  $\phi_c$  at which total internal reflection can be lost is given by the formula

$$\phi_c = \sin^{-1} (n \sin \phi'_c) \quad ,$$

where

$$\phi'_c = \tan^{-1} \sqrt{2} - \sin^{-1} (1/n) \quad .$$

The index of refraction is  $n = 4.00$  for germanium so that the cutoff angle after entering the front surface is  $\phi'_c = 40^\circ.258$ . The angle outside the cube corner is

$$\phi_c = \sin^{-1} (2.5849) \quad .$$

Since the sine of the cutoff angle  $\phi_c$  is greater than unity, no loss of total internal reflection occurs.

The reflectivity of the infrared cube corners is listed in Table 18 and plotted in Figure 12 as a function of the incidence angle  $\phi$  for  $\theta = 0$ , where the angles  $\theta$  and  $\phi$  are defined in Figure 4 (Section 6). Since the front face is circular and no loss of total internal reflection occurs, the reflectivity is nearly independent of  $\theta$ . There is a slight dependence on  $\theta$  due to polarization effects. The reflected energy is largely in the same polarization state as the input illumination, although some depolarization does occur as shown in Table 19. Except at normal incidence, the reflection losses at the front face are a strong function of the input polarization. The return is strongest when the electric vector is parallel to the plane of incidence and weakest when it is perpendicular. The signal for circular polarization is at least half as strong as the return for parallel polarization. The reflectivity listed is the average in the annulus between 32 and 41  $\mu$ rad from the center of the pattern. This is close to the top of the central lobe of the diffraction pattern, which is fairly wide at this long wavelength. The intensity has been normalized to the peak of the Airy diffraction pattern, which is the pattern for a perfect circular reflector. Reflection losses at the front face, and phase changes due to total internal reflection, which spread the pattern, together account for the fact that the intensity is down by about a factor of five from the center of the Airy

pattern. To convert the reflectivities in the table to gain the values are multiplied by  $G_{106000}$  where

$$G_{106000} = \frac{A}{\lambda^2} = \frac{11.4009 \text{ cm}^2}{(10.6 \times 10^{-4} \text{ cm})^2}$$

$$= 1.01468 \times 10^7 .$$

The cross section is  $ARG_{106000}$  where R is the reflectivity from Table 18. At normal incidence the cross section is  $2.55 \times 10^3 \text{ m}^2$  (in standard units of gain and cross section we have  $4\pi \times 2.55 \times 10^3 \text{ m}^2 = 3.2 \times 10^4 \text{ m}^2$ ).

Table 18. The reflectivity in units of  $A/\lambda^2$  for the Lageos infrared cube corners for input illumination, which is polarized parallel or perpendicular to plane of incidence or circularly polarized.

PHI	PARALLEL	PERPENDICULAR	CIRCULAR
0	.220740	.220740	.220740
5	.203725	.201985	.202860
10	.186730	.180403	.183602
15	.169991	.157213	.163702
20	.153655	.133528	.143784
25	.137848	.110358	.124401
30	.122625	.088528	.105975
35	.108039	.068704	.088851
40	.094131	.051364	.073278
45	.080858	.036751	.059349
50	.068216	.024957	.047109
55	.056140	.015884	.036482
60	.044598	.009303	.027342
65	.033539	.004866	.019503
70	.023071	.002164	.012821
75	.013469	.000743	.007221
80	.005585	.000160	.002917
83	.002277	.000040	.001176
85	.000885	.000011	.000454
86	.000450	.000005	.000231
87	.000179	.000001	.000092
88	.000045	0.000000	.000023

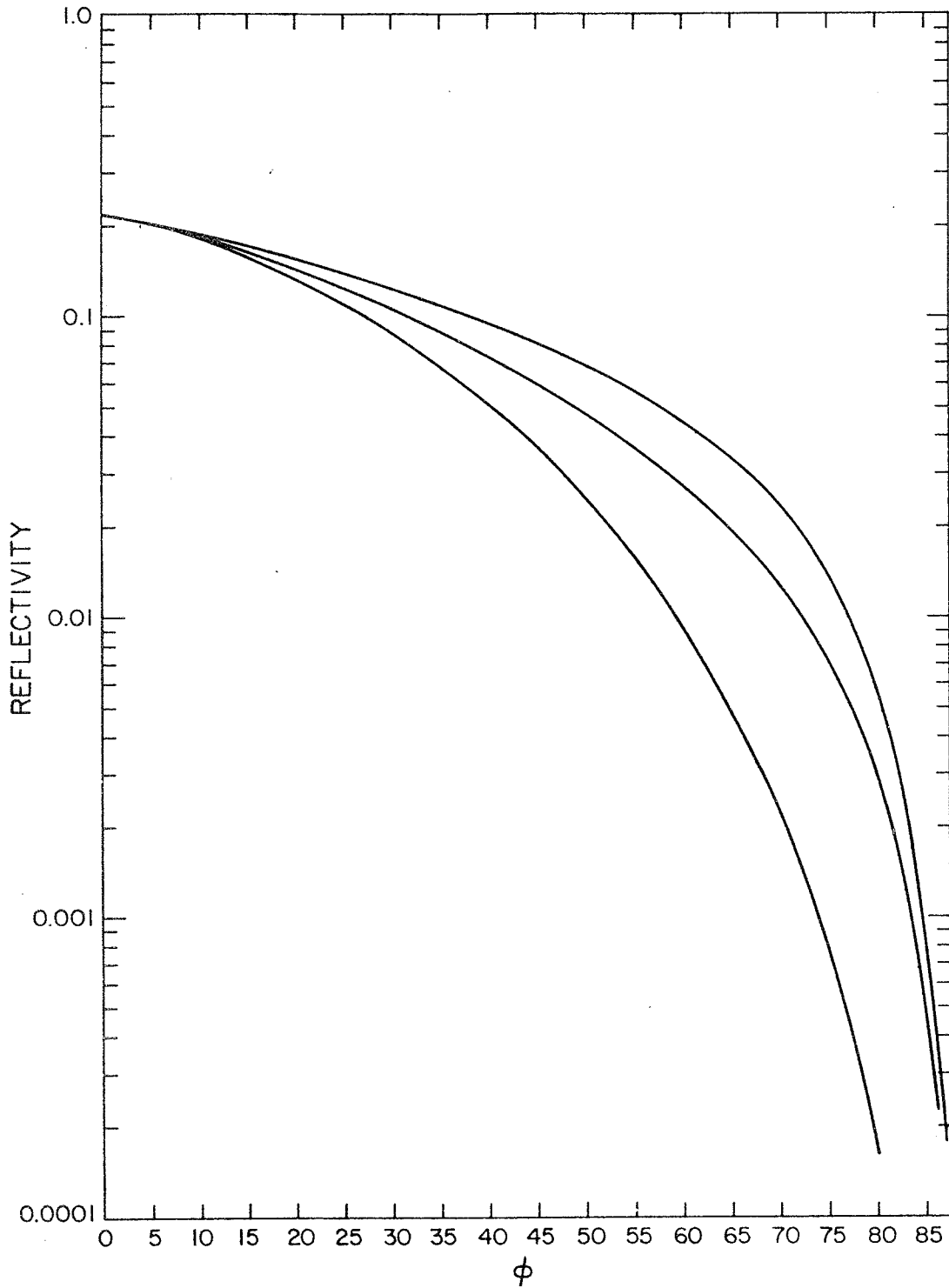


Figure 12. The reflectivity of the Lageos infrared cube corners in units of  $A/\lambda^2$ . The top curve is for input illumination parallel to the plane of incidence, the bottom curve for perpendicular to the plane of incidence, and the middle curve for circularly polarized illumination.

Table 19. The components of the reflected signal from the Lageos infrared cube in the same polarization state as the incident illumination and the orthogonal polarization state for some sample cases.

Incidence angle (°)	Transmitted polarization	Reflected intensity	
		Original polarization	Orthogonal polarization
0	Circular	0.2207	0.000012
60	Circular	0.0234	0.003925
0	Linear	0.2207	0.000006
60	Linear ( $E_{\parallel}$ )	0.0446	0.000012
60	Linear ( $E_{\perp}$ )	0.0093	0.000012

The transmission factor of the germanium cube corners decreases rapidly as the temperature of the material increases. The distance traveled by the ray inside the material varies from 5.57 to 5.75 cm. In Table 20, the absorption coefficient per centimeter, and the transmission factor for the cube corner are listed for various temperatures using a path length of 5.7 cm.

Table 20. Absorptance/cm and transmission factor for the Lageos infrared reflectors.

Temperature (°C)	Absorptance/cm	Transmission factor
27	0.027	0.857
40	0.028	0.852
45	0.033	0.829
50	0.045	0.774
60	0.085	0.616
70	0.143	0.443
80	0.241	0.253
90	0.386	0.111

The transmission factor should be included in the constant  $\eta$  when computing signal strengths using the formula in Section 5. Thermal vacuum tests run on two of the infrared cube corners gave temperatures of 104.4 and 106.7 °C with full solar illumination. The cube corners would be opaque at this temperature. With the solar illumination reduced by the factor  $1/\pi$ , the temperatures fell to 55.5 and 52.8 °C for the two cubes. This illumination corresponds to an incidence angle of 71.4°. With no solar illumination, the temperatures were 12.2 and 26.6°. In conclusion, the cube corners should operate well except when they are facing close to the direction of the sun.

By use of the reflectivity curve for the cube corners, calculations have been done to determine the probability over all possible viewing angles of obtaining single, double, and triple reflections. A return is considered double or triple if more than 0.1% of the reflected energy comes from a second or third cube corner. The results are tabulated for various cutoff intensities of the total signal (Table 21). The cutoff intensity is relative to the strongest return that can be obtained, which occurs when one cube corner is normal to the incident illumination. The results are shown for circular and linear polarization. A range of values is obtained for linear polarization since the reflectivity depends on the polarization angle. Strong returns are more likely to be single, and weak returns are more likely to be multiple.

Table 21. Probability over all viewing directions of getting single or multiple reflections for various cutoff levels of total intensity.

Cutoff intensity	Total probability	Single	Double	Triple
Circular Polarization				
0.01	1.000	0.223	0.632	0.135
0.1	0.980	0.233	0.632	0.115
0.2	0.781	0.233	0.516	0.031
0.5	0.256	0.206	0.050	0.000
Linear Polarization				
0.01	1.00-1.00	0.24-0.25	0.62-0.63	0.12-0.13
0.1	0.92-0.96	0.24-0.25	0.57-0.63	0.08-0.10
0.2	0.73-0.76	0.24-0.25	0.46-0.49	0.01-0.04

If the angle between the incident illumination and the normal to the front face of the infrared cube corner is known, the range correction from the apparent reflection point to the center of the satellite can be computed from the formula

$$C = R \cos \phi - L \sqrt{n^2 - \sin^2 \phi} ,$$

where

- C = the infrared range correction,
- R = the distance from the center of the satellite to the front face of the cube corner (29.807 cm),
- $\phi$  = the incidence angle of the illumination on the cube corner,
- L = the length of the cube corner from vertex to face (2.78384 cm),
- n = the index of refraction (4.0).

The first term is the position of the center of the front face of the cube corner along the line of sight, and the second term is the correction for optical path length in the cube corner. The range correction as a function of incidence angle is listed in Table 22. The negative values for large incidence angles indicate that the apparent reflection point is behind the center of the satellite. This effect is due to the optical path length in the cube corner.

Coherent interference can occur in the infrared reflection from Lageos in two different ways: The reflections from two or more cube corners can interfere with each other or multiply retroreflected beams from the same cube corner can interfere with each other. The beat frequency due to the first effect is  $2 \dot{\Delta C} / \lambda$ , where  $\lambda$  is the wavelength and  $\dot{\Delta C}$  is the rate of change of the difference in the range corrections for the two cube corners. The second effect is due to the fact that some of the radiation is reflected back into the cube corner each time a beam exits from the front face. A pulse of radiation therefore produces a train of reflected pulses each of lower intensity than the previous one. Alternate reflections are in the same direction as the incident beam. The reflections are of significant intensity because of the high index of refraction of germanium. The optical path length difference between the primary retroreflected beam and the next beam, which is parallel to the incident beam, is

Table 22. Infrared range correction vs the angle between the incident illumination and the normal to the front face of the reflector.

PHI (DEG)	RANGE CORRECTION (METERS)	*
0.0	.1867	*
1.0	.1867	*
2.0	.1865	*
3.0	.1863	*
4.0	.1860	*
5.0	.1856	*
6.0	.1851	*
7.0	.1845	*
8.0	.1839	*
9.0	.1831	*
10.0	.1823	*
11.0	.1814	*
12.0	.1804	*
13.0	.1793	*
14.0	.1781	*
15.0	.1768	*
16.0	.1754	*
17.0	.1740	*
18.0	.1725	*
19.0	.1708	*
20.0	.1691	*
21.0	.1674	*
22.0	.1655	*
23.0	.1636	*
24.0	.1615	*
25.0	.1594	*
26.0	.1572	*
27.0	.1549	*
28.0	.1526	*
29.0	.1502	*
30.0	.1477	*
31.0	.1451	*
32.0	.1424	*
33.0	.1397	*
34.0	.1369	*
35.0	.1340	*
36.0	.1310	*
37.0	.1280	*
38.0	.1249	*
39.0	.1217	*
40.0	.1184	*
41.0	.1151	*
42.0	.1117	*
43.0	.1083	*
44.0	.1048	*
45.0	.1012	*
46.0	.0975	*
47.0	.0938	*
48.0	.0900	*
49.0	.0862	*
50.0	.0823	*
51.0	.0783	*
52.0	.0743	*
53.0	.0703	*
54.0	.0661	*
55.0	.0620	*
56.0	.0577	*
57.0	.0535	*
58.0	.0491	*
59.0	.0448	*
60.0	.0403	*
61.0	.0358	*
62.0	.0313	*
63.0	.0268	*
64.0	.0222	*
65.0	.0175	*
66.0	.0128	*
67.0	.0081	*
68.0	.0033	*
69.0	-.0015	*
70.0	-.0063	*
71.0	-.0112	*
72.0	-.0161	*
73.0	-.0210	*
74.0	-.0259	*
75.0	-.0309	*
76.0	-.0359	*
77.0	-.0409	*
78.0	-.0460	*
79.0	-.0511	*
80.0	-.0562	*
81.0	-.0613	*
82.0	-.0664	*
83.0	-.0715	*
84.0	-.0767	*
85.0	-.0819	*
86.0	-.0870	*
87.0	-.0922	*
88.0	-.0974	*
89.0	-.1026	*
90.0	-.1078	*



$$\frac{4n L}{\cos \phi'} = \frac{4n^2 L}{\sqrt{n^2 - \sin^2 \phi}},$$

where

- $n$  = the index of refraction (4.0),
- $L$  = the length of the cube corner (2.78384 cm),
- $\phi$  = the incidence angle on the cube corner,
- $\phi'$  = the angle of the beam after refraction at the front face.

As the angle of incidence on the cube corner changes, the optical path length between the two retroreflected beams changes. The beat frequency due to this change is

$$\frac{\dot{\phi}}{\lambda} \frac{d}{d\phi} \left( \frac{4n^2 L}{\sqrt{n^2 - \sin^2 \phi}} \right) = \frac{\dot{\phi}}{\lambda} \frac{4Ln^2 \sin \phi \cos \phi}{(n^2 - \sin^2 \phi)^{3/2}}.$$

The cutoff angle for this interference is  $66^\circ 59'$  because the active reflecting area for secondary retroreflection goes to zero at this angle.

In order to use infrared data for deriving satellite positions to an accuracy better than 10 cm, it is necessary to know the orientation of the satellite. The orientation and angular velocity of the satellite affect the return signal in various ways that can, in principle, be used to infer the orientation as a function of time. If the satellite is spinning rapidly compared to the orbital frequency, the reflected intensity and measured range to each cube corner vary periodically. However, if the spin rate is low, or the change in orientation of the satellite relative to the observer is due only to the orbital motion, the variations in range and intensity would be difficult to separate from the variations due to orbital motion or other factors. The coherent interference between pairs of cube corners provides a precise measure of the change in distance to the two cube corners along the line of sight. The coherent interference between the primary and secondary retroreflected signals from one cube corner is a function of the incidence angle of the illumination on the cube corner. The rate of change of phase with incidence angle is zero at normal incidence and reaches a maximum value of 24 cycles/deg at  $46^\circ$  for a wavelength of  $106000 \text{ \AA}$ . Except at normal incidence, the

reflected intensity for linearly polarized illumination is a function of the angle of the polarization vector with respect to the plane of incidence on the cube corner. If the plane of polarization is rotated, the maximum intensity will occur when the polarization vector is in the plane of incidence, and the minimum will occur when it is perpendicular. The ratio of the maximum to the minimum is a function of the angle of incidence. Aside from an ambiguity of  $180^\circ$  in azimuth, such a measurement indicates the angle between the line of sight and the normal to the cube corner, and the azimuth of the cube corner about the line of sight.

#### 14. ACKNOWLEDGMENTS

The author wishes to express his appreciation to all those people who provided information used in this report. In particular, Mr. William Johnson of Marshall Space Flight Center provided technical data on the design of the satellite and retro-reflectors, and Mr. John Brueger of Bendix Aerospace Systems Division provided data on the thermal vacuum testing of the infrared cube corners.



## 15. REFERENCES

ARNOLD, D. A.

- 1972. Calculation of retroreflector array transfer functions. Final Technical Report, NASA Grant NGR 09-015-196, December. [This report gives results computed for satellites BE-B (6406401), BE-C (6503201), Geos 1 (6508901), D1C (6701101), D1D (6701401), Geos 2 (6800201), Peole (7010901), and Geos 3].
- 1974. Optical transfer function of NTS-1 retroreflector array. Technical Report RTOP 161-05-02, NASA Grant 09-015-002, Supplement No. 57, October.
- 1975a. Optical transfer function of Starlette retroreflector array. Technical Report RTOP 161-05-02, NASA Grant NGR 09-015-002, Supplement No. 57, February.
- 1975b. Optical and infrared transfer function of the Geos 3 retroreflector array. Technical Report RTOP 161-05-02, NASA Grant NGR 09-015-002 Supplement No. 57, October.

FITZMAURICE, M. W., MINOTT, P. O., ABSHIRE, J. B., and ROWE, H. E.

- 1977. Prelaunch testing of the laser geodynamic satellite (Lageos), March.

WEIFFENBACH, G. C.

- 1973. Use of a passive stable satellite for earth physics applications. Final Report, NASA Grant NGR 09-015-164, April.